Synthesis of Dualsteric Ligands for Muscarinic Acetylcholine Receptors and Cholinesterase Inhibitors

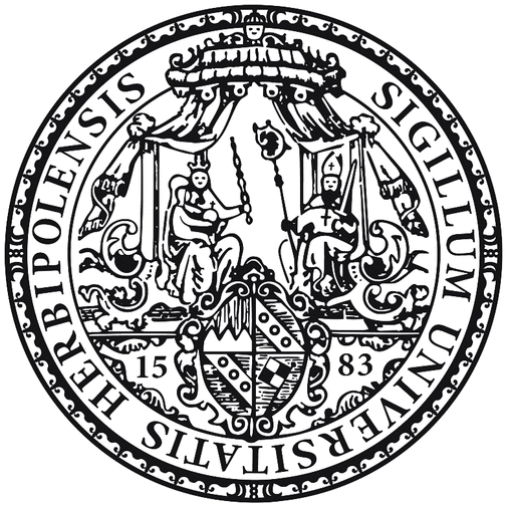

DISSERTATION

zur Erlangung des

naturwissenschaftlichen Doktorgrades

der Julius-Maximilians-Universität Würzburg

vorgelegt von

Regina Messerer

aus Wassertrüdingen

Würzburg 2017

Eingereicht bei der Fakultät für Chemie und Pharmazie am:

……

Gutachter der schriftlichen Arbeit:

1. Gutachter ……..

2. Gutachter ……..

Prüfer des öffentlichen Promotionskolloquiums:

1. Prüfer ……..

2. Prüfer ……..

3. Prüfer ……..

Datum des öffentlichen Promotionskolloquiums:

……..

Doktorurkunde ausgehändigt am:

……..

Die vorliegende Arbeit wurde auf Anregung und unter Anleitung von

Frau Prof. Dr. Ulrike Holzgrabe

am Lehrstuhl für Pharmazeutische Chemie

des Instituts für Pharmazie und Lebensmittelchemie

der Julius-Maximilians-Universität Würzburg angefertigt.

Ihr gilt mein besonderer Dank für die freundliche Aufnahme in den Arbeitskreis, das interessante Themengebiet und für ihre wertvollen Anregungen in allen Phasen der Promotion. Vielen Dank für das stets in mich gesetzte Vertrauen, welches mir die eigenverantwortliche Anfertigung dieser Dissertation ermöglichte.

Weiterhin möchte ich mich bei meinen Kooperationspartnern bedanken:

- **Prof. Dr. Carsten Hoffmann** und **Michael Kauk**, Pharmakologie Würzburg, für die Durchführung der FRET-Messungen sowie für die zahlreichen Auswertungen und Interpretationen. Vielen Dank für die sehr gute Zusammenarbeit!
- **Dr. Andreas Bock**, Pharmakologie Würzburg, für die hilfreichen sowie aufschlussreichen Diskussionen.
- **Prof. Dr. Marco De Amici**, **Dr. Clelia Dallanoce** und **Dr. Carlo Matera**, Scienze Farmaceutiche, Milano, für die gute und stets freundliche Zusammenarbeit. Grazie mille!
- **Prof. Dr. Klaus Mohr**, **PD Dr. Christian Tränkle**, **Anna Krüger**, **Paul Bannenberg, Mechthild Kepe** und **Matthias Irmen**, Pharmakologie und Toxikologie Bonn, für die Durchführung der Radioligandbindungsstudien.
- **Prof. Dr. Christoph Sotriffer**, **Prof. Dr. Michael Decker** und **Dr. Sarah Wehle**, Pharmazie und Lebensmittelchemie Würzburg, für die Durchführung der Dockingstudien an den Cholinesterase-Inhibitoren.
- **Prof. Dr. Elisabetta Barocelli** und **Lisa Flammini** für die Messung der Cholinesterase-Hemmung am Rattenhirn.

Ebenso danke ich **Dr. Eberhardt „Ebi“ Heller** und **Dr. Jens Schmitz**, die bei auftretenden Fragen zur Synthese, Aufarbeitung oder zu Reaktionsmechanismen jederzeit mit Rat und Tat zur Seite standen.

Dir liebe **Liana „Lina“ Pogorelaja** möchte ich für das ein oder andere nachsynthetisierte Iperoxo danken, womit du mir sehr viel Arbeit abgenommen hast. Vielen Dank auch für die netten Gespräche und Lebensweisheiten.

Ganz herzlich bedanke ich mich bei allen (ehemaligen) Laborkollegen und Freunden für die gute Zusammenarbeit, die tolle Arbeitsatmosphäre und natürlich auch für die gemeinsame Zeit die wir außerhalb des Labors hatten: **Alex**, **Andi**, **Anja**, **Anna**, **Antonio**, **Christiane**, **Christine E.**, **Christine H.**, **Daniela**, **David**, **Edgar**, **Flo G.**, **Flo S.**, **Georg**, **Ines**, **Jan**, **Jogi**, **Johannes**, **Katja**, **Klaus**, **Lu**, **Markus**, **Michi**, **Miri**, **Niclas**, **Nils**, **Nina**, **Olli**, **Patrick**, **Paul**, **Raphael** und **Steffi**.

Danke

Meinen Eltern und
Geschwistern

Table of contents

A. Introduction

1. The cholinergic system

The vegetative nervous system is subdivided into the sympathetic and parasympathetic nervous system due to their different morphological and functional properties. Stimuli of both systems are transferred by preganglionic and postganglionic neurons to nerve endings and eventually to effector organs. Stimuli of the sympathetic nervous system are mediated by the neurotransmitter noradrenaline (NA), whereas the parasympathetic nervous system is effected by the neurotransmitter acetylcholine (ACh). Neurons released by acetylcholine are referred to as cholinergic system (Figure 1).[1]

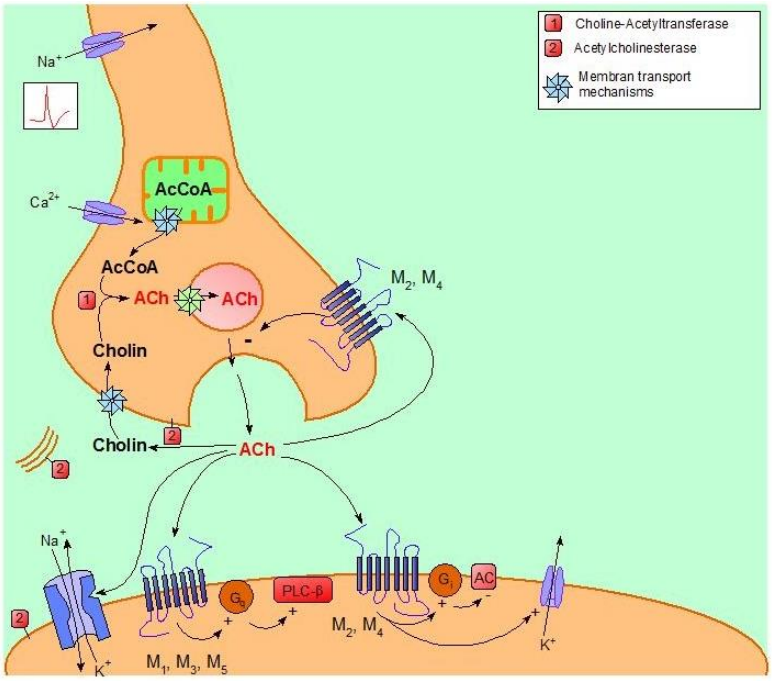

Figure 1: Schematic depiction of general cholinergic nerve junction. Biosynthesis, storage, release, hydrolysis of acetylcholine and location of receptor sites (modified according to Aktories et al.[2]).

Acetylcholine is one of the most important neurotransmitter, regulating basic cell functions such as energy-uptake and -storage, relevant e.g. for the regulation of heart rate and blood pressure. Acetylcholine is biosynthesized by choline and acetyl coenzyme A, catalyzed by the choline acetyltransferase in the presynaptic cell, followed by the storage in vesicles. Opening of the voltage-dependent calcium channels and subsequent influx of Ca^{2+} results in the release of acetylcholine from the storage vesicles into the synaptic cleft. There, acetylcholine can bind to e.g. cholinergic receptors on postsynaptic or presynaptic membranes, mediating cell responses. These receptors are classified either as muscarinic acetylcholinergic receptors (mAChR) or nicotinic acetylcholinergic receptors (nAChR), depending on the naturally occurring bound alkaloids muscarine or nicotine, respectively. mAChR are prototypical members of the G protein-coupled receptors, whereas nAChR

function as ligand-gated ion channels. Free, non-bound acetylcholine is hydrolyzed by acetylcholinesterase (AChE) to choline and acetate in the synaptic cleft.[2]

Chemical compounds are able to influence the regulation of the parasympathetic nervous system. Agonists and antagonists can bind to muscarinic and nicotinic acetylcholine receptors in order to stimulate or inhibit receptor function or ligands can act as inhibitors of AChE.[1]

2. Muscarinic acetylcholine receptors

2.1 Classification

The superfamily of G protein-coupled receptors (GPCRs) comprises the largest family of proteins in mammalian genomes.[3,4] Nowadays, about 50% of all modern drugs are targeting the G protein-coupled receptors, indicating the importance and the enormous potential of drug discovery in this field.[5] GPCRs can be activated by various organic, inorganic and physical stimuli, i.e. amines, odorants, proteins, peptides, lipids, nucleotides and photons to mediate extracellular signals into intracellular responses.[6]

The superfamily of G protein-coupled receptors is subdivided in five main families according to their amino acid sequences: rhodopsin (class A), secretin (class B), glutamate (class C), adhesion and frizzled/taste 2.[7] Among them, rhodopsin represents the largest family including the muscarinic acetylcholine receptors (mAChRs). The first high-resolution crystal structure was solved of bovine rhodopsin (class A) as prototypical template for further structural studies at GPCRs.[8] Since 2007, more crystal structures of class A GPCRs have been determined, including the *ß*-adrenergic receptors,[9-12] the adenosine A_{2A} receptor,[13] the chemokine CXCR4 receptor,[14] the dopamine D_3 receptor[15] and the muscarinic M_1, M_2, M_3, and M_4 receptors.[16-18] Numerous studies confirm the existence of homodimers, heterodimers and oligomers of GPCRs. Nevertheless, it is well known that also monomers effectively mediate signals. Therefore, the structures of the muscarinic acetylcholine receptors are in the following considered as monomeric structures.[19]

2.2 Structure and function

The muscarinic acetylcholine receptor consists of an extracellular N-terminal domain, an intracellular C-terminal domain, and seven transmembrane-spanning (TM) domains (TM1 – TM7) forming a channel-like cavity in the middle of the receptor. The domains are connected

by three extracellular and three intracellular loops. A guanine nucleotide binding protein (G-protein), consisting of an α-, β-, and γ-subunit, is bound to the cytosolic site of the membrane receptor.[20]

Receptor activation is induced by agonist binding to the receptor followed by conformational changes of α-transmembranal helixes. The activated receptor interacts with the heterotrimeric G-protein causing GDP dissociation und subsequent GTP binding and activation. Consequently, the heterotrimeric G-protein dissociates into an α subunit and a βγ dimeric subunit mediating different intracellular signaling responses through effector molecules. GTP is hydrolyzed by regulator proteins resulting in the reassociation of the α, β, and γ trimeric subunit and finally in the self-regulation of the activation cycle (Figure 2).[1,21]

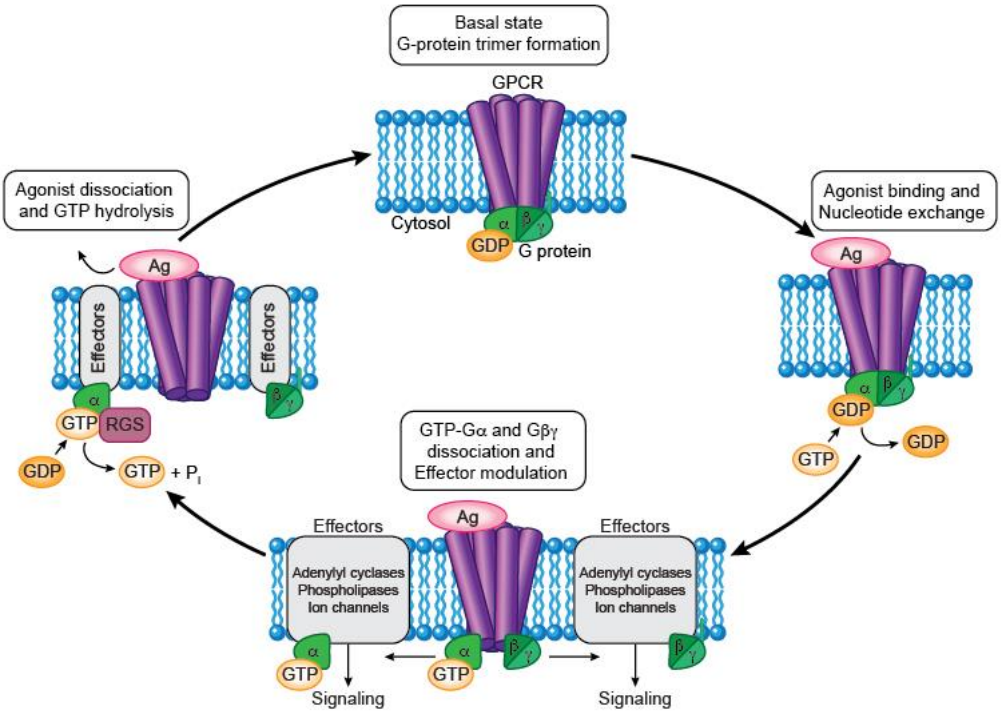

Figure 2: GPCR activation cycle. (Illustration by Peter Jurek. MUTAGENETIX (TM), B. Beutler and colleagues, Center for the Genetics of Host Defense, UT Southwestern, Dallas, TX.)

In 2012 the nobel prize in chemistry was awarded to Robert J. Lefkowitz and Brian K. Kobilka for their structural and signaling studies on G protein-coupled receptors, indicating the importance of this research field.

2.3 Subtpye differentiation

Five subtypes of muscarinic acetylcholine receptors M_1 – M_5 have been determined due to their different appearance and physiological function.[22,23] The M_1 AChRs are predominantly

expressed in the central nervous system especially in the forebrain, including cerebral cortex, striatum, and hippocampus.[24-26] M_2 is located in the central nervous system[24-26] and in the body periphery, above all in the heart and in smooth muscle tissues.[22,27,28] The M_3 mAChR subtype is found in different regions of the brain[29] and mediates smooth muscle contraction.[22,23,27] M_4 is widely expressed in the central nervous system[24-26] and M_5 receptors could be detected in the midbrain and may conduce to cognition-enhancing effects of acetylcholine.[30,31] Muscarinic subtypes expressed in the central nervous system are important targets for the treatment of major diseases of the CNS such as Alzheimer`s and Parkinson`s disease, schizophrenia, epilepsy, and depression.[32-34] The actions mediated by peripheral mAChRs include the regulation of the heart rate, smooth muscle contraction, and stimulation of glandular secretion.[22] The five mAChR subtypes can be divided into two major classes due to their ability to activate different classes of G-proteins. The even-numbered subtypes M_2 and M_4 are preferentially coupled with $G_{i/o}$-proteins. The activation of the $G_{i/o}$-proteins results in the inhibition of adenylate cyclase (AC) followed by a decrease of cyclic AMP (cAMP) and the blockage of voltage-gated calcium channels.[35] The odd-numbered subtypes M_1, M_3, and M_5 show selectivity for the $G_{q/11}$-family.[22,23] Stimulation of $G_{q/11}$ proteins results in phospholipase C (PLC) activation, followed by the mobilization of inositol-1,4,5-triphosphate (IP_3), and subsequent release of Ca^{2+} ions.[35] Nevertheless, the coupling of a muscarinic acetylcholine subtype is not exclusive for a preferred G-protein. For example the M_2 receptor may also couple to G_s and $G_{q/11}$.[36]

2.4 Binding sites of muscarinic receptors

The binding site of the endogenous ligand acetylcholine as well as of agonists and antagonists of muscarinic receptors is defined as “orthosteric site”.[37] This binding site is formed as a hydrophilic cavity within the transmembrane α-helixes in a depth of 15 Å.[38] Binding and point-mutation studies identified the involved amino acids crucial for the binding of acetylcholine within the orthosteric binding site (Figure 3). Herein, the negatively charged aspartate in TM3 plays an important role, forming ionic interactions with the positively charged amine of acetylcholine.[39] Furthermore, hydrogen bond interactions between the ester function of acetylcholine and the amino acids Thr^{231} and Thr^{234} (TM5), Thr^{148} (TM3) and Thr^{506} (TM4) as well as cation π-interactions with the aromatic amino acids phenylalanine, tyrosine, and tryptophan stabilize the ligand in the binding pocket.[40,41]

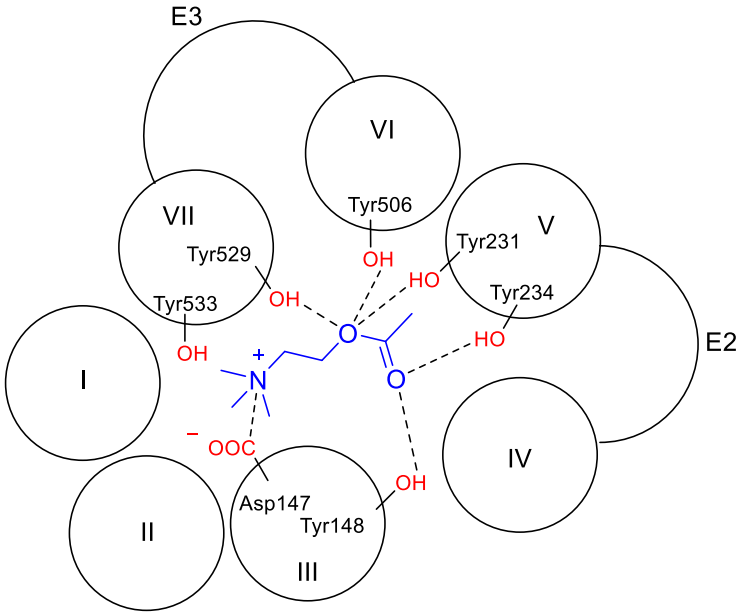

Figure 3: Model of ACh interaction with mAChRs. Circles represent seven transmembrane domains.

The existence of the orthosteric binding site was evidenced by the solved crystal structures of the active and inactive states of the M_2 receptor. Kruse et al. characterized the crystal structure of the M_2 receptor bound to the high-affinity agonist iperoxo, showing that the agonist is completely enclosed by the receptor (Figure 4, B). The closure of the orthosteric binding pocket results in hydrogen bond interactions between Tyr $403^{6.51}$, Tyr $104^{3.33}$, and Tyr $426^{7.39}$, forming a tyrosine lid which might be important for agonist binding and activation of the receptor.[42] Haga et al. reported the structure of the M_2 receptor bound to the antagonist quinuclidinyl benzilate (QNB) (Figure 4, A). The formation of the tyrosine lid hinders the ligand for dissociation of the orthosteric binding pocket.[17]

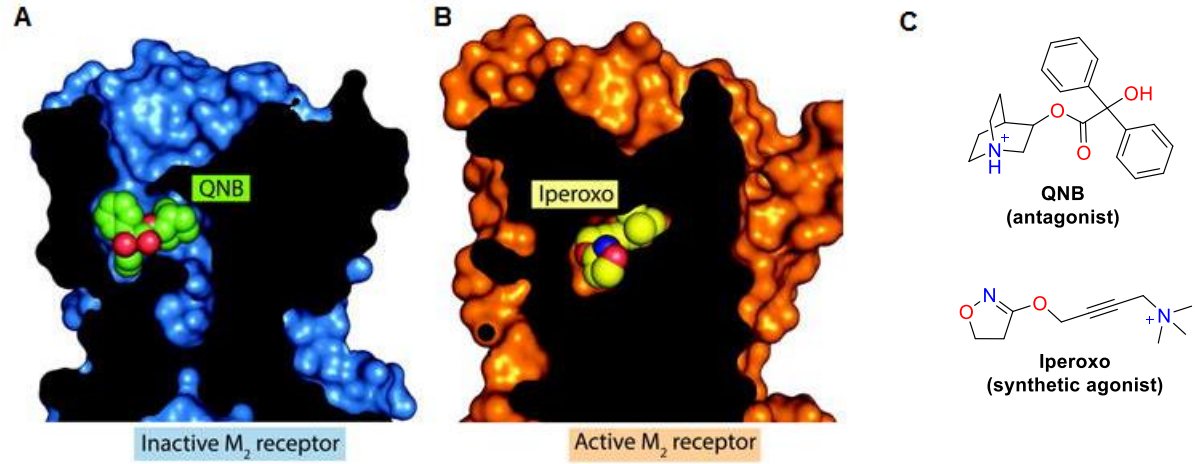

Figure 4: A: Inactive state of the hM_2-receptor bound to the antagonist QNB (green). **B:** Active state of the receptor bound to the agonist iperoxo (yellow). Iperoxo is completely covered within the receptor. **C:** Structures of the orthosteric ligands QNB and iperoxo used for crystallization.[42]

A huge advantage for drugs acting at the orthosteric binding site is the high ligand affinity achieved at this binding pocket. Nevertheless, the amine acid sequences of the orthosteric binding site is highly conserved among the subtypes M_1-M_5.[43-45] Consequently, drugs targeting the orthosteric binding site typically lack of therapeutically relevant subtype selectivity which may lead to unwanted side effects.

Next to the orthosteric binding site, there are one or two topographically distinct allosteric binding sites.[46,47] The allosteric binding site is located between the extracellular loop E2 and E3 in TM7 and is less conserved throughout the muscarinic receptor subtypes.[48,49] This remarkable diversity of the extracellular surface makes the allosteric binding site to a promising target region for the discovery of subtype-selective drugs with limited side effects. The M_2 receptor was crystallized in its active state bound simultaneously to the agonist iperoxo and to the positive allosteric modulator LY2119620 which resulted in conformational changes in the extracellular surface, giving rise to the existence of an allosteric binding site.[42]

2.5 Muscarinic agonists and antagonists

Historically, there are two kind of drugs, namely agonists and antagonists, interacting with GPCRs. Agonists are ligands which bind with high affinity to the active receptor and induce a physiological effect (= efficacy), whereas antagonists bind also to the receptor but do not influence the level of receptor activity. Partial agonists only mediate submaximal activation at a receptor. Inverse agonists bind to the receptor as an agonist, but mediate an opposite physiological effect.[50] Well known muscarinic agonists are listed in Figure 5. Acetylcholine has no therapeutic relevance due to its unselectivity as well as muscarine which only has toxicological significance. Iperoxo is known as superagonist at the M_2 receptor, due to its higher efficacy for receptor activation than mediated by the endogenous ligand acetylcholine.[51] Carbachol is a known drug for the treatment of glaucoma and bethanechol is therapeutically used against bladder atonia.

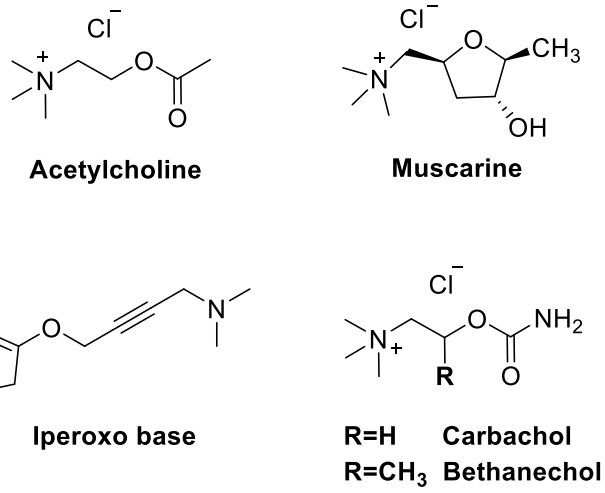

Figure 5: Structures of muscarinic agonists.

Therapeutic relevant antagonists are the alkaloids atropine and scopolamine (Figure 6) being applicable in the field of ophthalmology and as antiemetic, respectively. Positively charged antagonists mediate their effect only in the periphery because they are not able to pass the blood-brain barrier which prevents central nervous side effects. These include tiotropium bromide, a drug which is used in chronic obstructive pulmonary disease (COPD) and *N*-butylscopolamine bromide, used as spasmolytic drug (Figure 6).[1]

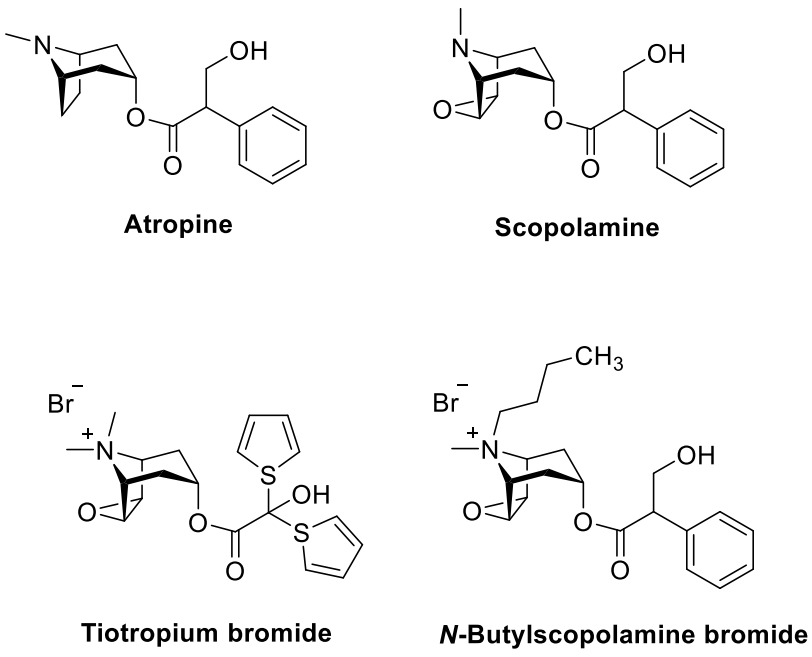

Figure 6: Structures of muscarinic antagonists.

2.6 Allosteric modulation of muscarinic receptors

Ligands bound to the allosteric binding site induces conformational changes to the receptor and can either directly activate the receptor, acting as allosteric agonists,[52] or can have influences on the ligand bound to the classical, orthosteric site. Ehlert established the ternary complex model (TCM), describing how two distinct ligands, orthosteric and allosteric, may influence the binding and function of each other (Figure 7).[53] In this model, an orthosteric ligand (A) and an allosteric ligand (B) can bind independently to the free receptor, forming the binary complexes AR and BR (Figure 7, II and III), respectively. Orthoster A binds to the orthosteric site with an affinity of K_a, whereas alloster B binds to the allosteric site with an affinity of K_b. When both ligands are simultaneously bound to the receptor, a ternary complex ARB is formed (Figure 7, IV). The magnitude by which the affinity of one ligand is influenced by the other ligand is described by the cooperativity factor α. It can result in a positive, neutral or negative outcome concerning the efficacy. Positive allosteric modulators (PAMs) induce positive cooperativity (α < 1) by enhancing the binding or the maximum effect of an orthosteric ligand.[54] Allosteric ligands which reduce the binding or the maximum effect of an orthosteric ligand (α > 1) are named negative allosteric modulators (NAMs).[55] Neutral (or silent) allosteric ligands (NALs) have neutral cooperativity (α = 1) by mediating no effect on the binding or maximum effect of an orthosteric ligand.[56] Consequently, the use of allosteric modulators makes it possible to control and fine-tune cellular signaling processes.

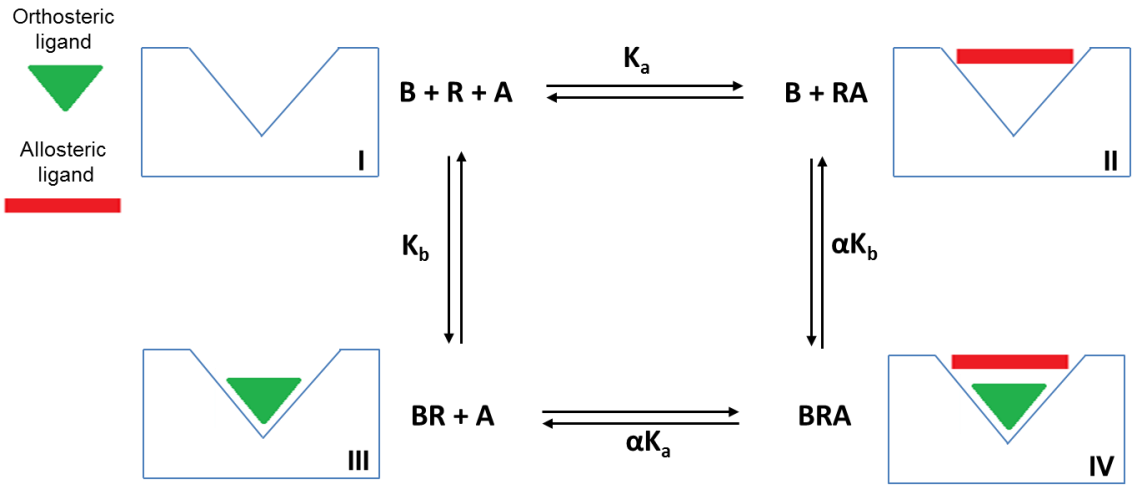

Figure 7: Ternary complex model (TCM) for the description of allosteric interactions (modified according to Ehlert[53]).

The first allosteric interaction at the muscarinic acetylcholine receptor was reported by Lüllmann and coworkers in 1968.[57] The mAChR antagonist atropine was used as an antidote for acetylcholinesterase intoxication with diisopropyl fluorophosphate in mice experiments. After the addition of the ganglion blocking alkane bis-ammonium compound W84 (Figure 8)

an over-additive antidote effect was observable, indicating an allosteric receptor interaction.[58] These findings were later evidenced by radioligand-binding studies using [^{3}H]-*N*-methylscopolamine ([^{3}H]NMS) for dissociation experiments.[59] Nowadays, a range of allosteric modulators exists, which differ in their subtype-selectivity and signaling outcome (Figure 8). The benzyl quinolone carboxylic acid BQCA was found to be an allosteric potentiator highly selective for M_1[60] and tacrine is known for its blockage of M_1 muscarinic receptors.[61] Therefore, these compounds are useful for the treatment of schizophrenia and Alzheimer`s disease. Furthermore, tacrine acts as antagonist at the M_2 receptor subtype.[61] The bis-phthalimidyl-substituted bis-ammoniumalkyl derivative W84 is a M_2 relatively selective allosteric ligand, acting as negative allosteric modulator (NAM) with respect to [^{3}H]NMS equilibrium binding at mAChRs. Other bis-ammonium derivatives, such as alcuronium and gallamine are antagonists at the nicotinic AChR. Alcuronium was found to be a positive allosteric modulator (PAM), whereas gallamine acts as negative allosteric modulator (NAM) with respect to [^{3}H]NMS equilibrium binding at the M_2 AChR.[62] The use of allosteric modulators for GPCR signaling has several advantages in comparison to standard orthosteric drugs. Firstly, if the allosteric site is completely occupied by allosteric modulators a saturation effect occurs. Therefore, allosteric modulators can be given in high concentrations to the receptor without fearing an overstimulation or overinhibition of the system. Another advantage is that allosteric modulators, especially PAMs are only able to mediate responses in the presence of the endogenous ligand. In contrast, orthosteric agonists are able to mediate their effect as long as they are available. Therefore, allosteric modulators are able to process temporal and special information in order to obtain an optimum effect. An important benefit is that allosteric modulators binding to the allosteric site of the receptor achieve subtype-selectivity due to the less conserved allosteric sites among the five muscarinic receptors in contrast to the very conserved orthosteric site. These properties make allosteric modulators to attractive tools for novel therapeutics, e.g. for cognitive dysfunction, schizophrenia, pain or organophosphorus poisoning.[63]

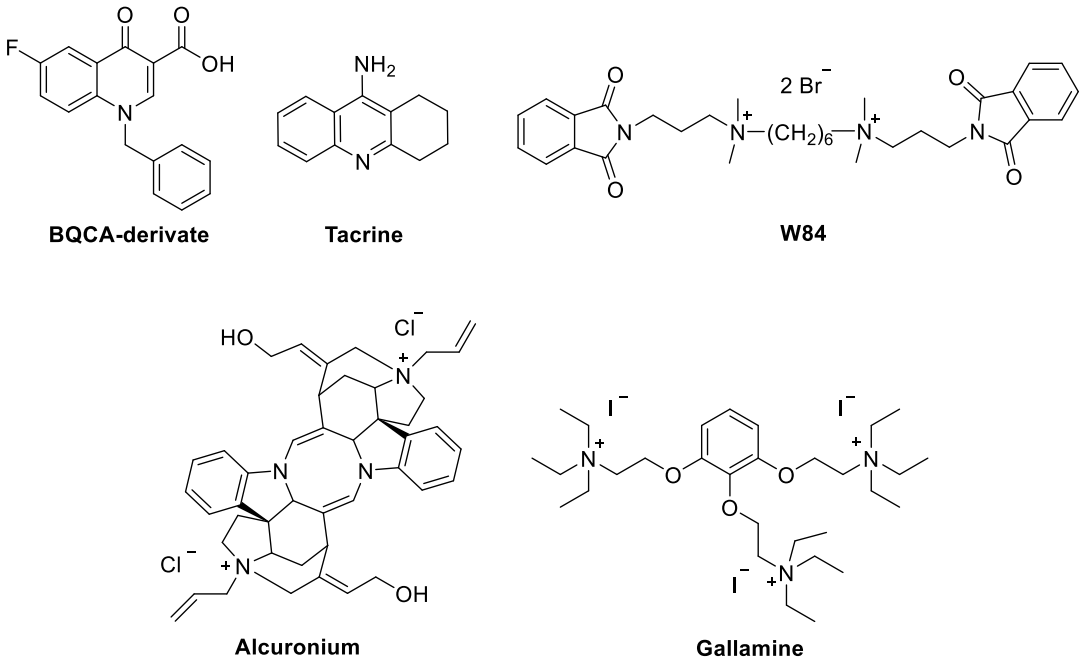

Figure 8: Structures of allosteric modulators.

2.7 Development of dualsteric/bitopic ligands for muscarinergic receptors

The use of allosteric modulators as therapeutic agents is controversial due to the lack of high-affinity to the receptor leading to side effects. Thus, no high-affinity allosteric modulators have been reported to date. Therefore, the concept of dualsteric ligands was developed which combines the advantages of high-affinity (orthosteric site) and subtype-selectivity (allosteric site) within one molecule.[64-67] Here, an orthosteric and an allosteric ligand are connected through an appropriate linker resulting in pharmacological interesting compounds. This approach was first described by Schwyzer in the late 1970s as "message-address concept" (Figure 9).[68] The orthosteric moiety of the dualsteric ligand may serve as message and transduces the signal from the receptor to the effector whereas the allosteric moiety acts as address and provides additional ligand receptor interactions in the less conserved allosteric binding site thus providing subtype-selectivity.

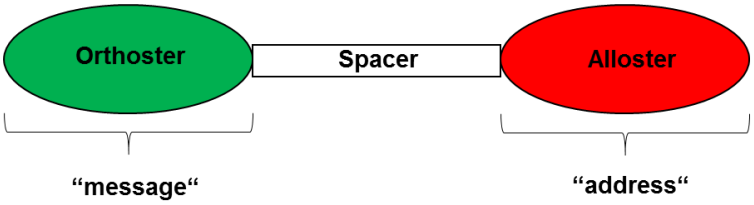

Figure 9: "Message-address concept" by Schwyzer.

Dualsteric ligands can in principal bind to the receptor in two different orientations (Figure 10, left).[69] Either they bind purely allosteric in the presence (Figure 10, pose 3) or absence (Figure 10, pose 2) of an orthosteric ligand or in a dualsteric binding mode (Figure 10, pose 1). Here, the orthosteric and allosteric binding site is simultaneously occupied within one receptor. Only this bitopic binding mode can activate the receptor and mediates different signaling pathways like G_s- or G_i-signaling in the case of M_2 receptor activation. The binding of the orthosteric agonist iperoxo induces $G_{i/o}$, G_s, and also ß-arrestin recruitment. By contrast, binding of an dualsteric ligand results exclusively in the activation of one preferred pathway (Figure 10, right).[70] This concept is termed bias signaling. Here, therapeutically significant pathways can be selectively activated while signaling pathways mediating undesirable side effects are almost excluded.[71] Thus, the rational design of biased bitopic ligands is desirable.

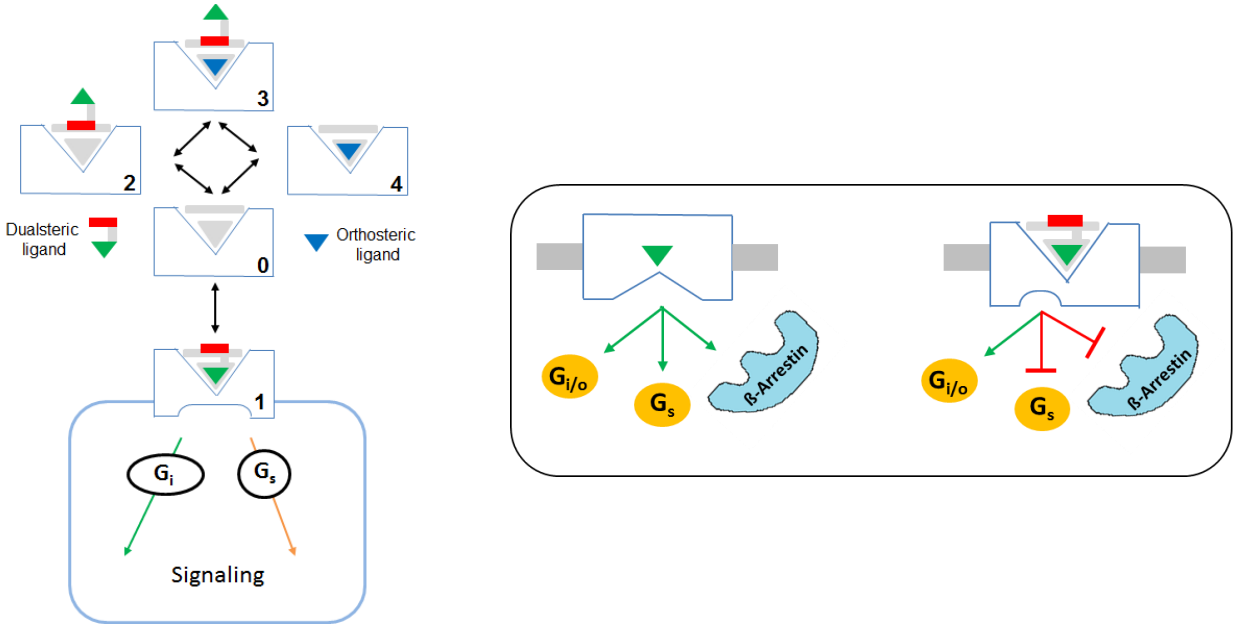

Figure 10: Receptor binding poses of dualsteric probes (left) (modified according to Bock et al.[69]). Concept of bias signaling (right) (modified according to Bock et al.[70]).

The first bitopic ligand was designed by Disingrini et al. through the connection of the high-affinity orthosteric agonist iperoxo with a M_2 receptor-selective allosteric ligand, containing either a W84 or a naphmethonium fragment, generating a M_2 receptor-selective agonist (Figure 11).[72] Simultaneous allosteric/orthosteric binding was evidenced by binding and functional assays and showed a preferred G_i signaling pathway activation.[73] Further hybrid molecules consisting of a benzyl quinolone carboxylic acid moiety (BQCA) and of the superagonist iperoxo were designed, and found to act as partial hM_1 agonists (Figure 11).[74] Schmitz et al. reported the concept of bivalent antagonism by the connection of an allosteric antagonist (phthal- or naphthalimide moiety) with an orthosteric antagonist (atropine or

scopolamine) resulting in hybrids with bitopic binding modes and pathway-specific signaling (Figure 11).[75] Besides heterobivalent molecules, also homobivalent ligands were designed by the linkage of two identical pharmacophores. Carbachol homodimers linked through a methylene chain of variable length (Figure 11) showed antagonistic properties on hM_1, hM_2, and hM_3 receptors. Docking simulations suggest a bitopic behavior of these homodimers as investigated on hM_1 and hM_2 receptors.[76]

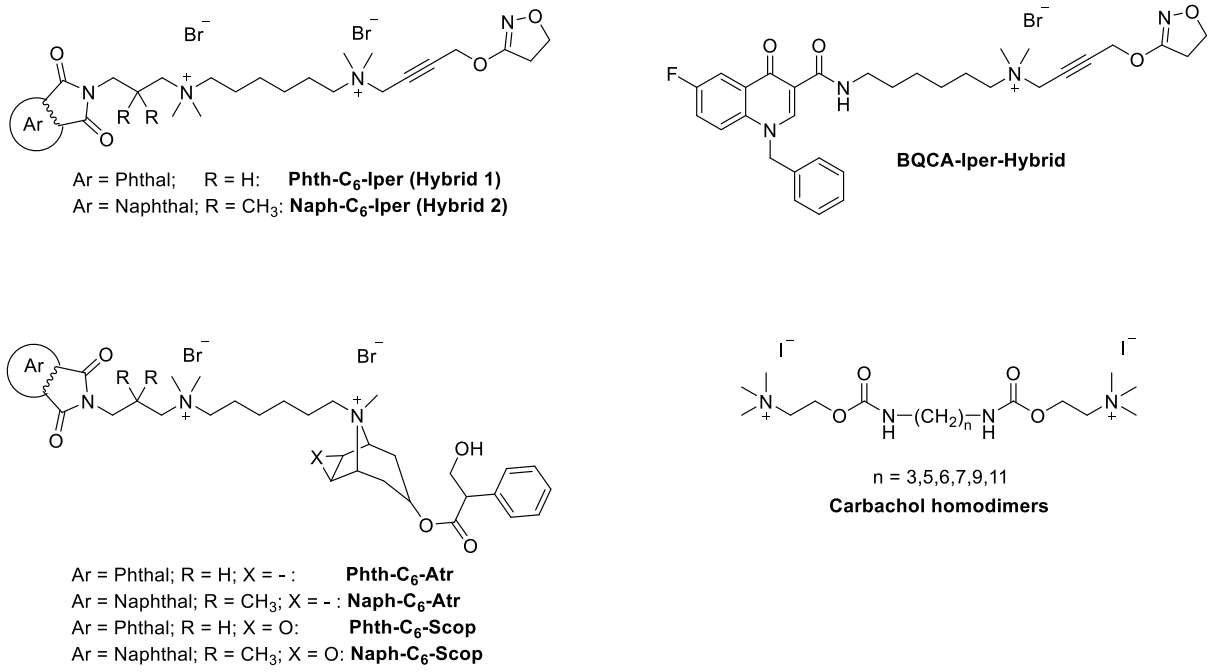

Figure 11: Structures of dualsteric compounds.

The development of bitopic ligands represents a new route towards the design of subtype-selective and high-affinity GPCR-targeting ligands as well as pathway-biased signaling, beside the tuning of the agonism.

3. The cholinesterases – AChE and BChE

3.1 Alzheimer`s disease

Alzheimer`s disease is a multifactorial, neurodegenerative disease which leads to the loss of cognitive function. In the course of the disease short-term memory and progressive memory impairments occur followed by mood changes, depression and the loss of reasoning ability. About one hundred years ago, Alois Alzheimer has already reported on this disease.[77] However, up to date there are still no effective drugs on the market or many of them are only able to retard the progression of the disease rather than curing the disease.[78] Worldwide

about 9% of the population aged over 65 are affected and most of the patients are older than 85.[79] Due to a democratic change of the society, the number of AD patients will increase continuously, from 24.3 million in 2011 to 81.1 million by 2040.[80] The rising number of patients clarifies the urgent need of highly effective drugs against AD.

So far, several hypotheses for the pathogenesis of AD exists:

(1) Reactive oxygen species (ROS), generated by dysfunctional mitochondria, are involved in the development of AD. A therapeutic approach is to improve mitochondrial function as well as to protect the brain from oxidative stress.[81,82]

(2) The τ-protein hyperphosphorylation: the τ-protein, mainly located in the neurofibrillary tangles, is responsible for the stability of microtubules in healthy people. However, in AD patients the τ-protein is hyperphosphorylated resulting in destroyed microtubules and impaired mitochondrial function.[83] Therefore, the hyperphosphorylation has to be reduced, for example by inhibition of GSK-3ß, a kinase mainly responsible for the phosphorylation of τ-protein.[84]

(3) Non-soluble amyloid plaques also contribute to the development of AD. Amyloid plaques are built out of amyloid ß, which is generated in the pathogenic way starting off with the amyloid precursor protein (APP). One therapeutic approach is to inhibit the amyloid ß assembly.[85]

(4) Today`s medication is above all based on the cholinergic hypothesis, describing that AD goes along with a decreased concentration of ACh in the brain. Responsible for the decomposition of ACh in the synaptic cleft are two cholinesterases, i.e. the acetylcholinesterase (AChE) and the butyrylcholinesterase (BChE). In the course of the disease the concentration of AChE decreases to 15%, whereas the concentration of BChE increases.[86] Therefore, BChE is also an important target in the treatment of AD.[87,88] Due to the structural similarities of BChE and AChE,[89] the structure and function of AChE is exemplarily described in the following.

3.2 Acetylcholinesterase – structure and function

Sussman et al. described a deep, narrow gorge (depth of 20 Å) in the AChE of *torpedo californica* composed of aromatic amino acids which guide the substrate from the peripheral anionic site (PAS), located at the entrance of the binding pocket, to the catalytic active site

(CAS), located at the bottom of the gorge.[90] The catalytic active site of AChE consists of an "anionic-binding site" where the cationic nitrogen of ACh is bound and fixed through cation-π interactions with tryptophan as well as of a catalytic triade (esteratic site), at which the hydrolysis of the ester takes place (Figure 12). The catalytic triade consists of the three amino acids glutamate, histidine, and serine, whereas the serine hydroxyl group acts as nucleophile, histidine serves as acid-base catalyst, and glutamate stabilizes the transition state. Furthermore, the hydrogen bond interactions between the two glycine residues, located next to the esteratic site, and the carbonyl oxygen contribute to the stabilization of the transition state. The hydrolysis of ACh starts with the interaction of the serine oxygen with the carbonyl group of ACh, resulting in an unstable state which collapses to choline and acetylated AChE. Hydrolysis of the acetylated AChE releases one molecule of acetic acid and regenerates the active form of AChE (Figure 12). However, if the enzyme is acetylated e.g. by a carbamyl or phosphate group instead of a carboxylate ester, the intermediate state is more stable and remains longer in the inactive state. This slow rate hydrolysis led to the discovery and design of inhibitors of cholinesterases as therapeutic approach in the treatment of AD.[1]

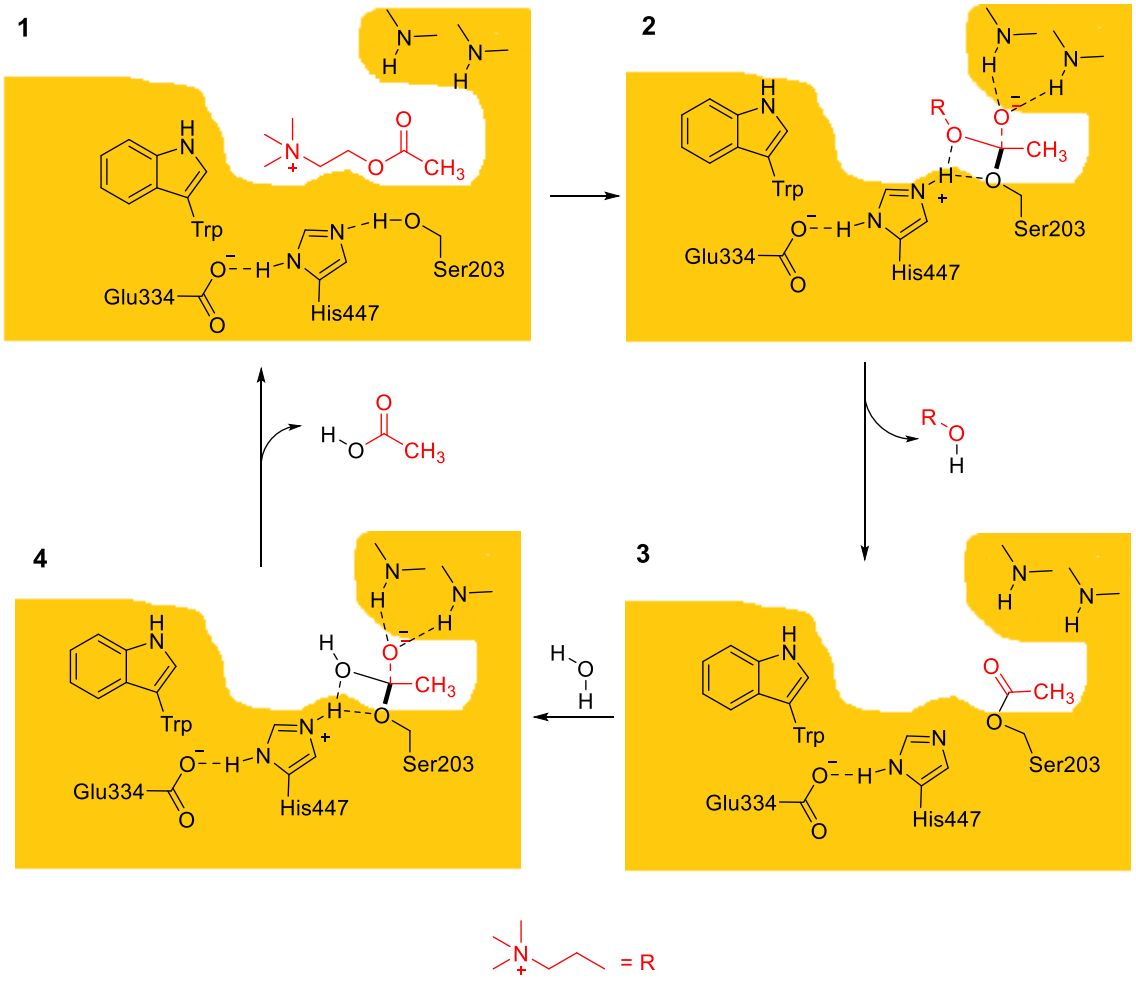

Figure 12: Mechanism of ACh-hydrolysis.

3.3 Acetylcholinesterase inhibitors

Acetylcholinesterase inhibitors can be subdivided into reversible (e.g. carbamate-derived) or irreversible (e.g. phosphoester-derived) inhibitors. Reversible AChEIs can either bind to the enzyme with a greater affinity than the endogenous ligand ACh but do not react with the enzyme or are able to react with the enzyme, forming an acylated enzyme which is more stable against hydrolysis and thus remains longer in the inactive state. Several reversible inhibitors were found so far and were applied for clinical use (Figure 13):

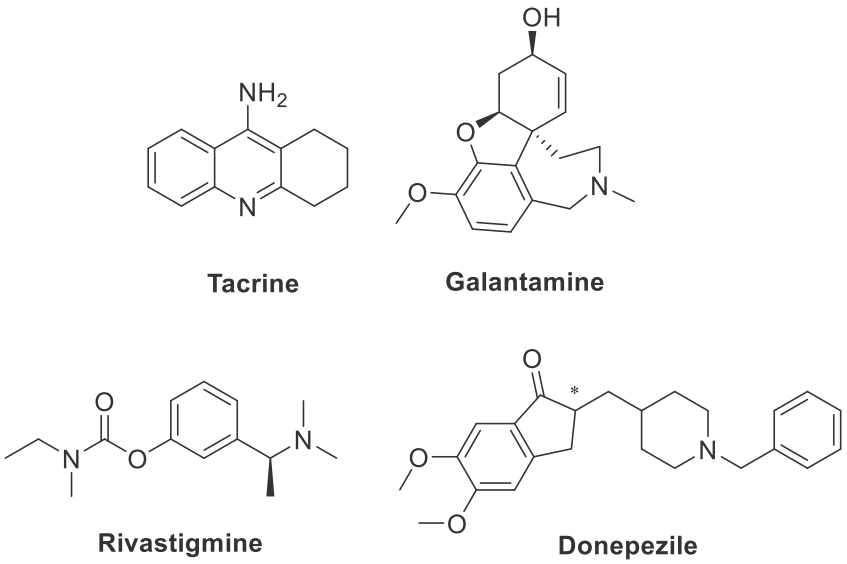

Figure 13: Structures of AChE-inhibitors.

Tacrine was the first drug approved for AD in 1993. This inhibitor binds to both cholinesterases, AChE and BChE, respectively. Nevertheless, the use of tacrine is currently limited due to its hepatotoxicity.[91] **Donepezil**, a AChEI, is used in the therapy of mild-to-moderate AD and dementia. It shows selectivity towards AChE and interacts with the catalytic active site, the peripheral anionic site as well as the choline-binding anionic site.[92] **Rivastigmine** is a slowly reversible arylcarbamate inhibitor of AChE and BChE. In 2000, Rivastigmine was approved as oral drug in the treatment of AD.[93] Another AChE-selective inhibitor is the plant alkaloid **galantamine**. Due to its tertiary structure, galantamine is able to pass the blood-brain barrier and is therefore an interesting inhibitor for the treatment of mild-to-moderate AD and dementia. Furthermore, galantamine is able to bind allosterically to nAChRs but its clinical application still remains unclear.[94] Nevertheless, the clinical application of these drugs in the treatment of AD is still under debate,[95] above all the use of tacrine, which shows serious hepatotoxicity.[91] Therefore, structural variations of tacrine were applied in order to improve its potency and selectivity in combination with reduced side effects. Thus, tacrine dimers (Figure 14) showed improved potency- and selectivity values

towards AChE (up to 3000-fold) in comparison to the monomer. These dimers were proved to bind simultaneously to the catalytic and peripheral site of the enzyme AChE.[96] Furthermore, tacrine has been used for the design and development of hybrid molecules. Fang et al. synthesized hybrids consisting of the cholinesterase inhibitor tacrine and of the orthosteric M_1 muscarinic receptor agonist xanomeline (Figure 14). These hybrids showed similar or higher acetylcholinesterase inhibition values than tacrine alone as well as enhanced M_1 allosteric affinity.[97] Elsinghorst et al. designed gallamine-tacrine hybrids (Figure 14) which show cholinesterase inhibition values in the nanomolar range and their allosteric potency at the M_2 receptor is increased in comparison to the monomers, gallamine and tacrine.[98]

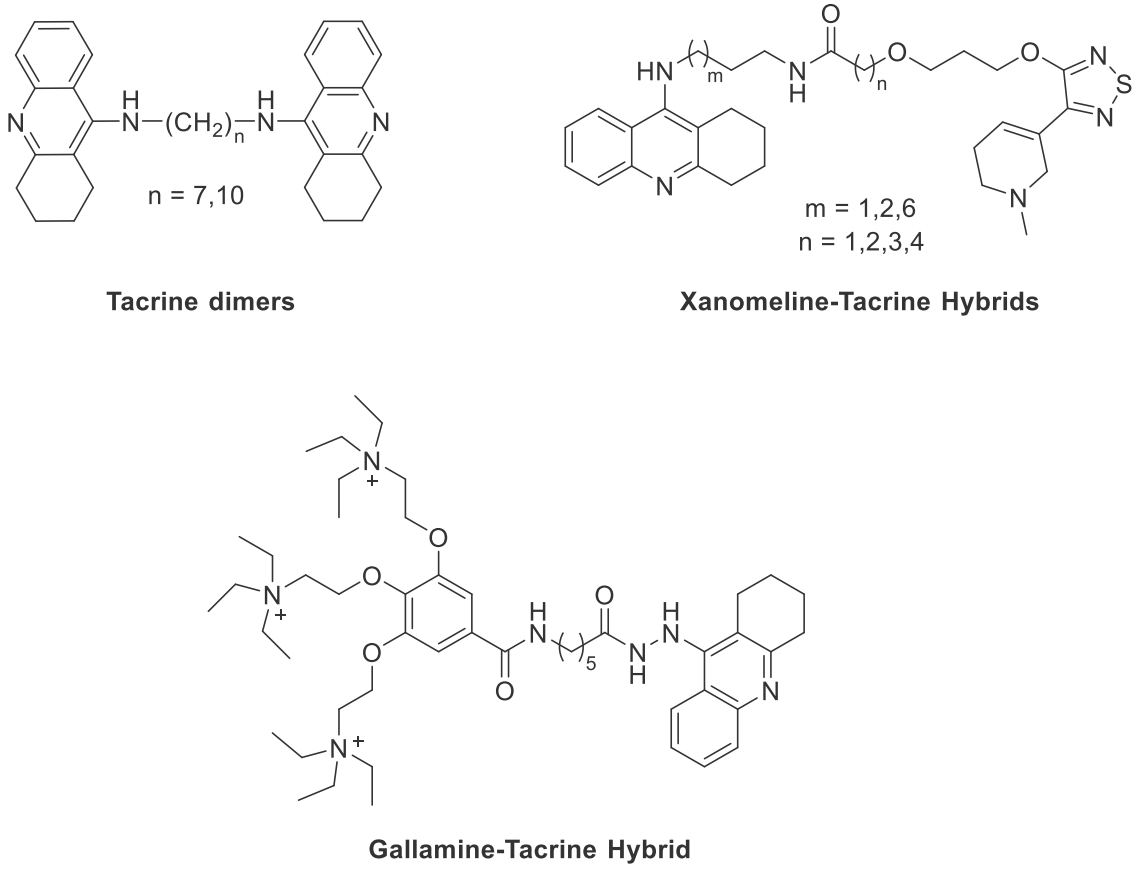

Figure 14: Structures of tacrine dimers and tacrine-related hybrids.

4. References

[1] Lemke, T. L., Williams, D. A., Roche, V. F., and Zito, S. W. (2013) *Foye`s Principles of Medicinal Chemistry*, Vol. 7th edition, Lippincott Williams & Wilkins, Two Commerce Square, 2001 Market Street, Philadelphia, PA 19103.

[2] Aktories, K., Förstermann, U., Hofmann, F. B., and Starke, K. (2009) *Allgemeine und spezielle Pharmakologie und Toxikologie*, Vol. 10. Auflage, Elsevier GmbH, München.

[3] Lander, E. S., and Linton, L. M. et al. (2001) Initial sequencing and analysis of the human genome, *Nature 409*, 860-921.

[4] Venter, J. C., and Adams, M. D. et al. (2001) The sequence of the human genome, *Science 291*, 1304-1351.

[5] Flower, D. R. (1999) Modelling G-protein-coupled receptors for drug design, *Biochimica et Biophysica Acta (BBA) - Reviews on Biomembranes 1422*, 207-234.

[6] Lagerström, M. C., and Schiöth, H. B. (2008) Structural diversity of G protein-coupled receptors and significance for drug discovery, *Nat. Rev. Drug. Discov. 7*, 339-357.

[7] Fredriksson, R., Lagerstrom, M. C., Lundin, L. G., and Schioth, H. B. (2003) The G-protein-coupled receptors in the human genome form five main families. Phylogenetic analysis, paralogon groups, and fingerprints, *Mol. Pharmacol. 63*, 1256-1272.

[8] Palczewski, K., Kumasaka, T., Hori, T., Behnke, C. A., Motoshima, H., Fox, B. A., Le Trong, I., Teller, D. C., Okada, T., Stenkamp, R. E., Yamamoto, M., and Miyano, M. (2000) Crystal structure of rhodopsin: A G protein-coupled receptor, *Science 289*, 739-745.

[9] Warne, T., Serrano-Vega, M. J., Baker, J. G., Moukhametzianov, R., Edwards, P. C., Henderson, R., Leslie, A. G., Tate, C. G., and Schertler, G. F. (2008) Structure of a beta1-adrenergic G-protein-coupled receptor, *Nature 454*, 486-491.

[10] Rosenbaum, D. M., Cherezov, V., Hanson, M. A., Rasmussen, S. G., Thian, F. S., Kobilka, T. S., Choi, H. J., Yao, X. J., Weis, W. I., Stevens, R. C., and Kobilka, B. K. (2007) GPCR engineering yields high-resolution structural insights into beta2-adrenergic receptor function, *Science 318*, 1266-1273.

[11] Rasmussen, S. G., Choi, H. J., Rosenbaum, D. M., Kobilka, T. S., Thian, F. S., Edwards, P. C., Burghammer, M., Ratnala, V. R., Sanishvili, R., Fischetti, R. F., Schertler, G. F., Weis, W. I., and Kobilka, B. K. (2007) Crystal structure of the human beta2 adrenergic G-protein-coupled receptor, *Nature 450*, 383-387.

[12] Cherezov, V., Rosenbaum, D. M., Hanson, M. A., Rasmussen, S. G., Thian, F. S., Kobilka, T. S., Choi, H. J., Kuhn, P., Weis, W. I., Kobilka, B. K., and Stevens, R. C. (2007) High-resolution crystal structure of an engineered human beta2-adrenergic G protein-coupled receptor, *Science 318*, 1258-1265.

[13] Jaakola, V. P., Griffith, M. T., Hanson, M. A., Cherezov, V., Chien, E. Y., Lane, J. R., Ijzerman, A. P., and Stevens, R. C. (2008) The 2.6 angstrom crystal structure of a human A2A adenosine receptor bound to an antagonist, *Science 322*, 1211-1217.

[14] Wu, B., Chien, E. Y., Mol, C. D., Fenalti, G., Liu, W., Katritch, V., Abagyan, R., Brooun, A., Wells, P., Bi, F. C., Hamel, D. J., Kuhn, P., Handel, T. M., Cherezov, V., and Stevens, R. C. (2010) Structures of the CXCR4 chemokine GPCR with small-molecule and cyclic peptide antagonists, *Science 330*, 1066-1071.

[15] Chien, E. Y., Liu, W., Zhao, Q., Katritch, V., Han, G. W., Hanson, M. A., Shi, L., Newman, A. H., Javitch, J. A., Cherezov, V., and Stevens, R. C. (2010) Structure of the human dopamine D3 receptor in complex with a D2/D3 selective antagonist, *Science 330*, 1091-1095.

[16] Thal, D. M., Sun, B., Feng, D., Nawaratne, V., Leach, K., Felder, C. C., Bures, M. G., Evans, D. A., Weis, W. I., Bachhawat, P., Kobilka, T. S., Sexton, P. M., Kobilka, B. K., and Christopoulos, A. (2016) Crystal structures of the M1 and M4 muscarinic acetylcholine receptors, *Nature 531*, 335-340.

[17] Haga, K., Kruse, A. C., Asada, H., Yurugi-Kobayashi, T., Shiroishi, M., Zhang, C., Weis, W. I., Okada, T., Kobilka, B. K., Haga, T., and Kobayashi, T. (2012) Structure of the human M2 muscarinic acetylcholine receptor bound to an antagonist, *Nature 482*, 547-551.

[18] Kruse, A. C., Hu, J., Pan, A. C., Arlow, D. H., Rosenbaum, D. M., Rosemond, E., Green, H. F., Liu, T., Chae, P. S., Dror, R. O., Shaw, D. E., Weis, W. I., Wess, J., and Kobilka, B. K. (2012) Structure and dynamics of the M3 muscarinic acetylcholine receptor, *Nature 482*, 552-556.

[19] Devi, L. A. (2001) Heterodimerization of G-protein-coupled receptors: pharmacology, signaling and trafficking, *Trends Pharmacol. Sci. 22*, 532-537.

[20] Wess, J. (1993) Molecular basis of muscarinic receptor function, *Trends Pharmacol. Sci. 14*, 308-313.

[21] Milligan, G., and Kostenis, E. (2006) Heterotrimeric G-proteins: a short history, *Br. J. Pharmacol. 147 Suppl 1*, S46-55.

[22] Caulfield, M. P. (1993) Muscarinic receptors--characterization, coupling and function, *Pharmacol. Ther. 58*, 319-379.

[23] Caulfield, M. P., and Birdsall, N. J. (1998) International Union of Pharmacology. XVII. Classification of muscarinic acetylcholine receptors, *Pharmacol. Rev. 50*, 279-290.

[24] Levey, A. I. (1993) Immunological localization of m1-m5 muscarinic acetylcholine receptors in peripheral tissues and brain, *Life Sci 52*, 441-448.

[25] Vilaró, M. T., Mengod, G., and Palacios, J. M. (1993) Chapter 9: Advances and limitations of the molecular neuroanatomy of cholinergic receptors: the example of multiple muscarinic receptors, *98*, 95-101.

[26] Wolfe, B. B., and Yasuda, R. P. (1995) Development of selective antisera for muscarinic cholinergic receptor subtypes, *Ann. N. Y. Acad. Sci. 757*, 186-193.

[27] Eglen, R. M., Hegde, S. S., and Watson, N. (1996) Muscarinic receptor subtypes and smooth muscle function, *Pharmacol. Rev. 48*, 531-565.

[28] Brodde, O. E., and Michel, M. C. (1999) Adrenergic and muscarinic receptors in the human heart, *Pharmacol. Rev. 51*, 651-690.

[29] Levey, A. I., Edmunds, S. M., Heilman, C. J., Desmond, T. J., and Frey, K. A. (1994) Localization of muscarinic M3 receptor protein and M3 receptor binding in rat brain, *Neuroscience 63*, 207-221.

[30] Vilaro, M. T., Palacios, J. M., and Mengod, G. (1990) Localization of m5 muscarinic receptor mRNA in rat brain examined by in situ hybridization histochemistry, *Neurosci. Lett. 114*, 154-159.

[31] Weiner, D. M., Levey, A. I., and Brann, M. R. (1990) Expression of muscarinic acetylcholine and dopamine receptor mRNAs in rat basal ganglia, *Proc. Natl. Acad. Sci. U. S. A. 87*, 7050-7054.

[32] Levine, R. R., Birdsall, N. J. M., and Nathanson, N. M. (2001) Proceedings of the 9th International Symposium on Subtypes of Muscarinic Receptors. October 31-November 4, 2000. Houston, Texas, USA, *Life Sci 68*, 2449-2644.

[33] Eglen, R. M., Choppin, A., Dillon, M. P., and Hegde, S. (1999) Muscarinic receptor ligands and their therapeutic potential, *Curr. Opin. Chem. Biol. 3*, 426-432.

[34] Felder, C. C., Bymaster, F. P., Ward, J., and DeLapp, N. (2000) Therapeutic opportunities for muscarinic receptors in the central nervous system, *J. Med. Chem. 43*, 4333-4353.

[35] Davie, B. J., Christopoulos, A., and Scammells, P. J. (2013) Development of M1 mAChR allosteric and bitopic ligands: prospective therapeutics for the treatment of cognitive deficits, *ACS Chem. Neurosci. 4*, 1026-1048.

[36] Michal, P., El-Fakahany, E. E., and Dolezal, V. (2007) Muscarinic M2 receptors directly activate Gq/11 and Gs G-proteins, *J. Pharmacol. Exp. Ther. 320*, 607-614.

[37] Proška, J., and Tuček, S. (1994) Mechanisms of steric and cooperative actions of alcuronium on cardiac muscarinic acetylcholine receptors, *Mol. Pharmacol. 45*, 709-717.

[38] Hibert, M. F., Trumpp-Kallmeyer, S., Hoflack, J., and Bruinvels, A. (1993) This is not a G protein-coupled receptor, *Trends Pharmacol. Sci. 14*, 7-12.

[39] Spalding, T. A., Birdsall, N. J., Curtis, C. A., and Hulme, E. C. (1994) Acetylcholine mustard labels the binding site aspartate in muscarinic acetylcholine receptors, *J. Biol. Chem. 269*, 4092-4097.

[40] Wess, J., Maggio, R., Palmer, J. R., and Vogel, Z. (1992) Role of conserved threonine and tyrosine residues in acetylcholine binding and muscarinic receptor activation. A study with m3 muscarinic receptor point mutants, *J. Biol. Chem. 267*, 19313-19319.

[41] Lu, Z.-L., Saldanha, J. W., and Hulme, E. C. (2002) Seven-transmembrane receptors: crystals clarify, *Trends Pharmacol. Sci. 23*, 140-146.

[42] Kruse, A. C., Ring, A. M., Manglik, A., Hu, J. X., Hu, K., Eitel, K., Hübner, H., Pardon, E., Valant, C., Sexton, P. M., Christopoulos, A., Felder, C. C., Gmeiner, P., Steyaert, J., Weis, W. I., Garcia, K. C., Wess, J., and Kobilka, B. K. (2013) Activation and allosteric modulation of a muscarinic acetylcholine receptor, *Nature 504*, 101-106.

[43] Wess, J. (1996) Molecular biology of muscarinic acetylcholine receptors, *Crit. Rev. Neurobiol. 10*, 69-99.

[44] Wess, J., Eglen, R. M., and Gautam, D. (2007) Muscarinic acetylcholine receptors: mutant mice provide new insights for drug development, *Nat. Rev. Drug. Discov. 6*, 721-733.

[45] Hulme, E. C., Lu, Z. L., and Bee, M. S. (2011) Scanning Mutagenesis Studies of the M 1 Muscarinic Acetylcholine Receptor, *Receptors Channels 9*, 215-228.

[46] Tuček, S., and Proška, J. (1995) Allosteric Modulation of Muscarinic Acetylcholine-Receptors, *Trends Pharmacol. Sci. 16*, 205-212.

[47] Christopoulos, A., and Kenakin, T. (2002) G protein-coupled receptor allosterism and complexing, *Pharmacol. Rev. 54*, 323-374.

[48] Buller, S., Zlotos, D. P., Mohr, K., and Ellis, J. (2002) Allosteric site on muscarinic acetylcholine receptors: A single amino acid in transmembrane region 7 is critical to the subtype selectivities of caracurine V derivatives and alkane-bisammonium ligands, *Mol. Pharmacol. 61*, 160-168.

[49] Conn, P. J., Jones, C. K., and Lindsley, C. W. (2009) Subtype-selective allosteric modulators of muscarinic receptors for the treatment of CNS disorders, *Trends Pharmacol. Sci. 30*, 148-155.

[50] De Amici, M., Dallanoce, C., Holzgrabe, U., Tränkle, C., and Mohr, K. (2010) Allosteric ligands for G protein-coupled receptors: a novel strategy with attractive therapeutic opportunities, *Med. Res. Rev. 30*, 463-549.

[51] Schrage, R., Seemann, W. K., Kloeckner, J., Dallanoce, C., Racke, K., Kostenis, E., De Amici, M., Holzgrabe, U., and Mohr, K. (2013) Agonists with supraphysiological efficacy at the muscarinic M2 ACh receptor, *Br. J. Pharmacol. 169*, 357-370.

[52] May, L. T., Avlani, V. A., Langmead, C. J., Herdon, H. J., Wood, M. D., Sexton, P. M., and Christopoulos, A. (2007) Structure-function studies of allosteric agonism at M2 muscarinic acetylcholine receptors, *Mol. Pharmacol. 72*, 463-476.

[53] Ehlert, F. J. (1988) Estimation of the Affinities of Allosteric Ligands Using Radioligand Binding and Pharmacological Null Methods, *Mol. Pharmacol. 33*, 187-194.

[54] Milligan, G., and Smith, N. J. (2007) Allosteric modulation of heterodimeric G-protein-coupled receptors, *Trends Pharmacol. Sci. 28*, 615-620.

[55] Langmead, C. J., and Christopoulos, A. (2006) Allosteric agonists of 7TM receptors: expanding the pharmacological toolbox, *Trends Pharmacol. Sci. 27*, 475-481.

[56] Burford, N. T., Watson, J., Bertekap, R., and Alt, A. (2011) Strategies for the identification of allosteric modulators of G-protein-coupled receptors, *Biochem. Pharmacol. 81*, 691-702.

[57] Kords, H., Lüllmann, H., Ohnesorge, F. K., and Wassermann, O. (1968) Action of atropine and some hexane-1.6-bis-ammonium derivatives upon the toxicity of DFP im mice, *Eur. J. Pharmacol. 3*, 341-346.

[58] Lüllmann, H., Ohnesorge, F. K., Schauwecker, G. C., and Wassermann, O. (1969) Inhibition of the actions of carbachol and DFP on guinea pig isolated atria by alkane-bis-ammonium compounds, *Eur. J. Pharmacol. 6*, 241-247.

[59] Jepsen, K., Lüllmann, H., Mohr, K., and Pfeffer, J. (1988) Allosteric Stabilization of3H-N-Methylscopolamine Binding in Guinea-Pig Myocardium by an Antidote against Organophosphate Intoxication, *Pharmacol. Toxicol. 63*, 163-168.

[60] Ma, L., Seager, M. A., Wittmann, M., Jacobson, M., Bickel, D., Burno, M., Jones, K., Graufelds, V. K., Xu, G., Pearson, M., McCampbell, A., Gaspar, R., Shughrue, P., Danziger, A., Regan, C., Flick, R., Pascarella, D., Garson, S., Doran, S., Kreatsoulas, C., Veng, L., Lindsley, C. W., Shipe, W., Kuduk, S., Sur, C., Kinney, G., Seabrook, G. R., and Ray, W. J. (2009) Selective activation of the M1 muscarinic acetylcholine receptor achieved by allosteric potentiation, *Proc. Natl. Acad. Sci. U. S. A. 106*, 15950-15955.

[61] Kiefer-Day, J. S., Campbell, H. E., Towles, J., and el-Fakahany, E. E. (1991) Muscarinic subtype selectivity of tetrahydroaminoacridine: possible relationship to its capricious efficacy, *Eur. J. Pharmacol. 203*, 421-423.

[62] Müller, C. E., Schiedel, A. C., and Baqi, Y. (2012) Allosteric modulators of rhodopsin-like G protein-coupled receptors: opportunities in drug development, *Pharmacol. Ther. 135*, 292-315.

[63] Christopoulos, A. (2002) Allosteric binding sites on cell-surface receptors: novel targets for drug discovery, *Nat. Rev. Drug. Discov. 1*, 198-210.

[64] Mohr, K., Schmitz, J., Schrage, R., Tränkle, C., and Holzgrabe, U. (2013) Molecular alliance-from orthosteric and allosteric ligands to dualsteric/bitopic agonists at G protein coupled receptors, *Angew. Chem. Int. Ed. Engl. 52*, 508-516.

[65] Lane, J. R., Sexton, P. M., and Christopoulos, A. (2013) Bridging the gap: bitopic ligands of G-protein-coupled receptors, *Trends Pharmacol. Sci. 34*, 59-66.

[66] Valant, C., Robert Lane, J., Sexton, P. M., and Christopoulos, A. (2012) The best of both worlds? Bitopic orthosteric/allosteric ligands of g protein-coupled receptors, *Annu. Rev. Pharmacol. Toxicol. 52*, 153-178.

[67] Valant, C., Sexton, P. M., and Christopoulos, A. (2009) Orthosteric/allosteric bitopic ligands: going hybrid at GPCRs, *Mol. Interv. 9*, 125-135.

[68] Schwyzer, R. (1977) Acth: A Short Introductory Review, *Ann. N. Y. Acad. Sci. 297*, 3-26.

[69] Bock, A., Merten, N., Schrage, R., Dallanoce, C., Batz, J., Kloeckner, J., Schmitz, J., Matera, C., Simon, K., Kebig, A., Peters, L., Müller, A., Schrobang-Ley, J., Tränkle, C., Hoffmann, C., De Amici, M., Holzgrabe, U., Kostenis, E., and Mohr, K. (2012) The allosteric vestibule of a seven transmembrane helical receptor controls G-protein coupling, *Nat. Commun. 3*, 1044.

[70] Bock, A., Kostenis, E., Tränkle, C., Lohse, M. J., and Mohr, K. (2014) Pilot the pulse: controlling the multiplicity of receptor dynamics, *Trends Pharmacol. Sci. 35*, 630-638.

[71] Kenakin, T., and Christopoulos, A. (2013) Signalling bias in new drug discovery: detection, quantification and therapeutic impact, *Nat. Rev. Drug. Discov. 12*, 205-216.

[72] Disingrini, T., Muth, M., Dallanoce, C., Barocelli, E., Bertoni, S., Kellershohn, K., Mohr, K., De Amici, M., and Holzgrabe, U. (2006) Design, synthesis, and action of oxotremorine-related hybrid-type allosteric modulators of muscarinic acetylcholine receptors, *J. Med. Chem. 49*, 366-372.

[73] Antony, J., Kellershohn, K., Mohr-Andra, M., Kebig, A., Prilla, S., Muth, M., Heller, E., Disingrini, T., Dallanoce, C., Bertoni, S., Schrobang, J., Tränkle, C., Kostenis, E., Christopoulos, A., Holtje, H. D., Barocelli, E., De Amici, M., Holzgrabe, U., and Mohr, K. (2009) Dualsteric GPCR targeting: a novel route to binding and signaling pathway selectivity, *FASEB J. 23*, 442-450.

[74] Chen, X., Kloeckner, J., Holze, J., Zimmermann, C., Seemann, W. K., Schrage, R., Bock, A., Mohr, K., Tränkle, C., Holzgrabe, U., and Decker, M. (2015) Rational design of partial agonists for the muscarinic m1 acetylcholine receptor, *J. Med. Chem. 58*, 560-576.

[75] Schmitz, J., van der Mey, D., Bermudez, M., Klöckner, J., Schrage, R., Kostenis, E., Tränkle, C., Wolber, G., Mohr, K., and Holzgrabe, U. (2014) Dualsteric muscarinic antagonists--orthosteric binding pose controls allosteric subtype selectivity, *J. Med. Chem. 57*, 6739-6750.

[76] Matucci, R., Nesi, M., Martino, M. V., Bellucci, C., Manetti, D., Ciuti, E., Mazzolari, A., Dei, S., Guandalini, L., Teodori, E., Vistoli, G., and Romanelli, M. N. (2016) Carbachol dimers as homobivalent modulators of muscarinic receptors, *Biochem. Pharmacol. 108*, 90-101.

[77] Alzheimer, A. (1907) Über eine eigenartige Erkrankung der Hirnrinde, In *Allg. Zeitung Psychiatr. Psych.-Gerichtl. Med.*, pp 146-148.

[78] Massoud, F., and Gauthier, S. (2010) Update on the pharmacological treatment of Alzheimer's disease, *Curr. Neuropharmacol. 8*, 69-80.

[79] (2014) Deutsche Alzheimer Gesellschaft, Factsheet "Das Wichtigste 1 – Die Häufigkeit von Demenzerkrankungen".

[80] Ballard, C., Gauthier, S., Corbett, A., Brayne, C., Aarsland, D., and Jones, E. (2011) Alzheimer's disease, *The Lancet 377*, 1019-1031.

[81] Benzi, G., and Moretti, A. (1995) Are reactive oxygen species involved in Alzheimer's disease?, *Neurobiol. Aging 16*, 661-674.

[82] Christen, Y. (2000) Oxidative stress and Alzheimer disease, *Am. J. Clin. Nutr. 71*, 621S-629S.

[83] Schulz, K. L., Eckert, A., Rhein, V., Mai, S., Haase, W., Reichert, A. S., Jendrach, M., Müller, W. E., and Leuner, K. (2012) A new link to mitochondrial impairment in tauopathies, *Mol. Neurobiol. 46*, 205-216.

[84] Berg, S., Bergh, M., Hellberg, S., Högdin, K., Lo-Alfredsson, Y., Söderman, P., von Berg, S., Weigelt, T., Ormö, M., Xue, Y., Tucker, J., Neelissen, J., Jerning, E., Nilsson, Y., and Bhat, R. (2012) Discovery of Novel Potent and Highly Selective Glycogen Synthase Kinase-3β (GSK3β) Inhibitors for Alzheimer's Disease: Design, Synthesis, and Characterization of Pyrazines, *J. Med. Chem. 55*, 9107-9119.

[85] Hardy, J. (2009) The amyloid hypothesis for Alzheimer's disease: a critical reappraisal, *J. Neurochem. 110*, 1129-1134.

[86] Greig, N. H., Utsuki, T., Ingram, D. K., Wang, Y., Pepeu, G., Scali, C., Yu, Q. S., Mamczarz, J., Holloway, H. W., Giordano, T., Chen, D., Furukawa, K., Sambamurti, K., Brossi, A., and Lahiri, D. K. (2005) Selective butyrylcholinesterase inhibition elevates brain acetylcholine, augments learning and lowers Alzheimer beta-amyloid peptide in rodent, *Proc. Natl. Acad. Sci. U. S. A. 102*, 17213-17218.

[87] Tasker, A., Perry, E. K., and Ballard, C. G. (2005) Butyrylcholinesterase: impact on symptoms and progression of cognitive impairment, *Expert Rev. Neurother. 5*, 101-106.

[88] Giacobini, E. (2004) Cholinesterase inhibitors: new roles and therapeutic alternatives, *Pharmacol. Res. 50*, 433-440.

[89] Nicolet, Y., Lockridge, O., Masson, P., Fontecilla-Camps, J. C., and Nachon, F. (2003) Crystal structure of human butyrylcholinesterase and of its complexes with substrate and products, *J. Biol. Chem. 278*, 41141-41147.

[90] Sussman, J. L., Harel, M., Frolow, F., Oefner, C., Goldman, A., Toker, L., and Silman, I. (1991) Atomic structure of acetylcholinesterase from Torpedo californica: a prototypic acetylcholine-binding protein, *Science 253*, 872-879.

[91] Watkins, P. B., Zimmerman, H. J., Knapp, M. J., Gracon, S. I., and Lewis, K. W. (1994) Hepatotoxic effects of tacrine administration in patients with Alzheimer's disease, *JAMA 271*, 992-998.

[92] Dooley, M., and Lamb, H. M. (2000) Donepezil - A review of its use in Alzheimer's disease, *Drugs Aging 16*, 199-226.

[93] Onor, M. L., Trevisiol, M., and Aguglia, E. (2007) Rivastigmine in the treatment of Alzheimer's disease: an update, *Clin. Interv. Aging 2*, 17-32.

[94] Ago, Y., Koda, K., Takuma, K., and Matsuda, T. (2011) Pharmacological aspects of the acetylcholinesterase inhibitor galantamine, *J. Pharmacol. Sci. 116*, 6-17.

[95] Munoz-Torrero, D. (2008) Acetylcholinesterase Inhibitors as Disease-Modifying Therapies for Alzheimers Disease, *Curr. Med. Chem. 15*, 2433-2455.

[96] Han, Y. F., Li, C. P., Chow, E., Wang, H., Pang, Y. P., and Carlier, P. R. (1999) Dual-site binding of bivalent 4-aminopyridine- and 4-aminoquinoline-based AChE inhibitors: contribution of the hydrophobic alkylene tether to monomer and dimer affinities, *Bioorg. Med. Chem. 7*, 2569-2575.

[97] Fang, L., Jumpertz, S., Zhang, Y., Appenroth, D., Fleck, C., Mohr, K., Tränkle, C., and Decker, M. (2010) Hybrid molecules from xanomeline and tacrine: enhanced tacrine actions on cholinesterases and muscarinic M1 receptors, *J. Med. Chem. 53*, 2094-2103.

[98] Elsinghorst, P. W., Cieslik, J. S., Mohr, K., Tränkle, C., and Gütschow, M. (2007) First gallamine-tacrine hybrid: design and characterization at cholinesterases and the M2 muscarinic receptor, *J. Med. Chem. 50*, 5685-5695.

B. Aim of the work

In the field of GPCR many agonists and antagonists are known to act as drugs on the muscarinic acetylcholine receptor. Nevertheless, the use of many therapeutic agents is limited due to the lack of subtype-selectivity to the receptor leading to side effects. The development of dualsteric ligands through the connection of two pharmacophoric units linked by an appropriate linker opens the way to high-affinity and subtype-selective compounds.

In order to get a better understanding of receptor activation and signaling, the design of new bipharmacophoric ligands is urgently needed. Hence, the aim of this thesis was the synthesis and pharmacological investigation of newly designed dualsteric compounds for the muscarinic acetylcholine receptor which show subtype-selectivity as well as pathway-biased signaling. Such tools can help to understand the activation process of the receptor or the reason for partial agonism (Figure 1).

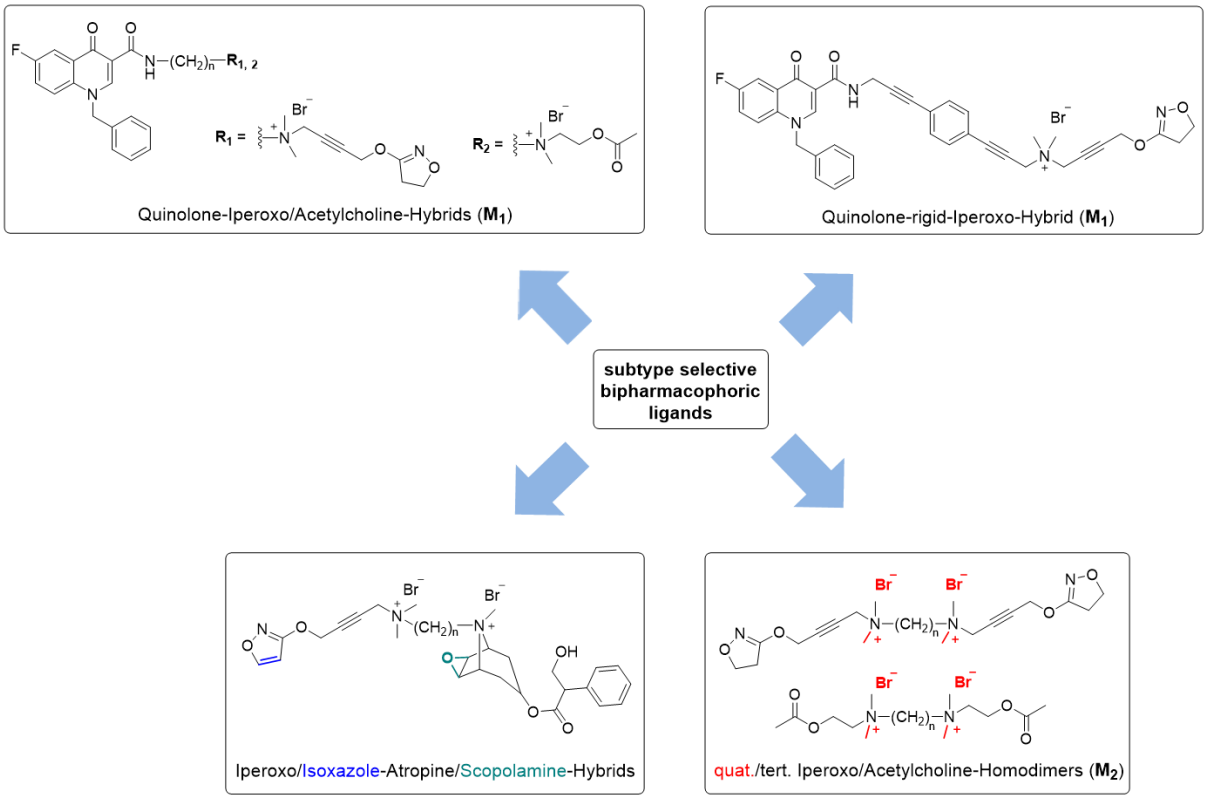

Figure 1: Overview of the projects.

On this basis, hybrids, consisting of a quinolone derived moiety linked via an alkyl chain to the agonist iperoxo and acetylcholine, respectively, were synthesized. Additionally, the flexible alkyl chain linker should be exchanged by a rigidified linker. The M_1 subtype selectivity of these hybrids as well as their binding properties were studied by means of FRET-experiments, performed in cooperation with Prof. Dr. Hoffmann by Michael Kauk (Pharmacology and Toxicology, University of Würzburg, Germany).

Furthermore, hybrids were built out of two orthosteric ligands, agonist and antagonist, which have different affinities to the orthosteric binding site. These designed iperoxo/isoxazole-atropine/scopolamine-hybrids could specifically control the extend of bias agonism.

Moreover, homodimers consisting of iperoxo and acetylcholine, respectively, linked through an alkyl chain of different length were synthesized as quaternary salts and tertiary compounds, respectively. Tertiary ligands are of interest due to their ability of passing the blood-brain-barrier. The quaternary dimers were investigated on radioligand binding assays at the M_2 receptor for their G_i- and G_s-signaling behavior and their extent concerning bias agonism. The binding studies were performed in cooperation with PD Dr. Tränkle and Prof. Dr. Mohr by Anna Krüger (Pharmacology and Toxicology, Institute of Pharmacy, University of Bonn, Germany).

Alzheimer`s disease is the most prominent form of dementia leading to the loss of cognitive function. One major therapeutic approach is the development of inhibitors for the cholinesterases AChE and BChE in order to increase the concentration of ACh in the synaptic cleft. In addition, agonists of the M_1 receptor are of interest. Hybrids should be developed in which the pharmacological benefits of two ligands are combined within one molecule which are able to address both the AChE/BChE and the M_1 receptor. The hybrids phth-C_n-isox (Figure 2) were found to have good anticholinesterase activity. On that basis, structural modifications of the pharmacophores as well as of the alkyl linker length should lead to newly designed hybrid molecules with improved anticholinesterase activity for AChE and BChE, respectively, whilst reduced side effects.

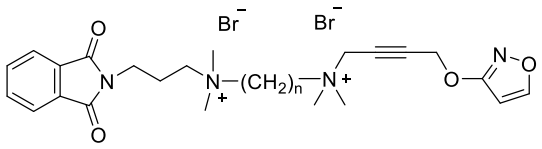

Phthalimide-C_n-Isoxazole

Figure 2: Structure of phthalimide-C_n-isoxazole.

C. Results

1. FRET studies of quinolone-based bitopic ligands and their structural analogues at the muscarinic M_1 receptor

Messerer, R., Kauk, M., Volpato, D., Alonso Canizal, M.C., Klöckner, J., Zabel, U., Nuber, S., Hoffmann, C., Holzgrabe, U.

Reprinted with permission from
Messerer, R., Kauk, M., Volpato, D., Alonso Canizal, M.C., Klöckner, J., Zabel, U., Nuber, S., Hoffmann, C., Holzgrabe, U., FRET Studies of Quinolone-Based Bitopic Ligands and Their Structural Analogues at the Muscarinic M_1 Receptor, ACS Chem. Biol., 2017, 12 (3), 833-843.

Abstract

Aiming to design partial agonists as well as allosteric modulators for the M_1 muscarinic acetylcholine (M_1AChR) receptor, two different series of bipharmacophoric ligands and their structural analogues were designed and synthesized. The hybrids were composed of the benzyl quinolone carboxylic acid (BQCA)-derived subtype selective allosteric modulator **3** and the orthosteric building block 4-((4,5-dihydroisoxazol-3-yl)oxy)-*N*,*N*-dimethylbut-2-yn-1-amine (base of iperoxo) **1** or the endogenous ligand 2-(dimethylamino)ethyl acetate (base of acetylcholine) **2**, respectively. The two pharmacophores were linked via alkylene chains of different lengths (C4, C6, C8, and C10). Furthermore, the corresponding structural analogues of **1** and **2** and of modified BQCA **3** with varying alkyl chain length between C2 and C10 were investigated. Fluorescence resonance energy transfer (FRET) measurements in a living single cell system were investigated in order to understand how these compounds interact with a G protein-coupled receptor (GPCR) on a molecular level and how the single moieties contribute to ligand receptor interaction. The characterization of the modified orthosteric ligands indicated that a linker attached to an orthoster rapidly attenuates the receptor response. Linker length elongation increases the receptor response of bitopic ligands, until reaching a maximum, followed by a gradual decrease. The optimal linker length was found to be six methylene groups at the M_1AChR. A new conformational change is described that is not of inverse agonistic origin for long linker bitopic ligands and was further investigated by exceptional fragment based screening approaches.

Abbreviations:

ACh, acetylcholine; BQCA, benzyl quinolone carboxylic acid; CFP, cyan fluorescent protein; DAG, diacylglycerol; FlAsH, fluoresceine arsenical hairpin binder; FRET, fluorescence resonance energy transfer; GPCR, G protein-coupled receptor; IL, intracellular loop; M_1, muscarinic acetylcholine subtype 1; mAChR, muscarinic acetylcholine receptor; PAM, positive allosteric modulator; YFP, yellow fluorescent protein.

1. Introduction

Muscarinic acetylcholine receptors (mAChRs) belong to class A of G protein-coupled receptors (GPCRs) and are divided into five M receptor subtypes (M_1-M_5). These subtypes regulate the activity of many important functions of the peripheral and central nervous system. They differ in their appearance and physiological function; e.g. the M_1 muscarinic acetylcholine receptor is mostly expressed in the central nervous system (cortex, hippocampus and striatum) and is therefore an interesting therapeutic target for the treatment of Alzheimer`s disease and schizophrenia.[1,2]

The orthosteric binding pocket appears to be homologues among the five receptor subtypes.[3] This issue is challenging for developing subtype selective therapeutics. To our knowledge Spalding et al.[4] described for the first time an alternative - allosteric binding region at M_1 receptors. This region does not show a high sequence identity and is thus a promising target for developing subtype selective allosteric modulators. Allosteric modulators can influence the affinity of ligands bound to the topographically distinct orthosteric site, either in a positive, neutral, or negative manner.[5] The benzyl quinolone carboxylic acid (BQCA) and its analogues were among others reported by Kuduk et al. to be positive allosteric modulators (PAMs) with respect to orthosteric agonist binding, including the endogenous neurotransmitter acetylcholine, and function in M_1 receptors.[6-9] To combine the advantages of the two binding sites, the concept of bitopic ligands was developed.[10] These ligands engage the allosteric and orthosteric site simultaneously. Recently, bipharmacophoric ligands consisting of the base of the superagonist iperoxo **1**[11,12] and a benzyl quinolone carboxylic acid moiety **3** were designed, and found to act as partial *h*M_1 receptor agonists.[13]

For the last two decades a series of different receptor sensors, based on fluorescence resonance energy transfer (FRET), were generated for different GPCRs.[14-16] Usually, such sensors are tagged C-terminally with cyan fluorescent protein (CFP) and in the third intracellular loop (IL) region with a yellow fluorescent protein (YFP) or a tetracysteine motif capable of binding a small soluble fluorophore called fluoresceine arsenical hairpin binder

(FlAsH). These receptor sensors proved to be valuable tools for pharmacological characterizations in intact cells, especially for monitoring receptor activation in real time and to investigate receptor ligand interaction on a molecular level.[17,18] According to Chen et al., structure-activity relationships (SARs) showed that the BQCA analogue containing a benzyl moiety at the nitrogen atom as well as a 6-fluoro substituted aromatic ring resulted in a partial *h*M_1 receptor agonist.[13] Due to these findings, the same structural BQCA modification was used for the herein newly designed compounds. Thus, analogues of the superagonist **1** and orthosteric agonist **2** and of the BQCA-derived subtype selective allosteric modulator **3** were designed, synthesized, and characterized, resulting in modified analogues with varying alkyl chain length between C2 and C10 (**1-Cn**, **2-Cn**, and **4-Cn**, where n gives the length of the linker, i.e., the number of C atoms, Scheme 1 and 2). The attachment point was chosen on the tetramethyl moiety as this group points out of the orthosteric binding pocket as seen for iperoxo.[19] Furthermore, the fluoro-substituted allosteric BQCA moieties were linked to the base of orthosteric agonists iperoxo and to the base of acetylcholine, aiming to design bipharmacophoric M_1 receptor agonists (**5-C** and **6-C**, Scheme 2). The linker elongation on the BQCA modified pharmacophore was attached on the carboxylic acid residue due to molecular modeling studies suggesting that the carboxylic acid position points out toward the extracellular site of the receptor.[20] Furthermore, the carboxylic moiety is a suitable attachment point for improving allosteric modulation. For the pharmacological characterization of these ligands, a novel M_1 FRET sensor was used. This study provides an insight into M_1 receptor activation, receptor conformational changes monitored by the movement of fluorescent labeled domains, and signaling behavior.

2. Results and discussion

2.1 Chemistry

The reaction sequences of the iperoxo analogues **1-C2** to **1-C10** and of the acetylcholine analogues **2-C4**, **2-C6**, **2-C8**, and **2-C10** are illustrated in Scheme 1. 4-((4,5-dihydroisoxazol-3-yl)oxy)-*N*,*N*-dimethylbut-2-yn-1-amine[11] (base of iperoxo) **1** and 2-(dimethylamino)ethyl acetate (base of acetylcholine) **2** were reacted with the corresponding bromoalkane in acetonitrile, affording the final monoquaternary ammonium salts **1-C2** to **1-C10** and **2-C4**, **2-C6**, **2-C8**, and **2-C10** in 48-91% yield. The synthesis of the acetylcholine analogues **2-C4**, **2-C6**, and **2-C8** were described previously using a different synthetic pathway.[21]

Scheme 1: Synthesis of orthosteric M_1 agonist agents based on iperoxo – and acetylcholine analogues.

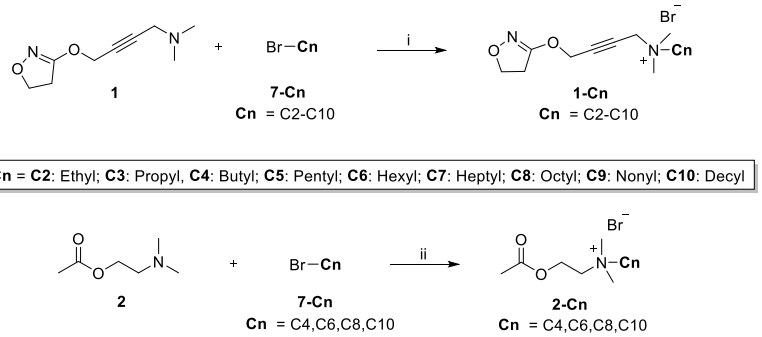

Reagents and conditions: (i) KI/K_2CO_3, $CH_3CN/CHCl_3$, 70 °C (48-89%); (ii) KI/K_2CO_3, CH_3CN, 70 °C (microwave) (65-91%).

As already reported, the fluoro-4-oxo-quinolone skeleton of **8** was synthesized using the Gould-Jacobs procedure, starting off with the condensation of 4-fluoroaniline with diethyl 2-(ethoxymethylene)-malonate and subsequent cyclization in boiling diphenyl ether.[22-24] Ester hydrolysis led to compound **3**.[25] Conversion of the ester function (**9**) with the aminoalcohols of the corresponding spacer length (C4, C6, C8, C10), substitution of the alcohol function with a bromine atom using HBr/H_2SO_4, and subsequent reaction with trimethylamine in acetonitrile at 40 °C led to the monoquaternary ammonium salts **4-C4**, **4-C6**, **4-C8**, and **4-C10** in 53-96% yield. For the preparation of the final BQCA/iperoxo hybrids **5-C4**, **5-C6**[13], **5-C8**, and **5-C10** as well as the BQCA/ACh hybrids **6-C4**, **6-C6**, **6-C8**, and **6-C10**, the intermediate bromides were connected to the base of iperoxo and to the base of acetylcholine, respectively, in the presence of KI/K_2CO_3 in acetonitrile (Scheme 2).

Scheme 2: Synthesis of quinolone analogues, BQCA/iperoxo hybrids and BQCA/ACh hybrids.

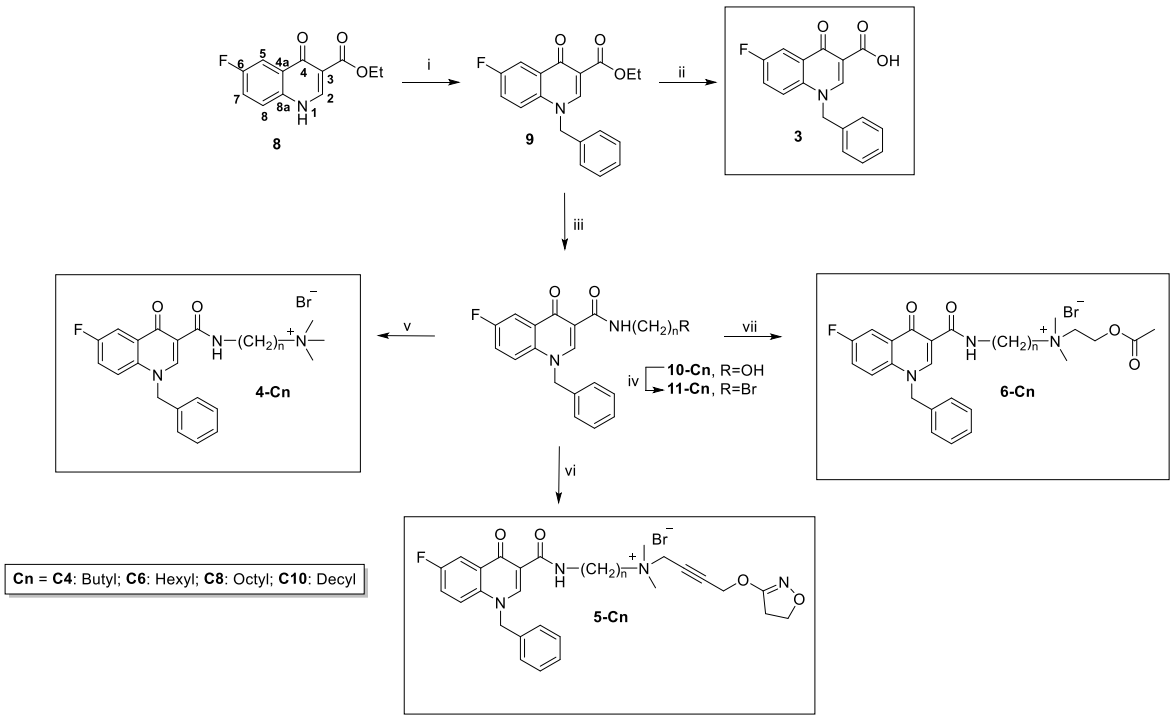

Reagents and conditions: (i) benzyl chloride, K_2CO_3, DMF, 80 °C (72%); (ii) 6 N HCl, MeOH, reflux (77%); (iii) $H_2N(CH_2)_nOH$, 150 °C (28-33%); (iv) HBr (48%), H_2SO_4, reflux (73-93%); (v) trimethylamine, CH_3CN, 40 °C (53-96%); (vi) **1**, KI/K_2CO_3, CH_3CN, 80 °C (microwave) (37-66%); (vii) **2**, KI/K_2CO_3, CH_3CN, 80 °C (microwave) (19-73%).

2.2 Pharmacology/FRET measurements

2.2.1 Receptor sensor and ligand characterization

In comparison to the previously reported M_1-, M_3-, M_5-[26] and M_2-ACh receptor FRET-sensors,[27] we created a novel full length FRET sensor of the human M_1-ACh receptor which was not truncated in the third intracellular loop (IL3). This novel sensor consists of the native amino acid sequence fused at the receptor C-terminus to CFP by adding the amino acids Ser/Arg encoding for an XbaI site. Additionally, a FlAsH binding motif CCPGCC was inserted between Gly227 and Ser228 (Figure 1a) at the N-terminal part of IL3 shortly underneath transmembrane domain 5 outside of the G protein-coupling region.[28] The receptor construct M_1-I3N-CFP expressed well at the cell surface as analyzed by confocal scanning laser microscopy (Figure 2). Since the previously published truncated sensors were not different from wild-type receptors in radioligand binding,[17] we characterized only functional response of the novel sensor. To evaluate the effect of the six amino acid insertion into the M_1-CFP receptor we used a dual fluorescence probe, which responds with an increase in red fluorescence intensity upon increase in Ca^{2+} and a decrease in green fluorescence upon binding to diacylglycerol (DAG). Therefore, the probe can specifically report on the activation

of Gq-signalling.[29] The dual fluorescent probe was transfected in HEK293 cells either alone or coexpressed with the M_1-CFP or the novel M_1-I3N-CFP sensor and analyzed by confocal microscopy. The dual probe did not respond to carbachol if no receptor was co-transfected. As shown in Figure 3, the carbachol stimulated response was indistinguishable for the M_1-CFP receptor or the M_1-I3N-CFP sensor. In combination with previous binding experiments on a truncated sensor version,[17] it was concluded that this sensor is not disturbed in its signaling properties by insertion of the CCPGCC sequence. For further FRET experiments, the M_1-I3N-CFP was stably expressed in HEK293 cells, and single cells were used for further analysis. To study dynamic conformational changes in real time, the M_1-I3N-CFP sensor was exposed to the endogenous agonist ACh and the synthetic full agonist iperoxo. To eliminate potential artefacts from changes in flow rates, the cells were constantly superfused with buffer. Under these conditions the receptor sensor shows a constant baseline. Upon ligand addition, a sharp antiparallel movement of the CFP and FlAsH signal was observed (Figure 4), resulting in a concentration dependent change in the FRET signal of 8-12% for iperoxo (Figure 1b). When the superfusion solution was switched back from agonist to buffer, the signal returned to the baseline. A slight reduction of the FRET signal over time was detectable and could be due to photobleaching. To prevent artificial underestimation of ligand efficacy, reference and ligand were measured in an alternating exposure regime. Thus, we were able to generate concentration dependent response (Figure 1c) curves for the endogenous agonist ACh (EC_{50} = 2.91 µM) and the synthetic full agonist iperoxo (EC_{50} = 0.57 µM). The observed EC_{50} value for ACh is in very good agreements with previously obtained value using the truncated receptor sensor.[17] Due to a 5-fold higher potency of iperoxo compared to ACh, the base of iperoxo **1** was chosen as the orthosteric building block for the studied bitopic ligands to ensure high receptor activation via the orthosteric binding site.

As allosteric building block a structural analogue of benzyl quinolone carboxylic acid (BQCA) origin was chosen. In 2009, BQCA was reported to be a M_1 selective positive allosteric modulator (PAM)[9] whose binding region was studied in detail.[20] However, an essential property of allosteric modulators is probe dependency. Thus, an experimental approach to show this cooperative effect of BQCA analogue (**3**) combined with iperoxo (Figure 1d) was designed. To study positive modulation, a concentration of iperoxo which results in approximately 20% of the maximal observed signal (EC_{20}) was chosen. This way, a clear signal was observed, and still a large detection range to observe positive allosteric modulation was available. As seen in Figure 1d by applying the allosteric modulator **3** alone, a small conformational change was found. This small response was not clearly detectable for all cells measured. This might be explained by the very small signal that could not always be distinguished from noise. When applying saturating concentrations of iperoxo, a significant

signal was monitored. Next, iperoxo at 0.1 µM concentration was applied, which results in 25% signal compared to saturating ligand concentrations. Now, the superfusion was changed to a mix of iperoxo and **3** and again back to iperoxo alone. A clear enhanced receptor response was observed by applying **3** and iperoxo at the same time, compared with the appropriate iperoxo response. This enhanced response is higher than a theoretical additive effect of the conformational changes induced by **3** and iperoxo alone and can be described as positive allosteric modulation.

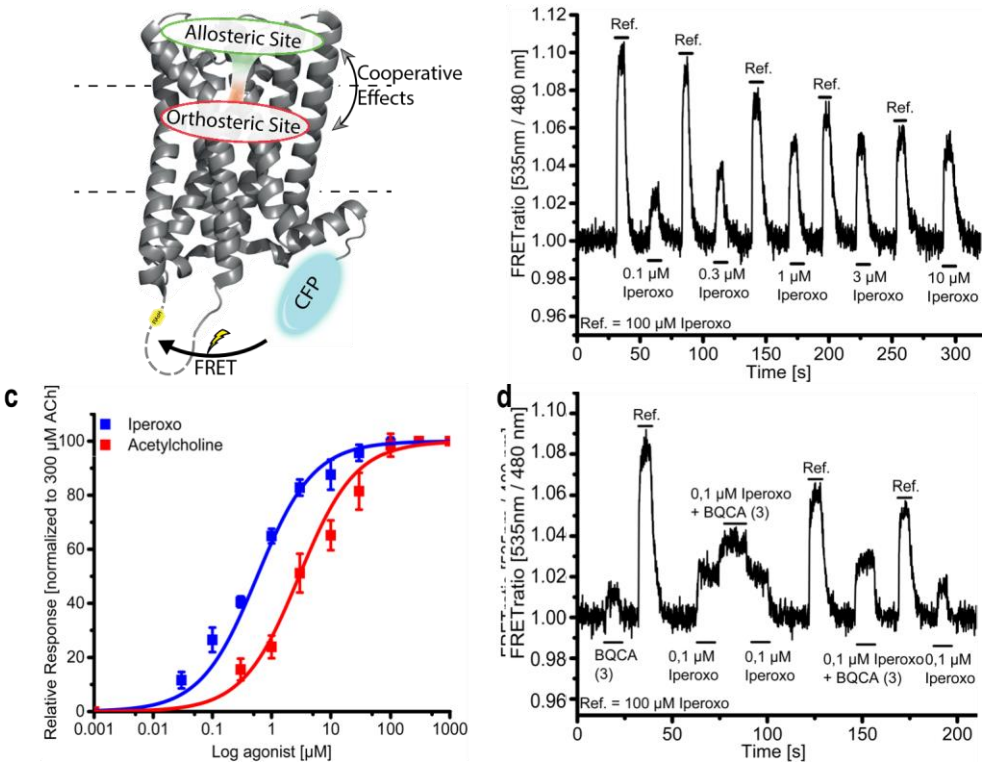

Figure 1: Receptor sensor and ligand characterization. (**a**) Schematic representation of the M_1-I3N-CFP receptor sensor with insertion of the CCGPCC FlAsH-binding site in intracellular loop 3 and fusion of CFP at the C-terminus. Schematically, the allosteric and orthosteric regions for ligand binding are highlighted as well. (**b**) An example of a single cell FRET-recording of the M_1-I3N-CFP stably expressed in HEK293 cells is shown. One-hundred micromolar iperoxo was used as reference ligand throughout the recording as indicated by black bars above the recorded signal. Different concentrations of iperoxo were applied as indicated at the appropriate time points by black bars underneath the recorded signal. The trace is representative of 30 cells measured at four different experimental days. Changes in FRET ratio for 100 µM iperoxo varied between 9 and 11% at all cells. (**c**) Concentration response curves of ACh (red, EC_{50} = 2.91 ± 0.07 µM) and iperoxo (blue, EC_{50} = 0.57 ± 0.02 µM) as calculated form FRET experiments using the M_1-I3N-CFP receptor sensor. Each ligand concentration is represented by an average value of at least 10 cells. (**d**) One-hundred micromolar iperoxo was used as reference throughout the recording as indicated by black bars above the recorded signal. Different concentrations and combinations of iperoxo and/or **3** were applied as indicated at the appropriate time points by black bars underneath the recorded signal. The trace is representative of 15 cells measured at four different experimental days.

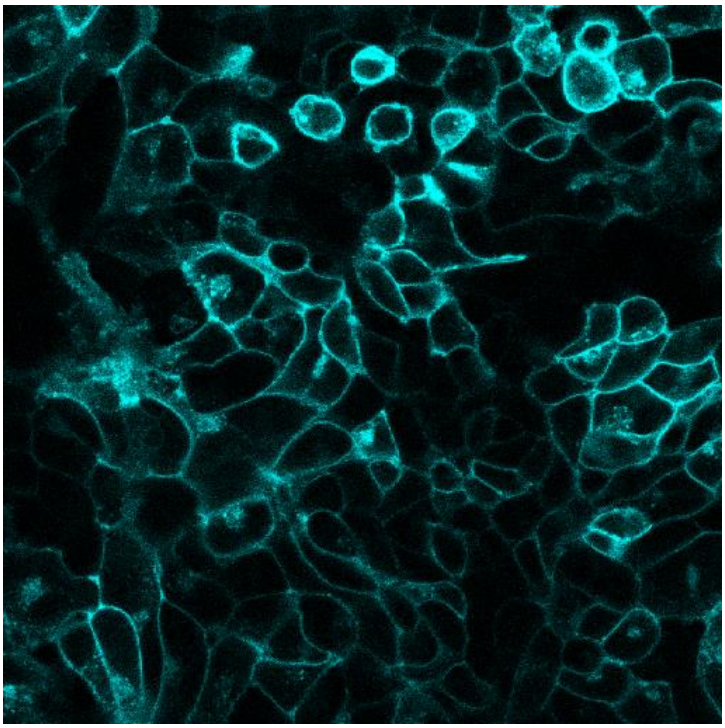

Figure 2: Cell surface expression of the M_1-I3N-CFP receptor sensor in HEK 293 cells was investigated using confocal scanning laser microscopy.

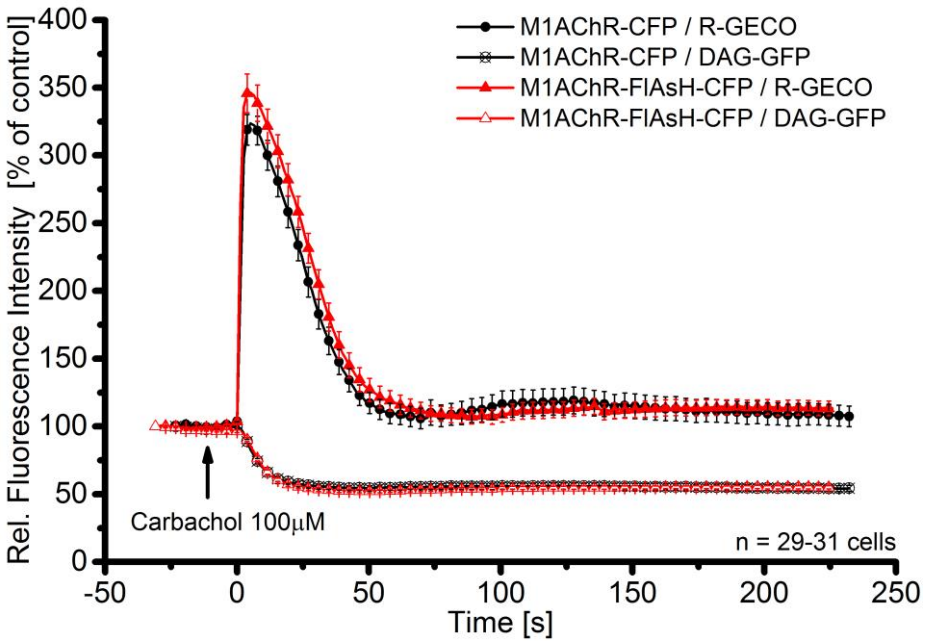

Figure 3: M_1-I3N-CFP receptor sensor characterization was performed using a dual fluorescence probe from Montana Molecular. With the help of this fluorescence tool it is possible to monitor DAG formation and Ca^{2+} release simultaneously. The stimulated response was indistinguishable for the M_1-CFP receptor and the M_1I3N-CFP receptor.

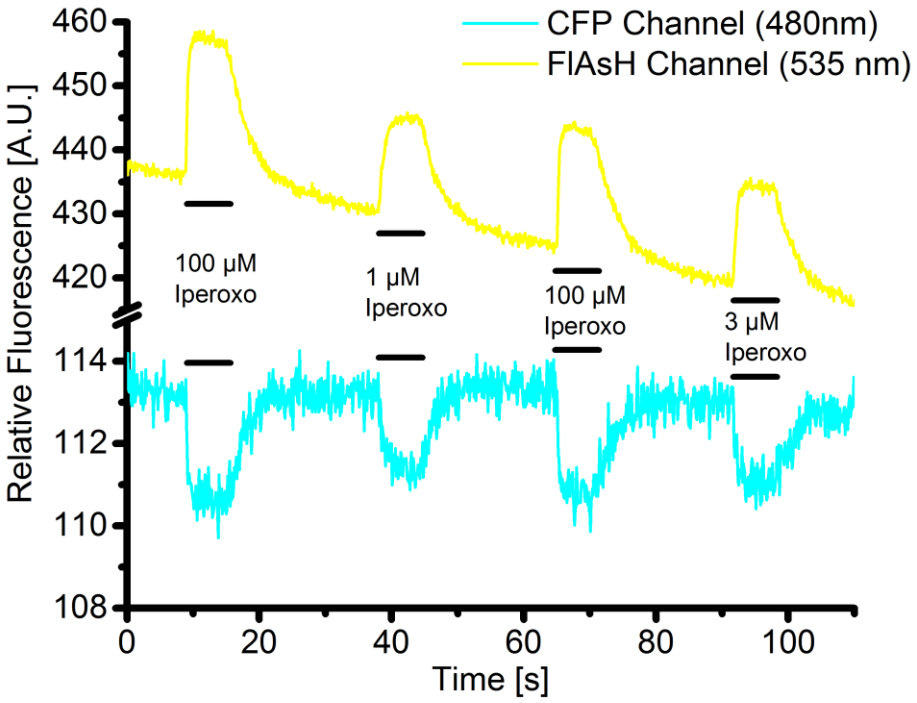

Figure 4: Effect of agonist addition to the receptor sensor. Upon ligand exposure sharp concentration dependent, antiparallel movements of the different FRET channels were detectable. Constant superfusion of buffer results in a constant baseline.

2.2.2 Linker elongation attenuates orthosteric properties

Besides their orthosteric and allosteric moieties, bitopic ligands consist of a linker region that is often not investigated in a systematic way, and hence, the linker is often inappropriately treated. To date, the molecular effects of additional carbon atoms at an orthosteric ligand for muscarinic receptors are still unknown. Therefore, nine different structural analogues of **1** with a linker attached to the amine group were synthesized (Scheme 1, **1-C2** to **1-C10**). These compounds were investigated via FRET for their ability to induce a conformational change at the M_1 receptor. The results are summarized in Figure 5. Figure 5a shows a single FRET experiment comparing the effect of iperoxo and different concentrations of **1-C2** and **1-C3**. Even saturating concentrations of **1-C2** exhibit a much reduced FRET signal compared to the reference compound iperoxo. From these data, it can be concluded that additional methylene units significantly reduce the efficacy to 65% compared to iperoxo. Nonetheless, it was possible to generate a concentration response curve for **1-C2**. Besides the reduced efficacy, a 3-fold lower affinity (EC_{50} (**1-C2**) = 1.65 µM) to the receptor sensor became evident (Figure 5b). For **1-C3**, a more than 80% reduced conformational change was found. These signals were too small to establish a reliable concentration response curve. The iperoxo analogues (**1-C4** to **1-C10**) did not induce any conformational change at the receptor sensor (Figure 5c). In order to test whether the linker extended ligands were able to bind the receptor sensor at the orthosteric binding site, competition experiment were performed

shown in Figure 5d. To test for binding of **1-C6**, first 10 µM of iperoxo as a concentration which induces 80% of the maximal signal response (EC_{80}) was applied. In the first case, a single ligand to the receptor sensor was superfused (Figure 5d). Next, a 10 µM solution of iperoxo with 100 µM of the linker analogue **1-C6** was added. As can be seen in Figure 5d, the receptor response induced by the ligand mix was significantly reduced compared to the signal induced by iperoxo alone, most likely indicating that the two ligands compete for the orthosteric binding site and that the **1-C6** analogue shows affinity to the orthosteric binding site but does not exhibit efficacy as shown by the lack of conformational changes in Figure 5c. In Figure 5e, the results for a corresponding set of ligands of ACh origin (Scheme 1) are displayed. The given FRET trace proves that a distinct linker elongation at an orthosteric ligand attenuates orthosteric efficacy. This phenomenon could be due to a steric hindrance within the binding pocket or due to preventing an essential receptor movement like closing the aromatic lid, which was proposed before to be essential for receptor activation.[19]

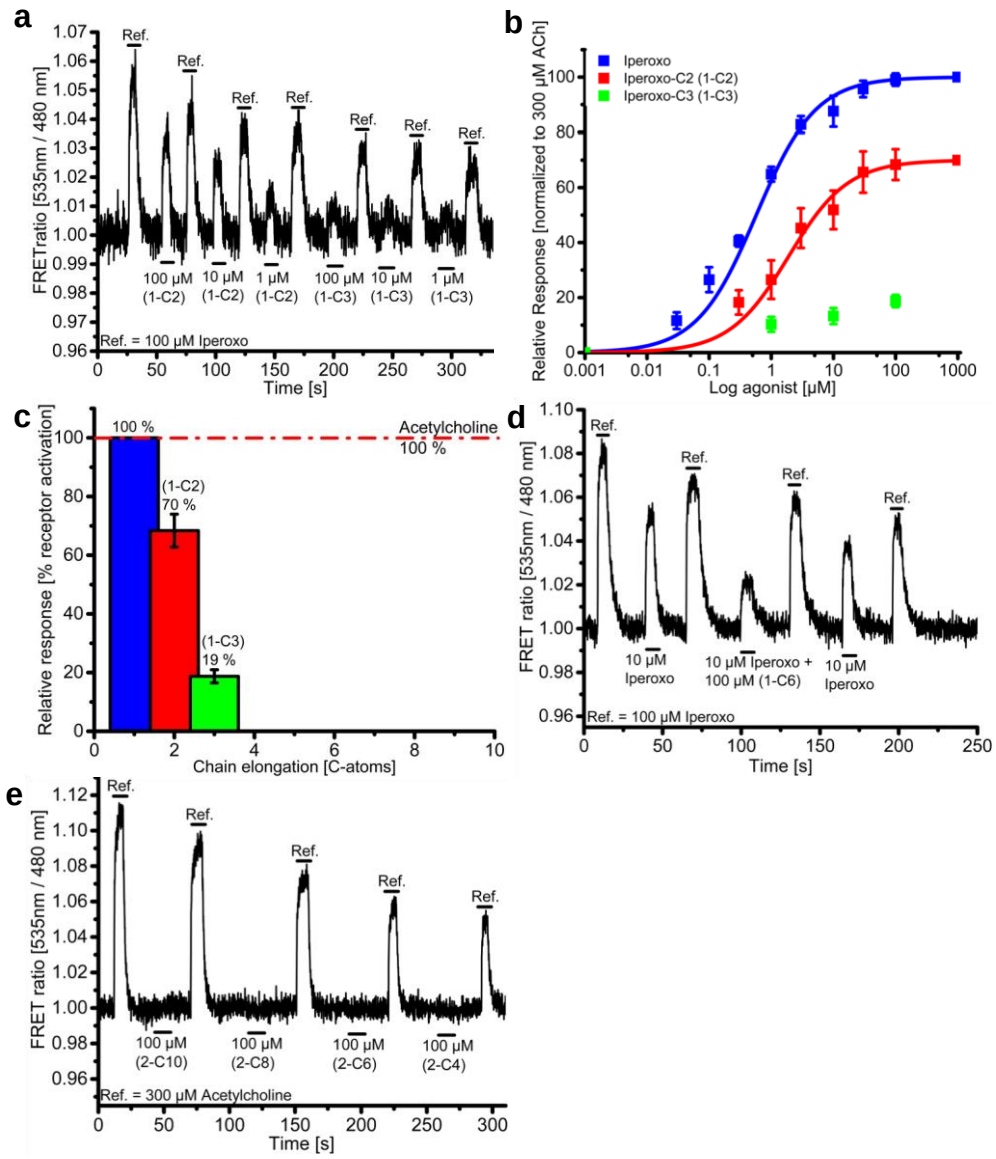

Figure 5: Characterization of iperoxo-linker elongated derivatives using FRET. (**a**) An example of a single cell FRET recording of the M_1-I3N-CFP stably expressed in HEK293 cells is shown. One-hundred micromolar iperoxo was used as reference throughout the recording, as indicated by black bars above the recorded signal. Different concentrations of **1-C2** or **1-C3** were applied as indicated at the appropriate time points by black bars underneath the recorded signal. The trace is representative of 20 cells measured at three different experimental days. (**b**) Calculated concentration response curves of iperoxo (data from Figure 1c) and **1-C2** (EC_{50} = 1.67 ± 0.14 µM) are shown. Each ligand concentration is represented by an average value of at least 10 cells. For **1-C3**, an 80% reduced conformational change was observed. (**c**) Observed FRET response of linker elongated derivatives (**1-C2** to **1-C10**) as percent of control (100 µM iperoxo). Each bar represents the average of at least 10 independent measurements. (**d**) Ligand competition observed at a single cell level. One-hundred micromolar iperoxo was used as reference throughout the recording, as indicated by black bars above the recorded signal. Application of 10 µM iperoxo alone or in combination with 100 µM **1-C6**, as indicated at the appropriate time points by black bars underneath the recorded signal, is indicative for binding of **1-C6** by reducing the effect of iperoxo in comparison to 10 µM iperoxo when applied alone. The trace is representative of 10 cells measured at three different experimental days. (**e**) Three-hundred micromolar ACh was used as a reference throughout the recording as indicated by black bars above the recorded signal. Maximal concentrations of **2-C4** to **2-C10** were applied as indicated at the appropriate time points and indicated by black bars underneath the recorded signal. The trace is representative of 15 cells measured at three different experimental days.

2.2.3 Evaluation of bitopic ligands

Bitopic ligands are thought to interact with both orthosteric and the allosteric binding site at the same time.[10] They are also thought to interact with the receptor in a dynamic binding mode, which consist at least of two different states.[30,31] Abdul-Ridha et al.[20] investigated both binding sites in great detail by mutational analysis. Using this approach, it was possible to restrict the relative position of both moieties to a certain area of the receptor.[20] In combination with the crystal structure of iperoxo bound to the M_2-receptor subtype[19] and the recently published crystal structure of the M_1-receptor subtype[3], we focused on bitopic ligands with different linker length consisting of either four, six, eight, or 10 carbon atoms. Thus, these ligands cover a relative distance of 6 Å to 15 Å between both pharmacophore moieties and hence representing the seven transmembrane helical core. A series of bitopic ligands consisting of the base of iperoxo (**1**) and the BQCA analogue (**3**) were synthesized (Scheme 2). Correspondingly, these ligands are called **5-Cn**, with **n** reflecting the linker length (**4**, **6**, **8**, **10**; Scheme 2). As can be seen in Figure 6a, showing a representative FRET trace of **5-C6**, a clear concentration-dependent increase in conformational change has taken place. This is the largest conformational change at this FRET sensor compared to all other structural analogues in this series. All other ligands were also able to induce a conformational change at the M_1 receptor sensor. Figure 6b shows the maximal ligand induced changes in comparison to iperoxo. The dashed line indicates the maximal observed signal for the allosteric moiety **3** when tested alone. Since all corresponding iperoxo linker analogues (**1-C4** to **1-C10**) alone did not induce a conformational change (cf. Figure 5c), the difference in conformational changes of the hybrids above the dashed line should either result from the positive cooperativity between the orthosteric and allosteric moieties or from an alternative binding pose. Moreover, for the M_1 receptor, the optimal linker length for the combination of **1** and **3** is in the range of six methylene groups (see Figure 6b), whereas for the M_2-receptor subtype, longer linker lengths are necessary to improve bitopic ligand efficacy.[30] Thus, the optimal linker length as well as the nature of the linker chain are crucial for receptor activation and are different for each receptor subtype, depending on their tertiary structure. A first indication for receptor subtype selectivity among acetylcholine receptors is shown in Figure 7. Compound **5-C6** was tested at a previously published M_3-ACh receptor FRET sensor[26] and did not evoke a conformational change as observed for iperoxo. Furthermore, after reaching an optimal linker length, the efficacy of bitopic ligands decline by further linker elongation (Figure 6b). Surprisingly, when investigating compound **5-C10**, a concentration dependent signal with opposite signal direction compared to iperoxo was found (Figure 6c). Since changes in FRET signals in general represent a relative distance change, this property was used as a readout for conformational changes at GPCRs. The opposite FRET signal induced by **5-C10** was not observed before for any bitopic ligand at M-receptors.

Comparable inverse FRET signals were reported for inverse agonistic responses at constitutively active mutants of the α_{2a} adrenergic receptor[32] and the M_3 mutant[33]. At constitutively active M_3 receptors, atropine behaves as an inverse agonist. Hence, to compare the effect found for **5-C10** at the M_1-I3N-CFP with eventual constitutive activity, the effect of atropine at this construct was studied. However, neither atropine nor tiotropium did induce any conformational change (see Figure 6d or Figure 8), arguing against constitutive activity as an explanation for the behavior of **5-C10**. Of note, the high receptor affinity of atropine becomes visible by the fact that it was almost impossible to induce a second signal for iperoxo after the first application of 10 µM atropine. To further study the surprising effect of **5-C10**, a series of bitopic ligands based on acetylcholine as orthosteric building block **6-C4** to **6-C10** (Scheme 2) was investigated. Figure 6e displays a representative FRET trace of acetylcholine based bitopic ligands, and the bar graph in Figure 6f summarizes the measured FRET signals. Again, a linker-length-dependent receptor response was found. Moreover, again, inverse FRET-signals for bitopic ligands of longer chain length were detected. Interestingly, for this compound series, a FRET-signal with similar direction as observed for ACh was never detected.

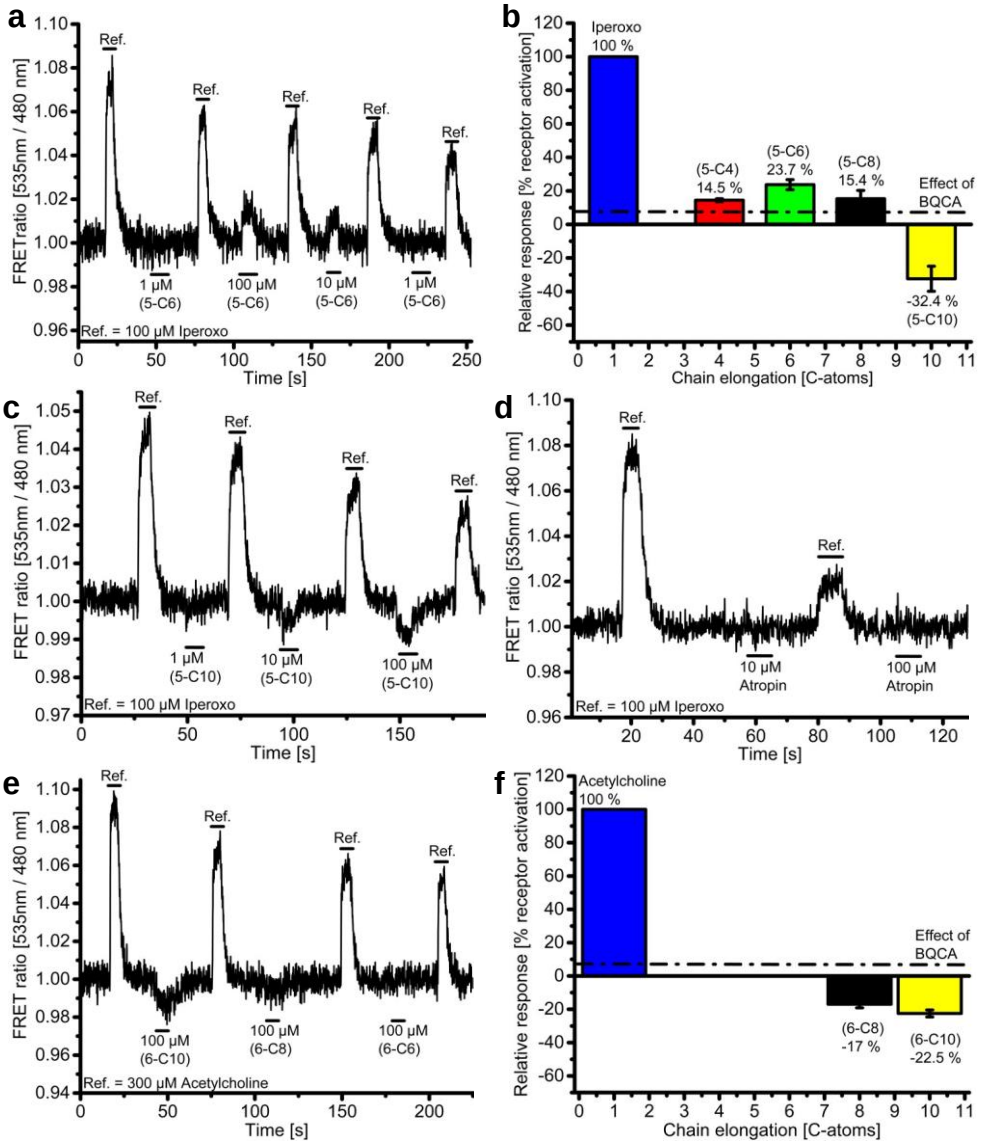

Figure 6: Evaluation of bitopic ligands at the M_1-I3N-CFP receptor sensor. (**a**) An example of a single cell FRET recording of the M_1-I3N-CFP stably expressed in HEK293 cells is shown. One-hundred micromolar iperoxo was used as reference ligand throughout the recording as indicated by black bars above the recorded signal. Different concentrations of **5-C6** were applied as indicated at the appropriate time points by black bars underneath the recorded signal. The trace is representative of 20 cells measured at four different experimental days. The maximal detected signal for **5-C6** was 23.7% compared to the reference. (**b**) Quantified maximal ligand induced FRET response of compounds **5-C4** to **5-C10** as percent of control (100 µM iperoxo). Each bar represents the average of at least 10 independent measurements. (**c**) One-hundred micromolar iperoxo was used as a reference ligand throughout the recording as indicated by black bars above the recorded signal. Different concentrations of **5-C10** were applied as indicated at the appropriate time points by black bars underneath the recorded signal. The trace is representative of 15 cells measured at three different experimental days. Note, the concentration dependent responses of **5-C10** showed an inverse signal direction compared to iperoxo. (**d**) The antagonist atropine did not induce a conformational change at the M_1-I3N-CFP receptor sensor. (**e**) Three-hundred micromolar ACh was used as a reference ligand throughout the recording as indicated by black bars above the recorded signal. Different responses to acetylcholine-based bitopic ligands were determined for **6-C4** to **6-C10**. The trace is representative of 20 cells measured at four different experimental days. Acetylcholine-based bitopic ligands results in an inverse FRET signal for derivatives with elongated chain length. (**f**) Quantified maximal ligand induced FRET response of compounds **6-C4** to **6-C10** as percent of control (300 µM acetylcholine). Each bar represents the average of at least 10 independent measurements.

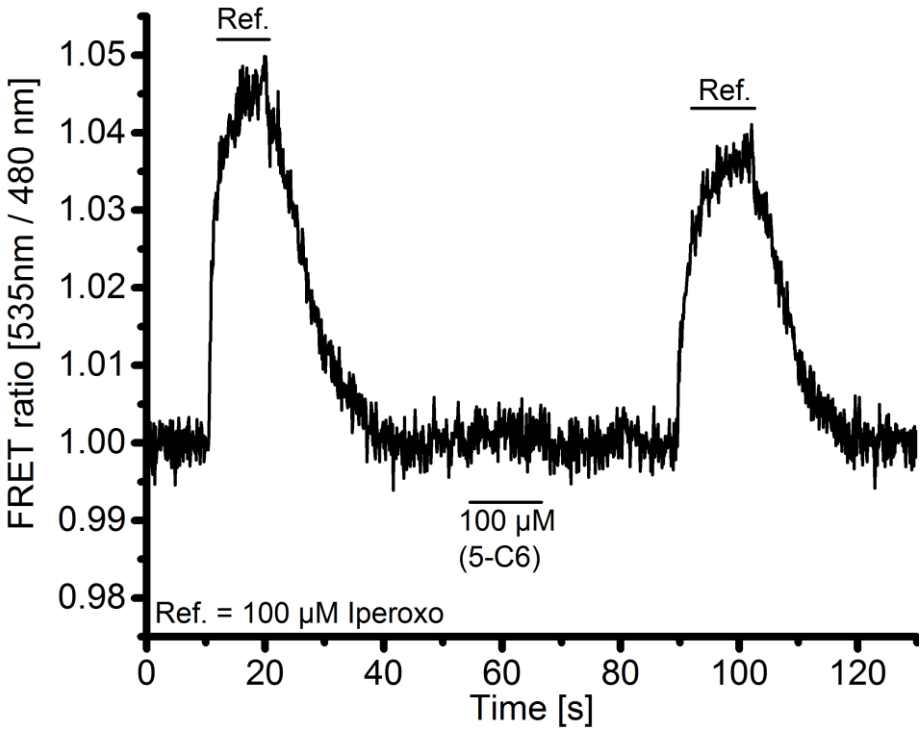

Figure 7: The hybrid **5-C6** was investigated at a M_3 receptor sensor that was reported before[26]. Iperoxo was used as the reference ligand. The hybrid **5-C6** was unable to induce a conformational change at the M_3 receptor subtype.

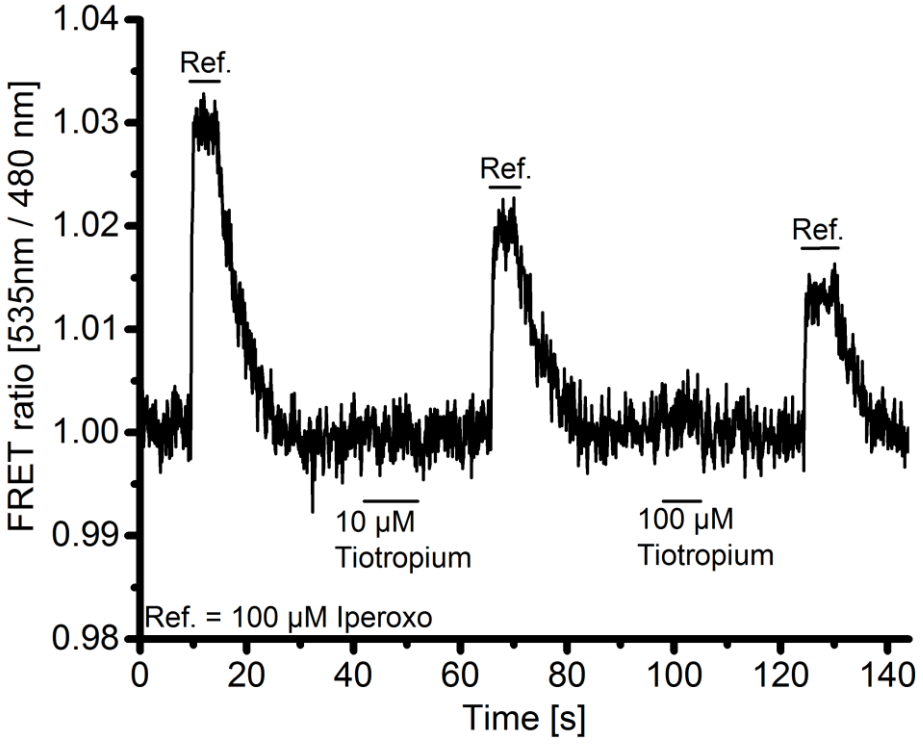

Figure 8: The antagonist tiotropium was investigated at the M_1-I3N-CFP sensor. Iperoxo was used as the reference ligand. Tiotropium was unable to induce a conformational change.

2.2.4 Linker fusion at the allosteric building block

In order to find out why bitopic ligands with longer linkers produce an inverse FRET signal, it was of interest to unravel the moiety of the ligands contributing to the observed signals. Additionally, the question arose whether it would be possible to reconstruct the signal derived by different bitopic ligands by combining the individual components in a fragment-based screening approach in a single cell. Therefore, the ligands **5-C6** and **5-C10** who showed the most extreme signals were studied. As shown in Figure 1d, the BQCA analogue (**3**) induces a small conformational change but the corresponding linker extended iperoxo analogue (**1-C6**) did not exhibit a detectable effect at our receptor sensor (Figure 5c). However, **1-C6** binds to the receptor (Figure 5d). Both effects are shown in Figure 9a, this time measured at the same cell. By applying both compounds (**3** and **1-C6**) at the same time, a receptor response was observed that was on the one hand significantly different to the BQCA response but on the other hand similar in the maximal signal intensity as reported before for the bitopic ligand **5-C6** (Figure 6a), indicating first that it is possible to reconstruct the effect of a bitopic ligand interacting with a receptor by applying the fragments at the same time as the receptor sensor and second that there is cooperativity between the allosteric modulator BQCA (**3**) and the ligand **1-C6**, which showed high affinity to the orthosteric binding site.

Comparable experiments were performed with the ligand **5-C10** and its respective building blocks (Figure 9b). Interestingly in this case, it was impossible to reconstruct the signal of the bitopic ligand by applying the single fragments, suggesting that the inverse signal is likely mechanistically different to the agonistic signal. Interestingly at the M_2 mAChR, iperoxo-based bitopic ligands have been shown to bind in at least two different binding poses,[31] and one of them was shown to be purely allosteric. This has recently been further investigated by molecular modeling.[34] In an attempt to explain the inverse FRET signal mechanistically, the set of compounds **4-C4** to **4-C10**, consisting of the allosteric moiety, was studied. Here, a linker moiety of different length and a tertiary amine are combined to imitate the positively charged amine of the orthosteric ligand (Scheme 2) in the presence of the allosteric moiety. Figure 9c displays a representative FRET trace recorded for a single cell that was superfused with the indicated ligands. Increasing linker length led to the appearance of an inverse signal for compound **4-C8** and **4-C10** even in the absence of the orthosteric moiety similar to the signal observed for compound **5-C10** or **6-C10**. This result supports the notion of an alternative second binding pose for the linker extended bitopic ligands at the M_1 receptor, as recently described for the M_2 receptor.[34] Another hypothesis is the possible binding of the ligands to two allosteric binding sites in a dimeric receptor.[35]

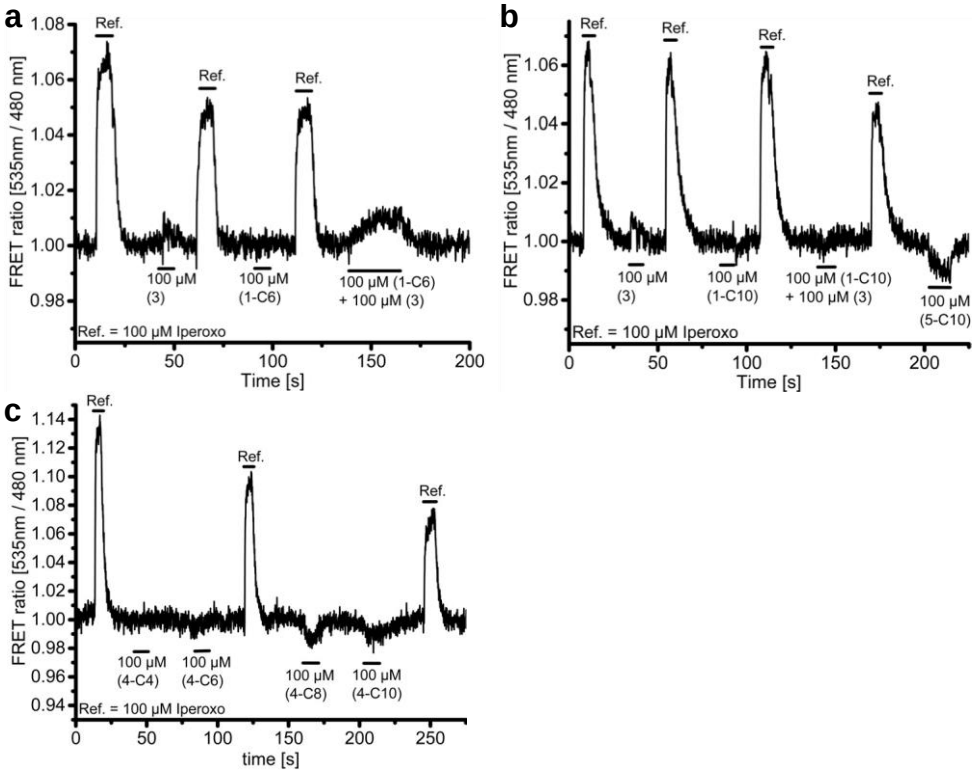

Figure 9: Fragment-based screening approach for reconstruction the signal induced by the bitopic ligand by combining the individual components in one assay. (**a**) An example of a single cell FRET recording of the M_1-I3N-CFP stably expressed in HEK293 cells is shown. One-hundred micromolar iperoxo was used as reference ligand throughout the recording as indicated by black bars above the recorded signal. Alternatively, 100 µM of **3** and **1-C6** were applied separately or in combination as indicated at the appropriate time points by black bars underneath the recorded signal. Note that the combination of individual fragments **1-C6** and **3** leads to a similar signal amplitude as induced by **5-C6** (Figure 6a). The trace is representative of 15 cells measured at three different experimental days. (**b**) One-hundred micromolar iperoxo was used as a reference ligand throughout the recording as indicated by black bars above the recorded signal. Alternatively, 100 µM of **3** and **1-C10** were applied separately or in combination as indicated at the appropriate time points by black bars underneath the recorded signal. Note that the combination of individual fragments **1-C10** and **3** was not able to reproduce a similar signal amplitude as **5-C10**. The trace is representative of 15 cells measured at three different experimental days. (**c**) One-hundred micromolar iperoxo was used as reference throughout the recording as indicated by black bars above the recorded signal. Maximal concentrations of **4-C4** to **4-C10** were applied as indicated at the appropriate time points and indicated by black bars underneath the recorded signal. The trace is representative of 15 cells measured at three different experimental days.

2.3 Concluding remarks

Bitopic ligands are molecular entities, which bind to more than one pharmacologically interesting region of membrane proteins, and are thought to have an impact on further drug development. This study provides a molecular insight of the interactions between GPCRs and bitopic ligands for a better understanding of ligand receptor interactions on a molecular level. Here, linker dependent responses of bitopic ligands at a M_1 receptor FRET sensor were investigated. The findings indicate an optimal linker length of the bitopic ligands for conformational changes at the M_1 mAChR. This optimal linker length is probably different for each receptor subtype and is likely dependent on the individual receptor architecture.

Furthermore, a previously unknown conformational change for GPCRs induced by bitopic ligands of long linker length was observed. Furthermore, an understanding of the origin of different conformational changes of GPCRs is provided. The influences of the reported movements on the downstream signaling of GPCRs are subjects of current studies. Bitopic ligands were discussed critically in terms of whether the lipophilic linker can pass the aromatic lid of muscarinic receptors. Here, it could be shown that an increased linker first hampers the orthoster to induce a conformational change although there is a distinct affinity to the orthosteric binding region. This phenomenon might be due to a steric clash with the aromatic lid structure in muscarinic acetylcholine receptors. Moreover, the findings indicate that this fact is no longer true for the bitopic analogues, indicating that here the linker is able to interact with the aromatic lid without being sterically hindered.

3. Methods

3.1 Chemistry

Melting points were determined with a Stuart melting point apparatus SMP3 (Bibby Scientific) and are uncorrected. ^{1}H (400.132 MHz) and ^{13}C (100.613 MHz) NMR spectra were recorded on a Bruker AV 400 instrument (Bruker Biospin). As internal standard, the signals of the deuterated solvents were used (DMSO-d_6: ^{1}H 2.5 ppm, ^{13}C 39.52 ppm; $CDCl_3$: ^{1}H 7.26 ppm, ^{13}C 77.16 ppm). Abbreviation for data quoted are: s, singlet; d, doublet; t, triplet; q, quartet; m, multiplet; b, broad; dd, doublet of doublets; dt, doublet of triplets; tt, triplet of triplets; tq, triplet of quartets. Coupling constants (*J*) are given in Hertz. TLC analyses were performed on commercial precoated plates, silica gel 60 F_{254} (Macherey-Nagel); spots were further evidenced by spraying with Dragendorff reagent[36] for amines. ESI mass spectra of the compounds were obtained on an Agilent LC/MSD Trap G2445D instrument. Data are reported as mass-to-charge ratio (*m/z*) of the corresponding positively charged molecular ions. Microwave assisted reactions were carried out on a MLS-rotaPREP instrument (Milestone). Chemicals were of analytical grade and purchased from Aldrich and Merck.

The purities of the compounds (**2-C4**, **2-C6**, **2-C8**, and **2-C10**) were determined using qNMR and were found to be $\geq$95%.1,2,4,5-Tetrachloro-3-nitrobenzene (Sigma Aldrich) was chosen as internal standard. qNMR data were acquired at 90° pulse tip angles with recovery delays of 60 s and acquisition time of 3.7 s in a non-spinning mode at a calibrated probe temperature of 300 K. Sixteen scans of 64 K data points for FID were acquired with a spectral width of 8012 Hz (16 ppm). Manuel phase and baseline correction were performed prior to integration. Preliminary data processing was carried out with Bruker software, TOPSPIN 3.0. Purities of the compounds **1-C2**, **1-C6**, **1-C7**, **1-C8**, **1-C9**, **1-C10**, **5-C4**, and **6-**

C6 were determined using capillary electrophoresis and were found to be ≥95%. The CE measurements were performed by means of a Beckman Coulter P/ACE System MDQ (Fullerton), equipped with a diode array detector measuring at wavelengths of 210 nm and 254 nm. A fused silica capillary (effective length 50.0 cm, total length 60.2 cm, inner diameter 50 µm) was used for the separation. A new capillary was conditioned by rinsing for 30 min with 0.1 mol L^{-1} NaOH, 2 min with H_2O, 10 min with 0.1 mol L^{-1} HCl and 2 min with H_2O. Before each run the capillary was rinsed for 2 min with H_2O and 5 min with the running buffer. All rinsing steps were performed with a pressure of 30.0 psi. The samples were injected with a pressure of 0.5 psi for 5.0 s at the anodic side of the capillary. The capillary was kept at 25 °C and a voltage of +25 kV was applied. A 50 mM aqueous sodium borate, pH 10.5, was prepared as running buffer, using ultrapure Milli-Q water (Millipore). The aqueous solutions were filtered through a 0.22 µm pore-size CME (cellulose mix ester) filter (Carl Roth GmbH). Compounds **1-C4** and **6-C4** (confirming purity ≥95%) and compounds **5-C8** and **5-C10** (confirming purity ≥90%) were measured on an HPLC system (Agilent 1100 series system with UV detector) using a C18 reversed-phase (Knauer) (150 x 4.6 mm) column. The mobile phase (MeOH/phosphate buffer = 70/30) was used at a flow rate of 1.5 mL/min, detecting at 254 nm. The HPLC analyses of compounds **4-C4** (confirming purity ≥90%) **4-C6**, **4-C8**, **4-C10**, **6-C8**, and **6-C10** (confirming purity >95%) were performed on a LCMS 2020 Shimadzu. The LCMS system from Shimadzu Products contained a DGU-20A3R degassing unit, a LC20AB liquid chromatograph, and a SPD-20A UV/vis detector. Mass spectra were obtained by a LCMS 2020. As stationary phase, a Synergi 4U fusion-RP (150 * 4.6 mm) column and, as mobile phase, a gradient of MeOH/water was used. Parameters for the method: solvent A, water with 0.1% formic acid; solvent B, MeOH with 0.1% formic acid. Solvent B from 0% to 90% in 13 min, then at 90% for 5 min, from 90% to 5% in 1 min, and then 5% for 4 min. The method was performed with a flow rate of 1.0 mL/min. UV detection was measured at 254 nm.

The compounds **1-C3**, **1-C5**,[12] and **3**[25] as well as **9**, **10-C6**, **11-C6**, and **5-C6**[13] were prepared according to previously reported procedures. The synthesis of the 4-oxo-quinoline skeleton **8**[37,38] was performed in analogy to the Gould-Jacobs procedure, using diethyl 2-(ethoxymethylene)-malonate for the condensation with 4-fluoroaniline followed by microwave assisted cyclization in diphenyl ether.[22-24]

Scheme 3: Synthesis of quinolone analogues, BQCA/iperoxo hybrids and BQCA/ACh hybrids.

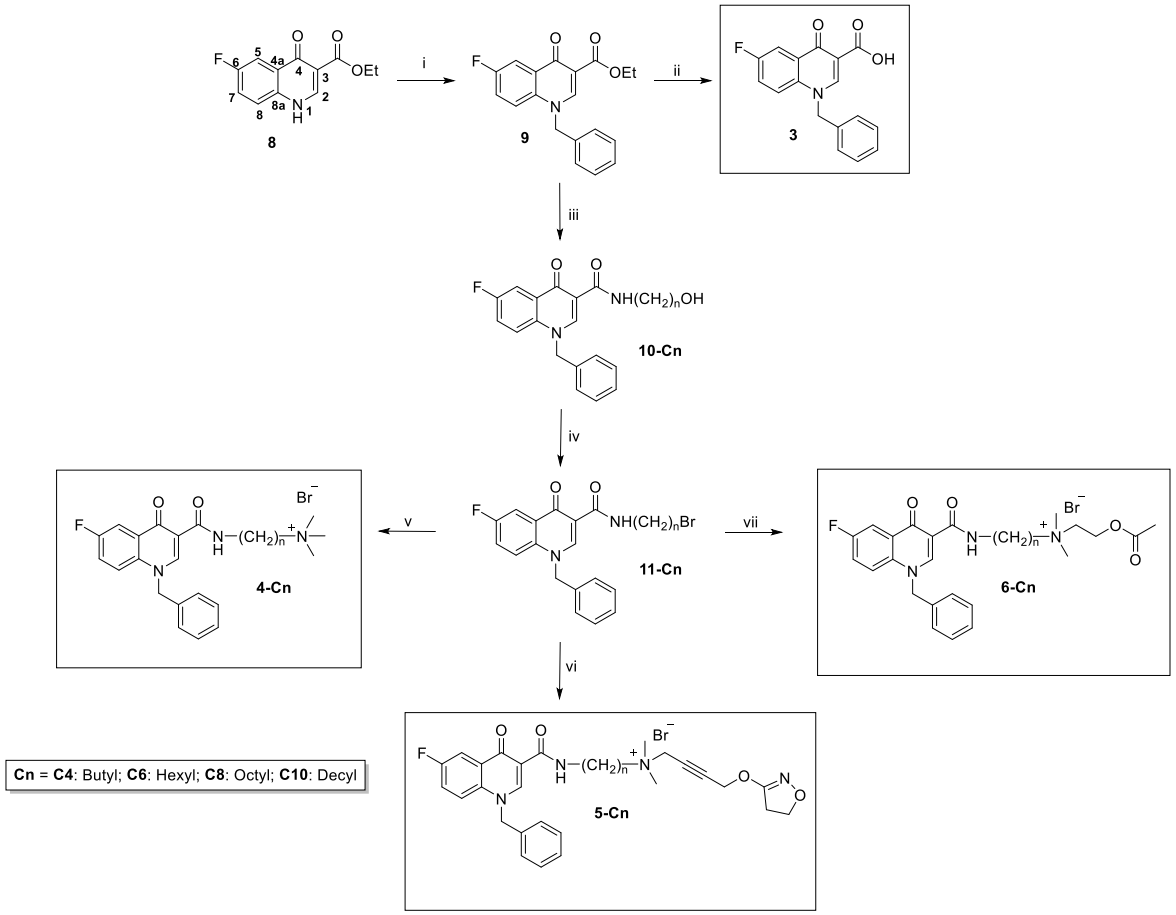

Reagents and conditions: (i) benzyl chloride, K_2CO_3, DMF, 80 °C (72%); (ii) 6 N HCl, MeOH, reflux (77%); (iii) $H_2N(CH_2)_nOH$, 150 °C (28-33%); (iv) HBr (48%), H_2SO_4, reflux (73-93%); (v) trimethylamine, CH_3CN, 40 °C (53-96%); (vi) **1**, KI/K_2CO_3, CH_3CN, 80 °C (microwave) (37-66%); (vii) **2**, KI/K_2CO_3, CH_3CN, 80 °C (microwave) (19-73%).

3.1.1 General procedure for the synthesis of the iperoxo analogues **1-C2**, **1-C4**, **1-C6**, **1-C7**, **1-C8**, **1-C9**, and **1-C10**

To a solution of 4-((4,5-dihydroisoxazol-3-yl)oxy)-*N*,*N*-dimethylbut-2-yn-1-amine[11] 0.45 g (2.47 mmol) in 10 mL of acetonitrile or chloroform, 5 - 10 equiv of the corresponding 1-bromoalkane **7-C2** to **7-C10** and a catalytic amount of KI/K_2CO_3 (1:1) were added. The mixture was stirred in a sealed container at a temperature between 55 and 70 °C. The precipitate obtained was filtered, and Et_2O was added to complete the precipitation. The solid was washed several times with Et_2O and dried over P_2O_5 *in vacuo*.

*4-((4,5-Dihydroisoxazol-3-yl)oxy)-N-ethyl-N,N-dimethylbut-2-yn-1-aminium bromide **1-C2***

Beige powder; 89% yield; mp 108-110 °C; ^{1}H NMR (DMSO): 1.26 (t, 3H, CH_2-C**H$_3$**, J = 7.2), 3.02 (t, 2H, **H**-4$_{2\text{-isox}}$, J = 9.6), 3.08 (s, 6H, $^+$N(C**H$_3$**)$_2$), 3.45 (m, 2H, N$^+$-C**H$_2$**-CH_3), 4.32 (t, 2H,

H-$5_{2\text{-isox}}$, *J* = 9.6), 4.50 (s, 2H, ≡C-C**H₂**-N^+), 4.93 (s, 2H, O-C**H₂**-C≡). ^{13}C NMR (DMSO): 7.8, 32.1, 49.1, 52.8, 57.1, 58.7, 69.5, 76.1, 85.7, 166.6. MS (ESI) m/z $[M]^+$ Calcd for $C_{11}H_{20}BrN_2O_2^+$ 211.3. Found: 221.2. CE purity 99.1%.

N-Butyl-4-((4,5-Dihydroisoxazol-3-yl)oxy)-N,N-dimethylbut-2-yn-1-aminium bromide ***1-C4***

White solid; 65% yield; mp 110-112 °C; ^{1}H NMR (DMSO): 0.93 (t, 3H, CH_2-C**H₃**, *J* = 7.5), 1.27-1.36 (m, 2H, CH_2-CH_2-C**H₂**-CH_3), 1.62-1.70 (m, 2H, CH_2-C**H₂**-CH_2-CH_3), 3.02 (t, 2H, **H**-$4_{2\text{-isox}}$, *J* = 9.5), 3.09 (s, 6H, $^+$N(C**H₃**)$_2$), 3.36-3.39 (m, 2H, N^+-C**H₂**-CH_2), 4.32 (t, 2H, **H**-$5_{2\text{-isox}}$, *J* = 9.47), 4.49 (s, 2H, ≡C-C**H₂**-N^+), 4.93 (s, 2H, O-C**H₂**-C≡). ^{13}C NMR (DMSO): 13.4, 19.1, 23.8, 32.2, 49.8, 53.3, 57.2, 63.0, 69.6, 76.2, 86.0, 166.7. MS (ESI) m/z $[M]^+$ Calcd for $C_{13}H_{23}N_2O_2^+$: 239.2. Found: 239.2. HPLC purity 96.1%.

N-(4-((4,5-Dihydroisoxazol-3-yl)oxy)but-2-yn-1-yl)-N,N-dimethylhexan-1-aminium bromide ***1-C6***

White solid, 85% yield; mp 121-122 °C; ^{1}H NMR (DMSO): 0.88 (t, 3H, CH_2-C**H₃**, *J* = 6.6), 1.30 (br, 6H, CH_2-CH_2-C**H₂**-C**H₂**-C**H₂**-CH_3), 1.62-1.73 (m, 2H, CH_2-C**H₂**-CH_2-CH_2-CH_2-CH_3), 3.01 (t, 2H, **H**-$4_{2\text{-isox}}$, *J* = 9.6), 3.09 (s, 6H, $^+$N(C**H₃**)$_2$), 3.33-3.38 (m, 2H, N^+-C**H₂**-CH_2), 4.32 (t, 2H, **H**-$5_{2\text{-isox}}$, *J* = 9.6), 4.48 (s, 2H, ≡C-C**H₂**-N^+), 4.93 (s, 2H, O-C**H₂**-C≡). ^{13}C NMR (DMSO): 13.7, 21.6, 21.7, 25.2, 30.5, 32.1, 49.7, 53.1, 57.1, 63.1, 69.5, 76.1, 85.8, 166.6. MS (ESI) m/z $[M]^+$ Calcd for $C_{15}H_{27}N_2O_2^+$: 267.2. Found: 267.3. CE purity 99.5%.

N-(4-((4,5-Dihydroisoxazol-3-yl)oxy)but-2-yn-1-yl)-N,N-dimethylheptan-1-aminium bromide ***1-C7***

White solid; 74% yield; mp 121-122 °C; ^{1}H NMR (DMSO): 0.87 (t, 3H, CH_2-C**H₃**, *J* = 6.8), 1.25-1.33 (br, 8H, CH_2-CH_2-C**H₂**-C**H₂**-C**H₂**-C**H₂**-CH_3), 1.63-1.72 (m, 2H, CH_2-C**H₂**-CH_2-CH_2-CH_2-CH_2-CH_3), 3.01 (t, 2H, **H**-$4_{2\text{-isox}}$, *J* = 9.6), 3.07 (s, 6H, $^+$N(C**H₃**)$_2$), 3.34-3.37 (m, 2H, N^+-C**H₂**-CH_2), 4.32 (t, 2H, **H**-$5_{2\text{-isox}}$, *J* = 9.6), 4.45 (s, 2H, ≡C-C**H₂**-N^+), 4.93 (s, 2H, O-C**H₂**-C≡). ^{13}C NMR (DMSO): 13.8, 20.8, 21.7, 21.9, 25.5, 28.0, 32.2, 49.7, 53.2, 57.1, 63.1, 69.5, 76.1, 85.9, 166.6. MS (ESI) m/z $[M]^+$ Calcd for $C_{16}H_{29}N_2O_2^+$: 281.2. Found: 281.3. CE purity 99.5%.

N-(4-((4,5-Dihydroisoxazol-3-yl)oxy)but-2-yn-1-yl)-N,N-dimethyloctan-1-aminium bromide ***1-C8***

White solid; 48% yield; mp 130-133 °C; ^{1}H NMR (DMSO): 0.87 (t, 3H, CH_2-C**H$_3$**, *J* = 6.9), 1.23-1.33 (br, 10H, CH_2-CH_2-C**H$_2$**-C**H$_2$**-C**H$_2$**-C**H$_2$**-C**H$_2$**-CH_3), 1.63-1.71 (m, 2H, CH_2-C**H$_2$**-CH_2-CH_2-CH_2-CH_2-CH_2-CH_3), 3.01 (t, 2H, **H**-$4_{2\text{-isox}}$, *J* = 9.6), 3.07 (s, 6H, $^{+}$N(C**H$_3$**)$_2$), 3.33-3.37 (m, 2H, N^{+}-C**H$_2$**-CH_2), 4.32 (t, 2H, **H**-$5_{2\text{-isox}}$, *J* = 9.6), 4.45 (s, 2H, ≡C-C**H$_2$**-N^{+}), 4.93 (s, 2H, O-C**H$_2$**-C≡). ^{13}C NMR (DMSO): 13.8, 21.7, 21.9, 25.6, 28.3, 31.0, 32.1, 49.7, 53.2, 57.1, 63.1, 69.5, 76.1, 85.9, 166.6. MS (ESI) m/z $[M]^{+}$ Calcd for $C_{17}H_{31}N_2O_2^{+}$: 295,2. Found: 295.3. CE purity 99.1%.

N-(4-((4,5-Dihydroisoxazol-3-yl)oxy)but-2-yn-1-yl)-N,N-dimethylnonan-1-aminium bromide ***1-C9***

White solid; 80% yield; mp 130-132 °C; ^{1}H NMR (DMSO): 0.86 (t, 3H, CH_2-C**H$_3$**, *J* = 6.7), 1.26 (br, 12H, CH_2-CH_2-C**H$_2$**-C**H$_2$**-C**H$_2$**-C**H$_2$**-C**H$_2$**-C**H$_2$**-CH_3), 1.62-1.71 (m, 2H, CH_2-C**H$_2$**-CH_2-CH_2-CH_2-CH_2-CH_2-CH_2-CH_3), 3.01 (t, 2H, **H**-$4_{2\text{-isox}}$, *J* = 9.6), 3.08 (s, 6H, $^{+}$N(C**H$_3$**)$_2$), 3.33-3.37 (m, 2H, N^{+}-C**H$_2$**-CH_2), 4.32 (t, 2H, **H**-$5_{2\text{-isox}}$, *J* = 9.6), 4.48 (s, 2H, ≡C-C**H$_2$**-N^{+}), 4.93 (s, 2H, O-C**H$_2$**-C≡). ^{13}C NMR (DMSO): 13.8, 21.7, 22.0, 25.6, 28.3, 28.6, 31.1, 32.1, 49.7, 53.2, 57.1, 63.1, 69.5, 76.1, 85.8, 166.6. MS (ESI) m/z $[M]^{+}$ Calcd for $C_{18}H_{33}N_2O_2^{+}$: 309.3. Found: 309.4. CE purity 98.8%.

N-(4-((4,5-Dihydroisoxazol-3-yl)oxy)but-2-yn-1-yl)-N,N-dimethyldecan-1-aminium bromide ***1-C10***

White solid; 83% yield; mp 135-137 °C; ^{1}H NMR (DMSO): 0.86 (t, 3H, CH_2-C**H$_3$**, *J* = 6.9), 1.26 (br, 14H, CH_2-CH_2-C**H$_2$**-C**H$_2$**-C**H$_2$**-C**H$_2$**-C**H$_2$**-C**H$_2$**-C**H$_2$**-CH_3), 1.67 (br, 2H, CH_2-C**H$_2$**-CH_2-CH_2-CH_2-CH_2-CH_2-CH_2-CH_2-CH_3), 3.01 (t, 2H, **H**-$4_{2\text{-isox}}$, *J* = 9.6), 3.08 (s, 6H, $^{+}$N(C**H$_3$**)$_2$), 3.33-3.37(m, 2H, N^{+}-C**H$_2$**-CH_2), 4.32 (t, 2H, **H**-$5_{2\text{-isox}}$, *J* = 9.6), 4.47 (s, 2H, ≡C-C**H$_2$**-N^{+}), 4.93 (s, 2H, O-C**H$_2$**-C≡). ^{13}C NMR (DMSO): 13.8, 21.7, 22.0, 25.6, 28.3, 28.5, 28.6, 28.7, 31.2, 32.1, 49.7, 53.1, 57.1, 63.1, 69.5, 76.1, 85.8, 166.6. MS (ESI) m/z $[M]^{+}$ Calcd for $C_{19}H_{35}N_2O_2^{+}$: 323.3. Found: 323.3 CE purity 99.8%.

3.1.2 General procedure for the synthesis of the acetylcholine analogues **2-C4**, **2-C6**, **2-C8**, and **2-C10**

To a solution of 2-(dimethylamino)ethyl acetate, 0.50 g (3.81 mmol) in acetonitrile (10 mL); 2 equiv of the corresponding 1-bromoalkane **7-C4**, **7-C6**, **7-C8**, and **7-C10** and a catalytic

amount of KI/K_2CO_3 (1:1) were added. The reaction mixture was heated in the microwave (500 W, 70 °C) for 4 h. After cooling to RT, the surplus of KI/K_2CO_3 was filtered, and the filtrate was evaporated to the half of the volume. After the addition of Et_2O, a viscous oil was formed. The solvent was decanted, and the product obtained was dried *in vacuo*.

N-(2-Acetoxyethyl)-N,N-dimethylbutan-1-aminium bromide ***2-C4***

White, viscose oil; yield 71%; ^{1}H NMR (DMSO): 0.93 (t, 3H, CH_2-C**H$_3$**, *J* = 7.2), 1.26-1.35 (m, 2H, CH_2-CH_2-C**H$_2$**-CH_3), 1.62-1.70 (m, 2H, CH_2-C**H$_2$**-CH_2-CH_3), 2.06 (s, 3H, CO-C**H$_3$**), 3.08 (s, 6H, $^+$N(C**H$_3$**)$_2$), 3.33-3.37 (m, 2H, $^+$N-C**H$_2$**-CH_2), 3.63-3.65 (m, 2H, C**H$_2$**-N$^+$), 4.42 (t, 2H, O-C**H$_2$**, *J* = 4.4). ^{13}C NMR (DMSO): 13.4, 19.1, 20.6, 23.6, 50.5, 57.4, 61.2, 63.6, 169.7. MS (ESI) m/z [M]$^+$ Calcd for $C_{10}H_{22}NO_2^+$: 188.2. Found: 188.2. qNMR purity 98.0%.

N-(2-Acetoxyethyl)-N,N-dimethylhexan-1-aminium bromide ***2-C6***

Transparent, viscose oil; yield 65%; ^{1}H NMR (DMSO): 0.88 (t, 3H, CH_2-C**H$_3$**, *J* = 6.8), 1.25-1.32 (m, 6H, CH_2-CH_2-C**H$_2$**-C**H$_2$**-C**H$_2$**-CH_3), 1.63-1.70 (m, 2H, CH_2-C**H$_2$**-CH_2-CH_2-CH_2-CH_3), 2.06 (s, 3H, CO-C**H$_3$**), 3.07 (s, 6H, $^+$N(C**H$_3$**)$_2$), 3.34-3.39 (m, 2H, $^+$N-C**H$_2$**-CH_2), 3.62-3.65 (m, 2H, C**H$_2$**-N$^+$), 4.41 (t, 2H, O-C**H$_2$**, *J* = 4,6). ^{13}C NMR (DMSO): 13.7, 20.6, 21.6, 21.7, 25.3, 30.6, 50.5, 57.4, 61.2, 63.8, 169.7. MS (ESI) m/z [M]$^+$ Calcd for $C_{12}H_{26}NO_2^+$: 216.2. Found: 216.2. qNMR purity 96.0%.

N-(2-Acetoxyethyl)-N,N-dimethyloctan-1-aminium bromide ***2-C8***

White, viscose oil; yield 91%; ^{1}H NMR (DMSO): 0.86 (t, 3H, CH_2-C**H$_3$**, *J* = 6.8), 1.26-1.29 (m, 10H, CH_2-CH_2-C**H$_2$**-C**H$_2$**-C**H$_2$**-C**H$_2$**-C**H$_2$**-CH_3), 1.63-1.70 (m, 2H, CH_2-C**H$_2$**-CH_2-CH_2-CH_2-CH_2-CH_2-CH_3), 2.05 (s, 3H, CO-C**H$_3$**), 3.08 (s, 6H, $^+$N(C**H$_3$**)$_2$), 3.33-3.37 (m, 2H, $^+$N-C**H$_2$**-CH_2), 3.63-3.66 (m, 2H, C**H$_2$**-N$^+$), 4.41 (t, 2H, O-C**H$_2$**, *J* = 4,6 Hz). ^{13}C NMR (DMSO): 13.8, 20.6, 21.6, 21.9, 25.6, 28.3, 31.0, 50.5, 57.4, 61.2, 63.8, 169.7. MS (ESI) m/z [M]$^+$ Calcd for $C_{14}H_{30}NO_2^+$: 244.2. Found: 244.3. qNMR purity 96.0%.

N-(2-Acetoxyethyl)-N,N-dimethyldecan-1-aminium bromide ***2-C10***

White, viscose oil; yield 88%; ^{1}H NMR (DMSO): 0.86 (t, 3H, CH_2-C**H$_3$**, *J* = 6.8), 1.26-1.28 (m, 14H, CH_2-CH_2-C**H$_2$**-C**H$_2$**-C**H$_2$**-C**H$_2$**-C**H$_2$**-C**H$_2$**-C**H$_2$**-CH_3), 1.63-1.70 (m, 2H, CH_2-C**H$_2$**-CH_2-CH_2-CH_2-CH_2-CH_2-CH_2-CH_2-CH_3), 2.05 (s, 3H, CO-C**H$_3$**), 3.07 (s, 6H, $^+$N(C**H$_3$**)$_2$), 3.32-3.35 (m,

2H, $^{+}$N-C**H$_2$**-CH$_2$), 3.62-3.64 (m, 2H, C**H$_2$**-N^{+}), 4.41 (t, 2H, O-C**H$_2$**, *J* = 4.6). ^{13}C NMR (DMSO): 13.8, 20.5, 21.6, 22.0, 25.6, 28.4, 28.5, 28.7, 28.8, 31.2, 50.5, 57.4, 61.2, 63.8, 169.7. MS (ESI) m/z [M]$^{+}$ Calcd for $C_{16}H_{34}NO_2^{+}$: 272.3. Found: 272.3. qNMR purity 96.0%.

3.1.3 General procedure for the amidation of **10-C4**, **10-C8**, and **10-C10**

1 equiv of ethyl 1-benzyl-6-fluoro-4-oxo-1,4-dihydroquinoline-3-carboxylate **9**[13] was reacted with 3 equiv of 4-aminobutanol, 8-aminooctanol, and 10-aminodecanol, respectively, and heated to 150 °C to melt the ester. The reaction was followed up by TLC (CH_2Cl_2/MeOH = 20:1, R_f = 0.35 – 0.54). After completion of the reaction (1.0 – 3.5 h), the mixture was cooled to RT. The so obtained solid was crystallized in ethanol and recrystallized from methanol.

1-Benzyl-6-fluoro-N-(4-hydroxybutyl)-4-oxo-1,4-dihydroquinoline-3-carboxamide ***10-C4***

White solid; yield 28%; mp 163-165 °C; R_f = 0.35 (CH_2Cl_2/MeOH = 20:1); ^{1}H NMR (DMSO): 1.47-1.61 (m, 4H, NH-CH$_2$-C**H$_2$**-C**H$_2$**), 3.34-3.46 (m, 4H, NH-C**H$_2$**/C**H$_2$**-OH), 4.42 (t, 1H, O**H**, *J* = 5.2), 5.80 (s, 2H, C**H$_2$**$_{benzyl}$), 7.21-7.24 (m, 2H, C**H**$_{phenyl}$), 7.27-7.37 (m, 3H, C**H**$_{phenyl}$), 7.67 (ddd, 1H, **H**-7, *J* = 3.1, J_{HF} = 8.0, *J* = 9.4), 7.84 (dd, 1H, **H**-8, J_{HF} = 4.3, *J* = 9.4), 7.99 (dd, 1H, **H**-5, *J* = 3.1, J_{HF} = 9.1), 9.08 (s, 1H, **H**-2), 9.88 (t, 1H, N**H**, *J* = 5.7). ^{13}C NMR (DMSO): 25.9, 29.9, 38.2, 56.0, 60.3, 110.5 (d, J_{CF} = 22.7), 110.7, 120.9 (d, J_{CF} = 8.4), 121.3 (d, J_{CF} = 25.0), 126.4, 127.9, 128.9, 128.9 (d, J_{CF} = 6.9), 135.7, 135.9, 148.7, 159.1 (d, J_{CF} = 245.3), 163.6, 174.7 (d, J_{CF} = 2.6).

1-Benzyl-6-fluoro-N-(8-hydroxyoctyl)-4-oxo-1,4-dihydroquinoline-3-carboxamide ***10-C8***

White solid; yield 28%; mp 154-156 °C; R_f = 0.54 (CH_2Cl_2/MeOH = 20:1); ^{1}H NMR (DMSO): 1.28-1.37 (m, 8H, NH-CH$_2$-CH$_2$-C**H$_2$**-C**H$_2$**-C**H$_2$**-C**H$_2$**), 1.39-1.42 (m, 2H, NH-CH$_2$-C**H$_2$**), 1.50-1.57 (m, 2H, C**H$_2$**-CH$_2$-OH), 3.33-3.39 (m, 4H, NH-C**H$_2$**/C**H$_2$**-OH), 4.30 (t, 1H, O**H**, *J* = 5.0), 5.80 (s, 2H, C**H$_2$**$_{benzyl}$), 7.21-7.23 (m, 2H, C**H**$_{phenyl}$), 7.27-7.37 (m, 3H, C**H**$_{phenyl}$), 7.67 (ddd, 1H, **H**-7, *J* = 3.1, J_{HF} = 8.0, *J* = 9.4), 7.84 (dd, 1H, **H**-8, J_{HF} = 4.4, *J* = 9.4), 7.99 (dd, 1H, **H**-5, *J* = 3.1, J_{HF} = 9.05), 9.08 (s, 1H, **H**-2), 9.87 (t, 1H, N**H**, ^3J = 5.6). ^{13}C NMR (DMSO): 25.4, 26.4, 28.7, 28.8, 29.2, 32.4, 38.3, 56.0, 60.6, 110.5 (d, J_{CF} = 22.4), 110.7, 120.9 (d, J_{CF} = 8.4), 121.3 (d, J_{CF} = 24.8), 126.4, 127.8, 128.9, 128.9 (d, J_{CF} = 7.2), 135.7, 135.8, 148.7, 159.1 (d, J_{CF} = 245.0), 163.6, 174.7 (d, J_{CF} = 2.5).

1-Benzyl-6-fluoro-N-(10-hydroxydecyl)-4-oxo-1,4-dihydroquinoline-3-carboxamide ***10-C10***

White solid; yield 31%; mp 152-154 °C; R_f = 0.37 (CH_2Cl_2/MeOH = 20:1); ^{1}H NMR (DMSO): 1.25-1.40 (m, 14H, NH-CH_2-C**H$_2$**-C**H$_2$**-C**H$_2$**-C**H$_2$**-C**H$_2$**-C**H$_2$**-C**H$_2$**), 1.50-1.55 (m, 2H, C**H$_2$**-CH_2-OH), 3.35-3.38 (m, 4H, NH-C**H$_2$**/C**H$_2$**-OH), 4.30 (t, 1H, O**H**, *J* = 5.0), 5.80 (s, 2H, C**H$_2$**$_{benzyl}$), 7.21-7.23 (m, 2H, C**H**$_{phenyl}$), 7.27-7.37 (m, 3H, C**H**$_{phenyl}$), 7.66 (ddd, 1H, **H**-7, *J* = 3.1, J_{HF} = 8.0, *J* = 9.4), 7.84 (dd, 1H, **H**-8, J_{HF} = 4.4, *J* = 9.4), 7.99 (dd, 1H, **H**-5, *J* = 3.1, J_{HF} = 9.05), 9.08 (s, 1H, **H**-2), 9.87 (t, 1H, N**H**, *J* = 5.6). ^{13}C NMR (DMSO): 25.4, 26.4, 28.6, 28.8, 28.9, 29.0, 29.1, 32.4, 38.3, 56.0, 60.6, 110.5 (d, J_{CF} = 22.9), 110.7, 120.9 (d, J_{CF} = 8.0), 121.3 (d, J_{CF} = 25.3), 126.4, 127.8, 128.9, 128.9 (d, J_{CF} = 6.8), 135.7, 135.8, 148.7, 159.1 (d, J_{CF} = 245.1), 163.6, 174.7 (d, J_{CF} = 2.6).

3.1.4 General procedure for the substitution of the alcohol group with a bromine group, compounds **11-C4**, **11-C8**, and **11-C10**

1 equiv of hydroxyalkyl fluoro substituted 4-oxo-quinolinecarboxamides **10-C4**, **10-C8**, and **10-C10**, respectively, were dissolved in 10 equiv of aqueous HBr (48%). Then, 4.2 equiv of conc. sulfuric acid was carefully added, and the reaction mixture was heated to reflux. The reaction was followed up by TLC (CH_2Cl_2/MeOH = 20:1, R_f = 0.81 – 0.95). After completion of the reaction (3.0 – 6.0 h), the solution was poured into water and extracted several times with chloroform. The combined organic phases were neutralized with K_2CO_3 and the solvent was evaporated to obtain the desired products.

1-Benzyl-N-(4-bromobutyl)-6-fluoro-4-oxo-1,4-dihydroquinoline-3-carboxamide ***11-C4***

White solid; yield 93%; mp 165-167 °C; R_f = 0.84 (CH_2Cl_2/MeOH = 20:1); ^{1}H NMR (DMSO): 1.64-1.71 (m, 2H, NH-CH_2-C**H$_2$**), 1.85-1.92 (m, 2H, NH-CH_2-CH_2-C**H$_2$**), 3.39 (dd, 2H, NH-C**H$_2$**, *J* = 6.9, *J* = 12.9), 3.59 (t, 2H, C**H$_2$**-Br, *J* = 6.7), 5.80 (s, 2H, C**H$_2$**$_{benzyl}$), 7.21-7.37 (m, 5H, C**H**$_{phenyl}$), 7.67 (ddd, 1H, **H**-7, *J* = 3.1, J_{HF} = 7.9, *J* = 9.4), 7.84 (dd, 1H, **H**-8, J_{HF} = 4.4, *J* = 9.4), 7.99 (dd, 1H, **H**-5, *J* = 3.1, J_{HF} = 9.1), 9.08 (s, 1H, **H**-2), 9.90 (t, 1H, N**H**, *J* = 5.8). ^{13}C NMR (DMSO): 28.0, 29.8, 34.7, 37.4, 56.0, 110.5 (d, J_{CF} = 22.7), 110.7, 120.9 (d, J_{CF} = 7.6), 121.3 (d, J_{CF} = 24.5), 126.4, 127.9, 128.9, 128.9 (d, J_{CF} = 7.0), 135.7, 135.9, 148.8, 159.1 (d, J_{CF} = 245.2), 163.8, 174.7 (d, J_{CF} = 2.5 Hz).

1-Benzyl-N-(8-bromooctyl)-6-fluoro-4-oxo-1,4-dihydroquinoline-3-carboxamide ***11-C8***

White solid; yield 88%; mp 168-171 °C; R_f = 0.81 (CH_2Cl_2/MeOH = 20:1); ^{1}H NMR (DMSO): 1.28-1.41 (m, 8H, NH-CH_2-CH_2-C**H$_2$**-C**H$_2$**-C**H$_2$**-C**H$_2$**), 1.51-1.57 (m, 2H, NH-CH_2-C**H$_2$**), 1.75-

1.82 (m, 2H, C**H₂**-CH₂-Br), 3.33-3.37 (m, 2H, NH-C**H₂**), 3.51 (t, 2H, C**H₂**-Br, *J* = 6.8), 5.80 (s, 2H, C**H₂**$_{benzyl}$), 7.21-7.37 (m, 5H, C**H**$_{phenyl}$), 7.66 (ddd, 1H, **H**-7, *J* = 3.1, J_{HF} = 8.0, *J* = 9.4), 7.84 (dd, 1H, **H**-8, J_{HF} = 4.4, *J* = 9.4), 7.99 (dd, 1H, **H**-5, *J* = 3.1, J_{HF} = 9.1), 9.08 (s, 1H, **H**-2), 9.87 (t, 1H, N**H**, *J* = 5.6 Hz). ^{13}C NMR (DMSO): 26.3, 27.4, 27.9, 28.4, 29.1, 33.1, 35.1, 38.2, 56.0, 110.4 (d, J_{CF} = 22.6), 110.7, 120.9 (d, J_{CF} = 8.4), 121.3 (d, J_{CF} = 24.9), 126.4, 127.8, 128.8, 128.9 (d, J_{CF} = 7.0), 135.7, 135.8, 148.7, 159.1 (d, J_{CF} = 245.2), 163.6, 174.7 (d, J_{CF} = 2.6).

1-Benzyl-N-(10-bromodecyl)-6-fluoro-4-oxo-1,4-dihydroquinoline-3-carboxamide ***11-C10***

White solid; yield 73%; mp 147-150 °C; R_f = 0.95 (CH_2Cl_2/MeOH = 20:1); ^{1}H NMR (DMSO): 1.26-1.35 (m, 12H, NH-CH₂-CH₂-C**H₂**-C**H₂**-C**H₂**-C**H₂**-C**H₂**-C**H₂**), 1.50-1.57 (m, 2H, NH-CH₂-C**H₂**), 1.73-1.80 (m, 2H, C**H₂**-CH₂-Br), 3.35-3.37 (m, 2H, NH-C**H₂**), 3.49 (t, 2H, C**H₂**-Br, *J* = 6.8), 5.80 (s, 2H, C**H₂**$_{benzyl}$), 7.21-7.37 (m, 5H, C**H**$_{phenyl}$), 7.66 (ddd, 1H, **H**-7, *J* = 3.1, J_{HF} = 8.0, *J* = 9.4), 7.84 (dd, 1H, **H**-8, J_{HF} = 4.4, *J* = 9.4), 7.99 (dd, 1H, **H**-5, *J* = 3.1, J_{HF} = 9.1), 9.08 (s, 1H, **H**-2), 9.87 (t, 1H, N**H**, *J* = 5.6). ^{13}C NMR (DMSO): 26.4, 27.4, 28.0, 28.5, 28.7, 28.7, 29.1, 32.1, 35.0, 38.3, 56.0, 110.5 (d, J_{CF} = 22.8), 110.7, 120.9 (d, J_{CF} = 8.4), 121.3 (d, J_{CF} = 25.2), 126.4, 127.8, 128.8, 128.9 (d, J_{CF} = 6.9), 135.7, 135.8, 148.7, 159.1 (d, J_{CF} = 244.9), 163.6, 174.7 (d, J_{CF} = 2.7).

3.1.5 General procedure for the synthesis of the quinolone analogues **4-C4**, **4-C6**, **4-C8**, and **4-C10**

To a solution of bromoalkyl 4-oxo-quinoline-3-carboxamides **11-C4**, **11-C6**, **11-C8**, and **11-C10** (0.11 mmol) in acetonitrile (5 mL), trimethylamine (45% in H_2O, 0.22 mmol) was added. The reaction was heated at 40 °C. After completion of the reaction (5 h) controlled by TLC (CH_2Cl_2/MeOH = 85:15, R_f = 0.10 – 0.45), the mixture was cooled to RT. The solvent was distilled off. The so obtained solid was crystallized from acetonitrile, filtered and dried *in vacuo*.

4-(1-Benzyl-6-fluoro-4-oxo-1,4-dihydroquinoline-3-carboxamido)-N,N,N-trimethylbutan-1-aminium bromide ***4-C4***

White solid; 53% yield; mp 176-179 °C; R_f = 0.18 (CH_2Cl_2/MeOH = 85:15); ^{1}H NMR (DMSO): 1.58-1.60 (m, 2H, NH-CH₂-C**H₂**), 1.74-1.78 (m, 2H, NH-CH₂-CH₂-C**H₂**), 3.06 (s, 9H, $^+$N(C**H₃**)₃), 3.33-3.45 (m, 4H, NH-C**H₂**/C**H₂**-N$^+$), 5.81 (s, 2H, C**H₂**$_{benzyl}$), 7.23-7.21 (m, 2H, C**H**$_{phenyl}$), 7.28-7.37 (m, 3H, C**H**$_{phenyl}$), 7.69 (ddd, 1H, **H**-7, *J* = 3.1, J_{HF} = 8.0, *J* = 9.4), 7.86 (dd,

1H, **H**-8, J_{HF} = 4.3, J = 9.4), 7.99 (dd, 1H, **H**-5, J = 3.1, J_{HF} = 9.0), 9.08 (s, 1H, **H**-2), 9.93 (t, 1H, N**H**, J = 5.8). ^{13}C NMR: (DMSO) 19.7, 26.2, 37.7, 52.1, 56.0, 64.8, 110.5, 110.6 (d, J_{CF} = 22.7), 121.0 (d, J_{CF} = 8.9), 121.5 (d, J_{CF} = 25.5), 126.4, 127.9, 128.9, 128.9, 135.6, 135.8, 148.7, 163.9, 169.7, 174.7 (d, J_{CF} = 2.5). MS (ESI) m/z $[M]^+$ Calcd for $C_{24}H_{29}FN_3O_2^+$: 410.2. Found: 410.1. LC purity 92.2%.

6-(1-Benzyl-6-fluoro-4-oxo-1,4-dihydroquinoline-3-carboxamido)-N,N,N-trimethylhexan-1-aminium bromide ***4-C6***

Ochre solid; 96% yield; mp 179-182 °C; R_f = 0.26 (CH_2Cl_2/MeOH = 85:15); ^{1}H NMR ($CDCl_3$): 1.48-1.49 (m, 4H, NH-CH_2-C**H₂**-C**H₂**), 1.64-1.68 (m, 2H, NH-CH_2-CH_2-CH_2-C**H₂**), 1.80-1.82 (m, 2H, C**H₂**-CH_2-N^+), 3.45 (s, 9H, $^+$N(C**H₃**)$_3$), 3.47-3.49 (m, 2H, NH-C**H₂**), 3.56-3.60 (m, 2H, C**H₂**-N^+), 5.51 (s, 2H, C**H₂**$_{benzyl}$), 7.14 (dd, 2H, C**H**$_{phenyl}$, J = 1.6, J = 7.7), 7.31-7.36 (m, 4H, C**H**$_{phenyl}$, **H**-8), 7.43 (dd, 1H, **H**-7, J = 4.2, J_{HF} = 9.4), 8.12 (dd, 1H, **H**-5, J = 3.0, J_{HF} = 8.8), 8.92 (s, 1H, **H**-2), 9.95 (t, 1H, N**H**, J = 5.7).^{13}C NMR: ($CDCl_3$) 22.9, 25.6, 26.3, 29.7, 38.7, 53.5, 58.1, 67.0, 111.9, 112.2 (d, J_{CF} = 22.8), 119.3 (d, J_{CF} = 7.9), 121.6 (d, J_{CF} = 25.4), 126.1, 128.8, 129.4, 134.0, 135.9, 148.4, 164.8, 167.2, 176.0 (d, J_{CF} = 2.7). MS (ESI) m/z $[M]^+$ Calcd for $C_{26}H_{33}FN_3O_2^+$: 438.3. Found: 438.1. LC purity 95.5%.

8-(1-Benzyl-6-fluoro-4-oxo-1,4-dihydroquinoline-3-carboxamido)-N,N,N-trimethyloctan-1-aminium bromide ***4-C8***

White solid; 53% yield; mp 185-187 °C; R_f = 0.10 (CH_2Cl_2/MeOH = 85:15); ^{1}H NMR (DMSO): 1.29-1.39 (m, 8H, NH-CH_2-CH_2-C**H₂**-C**H₂**-C**H₂**-C**H₂**), 1.55-1.58 (m, 2H, NH-CH_2-C**H₂**), 1.66-1.69 (m, 2H, C**H₂**-CH_2-N^+), 3.03 (s, 9H, N^+(C**H₃**)$_3$), 3.25-3.27 (m, 2H, NH-C**H₂**), 3.40-3.45 (m, 2H, C**H₂**-N^+), 5.81 (s, 2H, C**H₂**$_{benzyl}$), 7.20-7.24 (m, 2H, C**H**$_{phenyl}$), 7.30-7.38 (m, 3H, C**H**$_{phenyl}$), 7.69 (ddd, 1H, **H**-7, J = 3.1, J_{HF} = 8.0, J = 9.4), 7.86 (dd, 1H, **H**-8, J_{HF} = 4.4, J = 9.4), 7.99 (dd, 1H, **H**-5, J = 3.1, J_{HF} = 9.0), 9.07 (s, 1H, **H**-2), 9.89 (t, 1H, N**H**, J = 5.7). ^{13}C NMR (DMSO): 21.3, 25.0, 25.7, 27.7, 27.7, 28.5, 37.7, 51.5, 55.4, 64.6, 109.9, 110.1 (d, J_{CF} = 23.0), 120.4 (d, J_{CF} =8.1), 120.9 (d, J_{CF} = 24.8), 125.8, 127.3, 128.3, 128.3, 135.0, 135.2, 148.1, 163.1, 170.4, 174.2 (d, J_{CF} = 2.5). MS (ESI) m/z $[M]^+$ Calcd for $C_{28}H_{37}FN_3O_2^+$: 466.3. Found: 466.1. LC purity 95.5%.

10-(1-Benzyl-6-fluoro-4-oxo-1,4-dihydroquinoline-3-carboxamido)-N,N,N-trimethyldecan-1-aminium bromide ***4-C10***

White solid; 64% yield; mp 178-180 °C; R_f = 0.45 (CH_2Cl_2/MeOH = 8:2); ^{1}H NMR ($CDCl_3$) 1.31-1.42 (m, 12H, NH-CH_2-CH_2-C**H₂**-C**H₂**-C**H₂**-C**H₂**-C**H₂**-C**H₂**), 1.63-1.65 (m, 2H, NH-CH_2-C**H₂**), 1.73-1.76 (m, 2H, C**H₂**-CH_2-N^+), 3.46 (s, 9H, $^+$N(C**H₃**)$_3$), 3.47-3.55 (m, 4H, NH-C**H₂**/C**H₂**-N^+), 5.49 (s, 2H, C**H₂**$_{benzyl}$), 7.13-7.15 (dd, 2H, C**H**$_{phenyl}$, *J* = 1.7, *J* = 7.7), 7.31-7.35 (m, 4H, C**H**$_{phenyl}$/**H**-8), 7.40-7.44 (dd, 1H, **H**-7, *J* = 4.2, J_{HF} = 9.3), 8.15 (dd, 1H, **H**-5, *J* = 2.9, J_{HF} = 8.9), 8.93 (s, 1H, **H**-2), 9.92 (t, 1H, N**H**, *J* = 4.5). ^{13}C NMR ($CDCl_3$): 23.4, 26.4, 27.3, 29.3, 29.4, 29.5, 29.9, 30.0, 39.6, 53.8, 58.4, 67.6, 112.1, 112.5 (d, J_{CF} = 23.1), 119.5 (d, J_{CF} = 8.0), 121.8 (d, J_{CF} = 24.8), 126.4, 129.1, 129.7, 134.3, 136.1, 148.7, 164.9, 169.6, 176.3 (d, J_{CF} = 2.8). MS (ESI) m/z $[M]^+$ Calcd for $C_{30}H_{41}FN_3O_2^+$: 494.3. Found: 494.2. LC purity 97.8%.

3.1.6 General procedure for the synthesis of the quinolone-iperoxo hybrids **5-C4**, **5-C8**, and **5-C10**

To a solution of 1 equiv of the bromoalkyl 4-oxo-quinoline-3-carboxamides **11-C4**, **11-C8**, and **11-C10** in 20 mL acetonitrile, 2 equiv. 4-((4,5-dihydroisoxazol-3-yl)oxy)-*N*,*N*-dimethylbut-2-yn-1-amine[11] and a catalytic amount of KI/K_2CO_3 (1:1) were added. The reaction mixture was heated in the microwave (500 W, 80 °C) for 4 h. The reaction was monitored by TLC (MeOH/NH_4NO_2 (0.2 M) = 3:2, R_f = 0.54 – 0.68). After cooling to RT, the surplus of KI/K_2CO_3 was filtered. Et_2O was added to the filtrate to obtain a precipitation. The solid was filtered, washed with Et_2O, and dried *in vacuo*.

N-(4-(1-Benzyl-6-fluoro-4-oxo-1,4-dihydroquinoline-3-carboxamido)butyl)-4-((4,5-dihydroisoxazol-3-yl)oxy)-N,N-dimethylbut-2-yn-1-aminium bromide ***5-C4***

Beige solid; yield 37%; mp 94-101 °C; R_f = 0.54 (MeOH/NH_4NO_2 (0.2 M) = 3:2); ^{1}H NMR (DMSO): 1.57-1.63 (m, 2H, NH-CH_2-C**H₂**), 1.74-1.82 (m, 2H, NH-CH_2-CH_2-C**H₂**), 3.01 (t, 2H, **H**-4$_{2\text{-isox}}$, *J* = 9.6), 3.09 (s, 6H, $^+$N(C**H₃**)$_2$), 3.36-3.45 (m, 4H, NH-C**H₂**/C**H₂**-N^+), 4.31 (t, 2H, **H**-5$_{2\text{-isox}}$, *J* = 9.6), 4.45 (s, 2H, $^+$N-C**H₂**-C≡), 4.94 (s, 2H, ≡C-C**H₂**-O), 5.81 (s, 2H, C**H₂**$_{benzyl}$), 7.21-7.23 (m, 2H, C**H**$_{phenyl}$), 7.28-7.38 (m, 3H, C**H**$_{phenyl}$), 7.69 (ddd, 1H, **H**-7, *J* = 9.3, J_{HF} = 8.0, *J* = 3.1), 7.86 (dd, 1H, **H**-8, J_{HF} = 4.3, *J* = 9.5), 7.99 (dd, 1H, **H**-5, *J* = 3.0, J_{HF} = 9.0), 9.07 (s, 1H, **H**-2), 9.93 (t, 1H, N**H**, *J* = 5.7). ^{13}C NMR (DMSO): 19.5, 26.1, 32.1, 37.6, 49.8, 53.3, 56.0, 57.1, 62.8, 69.5, 76.0, 86.0, 110.4 (d, J_{CF} = 22.6), 110.6, 121.1 (d, J_{CF} = 8.4), 121.5 (d, J_{CF} = 24.8), 126.4, 127.9, 128.8, 128.9, 135.6, 135.9, 148.7, 159.1 (d, J_{CF} = 244.8), 163.9, 166.6, 175.4. MS (ESI) m/z $[M]^+$ Calcd for $C_{30}H_{34}FN_4O_4^+$: 533.3. Found: 533.4. CE purity 95.0%.

8-(1-Benzyl-6-fluoro-4-oxo-1,4-dihydroquinoline-3-carboxamido)-N-(4-((4,5-dihydroisoxazol-3-yl)oxy)but-2-yn-1-yl)-N,N-dimethyloctan-1-aminium bromide ***5-C8***

Beige solid; yield 60%; mp 112-118 °C; R_f = 0.56 (MeOH/NH_4NO_2 (0.2 M) = 3:2); ^{1}H NMR (DMSO): 1.28-1.39 (m, 8H, NH-CH_2-CH_2-C**H₂**-C**H₂**-C**H₂**-C**H₂**), 1.52-1.59 (m, 2H, NH-CH_2-C**H₂**), 1.67-1.73 (m, 2H, C**H₂**-CH_2-N^+), 3.00 (t, 2H, **H**-$4_{2\text{-isox}}$, *J* = 9.6), 3.08 (s, 6H, $^+$N(C**H₃**)$_2$), 3.35-3.37 (m, 4H, NH-C**H₂**/C**H₂**-N^+), 4.31 (t, 2H, **H**-$5_{2\text{-isox}}$, *J* = 9.6), 4.45 (s, 2H, $^+$N-C**H₂**-C≡), 4.93 (s, 2H, ≡C-C**H₂**-O), 5.81 (s, 2H, C**H₂**$_{benzyl}$), 7.21-7.38 (m, 5H, C**H**$_{phenyl}$), 7.68 (ddd, 1H, **H**-7, *J* = 9.3, J_{HF} = 8.0, *J* = 3.1), 7.85 (dd, 1H, **H**-8, J_{HF} = 4.0, *J* = 9.4), 7.98 (dd, 1H, **H**-5, *J* = 3.1, J_{HF} = 9.0), 9.07 (s, 1H, **H**-2), 9.88 (t, 1H, N**H**, *J* = 5.6). ^{13}C NMR (DMSO): 21.7, 25.5, 26.3, 28.2, 29.1, 32.2, 38.3, 49.7, 53.2, 56.0, 57.1, 64.8, 69.5, 76.0, 85.9, 110.4 (d, J_{CF} = 22.8), 110.7, 121.0, 121.5, 126.4, 127.9, 128.9, 128.9, 135.8, 148.7, 159.1 (d, J_{CF} = 245.3), 163.6, 166.6, 174.7. MS (ESI) m/z $[M]^+$ Calcd for $C_{34}H_{42}FN_4O_4^+$: 589.7. Found: 589.6. HPLC purity 91.1%.

10-(1-Benzyl-6-fluoro-4-oxo-1,4-dihydroquinoline-3-carboxamido)-N-(4-((4,5-dihydroisoxazol-3-yl)oxy)but-2-yn-1-yl)-N,N-dimethyldecan-1-aminium bromide ***5-C10***

Beige solid; yield 44%; mp 107-109 °C; R_f = 0.68 (MeOH/NH_4NO_2 (0.2 M) = 3:2); ^{1}H NMR (DMSO): 1.22-1.39 (m, 12H, NH-CH_2-CH_2-C**H₂**-C**H₂**-C**H₂**-C**H₂**-C**H₂**-C**H₂**), 1.53-1.56 (m, 2H, NH-CH_2-C**H₂**), 1.65-1.67 (m, 2H, C**H₂**-CH_2-N^+), 3.00 (t, 2H, **H**-$4_{2\text{-isox}}$, *J* = 9.6), 3.07 (s, 6H, $^+$N(C**H₃**)$_2$), 3.35-3.37 (m, 4H, NH-C**H₂**/C**H₂**-N^+), 4.31 (t, 2H, **H**-$5_{2\text{-isox}}$, *J* = 9.6), 4.44 (s, 2H, $^+$N-C**H₂**-C≡), 4.93 (s, 2H, ≡C-C**H₂**-O), 5.81 (s, 2H, C**H₂**$_{benzyl}$), 7.21-7.37 (m, 5H, C**H**$_{phenyl}$), 7.68 (ddd, 1H, **H**-7, *J* = 9.3, J_{HF} = 8.0, *J* = 3.1), 7.85 (dd, 1H, **H**-8, J_{HF} = 4.0, *J* = 9.4), 7.98 (dd, 1H, **H**-5, *J* = 3.1, J_{HF} = 9.0), 9.07 (s, 1H, **H**-2), 9.87 (t, 1H, N**H**, *J* = 5.6). ^{13}C NMR (DMSO): 21.7, 25.5, 26.5, 28.3, 28.6, 28.7, 29.1, 32.2, 38.3, 49.7, 53.2, 56.0, 57.1, 63.1, 69.5, 76.0, 85.9, 110.7, 110.8, 121.0, 121.2, 126.4, 127.9, 128.9, 128.9, 135.7, 135.8, 148.7, 160.3, 163.6, 166.6, 174.7. MS (ESI) m/z $[M]^+$ Calcd for $C_{36}H_{46}FN_4O_4^+$: 617.8. Found: 617.7. HPLC purity 93.1%.

3.1.7 General procedure for the synthesis of the quinolone-acetylcholine hybrids **6-C4**, **6-C6**, **6-C8**, and **6-C10**

To a solution of 1 equiv of the bromoalkyl 4-oxo-quinoline-3-carboxamides **11-C4**, **11-C8**, and **11-C10** in 15 mL acetonitrile, 2 equiv 2-(dimethylamino)ethyl acetate and a catalytic amount of KI/K_2CO_3 (1:1) were added. The reaction mixture was heated in the microwave (500 W, 80 °C) for 4.0 – 6.5 h. After cooling to RT, the surplus of KI/K_2CO_3 was filtered, and

Et_2O was added to the filtrate. The solid obtained was filtered, washed with Et_2O, and dried *in vacuo*.

N-(2-Acetoxyethyl)-4-(1-benzyl-6-fluoro-4-oxo-1,4-dihydroquinoline-3-carboxamido)-N,N-dimethylbutan-1-aminium bromide ***6-C4***

White solid; yield 73%; mp 153-156 °C; ^{1}H NMR (DMSO): 1.56-1.63 (m, 2H, NH-CH_2-C**H$_2$**), 1.73-1.81 (m, 2H, NH-CH_2-CH_2-C**H$_2$**), 2.06 (s, 3H, C**H$_3$**), 3.09 (s, 6H, $^+$N(C**H$_3$**)$_2$), 3.40-3.44 (m, 4H, NH-C**H$_2$**/C**H$_2$**-N$^+$), 3.63-3.66 (m, 2H, C**H$_2$**-CH_2-O), 4.43 (t, 2H, C**H$_2$**-O, *J* = 4.6), 5.81 (s, 2H, C**H$_2$**$_{benzyl}$), 7.21-7.38 (m, 5H, C**H**$_{phenyl}$), 7.69 (ddd, 1H, **H**-7, *J* = 3.1, *J* = 8.0, *J* = 9.4), 7.86 (dd, 1H, **H**-8, *J* = 4.3, *J* = 9.4), 7.98 (dd, 1H, **H**-5, *J* = 3.0, *J* = 9.0), 9.08 (s, 1H, **H**-2), 9.93 (t, 1H, N**H**, *J* = 5.8). ^{13}C NMR (DMSO): 19.4, 20.5, 26.2, 37.7, 50.6, 56.0, 57.4, 61.4, 63.4, 110.4 (d, J_{CF} = 22.6), 110.6, 121.0 (d, J_{CF} = 8.2), 121.5, 126.4, 127.9, 128.9, 128.9, 135.6, 135.8, 148.7, 159.1 (d, J_{CF} = 245.6), 163.9, 169.7, 174.7 (d, J_{CF} = 2.3). MS (ESI) m/z [M]$^+$ Calcd for $C_{27}H_{33}FN_3O_4^+$: 482.2. Found: 482.2. HPLC purity 95.0%.

N-(2-Acetoxyethyl)-6-(1-benzyl-6-fluoro-4-oxo-1,4-dihydroquinoline-3-carboxamido)-N,N-dimethylhexan-1-aminium bromide ***6-C6***

White solid; yield 19%; mp 184-188 °C; ^{1}H NMR (DMSO): 1.34-1.46 (m, 4H, NH-CH_2-CH_2-C**H$_2$**-C**H$_2$**), 1.55-1.62 (m, 2H, NH-CH_2-C**H$_2$**), 1.67-1.75 (m, 2H, C**H$_2$**-CH_2-N$^+$), 2.05 (s, 3H, C**H$_3$**), 3.08 (s, 6H, $^+$N(C**H$_3$**)$_2$), 3.33-3.39 (m, 4H, NH-C**H$_2$**/C**H$_2$**-N$^+$), 3.64 (t, 2H, C**H$_2$**-CH_2-O, *J* = 4.8), 4.42 (t, 2H, C**H$_2$**-O, *J* = 4.4), 5.81 (s, 2H, C**H$_2$**$_{benzyl}$), 7.22-7.37 (m, 5H, C**H**$_{phenyl}$), 7.68 (ddd, 1H, **H**-7, *J* = 3.1, *J* = 8.0, *J* = 9.3), 7.86 (dd, 1H, **H**-8, *J* = 4.3, *J* = 9.4), 7.98 (dd, 1H, **H**-5, *J* = 3.0, *J* = 9.0), 9.07 (s, 1H, **H**-2), 9.89 (t, 1H, N**H**, *J* = 5.6). ^{13}C NMR (DMSO): 20.6, 21.6, 25.4, 25.9, 28.9, 38.1, 50.5, 56.0, 57.4, 61.3, 63.8, 110.4 (d, J_{CF} = 22.8), 110.7, 121.0 (d, J_{CF} = 8.1), 121.4 (d, J_{CF} = 24.8), 126.4, 127.9, 128.9, 128.9, 135.6, 135.8, 148.7, 159.1 (d, J_{CF} = 245.0), 163.7, 169.7, 174.7 (d, J_{CF} = 2.3). MS (ESI) m/z [M]$^+$ Calcd for $C_{29}H_{37}FN_3O_4^+$: 510.3. Found: 510.4. CE purity 95.3%.

N-(2-Acetoxyethyl)-8-(1-benzyl-6-fluoro-4-oxo-1,4-dihydroquinoline-3-carboxamido)-N,N-dimethyloctan-1-aminium bromide ***6-C8***

White solid; yield 39%; mp 163-166 °C; ^{1}H NMR (DMSO): 1.29-1.35 (m, 8H, NH-CH_2-CH_2-C**H$_2$**-C**H$_2$**-C**H$_2$**-C**H$_2$**), 1.54-1.55 (m, 2H, NH-CH_2-C**H$_2$**), 1.65-1.72 (m, 2H, C**H$_2$**-CH_2-N$^+$), 2.05 (s, 3H, C**H$_3$**), 3.08 (s, 6H, $^+$N(C**H$_3$**)$_2$), 3.34-3.37 (m, 4H, NH-C**H$_2$**/C**H$_2$**-N$^+$), 3.64 (t, 2H, C**H$_2$**-CH_2-O, *J* = 4.8), 4.42 (t, 2H, C**H$_2$**-O, *J* = 4.6), 5.81 (s, 2H, C**H$_2$**$_{benzyl}$), 7.22-7.37 (m, 5H,

C**H**$_{phenyl}$), 7.67 (ddd, 1H, **H**-7, *J* = 3.1, *J* = 8.0, *J* = 9.4), 7.86 (dd, 1H, **H**-8, *J* = 4.4, *J* = 9.4), 7.98 (dd, 1H, **H**-5, *J* = 3.1, *J* = 9.0), 9.07 (s, 1H, **H**-2), 9.88 (t, 1H, N**H**, *J* = 5.6). ^{13}C NMR (DMSO): 20.6, 21.6, 25.6, 26.3, 28.3, 28.4, 29.1, 38.2, 50.5, 56.0, 57.4, 61.3, 63.8, 110.4 (d, J_{CF} = 22.8), 110.7, 121.0 (d, J_{CF} = 7.8), 121.3 (d, J_{CF} = 25.1), 126.4, 127.9, 128.8, 128.9, 135.6, 135.8, 148.7, 159.1 (d, J_{CF} = 245.2), 163.6, 169.7, 174.7 (d, J_{CF} = 2.4). MS (ESI) m/z $[M]^+$ Calcd for $C_{31}H_{41}FN_3O_4^+$: 538.3. Found: 538.5. LC purity 97.6%.

N-(2-Acetoxyethyl)-10-(1-benzyl-6-fluoro-4-oxo-1,4-dihydroquinoline-3-carboxamido)-N,N-dimethyldecan-1-aminium bromide ***6-C10***

White solid; yield 63%; mp 122-126 °C; ^{1}H NMR (DMSO): 1.27-1.33 (m, 12H, NH-CH_2-CH_2-C**H$_2$**-C**H$_2$**-C**H$_2$**-C**H$_2$**-C**H$_2$**-C**H$_2$**), 1.51-1.58 (m, 2H, NH-CH_2-C**H$_2$**), 1.63-1.71 (m, 2H, C**H$_2$**-CH_2-N^+), 2.05 (s, 3H, C**H$_3$**), 3.06 (s, 6H, $^+$N(C**H$_3$**)$_2$), 3.31-3.37 (m, 4H, NH-C**H$_2$**/C**H$_2$**-N^+), 3.60-3.63 (m, 2H, C**H$_2$**-CH_2-O), 4.41 (t, 2H, C**H$_2$**-O, *J* = 4.6), 5.81 (s, 2H, C**H$_2$**$_{benzyl}$), 7.21-7.38 (m, 5H, C**H**$_{phenyl}$), 7.68 (ddd, 1H, **H**-7, *J* = 3.1, *J* = 7.9, *J* = 9.4), 7.85 (dd, 1H, **H**-8, *J* = 4.4, *J* = 9.4), 7.98 (dd, 1H, **H**-5, *J* = 3.1, *J* = 9.0), 9.07 (s, 1H, **H**-2), 9.87 (t, 1H, N**H**, *J* = 5.6). ^{13}C NMR (DMSO): 20.5, 21.6, 25.6, 26.5, 28.4, 28.6, 28.6, 28.7, 29.1, 38.3, 50.5, 56.0, 57.4, 61.2, 63.8, 110.3, 110.5 (d, J_{CF} = 23.0), 110.7, 120.9 (d, J_{CF} = 6.9), 121.3 (d, J_{CF} = 24.4), 126.4, 127.9, 128.9, 128.9, 135.6, 135.8, 148.7, 157.9 (d, J_{CF} = 243.8), 163.7, 169.7, 174.7 (d, J_{CF} = 2.4). MS (ESI) m/z $[M]^+$ Calcd for $C_{33}H_{45}FN_3O_4^+$: 566.3. Found: 566.5. LC purity 100.0%.

3.2 Pharmacology

3.2.1 Construction of the *h*M_1 receptor FRET sensor

A muscarinic ACh receptor construct was C-terminally fused to the enhanced variants of cyan fluorescent protein (eCFP; BD Bioscience Clontech) by standard PCR extension overlap technique.[39] The amino acid sequence SR, coding for an Xba I restriction site, was inserted as a linker sequence between receptor and fluorescent protein. In the third intracellular loop (IL3), an amino acid motif was introduced; thus the novel sequence reads QG227CCPGCCSGS228E. It specifically binds the fluorescein arsenical hairpin binder (FlAsH) and codes for a restriction site. The construct was cloned into pcDNA3 (Invitrogen) and verified by sequencing, done by Eurofins Genomics.

3.2.2 Stable cell line generation

Cells were seeded into a culture dish with a confluency of 30% 3 h before transfecting the cells with the Effectene reagent ordered from Quiagene. Reagent concentration and incubation times were applied in accordance with the manufacturer's instructions. Twenty-four hours after transfecting, the normal culture medium was replaced by culture medium supplemented with 400 µg mL^{1} G-418. After that, the medium was refreshed every day until all untransfected cells died. Now the cells were counted, diluted, and applied to 48-well plates, resulting in a one cell to well distribution. This homogenous cell population were characterized with fluorescence microscopy and were investigated concerning their cDNA content.

3.2.3 Cell culture

HEK293 cells stably expressing the *h*M_1 receptor FRET sensor were maintained in DMEM with 4.5 g l^{-1} 10% (v/v) FCS, 100 U mL^{-1} penicillin, 100 µg mL^{-1} streptomycin sulfate and 2 mM L-glutamine, and 200 µg mL^{-1} G-418. The cells were kept at 37 °C in a humidified 7% CO_2 atmosphere and were routinely passaged every 2 to 3 days. Untransfected HEK cells were maintained in cell culture medium without G-418.

3.2.4 FlAsH labeling

A labeling protocol was applied as described previously.[15,40,41] In brief, cells were grown to near confluency on poly-D-lysine coated glass coverslips. Initially, cells were washed with labeling buffer (150 mM NaCl, 10 mM HEPES, 2.5 mM KCl, 4 mM $CaCl_2$, 2mM $MgCl_2$ supplemented with 10 mM glucose (pH 7.3)). After that, cells were incubated with labeling buffer containing 500 nM FlAsH and 12.5 µM 1,2-ethanedithiol (EDT) for 1 h at 37 °C followed by flushing with labeling buffer. To reduce nonspecific FlAsH binding, the cells were incubated for 10 min with labeling buffer containing 250 µM EDT. After flushing with labeling buffer, the cells were held in cell culture medium.

3.2.5 Description of calcium/DAG determination using confocal microscopy

To evaluate the effect of the six amino acid insertion into the M_1-CFP receptor we used a dual fluorescence probe from Montana Molecular (downward DAG2/R Geco)[29]. This fluorescence probe is composed of two sensors, fused in frame on both sides of a 2A

peptide sequence: first, a DAG sensor, which consist of a cpGFP fused to the C1 domain of a PKC; second, the red calcium sensor R-GECO. This dual sensor responds with an increase in red fluorescence intensity upon increase in Ca^{2+} and a decrease in green fluorescence upon binding to diacylglycerol (DAG). Therefore, the probe can specifically report on the activation of the Gq-signalling pathway. The dual fluorescent probe was used in HEK293 cells either alone or co-expressed with the M_1-CFP or the novel M_1-I3N-CFP sensor. In brief, round 24 mm cover slips were placed in six-well plates and coated for 20 min using 200µl of poly-d-lysine (1 mg/ml). After washing with sterile PBS, HEK293 cells stably expressing the calcium sensor were seeded onto these cover slips. Cells were transfected 3-4 hours later using Effectene (Quiagen), according to the manufacturer's instructions. For transfection, 500 ng DNA per well of each receptor construct were used, and cell culture medium was exchanged 16–18 h later. Analysis of the cells was done 48 h after transfection.

3.2.6 Confocal microscopy analysis and quantification of cell responses

48 h after transfection cells were placed in an Attofluor holder (Molecular probes), maintained in imaging buffer and analyzed using LeicaSP8 microscope equipped with four detection channels. CFP was excited using 440 nm line and emission was detected from 470-530nm; GFP was excited using the 488 nm line and detected from 510-560 nm; R-GECO was excited at 562 nm and detected from 610-660 nm. Time series were taken using 512*512 resolution and sequential scan mode, leading to total image acquisition times of 1.290 sec. Cells were monitored for 200 frames. After 15 seconds cells were stimulated by addition of 100 µM carbachol and analyzed for their agonist response. The dual probe did not respond to carbachol if no receptor was co-transfected. Fluorescence data were acquired using the Leica software. Only cell expressing CFP tagged receptors were used for analysis. Off line analysis was performed using Origin software. To account for none homogenous cell response due to bath application of carbachol, individual cell responses were manually aligned to the first time frame showing an increase in R-GECO and averaged after alignment.

3.2.7 Ligand application

The reference ligands were prepared from 1 mM stock solutions that were stored at -20 °C, taking into consideration that at least acetylcholine remains unstable in solution.[42] Used stock solutions have not been older than a couple of weeks. Bitopic ligands or analogues were stored at 4 °C and were weighed out directly before the experiment. Then, the ligands were

solubilized in measuring buffer (140 mM NaCl, 10 mM HEPES, 5.4 mM KCl, 2 mM $CaCl_2$, 1 mM $MgCl_2$ (pH 7.3)) to a final concentration of 100 µM.

3.2.8 Single cell FRET experiments

FRET measurements were performed using a Zeiss Axiovert 200 inverted microscope endued with a PLAN-Neoflar oil immersion 100 objective, a dual emission photometric system, and a Polychrome IV light source (Till Photonica) as described previously.[15,14] Experiments were conducted at 25 °C using live HEK293 cells stably expressing the *h*M_1 receptor FRET sensor or the previously published *h*M_3 receptor FRET sensor[26] that was maintained in an assay buffer. Single cells were excited at 436 nm (dichroic 460 nm) with a frequency of 10 Hz. Emitted light was recorded using 535/30 nm and 480/40 nm emission filters and a DCLP 505 nm beam splitter for FlAsH and CFP, respectively. FRET was observed as the ratio of FlAsH/CFP, which was corrected offline for bleed-through, direct FlAsH excitation, and photo-bleaching using the 2015 version of the Origin software as described recently. To investigate changes in FRET on ligand addition, cells were continuously super fused with FRET buffer complemented with various ligands in saturating concentrations as indicated. Superfusion was done using the ALA-VM8 (ALA Scientific Instruments).

3.2.9 Data processing

Data are shown as means ± SD for n independent observations. Fluorescence intensities were acquired using Clampex (Axon Instruments). Statistical analysis and curve fitting were performed using Origin (OriginLab).

Acknowledgments

M.K and D.V. were supported by the international doctoral college “Receptor Dynamics: Emerging Paradigms for Novel Drugs” funded within the framework of the Elite Network of Bavaria. M.C.A.C. was supported by the Marie Curie Initial Training Networks (ITN) “WntsApp” grant agreement number 608180. We thank Montana Molecular and Dr. Anne Marie Quinn for technical support and help to use the dual sensor.

References

[1] Wess, J. (2004) Muscarinic acetylcholine receptor knockout mice: novel phenotypes and clinical implications, *Annu. Rev. Pharmacol. Toxicol. 44*, 423-450.

[2] Kruse, A. C., Kobilka, B. K., Gautam, D., Sexton, P. M., Christopoulos, A., and Wess, J. (2014) Muscarinic acetylcholine receptors: novel opportunities for drug development, *Nat. Rev. Drug. Discov. 13*, 549-560.

[3] Thal, D. M., Sun, B., Feng, D., Nawaratne, V., Leach, K., Felder, C. C., Bures, M. G., Evans, D. A., Weis, W. I., Bachhawat, P., Kobilka, T. S., Sexton, P. M., Kobilka, B. K., and Christopoulos, A. (2016) Crystal structures of the M1 and M4 muscarinic acetylcholine receptors, *Nature 531*, 335-340.

[4] Spalding, T. A. (2002) Discovery of an Ectopic Activation Site on the M1 Muscarinic Receptor, *Mol. Pharmacol. 61*, 1297-1302.

[5] De Amici, M., Dallanoce, C., Holzgrabe, U., Tränkle, C., and Mohr, K. (2010) Allosteric ligands for G protein-coupled receptors: a novel strategy with attractive therapeutic opportunities, *Med. Res. Rev. 30*, 463-549.

[6] Mistry, S. N., Valant, C., Sexton, P. M., Capuano, B., Christopoulos, A., and Scammells, P. J. (2013) Synthesis and pharmacological profiling of analogues of benzyl quinolone carboxylic acid (BQCA) as allosteric modulators of the M1 muscarinic receptor, *J. Med. Chem. 56*, 5151-5172.

[7] Kuduk, S. D., Chang, R. K., Di Marco, C. N., Ray, W. J., Ma, L., Wittmann, M., Seager, M. A., Koeplinger, K. A., Thompson, C. D., Hartman, G. D., and Bilodeau, M. T. (2010) Quinolizidinone carboxylic acids as CNS penetrant, selective m1 allosteric muscarinic receptor modulators, *ACS Med. Chem. Lett. 1*, 263-267.

[8] Davie, B. J., Valant, C., White, J. M., Sexton, P. M., Capuano, B., Christopoulos, A., and Scammells, P. J. (2014) Synthesis and pharmacological evaluation of analogues of benzyl quinolone carboxylic acid (BQCA) designed to bind irreversibly to an allosteric site of the M (1) muscarinic acetylcholine receptor, *J. Med. Chem. 57*, 5405-5418.

[9] Ma, L., Seager, M. A., Wittmann, M., Jacobson, M., Bickel, D., Burno, M., Jones, K., Graufelds, V. K., Xu, G., Pearson, M., McCampbell, A., Gaspar, R., Shughrue, P., Danziger, A., Regan, C., Flick, R., Pascarella, D., Garson, S., Doran, S., Kreatsoulas, C., Veng, L., Lindsley, C. W., Shipe, W., Kuduk, S., Sur, C., Kinney, G., Seabrook, G. R., and Ray, W. J. (2009) Selective activation of the M1 muscarinic acetylcholine receptor achieved by allosteric potentiation, *Proc. Natl. Acad. Sci. U. S. A. 106*, 15950-15955.

[10] Mohr, K., Schmitz, J., Schrage, R., Tränkle, C., and Holzgrabe, U. (2013) Molecular alliance-from orthosteric and allosteric ligands to dualsteric/bitopic agonists at G protein coupled receptors, *Angew. Chem. Int. Ed. Engl. 52*, 508-516.

[11] Kloeckner, J., Schmitz, J., and Holzgrabe, U. (2010) Convergent, short synthesis of the muscarinic superagonist iperoxo, *Tetrahedron Lett. 51*, 3470-3472.

[12] Schrage, R., Seemann, W. K., Kloeckner, J., Dallanoce, C., Racke, K., Kostenis, E., De Amici, M., Holzgrabe, U., and Mohr, K. (2013) Agonists with supraphysiological efficacy at the muscarinic M2 ACh receptor, *Br. J. Pharmacol. 169*, 357-370.

[13] Chen, X., Kloeckner, J., Holze, J., Zimmermann, C., Seemann, W. K., Schrage, R., Bock, A., Mohr, K., Tränkle, C., Holzgrabe, U., and Decker, M. (2015) Rational design of partial agonists for the muscarinic m1 acetylcholine receptor, *J. Med. Chem. 58*, 560-576.

[14] Vilardaga, J. P., Bünemann, M., Krasel, C., Castro, M., and Lohse, M. J. (2003) Measurement of the millisecond activation switch of G protein-coupled receptors in living cells, *Nat. Biotechnol. 21*, 807-812.

[15] Hoffmann, C., Gaietta, G., Bünemann, M., Adams, S. R., Oberdorff-Maass, S., Behr, B., Vilardaga, J. P., Tsien, R. Y., Ellisman, M. H., and Lohse, M. J. (2005) A FlAsH-based FRET approach to determine G protein-coupled receptor activation in living cells, *Nat. Methods 2*, 171-176.

[16] Stumpf, A. D., and Hoffmann, C. (2016) Optical probes based on G protein-coupled receptors - added work or added value?, *Br. J. Pharmacol. 173*, 255-266.

[17] Vilardaga, J. P., Bünemann, M., Feinstein, T. N., Lambert, N., Nikolaev, V. O., Engelhardt, S., Lohse, M. J., and Hoffmann, C. (2009) GPCR and G proteins: drug efficacy and activation in live cells, *Mol. Endocrinol. 23*, 590-599.

[18] Lohse, M. J., Nuber, S., and Hoffmann, C. (2012) Fluorescence/bioluminescence resonance energy transfer techniques to study G-protein-coupled receptor activation and signaling, *Pharmacol. Rev. 64*, 299-336.

[19] Kruse, A. C., Ring, A. M., Manglik, A., Hu, J. X., Hu, K., Eitel, K., Hübner, H., Pardon, E., Valant, C., Sexton, P. M., Christopoulos, A., Felder, C. C., Gmeiner, P., Steyaert, J., Weis, W. I., Garcia, K. C., Wess, J., and Kobilka, B. K. (2013) Activation and allosteric modulation of a muscarinic acetylcholine receptor, *Nature 504*, 101-106.

[20] Abdul-Ridha, A., Lopez, L., Keov, P., Thal, D. M., Mistry, S. N., Sexton, P. M., Lane, J. R., Canals, M., and Christopoulos, A. (2014) Molecular determinants of allosteric modulation at the M1 muscarinic acetylcholine receptor, *J. Biol. Chem. 289*, 6067-6079.

[21] Ogino, K., Tokuda, Y., Nakai, T., and Tagaki, W. (1994) Hydrolysis of acetylcholine analogs catalyzed by an anionic surfactant containing 2-hydroxymethylimidazole and sulfate groups in the absence and presence of Cu2+ ion in mixed micellar systems, *Mem. Fac. Eng., Osaka City Univ. 35*, 187-197.

[22] Gould, R. G., and Jacobs, W. A. (1939) The Synthesis of Certain Substituted Quinolines and 5,6-Benzoquinolines, *J. Am. Chem. Soc. 61*, 2890-2895.

[23] de la Cruz, A., Elguero, J., Goya, P., Martínez, A., and Pfleiderer, W. (1992) Tautomerism and acidity in 4-quinolone-3-carboxylic acid derivatives, *Tetrahedron 48*, 6135-6150.

[24] Shindikar, A. V., and Viswanathan, C. L. (2005) Novel fluoroquinolones: design, synthesis, and in vivo activity in mice against Mycobacterium tuberculosis H37Rv, *Bioorg. Med. Chem. Lett. 15*, 1803-1806.

[25] Zhi, Y., Gao, L. X., Jin, Y., Tang, C. L., Li, J. Y., Li, J., and Long, Y. Q. (2014) 4-Quinolone-3-carboxylic acids as cell-permeable inhibitors of protein tyrosine phosphatase 1B, *Bioorg. Med. Chem. 22*, 3670-3683.

[26] Ziegler, N., Bätz, J., Zabel, U., Lohse, M. J., and Hoffmann, C. (2011) FRET-based sensors for the human M1-, M3-, and M5-acetylcholine receptors, *Bioorg. Med. Chem. 19*, 1048-1054.

[27] Maier-Peuschel, M., Frölich, N., Dees, C., Hommers, L. G., Hoffmann, C., Nikolaev, V. O., and Lohse, M. J. (2010) A fluorescence resonance energy transfer-based M2 muscarinic receptor sensor reveals rapid kinetics of allosteric modulation, *J. Biol. Chem. 285*, 8793-8800.

[28] Wess, J. (1998) Molecular basis of receptor/G-protein-coupling selectivity, *Pharmacol. Ther. 80*, 231-264.

[29] Tewson, P., Westenberg, M., Zhao, Y., Campbell, R. E., Quinn, A. M., and Hughes, T. E. (2012) Simultaneous detection of Ca2+ and diacylglycerol signaling in living cells, *PLoS One 7*, e42791.

[30] Bock, A., Merten, N., Schrage, R., Dallanoce, C., Batz, J., Kloeckner, J., Schmitz, J., Matera, C., Simon, K., Kebig, A., Peters, L., Müller, A., Schrobang-Ley, J., Tränkle, C., Hoffmann, C., De Amici, M., Holzgrabe, U., Kostenis, E., and Mohr, K. (2012) The allosteric vestibule of a seven transmembrane helical receptor controls G-protein coupling, *Nat. Commun. 3*, 1044.

[31] Bock, A., Chirinda, B., Krebs, F., Messerer, R., Batz, J., Muth, M., Dallanoce, C., Klingenthal, D., Tränkle, C., Hoffmann, C., De Amici, M., Holzgrabe, U., Kostenis, E., and Mohr, K. (2014) Dynamic ligand binding dictates partial agonism at a G protein-coupled receptor, *Nat. Chem. Biol. 10*, 18-20.

[32] Vilardaga, J. P., Steinmeyer, R., Harms, G. S., and Lohse, M. J. (2005) Molecular basis of inverse agonism in a G protein-coupled receptor, *Nat. Chem. Biol. 1*, 25-28.

[33] Hoffmann, C., Nuber, S., Zabel, U., Ziegler, N., Winkler, C., Hein, P., Berlot, C. H., Bunemann, M., and Lohse, M. J. (2012) Comparison of the activation kinetics of the M3 acetylcholine receptor and a constitutively active mutant receptor in living cells, *Mol. Pharmacol. 82*, 236-245.

[34] Bock, A., Bermudez, M., Krebs, F., Matera, C., Chirinda, B., Sydow, D., Dallanoce, C., Holzgrabe, U., De Amici, M., Lohse, M. J., Wolber, G., and Mohr, K. (2016) Ligand Binding Ensembles Determine Graded Agonist Efficacies at a G Protein-coupled Receptor, *J. Biol. Chem. 291*, 16375-16389.

[35] Ilien, B., Glasser, N., Clamme, J. P., Didier, P., Piemont, E., Chinnappan, R., Daval, S. B., Galzi, J. L., and Mely, Y. (2009) Pirenzepine promotes the dimerization of muscarinic M1 receptors through a three-step binding process, *J. Biol. Chem. 284*, 19533-19543.

[36] Nayeem AA, K. A., Rahman MS, Rahman M. (2011) Evaluation of phytochemical and pharmacological properties of Mikania cordata (Asteraceae) leaves, *J. Pharmacognosy Phytother. 3*, 118-123.

[37] Leyva, E., Monreal, E., and Hernández, A. (1999) Synthesis of fluoro-4-hydroxyquinoline-3-carboxylic acids by the Gould–Jacobs reaction, *J. Fluor. Chem. 94*, 7-10.

[38] Niedermeier, S., Singethan, K., Rohrer, S. G., Matz, M., Kossner, M., Diederich, S., Maisner, A., Schmitz, J., Hiltensperger, G., Baumann, K., Holzgrabe, U., and Schneider-Schaulies, J. (2009) A small-molecule inhibitor of Nipah virus envelope protein-mediated membrane fusion, *J. Med. Chem. 52*, 4257-4265.

[39] Ho, S. N., Hunt, H. D., Horton, R. M., Pullen, J. K., and Pease, L. R. (1989) Site-Directed Mutagenesis by Overlap Extension Using the Polymerase Chain-Reaction, *Gene 77*, 51-59.

[40] Zürn, A., Zabel, U., Vilardaga, J. P., Schindelin, H., Lohse, M. J., and Hoffmann, C. (2009) Fluorescence resonance energy transfer analysis of alpha 2a-adrenergic receptor activation reveals distinct agonist-specific conformational changes, *Mol. Pharmacol. 75*, 534-541.

[41] Hoffmann, C., Gaietta, G., Zürn, A., Adams, S. R., Terrillon, S., Ellisman, M. H., Tsien, R. Y., and Lohse, M. J. (2010) Fluorescent labeling of tetracysteine-tagged proteins in intact cells, *Nat. Protoc. 5*, 1666-1677.

[42] Sletten, D. M., Nickander, K. K., and Low, P. A. (2005) Stability of acetylcholine chloride solution in autonomic testing, *J. Neurol. Sci. 234*, 1-3.

2. Synthesis and FRET studies of the quinolone-rigid-iper hybrid

1. Introduction

G protein-coupled receptors (GPCRs) belong to the largest class of membrane proteins in mammals.[1] Among them, one major subfamily is the muscarinic acetylcholine receptor (mAChR) which is divided into five classes $M_1 – M_5$ due to their different appearance and physiological response. The M_1 muscarinic acetylcholine receptor is typically located in the central nervous system (cortex, hippocampus, and striatum) and is therefore an interesting target for the treatment of neurodegenerative diseases such as Alzheimer.[2,3]

Agonist binding leads to receptor activation followed by downstream signaling. One of the most prominent agonists is the synthetic iperoxo[4] which is known as superagonist at the muscarinic receptors due to its higher efficiency to the orthosteric binding site in comparison to the endogenous ligand acetylcholine.[5] The crystal structure of the M_2 receptor bound to the high-affinity orthosteric agonist iperoxo showed that iperoxo is completely enclosed in the orthosteric binding site due to aromatic lid formation (i.e. a tyr) between the allosteric and orthosteric binding site which leads to full receptor activation.[6]

Besides the orthosteric binding site there is a topographically distinct allosteric binding site located in the extracellular vestibule.[7] Allosteric modulators can bind and influence the ligand bound to the orthosteric site in different manners, resulting in positive, neutral or negative cooperativity.[8] The benzyl quinolone carboxylic acid (BQCA) **2** is known as M_1-subtype selective positive allosteric modulator (PAM) (Figure 1).[9-13]

In order to combine the advantages of high-affinity (orthosteric binding site) and subtype-selectivity (allosteric binding site) the concept of dualsteric ligands was developed.[14] Such bipharmacophoric ligands are able to bind simultaneously to the orthosteric and allosteric binding site within one molecule named as bitopic binding. Chen et al. reported about the synthesis of quinolone-C_6-iper **3**, consisting of a benzyl quinolone carboxylic acid moiety and of the base of iperoxo **1** linked through an hexamethylene chain and was found to be a M_1-subtype selective partial agonist (Figure 1).[15] Furthermore, hybrids were designed where the two pharmacophores, a naphmethonium moiety and the base of iperoxo **1** were connected through a rigidified linker resulting in the compound naph-rigid-iper **4** which was investigated on the M_2AChR on the basis of dynamic ligand binding (Figure 1).[16] This concept describes the possibility of dualsteric ligands to bind either dualsteric (i.e. active states) or purely allosteric (i.e. inactive states) to the receptor. Depending on the ratio of active versus inactive states, such dualsteric ligands act as partial agonists.[17] Interestingly, binding studies of the hybrid naph-rigid-iper **4** showed that a purely allosteric binding mode is not observed. The

dualsteric ligand is forced to bind in a purely dualsteric binding mode resulting in full receptor activation and therefore full agonism due to the rigidified linker.[16]

On this basis, the hybrid naph-rigid-iper **4** was modified by replacing the naphmethonium group with a modified quinolone moiety in order to address the M_1-subtype only. The so obtained quinolone-rigid-iper **5** hybrid was further investigated in FRET studies.

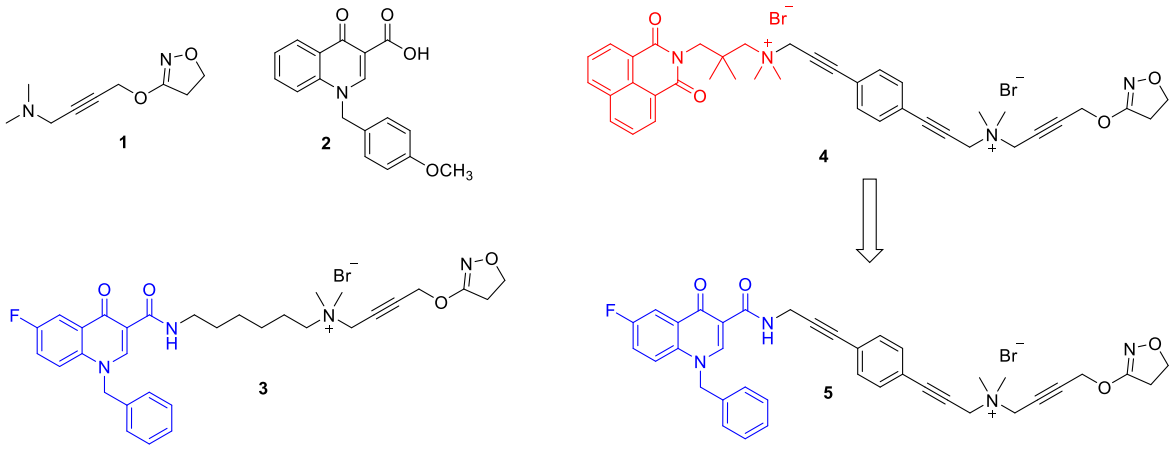

Figure 1: Structures of the base of iperoxo **1**, BQCA **2**, and of the hybrids quinolone-C_6-iper **3**, naph-rigid-iper **4**, and quinolone-rigid-iper **5**.

2. Results and discussion

2.1 Chemistry

The hybrid **5** was built up out of fluoro-4-oxo-quinolone skeleton **15** connected to the rigid spacer **8** (Scheme 1) and further connection to the base of iperoxo **1** (Scheme 2).

For the synthesis of the rigid spacer **8** different synthetic approaches were tested (Scheme 1). Firstly, 1-bromo-4-iodobenzene **6** was coupled to propargyl alcohol in the presence of $Pd(PPh_3)_2Cl_2$ and CuI in a Sonogashira-like reaction to yield 32% of **7**.[18] Further Sonogashira-like reaction using propargyl amine proved **8** as unreactive. Another attempt for the synthesis of the rigid linker **8** was the coupling of 1,4-dibromobenzene **9** and propargyl alcohol in a Sonogashira-like reaction yielding **10** in 95%.[19,20] The Appel reaction was applied to replace one OH-group by a bromine atom. Gabriel synthesis was used for the substitution of the bromine atom to the primary NH_2-group. The reaction with potassium phthalimide followed by hydrazine monohydrate resulted in the rigid spacer linker **8** in 77% yield.[21]

Scheme 1: Synthetic approaches for the synthesis of the rigid linker **8**.

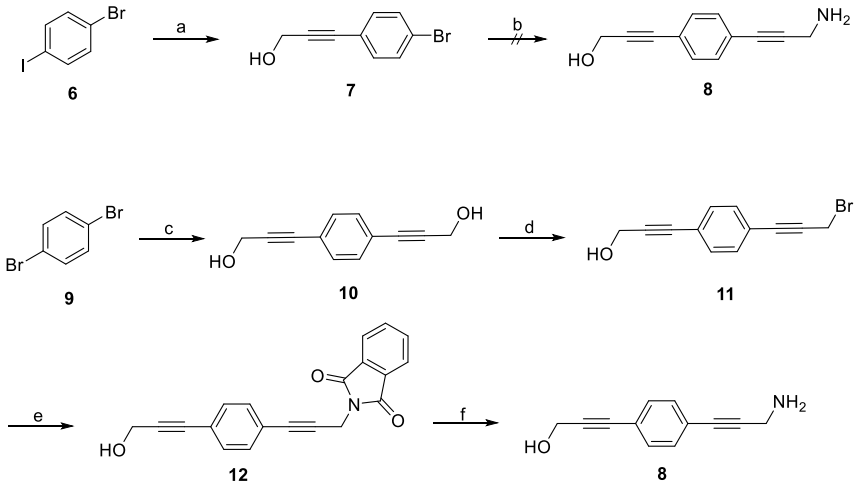

Reagents and conditions: a) propargyl alcohol (80% in toluene), $Pd(PPh_3)_2Cl_2$, CuI, piperidine, toluene, 35 °C; b) propargyl amine, $Pd(PPh_3)_2Cl_2$, CuI, piperidine, toluene, 35 °C; c) propargyl alcohol, $Pd(PPh_3)_4$, propylamine, 60 °C; d) CBr_4, PPh_3, CH_2Cl_2, 0 °C, rt.; e) potassium phthalimide, CH_3CN, 90 °C, rt.; f) hydrazine monohydrate, EtOH, 90 °C, rt.

The fluoro-4-oxo-quinolone core of BQCA **13**[22,23] was synthesized in two steps making use of the Gould-Jacobs synthetic pathway. Firstly, 4-fluoroaniline reacted with diethyl 2-(ethoxymethylene)-malonate followed by a microwave assisted cyclization reaction with diphenyl ether to afford the compound **13**.[24-26] *N*-Alkylation of **13** was achieved by using benzyl chloride in the presence of K_2CO_3 in DMF.[27] Hydrolysis of the ester function of **14** led to the M_1-selective allosteric moiety **15**. The amidation reaction between the M_1-selective allosteric moiety **15** and the linker **8** was accomplished in the presence of ethyl chloroformate and trimethylamine in DMF to build the intermediate compound **16**.[23] The Appel reaction converted the OH-group to a bromine group. The intermediate **17** was connected to the base of iperoxo **1** in the presence of KI/K_2CO_3 in acetonitrile to obtain the final hybrid compound **5** in 60% yield (Scheme 2).

Scheme 2: Synthetic pathway of the rigid quinolone-iperoxo hybrid **5**.

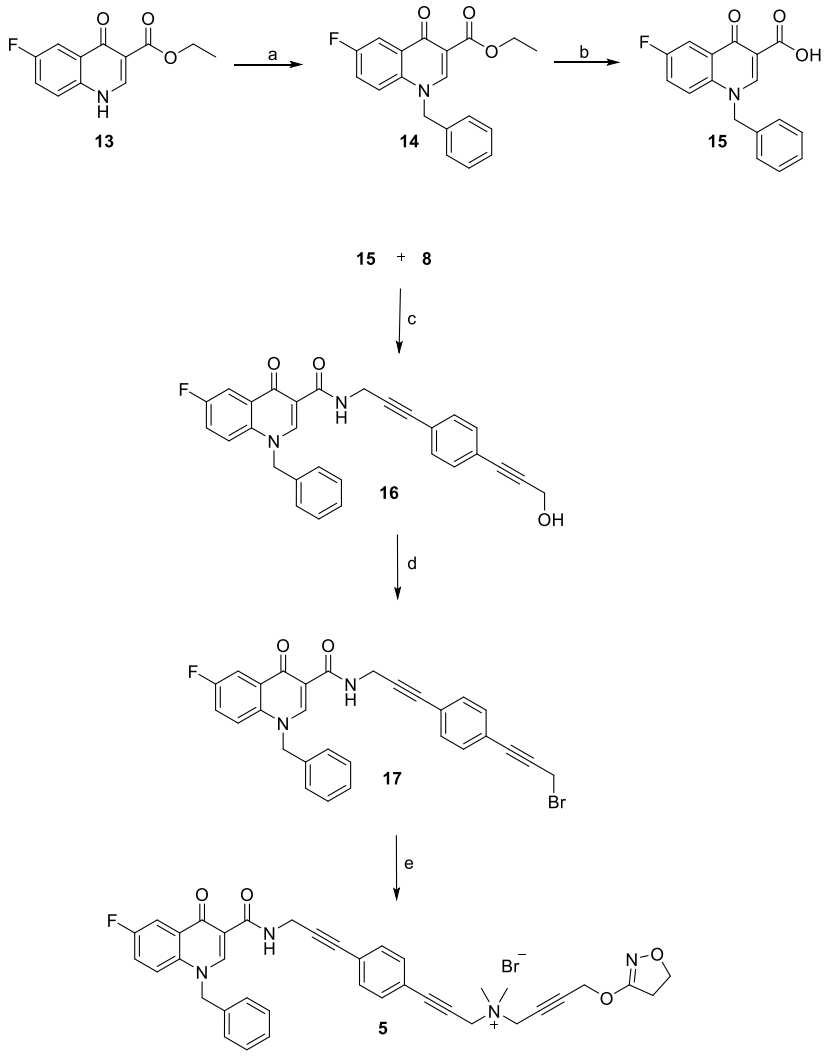

Reagents and conditions: a) benzyl chloride, K_2CO_3, DMF, 80 °C; b) 6 N HCl, MeOH, reflux; c) ethyl chlorofomate, NMe_3, DMF, 0 °C, rt.; d) CBr_4, PPh_3, CH_2Cl_2, 0 °C, rt.; e) base of iperoxo **1**, KI/K_2CO_3, CH_3CN, 80 °C (microwave).

2.2 Pharmacology

The hybrid compound **5** was further investigated in FRET studies. The experiments were performed in the working group of Prof. Dr. Hoffmann by Michael Kauk (Pharmacology and Toxicology, University of Würzburg, Germany). Figure 2 shows the FRET signal induced by **5**, displaying a time-delayed signal and therefore delayed kinetics. In comparison, FRET studies of hybrid **3**, consisting of the same pharmacophoric units but linked via a flexible hexamethylene chain, afforded a sharper FRET signal indicating that the delayed signal of **5** must result from the rigidified linker (Figure 2). Presumably, the rigidified linker is able to interact with the so-called tyrosine lid, formed by cation-π-interactions between three tyrosine

amino acids Y104$^{3.33}$, Y403$^{6.51}$, and Y426$^{7.39}$, separating the orthosteric from the allosteric binding site.[6] These interactions may contribute to the observed time-delayed FRET signal.

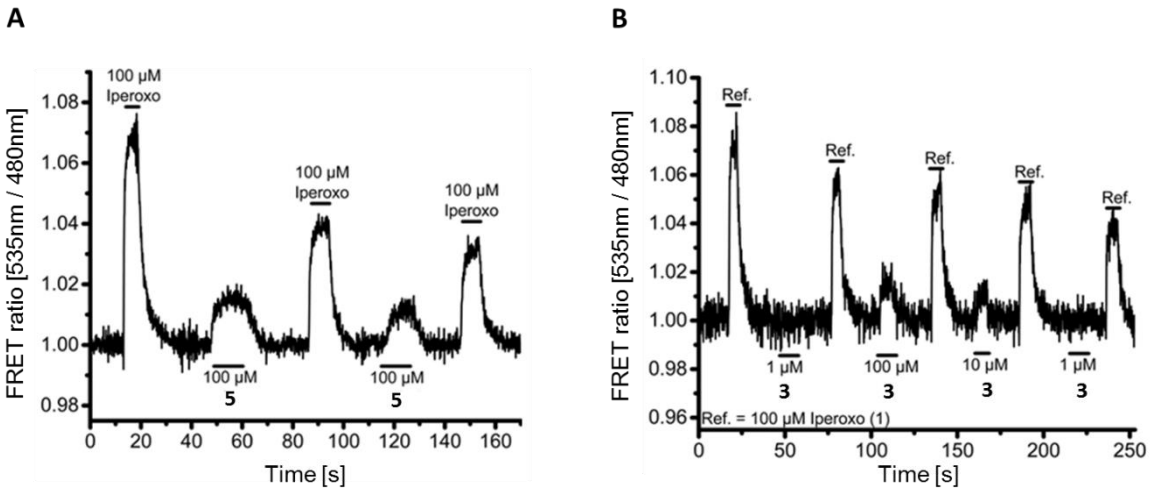

Figure 2: FRET measurements of rigidified hybrid **5** (**A**) and flexible hybrid **3** (**B**).

3. Methods

3.1 Chemistry

Reagents were obtained from commercial sources (Aldrich, Steinheim, Germany; Merck, Darmstadt, Germany) and used without any further purification. Microwave assisted reactions were carried out on a MLS-rotaPREP instrument (Milestone, Leutkirch, Germany). Thin-layer chromatography was performed on silica gel 60 F_{254} plates (Macherey-Nagel, Düren, Germany). Merck silica gel 60 (Merck, Darmstadt, Germany) was used for chromatography (230-400 mesh) columns. Column chromatography was also performed on an Interchim Puri Flash 430 (Ultra Performance Flash Purification) instrument (Montluçon, France) connected to an Interchim Flash ELSD. Used columns are: Silica 25 g – 30 µm, Alox-B 40 g – 32/63 µm, Alox-B 25 g – 32/63 µm (Interchim, Montluçon, France). Melting points were determined on a Stuart melting point apparatus SMP3 (Bibby Scientific, UK) and are uncorrected. ^{1}H (400.132 MHz) and ^{13}C (100.613 MHz) NMR spectra were recorded on a Bruker AV 400 instrument (Bruker Biospin, Ettlingen, Germany). As internal standard, the signals of the deuterated solvents were used (DMSO-d_6: ^{1}H 2.50 ppm, ^{13}C 39.52 ppm; $CDCl_3$: ^{1}H 7.26 ppm, ^{13}C 77.16 ppm; $(CD_3)_2CO$: ^{1}H 2.05 ppm, ^{13}C 39.52 ppm; MeOD-d_4: ^{1}H 3.31 ppm, ^{13}C 49.0 ppm). Abbreviation for data quoted are: s, singlet; d, doublet; t, triplet; q, quartet; m, multiplet; br, broad; dd, doublet of doublets; dt, doublet of triplets; tt, triplet of triplets; tq, triplet of quartets. Coupling constants (*J*) are given in Hz. FT-IR spectra were recorded on a Jasco FT-IR-6100 spectrometer (Gross-Umstadt, Germany) equipped with an ATR unit. ESI mass spectra of the compounds were obtained on an Agilent LC/MSD Trap

G2445D instrument (Waldbronn, Germany). Data are reported as mass-to-charge ratio (*m/z*) of the corresponding positively charged molecular ions. The purity of the new compound **5** was determined using HPLC analyses and was found to be ≥95%. The measurement was performed on a LCMS 2020 Shimadzu (Duisburg, Germany). The LCMS-system from Shimadzu Products, contained a DGU-20A3R degassing unit, a LC20AB liquid chromatograph and a SPD-20A UV/Vis detector. UV detection was measured at 254 nm. As stationary phase a Synergi 4U fusion-RP (150 * 4.6 mm) column and as mobile phase a gradient of MeOH/water was used. Parameters for method: Solvent A: water with 0.1% formic acid, solvent B: MeOH with 0.1% formic acid. Solvent B from 5% to 90% in 8 min, then 90% for 5 min, from 90% to 5% in 1 min, then 5% for 4 min. The method was performed with a flow rate of 1.0 mL/min. Mass spectra were also obtained by a LCMS 2020 as described above.

The compounds iperoxo base **1**[4], **7**[18], **10**[19, 20], **14**[15], and **15**[28] were prepared according to previously reported procedures. The synthesis of the 4-oxo-quinoline skeleton **13**[22,23] was performed according to the Gould-Jacobs procedure, describing the condensation reaction of 4-fluoroaniline with diethyl 2-(ethoxymethylene)-malonate followed by microwave assisted cyclization in diphenyl ether.[24-26]

3.1.1 Synthesis of 3,3'-(1,4-Phenylene)bis(prop-2-yn-1-ol) **10**

1,4-Dibromobenzene **9** (2.00 g, 8.47 mmol) and $Pd(PPh_3)_4$ (255 mg, 0.22 mmol) were dissolved in 40 mL of propylamine. After addition of 2-propyn-1-ol (2.80 g, 50.9 mmol), the reaction mixture was heated at 60 °C under nitrogen. The reaction was monitored through silica gel TLC (cyclohexane/ethyl acetate = 4:6, R_f = 0.50). After completion of the reaction (2.5 days), the mixture was quenched with 20 mL HCl. The aqueous layer was extracted with diethyl ether. The combined organic layers were dried over Na_2SO_4 and the solvent was removed under reduced pressure. The product was purified via column chromatography (silica gel flushed with cyclohexane/ethyl acetate = 7:3 to 4:6). The product was obtained as yellow solid. 95% yield; ^{1}H NMR ($CDCl_3$): 4.50 (s, 4H, C**H$_2$**-OH), 7.36 (s, 4H, C**H**$_{arom.}$).

3.1.2 Synthesis of 3-(4-(3-Bromoprop-1-yn-1-yl)phenyl)prop-2-yn-1-ol **11**

10 (0.63 g, 3.40 mmol) and tetrabromomethane (1.13 g, 3.40 mmol) were dissolved in 20 mL dichloromethane dry under argon. Triphenylphosphine (0.89 g, 3.40 mmol) was added at 0 °C. The reaction mixture was then allowed to warm up to room temperature, stirred overnight and monitored with silica gel TLC (cyclohexane/ethyl acetate = 4:6, R_f = 0.72). The

solvent was removed under reduced pressure and the product was purified via column chromatography (cyclohexane/ethyl acetate = 4:6) to yield a yellow solid. 17% yield; mp 81-89 °C; IR (ATR): 3330, 2999, 2912, 2859, 2250, 1507, 1200, 1031, 832 cm^{-1}; ^{1}H NMR ($CDCl_3$): 4.16 (s, 2H, C**H**$_2$-Br), 4.50 (s, 2H, C**H**$_2$-OH), 7.38 (s, 4H, C**H**$_{arom.}$). ^{13}C NMR ($CDCl_3$): 15.0, 51.7, 85.2, 86.0, 86.1, 89.3, 122.3, 123.1, 131.6, 131.8.

3.1.3 Synthesis of 2-(3-(4-(3-Hydroxyprop-1-yn-1-yl)phenyl)prop-2-yn-1-yl)isoindoline-1,3-dione **12**

11 (364 mg, 1.46 mmol) was dissolved in dry acetonitrile (10 mL) and potassium phthalimide (811 mg, 4.38 mmol) was added. The reaction mixture was stirred at 90 °C for 7.5 h and at room temperature overnight. The reaction was monitored by TLC (cyclohexane/ethyl acetate = 4:6, R_f = 0.72). The obtained solid was filtered off and the solvent was removed *in vacuo* to yield a beige solid. 100% yield; mp 142-145 °C; IR (ATR): 3439, 2950, 2300, 1706, 1028 cm^{-1}; ^{1}H NMR ($CDCl_3$): 4.48 (s, 2H, C**H**$_2$-OH), 4.68 (s, 2H, C**H**$_2$-N$_{phth.}$), 7.31-7.37 (m, 4H, C**H**$_{arom.}$), 7.74 (dd, 2H, C**H**$_{phth.}$, *J* = 3.0, *J* = 5.5), 7.90 (dd, 2H, C**H**$_{phth.}$, *J* = 3.0, *J* = 5.5). ^{13}C NMR ($CDCl_3$): 27.9, 51.6, 82.5, 84.5, 85.2, 89.0, 122.5, 122.7, 123.6, 131.5, 131.8, 132.1, 134.2, 167.1.

3.1.4 Synthesis of 3-(4-(3-Aminoprop-1-yn-1-yl)phenyl)prop-2-yn-1-ol **8**

12 (782 mg, 2.48 mmol) was suspended in 10 mL of ethanol. After addition of hydrazine monohydrate (0.48 mL, 9.92 mmol) a clear solution was obtained. While the reaction mixture was heated at 90 °C a solid was precipitated. Another 3 mL of ethanol were added. The reaction was monitored by TLC (CH_2Cl_2/MeOH = 8:2, R_f = 0.44). The suspension was stirred at 90 °C for 7.0 h and at room temperature overnight. For work-up the precipitate was filtered off and washed with ethanol. The filtrate was evaporated off and the crude product was purified by column chromatography (CH_2Cl_2/MeOH = 9:1 to 7:3) to yield a yellow solid. 77% yield; mp 148-151 °C; IR (ATR): 3346, 3282, 2742, 1600, 1497, 1341, 1038, 839 cm^{-1}; ^{1}H NMR (MeOD): 3.60 (s, 2H, C**H**$_2$-NH_2), 4.39 (s, 2H, C**H**$_2$-OH), 7.36 (s, 4H, C**H**$_{arom.}$). ^{13}C NMR (MeOD): 32.1, 51.2, 83.0, 85.0, 90.7, 92.1, 124.2, 124.7, 132.6.

3.1.5 Synthesis of 1-Benzyl-6-fluoro-*N*-(3-(4-(3-hydroxyprop-1-yn-1-yl)phenyl)prop-2-yn-1-yl)-4-oxo-1,4-dihydroquinoline-3-carboxamide **16**

15 (257 mg, 0.87 mmol) and trimethylamine (0.25 mL, 1.83 mmol) were dissolved in dry DMF (12 mL). Ethyl chloroformate (0.17 mL, 1.78 mmol) was slowly added under stirring at 0 °C

for 1.5 h. After addition of **8** (258 mg, 1.39 mmol), the reaction mixture was stirred at 0 °C for 2.5 h and subsequently at room temperature for 64 h. The reaction mixture was poured into ice-water and the solid was filtered off washed with water and petrol ether. The white solid was dried *in vacuo*. 91% yield; mp 205-207 °C; IR (ATR): 3058, 2990, 2260, 1655, 1611, 1494, 1230, 814, 735 cm^{-1}; ^{1}H NMR ($CDCl_3$): 4.42-4.52 (m, 4H, NH-C**H₂**/C**H₂**-OH), 5.47 (s, 2H, C**H₂**$_{arom.}$), 7.13-7.44 (m, 11H, C**H**$_{arom.}$/**H**-7/**H**-8), 8.17 (dd, 1H, **H**-5, *J* = 2.7, *J* = 8.7), 8.93 (s, 1H, **H**-2), 10.22 (br, 1H, N**H**). ^{13}C NMR ($CDCl_3$): 29.6, 51.6, 58.1, 82.3, 85.3, 87.4, 88.8, 111.3, 112.3, 119.1, 121.5, 122.3, 123.2, 126.0, 128.8, 129.5, 131.5, 131.7, 133.8, 135.8, 148.5, 159.9, 164.5, 175.9.

3.1.6 Synthesis of 1-Benzyl-*N*-(3-(4-(3-bromoprop-1-yn-1-yl)phenyl)prop-2-yn-1-yl)-6-fluoro-4-oxo-1,4-dihydroquinoline-3-carboxamide **17**

16 (300 mg, 0.65 mmol) and tetrabromomethane (0.43 g, 1.29 mmol) were dissolved in dry dichloromethane (15 mL) under argon. Triphenylphosphine (0.34 g, 1.29 mmol) was added at 0 °C. The reaction mixture was then allowed to warm to room temperature and stirred for further 2.0 d. The solvent was evaporated and the residue was crystallized in ethanol and recrystallized in methanol to afford a beige solid. 54% yield; mp 197-200 °C; IR (ATR): 3041, 2901, 2190, 1657, 1609, 1492, 1230, 814, 732 cm^{-1}; ^{1}H NMR ($(CD_3)_2CO$): 4.39 (s, 2H, C**H₂**-Br), 4.50 (d, 2H, NH-C**H₂**, *J* = 5.6), 5.85 (s, 2H, C**H₂**$_{arom.}$), 7.33-7.57 (m, 10H, C**H**$_{arom.}$/**H**-8), 7.86 (dd, 1H, **H**-7, *J* = 4.3, *J* = 9.4), 8.06 (dd, 1H, **H**-5, *J* = 3.1, *J* = 9.1), 9.03 (s, 1H, **H**-2), 10.22 (dt, 1H, N**H**, *J* = 1.2, *J* = 5.0). ^{13}C NMR ($(CD_3)_2CO$): 16.9, 31.1, 59.0, 83.1, 87.3, 88.5, 90.8, 112.9, 112.9, 122.6, 123.0, 123.9, 128.5, 130.1, 131.0, 133.6, 137.5, 138.0, 138.3, 150.9, 161.7, 165.9, 177.2. MS (ESI) m/z [M^+] Calcd for $C_{29}H_{21}BrFN_2O_2^+$: 527.1. Found: 527.2.

3.1.7 Synthesis of *N*-(3-(4-(3-(1-Benzyl-6-fluoro-4-oxo-1,4-dihydroquinoline-3-carboxamido)prop-1-yn-1-yl)phenyl)prop-2-yn-1-yl)-4-((4,5-dihydroisoxazol-3-yl)oxy)-*N*,*N*-dimethylbut-2-yn-1-aminium bromide **5**

To a solution of iperoxo base[4] **1** (104 mg, 0.57 mmol) in 10 mL acetonitrile, **17** (150 mg, 0.28 mmol) and a catalytic amount of KI/K_2CO_3 (1:1) were added. The reaction mixture was heated in the microwave (500 W, 80 °C) for 6 h. After cooling to room temperature the surplus of KI/K_2CO_3 was filtered off and the solvent was evaporated to half volume. Diethyl ether was added and the solution was kept in the fridge overnight. The precipitate obtained was filtered, washed with Et_2O and dried *in vacuo* to yield a beige solid. 60% yield; mp 148-149 °C; IR (ATR): 3182, 2990, 2362, 1650, 1610, 1495, 1340, 1231, 814, 739 cm^{-1}; ^{1}H NMR

(DMSO): 3.01 (t, 2H, **H**-$4_{2\text{-isox}}$, *J* = 9.6), 3.22 (s, 6H, $^{+}N(C\mathbf{H_3})_2$), 4.32 (t, 2H, **H**-$5_{2\text{-isox}}$, *J* = 9.6) 4.47 (d, 2H, NH-C$\mathbf{H_2}$, *J* = 5.5), 4.59 (s, 2H, ≡C-C$\mathbf{H_2}$-O), 4.68 (s, 2H, C$\mathbf{H_2}$-N^{+}), 4.95 (s, 2H, $^{+}$N-C$\mathbf{H_2}$-C≡), 5.83 (s, 2H, C$\mathbf{H_{2arom.}}$), 7.23-7.53 (m, 9H, $\mathbf{H}_{arom.}$), 7.69 (ddd, 1H, **H**-8, *J* = 3.1, *J* = 8.0, *J* = 9.4), 7.86 (dd, 1H, **H**-7, *J* = 4.3, *J* = 9.4), 8.00 (dd, 1H, **H**-5, *J* = 3.1, *J* = 9.0), 9.13 (s, 1H, **H**-2), 10.19 (t, 1H, N**H**, *J* = 5.6). ^{13}C NMR (DMSO): 28.6, 32.1, 49.8, 53.4, 53.4, 53.9, 56.1, 57.2, 69.5, 75.7, 78.9, 80.9, 86.5, 89.8, 90.0, 110.2, 110.5 (d, J_{CF} = 23.3), 120.1, 121.1 (d, J_{CF} = 7.6), 121.5 (d, J_{CF} = 25.3), 123.5, 126.4, 127.9, 128.9, 128.9, 129.0, 131.6, 132.1, 135.6, 149.0, 159.2 (d, J_{CF} = 245.4), 163.7, 166.6, 174.6 (d, *J* = 1.6). MS (ESI) m/z [M^{+}] Calcd for $C_{38}H_{34}FN_4O_4^{+}$: 629.3. Found: 629.1.

References

[1] Lander, E. S., and Linton, L. M. et al. (2001) Initial sequencing and analysis of the human genome, *Nature 409*, 860-921.

[2] Wess, J. (2004) Muscarinic acetylcholine receptor knockout mice: novel phenotypes and clinical implications, *Annu. Rev. Pharmacol. Toxicol. 44*, 423-450.

[3] Kruse, A. C., Kobilka, B. K., Gautam, D., Sexton, P. M., Christopoulos, A., and Wess, J. (2014) Muscarinic acetylcholine receptors: novel opportunities for drug development, *Nat. Rev. Drug. Discov. 13*, 549-560.

[4] Kloeckner, J., Schmitz, J., and Holzgrabe, U. (2010) Convergent, short synthesis of the muscarinic superagonist iperoxo, *Tetrahedron Lett. 51*, 3470-3472.

[5] Schrage, R., Seemann, W. K., Kloeckner, J., Dallanoce, C., Racke, K., Kostenis, E., De Amici, M., Holzgrabe, U., and Mohr, K. (2013) Agonists with supraphysiological efficacy at the muscarinic M2 ACh receptor, *Br. J. Pharmacol. 169*, 357-370.

[6] Kruse, A. C., Ring, A. M., Manglik, A., Hu, J., Hu, K., Eitel, K., Hübner, H., Pardon, E., Valant, C., Sexton, P. M., Christopoulos, A., Felder, C. C., Gmeiner, P., Steyaert, J., Weis, W. I., Garcia, K. C., Wess, J., and Kobilka, B. K. (2013) Activation and allosteric modulation of a muscarinic acetylcholine receptor, *Nature 504*, 101-106.

[7] Tuček, S., and Proška, J. (1995) Allosteric Modulation of Muscarinic Acetylcholine-Receptors, *Trends Pharmacol. Sci. 16*, 205-212.

[8] De Amici, M., Dallanoce, C., Holzgrabe, U., Tränkle, C., and Mohr, K. (2010) Allosteric ligands for G protein-coupled receptors: a novel strategy with attractive therapeutic opportunities, *Med. Res. Rev. 30*, 463-549.

[9] Ma, L., Seager, M. A., Wittmann, M., Jacobson, M., Bickel, D., Burno, M., Jones, K., Graufelds, V. K., Xu, G., Pearson, M., McCampbell, A., Gaspar, R., Shughrue, P., Danziger, A., Regan, C., Flick, R., Pascarella, D., Garson, S., Doran, S., Kreatsoulas, C., Veng, L., Lindsley, C. W., Shipe, W., Kuduk, S., Sur, C., Kinney, G., Seabrook, G. R., and Ray, W. J. (2009) Selective activation of the M1 muscarinic acetylcholine receptor achieved by allosteric potentiation, *Proc. Natl. Acad. Sci. U. S. A. 106*, 15950-15955.

[10] Kuduk, S. D., and Beshore, D. C. (2014) SAR Studies on Carboxylic Acid Series M1 Selective Positive Allosteric Modulators (PAMs), *Curr. Top. Med. Chem. 14*, 1738-1754.

[11] Mistry, S. N., Valant, C., Sexton, P. M., Capuano, B., Christopoulos, A., and Scammells, P. J. (2013) Synthesis and pharmacological profiling of analogues of benzyl quinolone carboxylic acid (BQCA) as allosteric modulators of the M1 muscarinic receptor, *J. Med. Chem. 56*, 5151-5172.

[12] Kuduk, S. D., Chang, R. K., Di Marco, C. N., Ray, W. J., Ma, L., Wittmann, M., Seager, M. A., Koeplinger, K. A., Thompson, C. D., Hartman, G. D., and Bilodeau, M. T. (2010) Quinolizidinone carboxylic acids as CNS penetrant, selective m1 allosteric muscarinic receptor modulators, *ACS Med. Chem. Lett. 1*, 263-267.

[13] Davie, B. J., Valant, C., White, J. M., Sexton, P. M., Capuano, B., Christopoulos, A., and Scammells, P. J. (2014) Synthesis and pharmacological evaluation of analogues of benzyl quinolone carboxylic acid (BQCA) designed to bind irreversibly to an allosteric site of the M (1) muscarinic acetylcholine receptor, *J. Med. Chem. 57*, 5405-5418.

[14] Mohr, K., Schmitz, J., Schrage, R., Tränkle, C., and Holzgrabe, U. (2013) Molecular alliance-from orthosteric and allosteric ligands to dualsteric/bitopic agonists at G protein coupled receptors, *Angew. Chem. Int. Ed. Engl. 52*, 508-516.

[15] Chen, X., Kloeckner, J., Holze, J., Zimmermann, C., Seemann, W. K., Schrage, R., Bock, A., Mohr, K., Tränkle, C., Holzgrabe, U., and Decker, M. (2015) Rational design of partial agonists for the muscarinic m1 acetylcholine receptor, *J. Med. Chem. 58*, 560-576.

[16] Bock, A., Bermudez, M., Krebs, F., Matera, C., Chirinda, B., Sydow, D., Dallanoce, C., Holzgrabe, U., De Amici, M., Lohse, M. J., Wolber, G., and Mohr, K. (2016) Ligand Binding Ensembles Determine Graded Agonist Efficacies at a G Protein-coupled Receptor, *J. Biol. Chem. 291*, 16375-16389.

[17] Bock, A., Chirinda, B., Krebs, F., Messerer, R., Batz, J., Muth, M., Dallanoce, C., Klingenthal, D., Tränkle, C., Hoffmann, C., De Amici, M., Holzgrabe, U., Kostenis, E., and Mohr, K. (2014) Dynamic ligand binding dictates partial agonism at a G protein-coupled receptor, *Nat. Chem. Biol. 10*, 18-20.

[18] Kleinbeck, F., and Toste, F. D. (2009) Gold(I)-catalyzed enantioselective ring expansion of allenylcyclopropanols, *J. Am. Chem. Soc. 131*, 9178-9179.

[19] Hopf, H., Jones, P. G., Bubenitschek, P., and Werner, C. (1995) Para-Quinodimethane and Ortho-Quinodimethane Intermediates with Cumulative Double-Bonds, *Angew. Chem. Int. Ed. Engl. 34*, 2367-2368.

[20] Werner, C., Hopf, H., Dix, I., Bubenitschek, P., and Jones, P. G. (2007) 1,x-elimination reactions: extending the limits of a classical organic reaction, *Chemistry (Easton) 13*, 9462-9477.

[21] Farber, K. M., Haddadin, M. J., and Kurth, M. J. (2014) Davis-Beirut reaction: route to thiazolo-, thiazino-, and thiazepino-2H-indazoles, *J. Org. Chem. 79*, 6939-6945.

[22] Leyva, E., Monreal, E., and Hernández, A. (1999) Synthesis of fluoro-4-hydroxyquinoline-3-carboxylic acids by the Gould–Jacobs reaction, *J. Fluor. Chem. 94*, 7-10.

[23] Niedermeier, S., Singethan, K., Rohrer, S. G., Matz, M., Kossner, M., Diederich, S., Maisner, A., Schmitz, J., Hiltensperger, G., Baumann, K., Holzgrabe, U., and Schneider-Schaulies, J. (2009) A small-molecule inhibitor of Nipah virus envelope protein-mediated membrane fusion, *J. Med. Chem. 52*, 4257-4265.

[24] Gould, R. G., and Jacobs, W. A. (1939) The Synthesis of Certain Substituted Quinolines and 5,6-Benzoquinolines, *J. Am. Chem. Soc. 61*, 2890-2895.

[25] de la Cruz, A., Elguero, J., Goya, P., Martínez, A., and Pfleiderer, W. (1992) Tautomerism and acidity in 4-quinolone-3-carboxylic acid derivatives, *Tetrahedron 48*, 6135-6150.

[26] Shindikar, A. V., and Viswanathan, C. L. (2005) Novel fluoroquinolones: design, synthesis, and in vivo activity in mice against Mycobacterium tuberculosis H37Rv, *Bioorg. Med. Chem. Lett. 15*, 1803-1806.

[27] Koga, H., Itoh, A., Murayama, S., Suzue, S., and Irikura, T. (1980) Structure-activity relationships of antibacterial 6,7- and 7,8-disubstituted 1-alkyl-1,4-dihydro-4-oxoquinoline-3-carboxylic acids, *J. Med. Chem. 23*, 1358-1363.

[28] Zhi, Y., Gao, L. X., Jin, Y., Tang, C. L., Li, J. Y., Li, J., and Long, Y. Q. (2014) 4-Quinolone-3-carboxylic acids as cell-permeable inhibitors of protein tyrosine phosphatase 1B, *Bioorg. Med. Chem. 22*, 3670-3683.

3. Dynamic ligand binding dictates partial agonism at a G protein-coupled receptor

Bock, A., Chirinda, B., Krebs, F., Messerer, R., Bätz, J., Muth, M., Dallanoce, C., Klingenthal, D., Tränkle, C., Hoffmann, C., De Amici, M., Holzgrabe, U., Kostenis, E., and Mohr, K.

Reprinted with permission from
Macmillan Publishers Ltd: Nature Chemical Biology, 2014, 10, 18-20; © 2014.

Abstract

We present a new concept of partial agonism at G protein-coupled receptors. We demonstrate the coexistence of two functionally distinct populations of the muscarinic M_2 receptor stabilized by one dynamic ligand, which binds in two opposite orientations. The ratio of orientations determines the cellular response. Our concept allows predicting and virtually titrating ligand efficacy which opens unprecedented opportunities for the design of drugs with graded activation of the biological system.

1. Introduction

G protein-coupled receptors (GPCRs) induce intracellular biological responses upon binding agonist ligands[1,2]. The term 'efficacy' at a GPCR is defined as the capacity of a ligand to exert a change in receptor behavior towards the cell when the ligand is bound to the receptor[3,4]. According to their efficacy, agonists are subclassified as full and partial agonists depending on whether they trigger a maximal biological response or induce a submaximal effect even at saturating concentrations, respectively[5]. Mechanistic explanations for different agonist efficacies include an impaired engagement of receptor epitopes used by full agonists[6], a weaker stabilization of the contracted agonist-binding cavity[6], and a partial disruption of microswitches necessary for full receptor activation[7,8]. Taken together, a partial agonist shares the general binding topography of full agonists but most likely stabilizes distinct receptor conformations with diminished efficacy on cell signaling[9-12]. This includes that an agonist is bound to the receptor exclusively in one orientation and stabilizes somewhat fluffy receptor states able to couple to multiple intracellular effector proteins[13]. Here, we demonstrate a new concept of graded ligand efficacy at GPCRs. We show that

partial agonism can emerge from a stochastic switch of ligand binding between two functionally distinct orientations.

2. Results and discussion

First, we delineated a model to quantify binding affinity and efficacy of such dynamic ligands (mathematical derivation is in **Note 1**). Let an agonist molecule consist of two pharmacophores: one may activate the receptor protein (active moiety; **Fig. 1a**) and the other may stabilize an inactive receptor conformation (inactive moiety; **Fig. 1a**). Then let this bipharmacophoric ligand be able to dynamically bind in two orientations: an active signaling-competent pose and an inactive binding pose. The ligand stochastically distributes over the receptor population with the fraction of the respective subpopulation determined by the affinity ratio between the active signaling-competent and the inactive orientation (equilibrium dissociation constants K_{active} and $K_{inactive}$, respectively). Assuming that only the ligand-receptor complex in the active pose canonically couples to intracellular G proteins and induces downstream signaling, the measured biological effect is a function of the ratio of orientations, R_{pose} (**Fig. 1a,b**). To simulate and predict the role of R_{pose} for receptor activation and subsequent cellular response, we extended the operational model of agonism[14] to incorporate dynamic switching of a ligand between an active and an inactive binding pose (derivation is in **Note 1**). Simulations predicted that the level of receptor activation (**Fig. 1b**) as well as the downstream biological response (**Fig. 2**) were highly sensitive to the active/inactive orientation ratio R_{pose}.

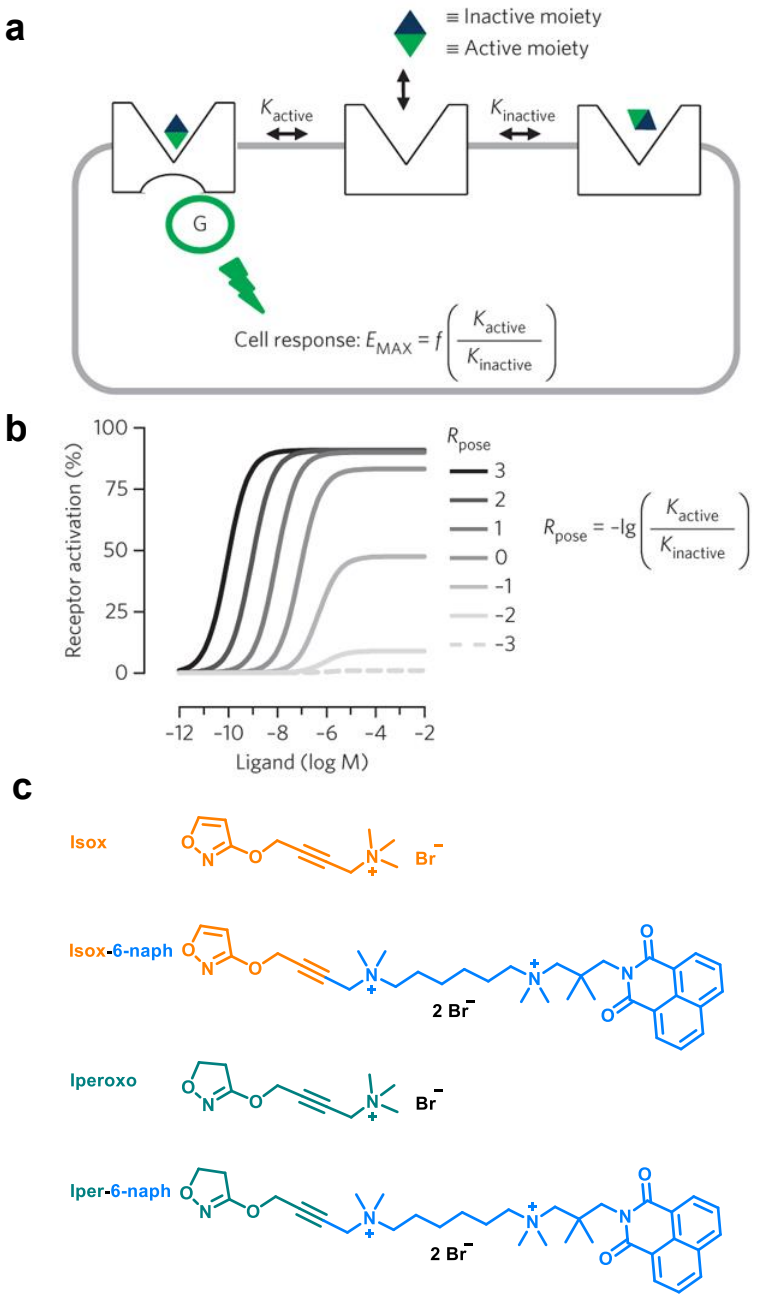

Figure 1: Dynamic ligand binding dictates partial agonism: model, predictions and chemical tools. (**a**) A bipharmacophoric ligand consisting of an active moiety (green triangle) and an inactive moiety (blue triangle) will bind in two distinct binding poses, that is, the active signaling-competent pose (left) and the inactive nonsignaling pose (right). The orientation ratio R_{pose} is determined by the affinity in the active pose (represented by the equilibrium dissociation constant K_{active}) versus the inactive pose (represented by the equilibrium dissociation constant $K_{inactive}$). The overall cell response (E_{MAX}) is a function of the orientation ratio $K_{active}/K_{inactive}$. (**b**) Predicted concentration-effect curves (receptor activation as a function of dynamic ligand concentration) depending on the orientation ratio R_{pose}, as simulated by the operational model of agonism for dynamic ligands (Online Methods and **Note 1**). Receptor activation is plotted on the y-axis as the percentage of the maximum receptor activation. Parameters used for simulation are $\varepsilon = 10$; $\log K_b = -6$; $R_T/K_E = 1$; $\log K_{active}$ was varied to yield the indicated orientation ratio R_{pose}. (**c**) Structures of the orthosteric agonists isox and iperoxo and the bipharmacophoric tools thereof, isox-6-naph and iper-6-naph, which were used for validation of the model. Orthosteric agonists isox and iperoxo are shown in orange and green, respectively. The allosteric inactive moiety 6-naph is shown in blue.

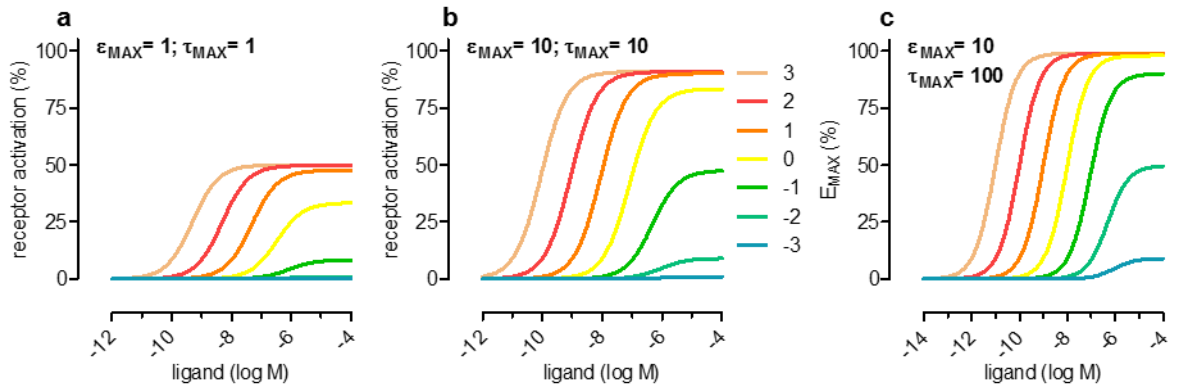

Figure 2: The orientation ratio fine-tunes receptor activation and downstream signaling of ligands with various intrinsic efficacies. (**a,c**) Shown are simulated concentration-effect-curves of dynamic ligands computed with the operational model for dynamic ligands. Fixed parameters for simulation are as follows: Effect_{MAX} = 100; $\log K_{inactive} = -6$; $\log K_{active}$ was varied to yield the indicated orientation ratios $R_{pose} = -\log\left(\frac{K_{active}}{K_{inactive}}\right)$ (see color code in **b**); $\frac{R_T}{K_E}$ was set to 1 (**a,b**) and 10 (**c**). (**a**) Low-efficacy dynamic ligands ($\varepsilon_{MAX} = 1$) are not able to fully activate the receptor even at full occupancy ($R_{pose} > 2$) in the active pose. The y-axis directly reflects receptor activation. (**b**) High-efficacy dynamic ligands ($\varepsilon_{MAX} = 10$) are able to fully activate the receptor at high orientation ratios ($R_{pose} > 2$). For these ligands the orientation ratio covers the whole range of efficacy, i.e. from weak partial to almost maximum receptor activation. The y-axis directly reflects receptor activation. (**c**) In a system with high receptor reserve ($\frac{R_T}{K_E} = 10$, $\tau_{MAX} = 100$), high-efficacy dynamic ligands ($\varepsilon_{MAX} = 10$) are able to fully activate the receptor even at low orientation ratios (e.g. $R_{pose} = 0$). The y-axis displays the downstream response.

The phenomenon of dynamic ligand binding was initially discovered in estrogen receptors[15]. We here expand this concept to the therapeutically highly relevant class of GPCRs[16]. To directly demonstrate the coexistence of two distinct receptor populations, we established an experimental test system characterized by two essential features: (i) an assay providing unidirectional signaling and (ii) bipharmacophoric test compounds encompassing two fragments that target two distinct binding sites on the receptor protein. To attain this goal, we used the muscarinic M_2 receptor as a paradigm for class A GPCRs and applied the recently developed G_i-biased ligands iper-6-naph (**1**) and iper-6-phth (**2**) (the structures of all of the compounds are in **Fig. 3**) as well as the G_i-biased ligands isox-6-naph (**3**) and isox-6-phth (**4**) (**Fig. 4**). These ligands allow restricting pleiotropic receptor signaling to the physiologically most relevant G_i signaling pathway[17,18]. The applied bipharmacophoric probes iper-6-naph and isox-6-naph (**Fig. 1c**) are composed of orthosteric active moieties iperoxo (**5**) and isox (**6**) covalently linked to the inactive allosteric moiety '6-naph' (**7**) (**Fig. 1c**). The active binding pose of such bipharmacophoric ligands is characterized by dualsteric binding, that is,

simultaneous bitopic orthosteric/allosteric binding, and the inactive pose reflects purely allosteric binding (**Fig. 1a**). Most importantly, iperoxo and isox showed equal efficacy for receptor activation, as reflected by [^{35}S]GTPγS binding, and additionally displayed equal operational efficacies in downstream signaling, as reflected by dynamic mass redistribution (DMR) measurements (**Fig. 5**). Moreover, the negative cooperativity of efficacy between iperoxo and 6-naph as well as isox and 6-naph was in the same range (**Fig. 6**). This implied that differences in receptor activation by iper-6-naph and isox-6-naph are mainly due to a different orientation ratio of the respective ligands. The applied inactive 6-naph moiety is known to interact with an allosteric site of the receptor protein and to enhance orthosteric radioligand binding (**Fig. 6**) which is unequivocal evidence for purely allosteric binding of the bipharmacophoric probe in the inactive pose.

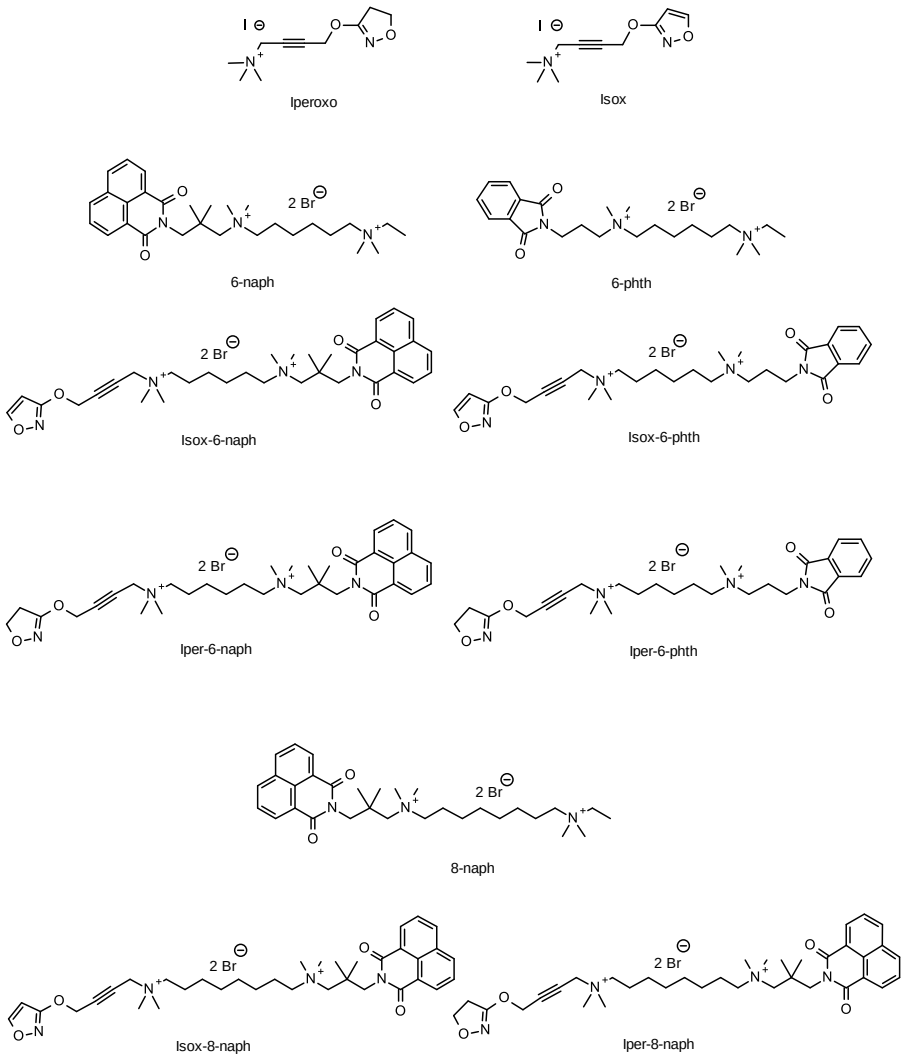

Figure 3: Structures of dynamic ligands and their building blocks.

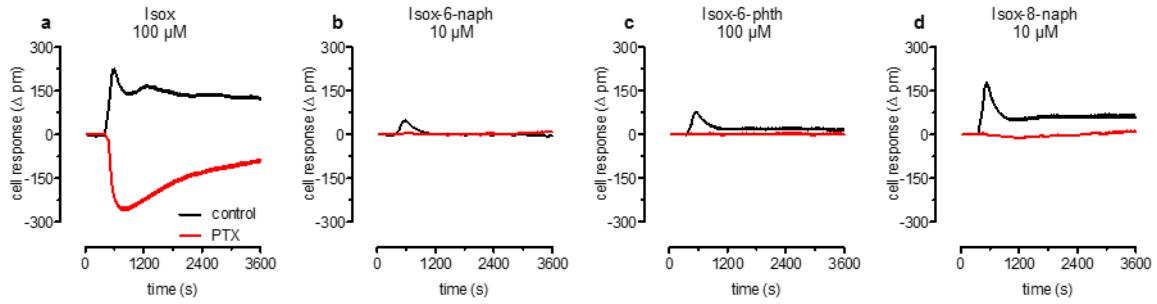

Figure 4: Isox-derived dynamic ligands exclusively signal *via* G_i proteins. Shown are baseline-corrected DMR responses measured as wavelength shifts (Δ pm) and recorded over time after addition of maximal concentrations of (**a**) isox, (**b**) isox-6-naph, (**c**) isox-6-phth, and (**d**) isox-8-naph to live CHO-hM_2 cells. DMR responses under control conditions and after PTX-pretreatment (100 ng/ml, overnight) are indicated as black and red traces, respectively. Data are means and s.e.m. of one out of 3 independent experiments conducted in quadruplicate.

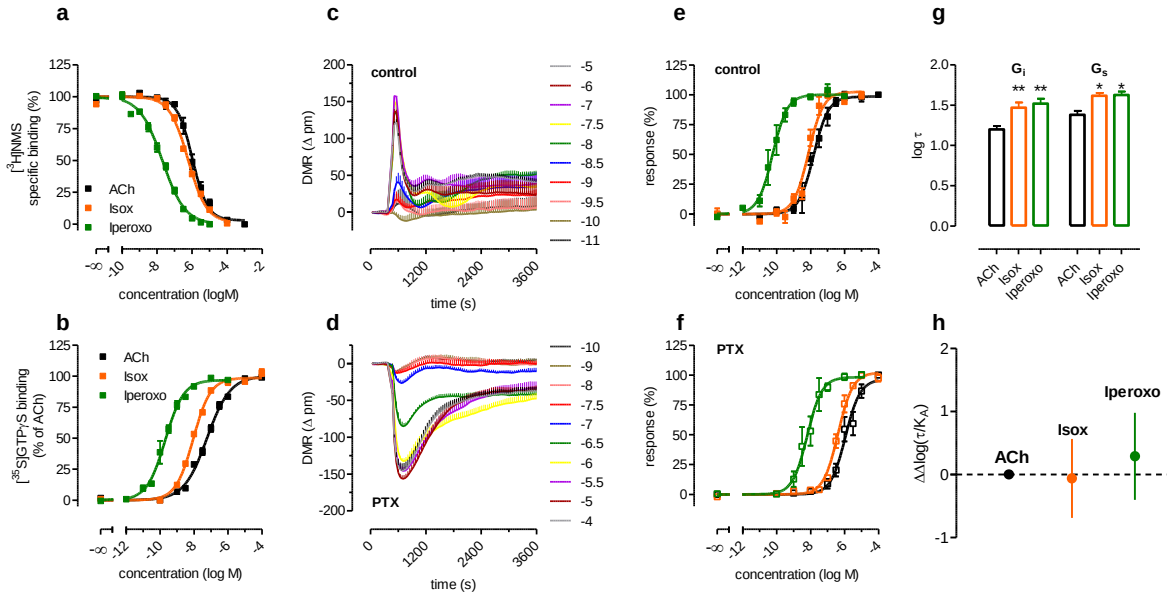

Figure 5: Isox is an unbiased orthosteric agonist with iperoxo-like efficacy and acetylcholine-like affinity. (**a**) Equilibrium binding of indicated orthosteric agonists to M_2 receptors stably expressed in live CHO-hM_2 cells using [^{3}H]NMS as the radioactive probe. Total binding in the absence of test compounds was set to 100 %. Data points were fitted by a four-parameter logistic function and affinity values were calculated using subsequent Cheng-Prusoff correction. Data are means ± s.e.m. of 3-4 independent experiments conducted in triplicate. (**b**) [^{35}S]GTPγS binding to membranes of CHO-hM_2 cells represents M_2 receptor-mediated G_i activation induced by the indicated orthosteric agonists. Total [^{35}S]GTPγS binding in the absence of test compounds was set to 0 %; maximum ACh-induced [^{35}S]GTPγS binding was set to 100 %. Data are means ± s.e.m. from 4-6 independent experiments conducted in triplicate. (**c,d**) Shown are baseline-corrected DMR responses measured as wavelength shifts (Δ pm) and recorded over time after addition of indicated concentrations of isox to live CHO-hM_2 cells under control conditions **(c)** and after PTX -pre-treatment (100 ng/ml, overnight) (**d**). Data are means and s.e.m. of one representative out of 4 independent experiments. (**e,f**) Concentration-effect curves of maximum positive peak DMR (reflecting G_i activation) (**e**) and negative peak DMR (reflecting G_s activation) (**f**) induced by ACh, isox and iperoxo are shown in black, orange and green, respectively. The operational model of agonism was fitted to the data points in (**e**) and (**f**). DMR of solvent controls was set to 0 %. The maximum positive and negative DMR responses of all orthosteric agonists were set to 100 %. The slope was constrained to 1. Data are means ± s.e.m. from 3-7 independent experiments conducted in triplicate. (**g**) Operational efficacies (log τ) for both G_i and G_s activation as derived from the fits to the data in (**e**) and (**f**). Isox and iperoxo are superagonists with respect to both G_i and G_s activation (*,**: $P < 0.05$, $P < 0.01$, according to One-way ANOVA and Bonferroni's multiple comparison test). (**h**) $\Delta\Delta\log(\tau/K_A)$ values display true ligand bias relative to ACh which is taken as balanced agonist. Data are means with 95% confidence intervals (CIs). Isox and iperoxo are unbiased relative to ACh as their 95% CIs include zero.

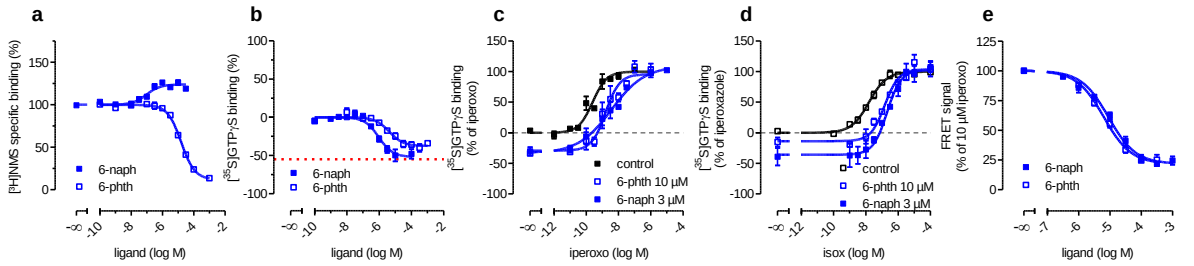

Figure 6: The allosteric moieties do not activate M_2 receptors. (**a**) Equilibrium binding of 6-naph and 6-phth to membranes of CHO-hM_2 cells using [^{3}H]NMS as an orthosteric probe. Total binding in the absence of test compounds was set to 100 %. Curve fitting was based on the allosteric ternary complex model. Data are means ± s.e.m. from 4 independent experiments conducted in triplicate. (**b**) 6-phth and 6-naph by themselves reduce basal [^{35}S]GTPγS binding to membranes of CHO-hM_2 cells in a concentration-dependent manner. Total [^{35}S]GTPγS binding in the absence of test compounds was set to 0 %; maximum iperoxo-induced [^{35}S]GTPγS binding was set to 100 %. The red dotted line indicates the inverse agonistic effect of 10 µM atropine. Data are means ± s.e.m. from 3-4 independent experiments conducted in triplicate. (**c,d**) 6-phth and 6-naph antagonize iperoxo (**c**) and isox (**d**)-induced [^{35}S]GTPγS binding. Concentrations used approximately account for a half-maximal reduction of basal [^{35}S]GTPγS binding. (**e**) 6-phth (open squares) and 6-naph (filled squares) allosterically inhibit iperoxo-induced activation of an N-FLAG-tagged hM_2 FlAsH–eCFP fusion protein stably expressed in HEK293 cells. Maximum agonist-induced FRET in the absence of allosteric moieties was set to 100 %. Data are means ± s.e.m. from at least 12 independent experiments.

Radioligand competition binding experiments uncovered two dynamic orientations for each of the ligands iper-6-naph and isox-6-naph which differed in their orientation ratio (**Fig. 7a**). Iper-6-naph and its active moiety iperoxo both displaced the orthosteric radioligand [^{3}H]N-methylscopolamine ([^{3}H]NMS), which indicated preferential binding of iper-6-naph in the active pose. However, [^{3}H]NMS displacement by iper-6-naph was incomplete, thus revealing that a small population of [^{3}H]NMS-bound receptors was additionally occupied by iper-6-naph in the purely allosteric inactive orientation. Quantification of the fractional receptor occupancy showed a pronounced preference of iper-6-naph for the active pose (79% versus 21%, **Fig. 8** and **Table 1**). Replacement of the active 'iper' moiety in iper-6-naph by the less affine 'isox' moiety shifted binding towards the purely allosteric inactive orientation: isox-6-naph, unlike its active building block isox, enhanced rather than displaced [^{3}H]NMS binding by ternary complex formation (**Fig. 7a**), thus demonstrating a pronounced preference for the allosteric, inactive pose (7% versus 93%; **Fig. 8** and **Table 1**). Yet, isox-6-naph was still able to induce some [^{35}S]GTPγS binding (**Fig. 7b**) confirming the existence and functionality of a small receptor population bound by isox-6-naph in the active orientation (**Fig. 7b**). Of note, the allosteric inactive fragment 6-naph by itself reduced ligand-independent, spontaneous [^{35}S]GTPγS binding of the receptor and antagonized [^{35}S]GTPγS binding induced by iperoxo and isox (**Fig. 6**). Regarding receptor structure, fluorescence resonance energy transfer (FRET) experiments using a recently established M_2 fluorescein arsenical hairpin binder-enhanced CFP sensor (FlAsH-eCFP) sensor[18] indicated a 6-naph-mediated allosteric reversal of the active receptor conformation induced by orthosteric iperoxo (**Fig. 6** and

Table 1). This implied that binding of iper-6-naph and isox-6-naph in the inactive, 6-naph-like orientation stabilizes receptor conformations structurally and functionally opposite to that induced by iperoxo.

In line with its higher binding preference for the active orientation, iper-6-naph induced a significantly ($P < 0.0001$) higher biological response than isox-6-naph (**Fig. 7b** and **Table 1**). This was mainly caused by their deviating orientation ratios; iperoxo had a more than tenfold higher affinity than the inactive moiety 6-naph, whereas the affinities of isox and 6-naph were in the same range (**Fig. 7a** and **Table 1**). This favored the active orientation in case of iper-6-naph and, in contrast, led to an increased fraction of inactive receptors in case of isox-6-naph.

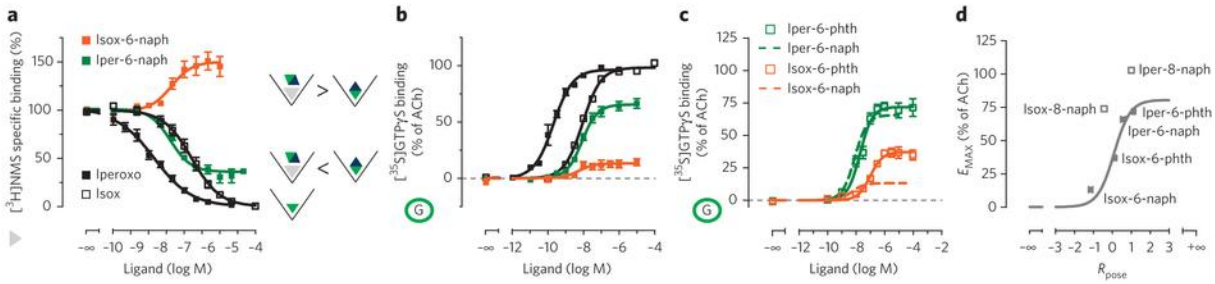

Figure 7: The orientation ratio determines graded ligand efficacy. (**a**) Influence on [^{3}H]NMS equilibrium binding of indicated test compounds to membranes of CHO-hM_2 cells reveals two co-existing receptor populations. Symbols show the receptor's binding cavity and its occupancy by either the bipharmacophoric ligand (green-blue diamond) alone, bound together with [^{3}H]NMS (gray triangle) or by the active moieties iperoxo or isox (green triangle). (**b**) [^{35}S]GTPγS binding to membranes of CHO-hM_2 cells represents M_2 receptor-mediated G_i activation. Total [^{35}S]GTPγS binding in the absence of test compounds was set to 0% (dashed line), and maximum ACh-induced [^{35}S]GTPγS binding was set to 100%. Compounds are the same as in **a**. The ´G´ enclosed in the green circle symbolizes G-protein activation. (**c**) [^{35}S]GTPγS binding induced by iper-6-phth and isox-6-phth compared with the respective X-6-naph congeners (where X is 'iper', 'isox'; represented by dashed lines in green and orange, respectively). Fitted parameter values from **b** and **c** are compiled in **Tables 1** and **3** (**d**) Maximum [^{35}S]GTPγS binding (gray squares) is plotted against the orientation ratios R_{pose} of indicated hexamethylene-type test compounds, yielding a sigmoidal orientation-efficacy relationship (filled squares, gray curve). Octamethylene-linker compounds isox-8-naph and iper-8-naph (open squares) reveal the role of the linker and are not included into the curve fit. Effects were normalized to the maximum effect of ACh, which was set to 100%. Where not visible, error bars did not exceed the symbols. Data in **a-d** represent mean ± s.e.m. from 4-8 independent experiments, conducted in triplicate.

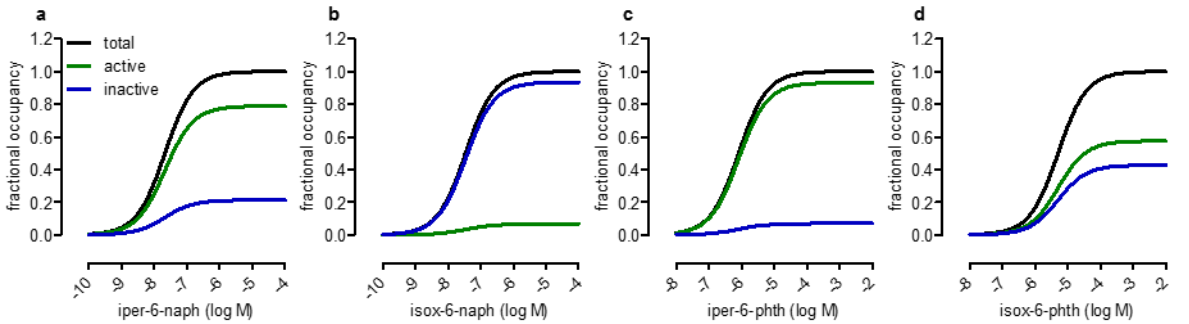

Supplementary Figure 8: Fractional binding of hexamethylene-type dynamic ligands. Computation of the concentration-dependent fractional receptor occupancy of (**a**) iper-6-naph, (**b**) isox-6-naph, (**c**) iper-6-phth, and (**d**) isox-6-phth. Concentration-dependent total binding and fractional receptor occupancies in both the active and inactive poses are illustrated as black, green and blue lines, respectively. Computation was based on the following equations:

Total binding: $Y_{tot} = \frac{[AB] \cdot R_T}{[AB] + K_{obs}}$ with $K_{obs} = \frac{K_A \cdot K_B}{K_A + K_B}$;

fractional occupancy of the active pose: $Y_{RAB} = \frac{f_{RAB} \cdot [AB] \cdot R_T}{[AB] + K_{obs}}$ with $f_{RAB} = \frac{K_B}{K_A + K_B}$, and

fractional occupancy of the inactive pose: $Y_{ABR} = \frac{f_{ABR} \cdot [AB] \cdot R_T}{[AB] + K_{obs}}$ with $f_{ABR} = \frac{K_A}{K_A + K_B}$.

R_T represents the total number of receptors, $[AB]$ denotes the concentration of the dynamic ligand, K_{obs} is the observed equilibrium dissociation constant of the dynamic ligand, K_A and K_B denote the equilibrium dissociation constants of the dynamic ligand for the active and inactive pose, respectively, and represent the affinities for the respective poses, and f_{RAB} and f_{ABR} are the maximal fractional occupancies at receptor saturation of the active and inactive pose, respectively. For delineation of the equations see **Note 1.** Parameter values used for the computation were determined in equilibrium binding assays and are compiled in **Table 1**.

CHO-M_2 membranes	[^{3}H]NMS binding				[^{35}S]GTPγS binding	
	Dissociation binding	Equilibrium binding			4-PL function	
Ligand	**$pEC_{50,diss}$ ± s.e.m.**	**pK_{active} ± s.e.m.**	**$pK_{inactive}$ (α) ± s.e.m.**	**pK ± s.e.m.$_i$ (n ± s.e.m.)**	**% E_{max} (mean ± s.e.m.)**	**pEC_{50} ± s.e.m. (n ± s.e.m.)**
Acetylcholine	n.d.	n.a.	n.a.	n.d.	100 ± 2	7.27 ± 0.06 (0.64 ± 0.03)
Iperoxo	n.d.	n.a.	n.a.	8.35 ± 0.12 (-0.55 ± 0.05)	97 ± 2	9.69 ± 0.11 (0.80 ± 0.06)
Isox	n.d.	n.a.	n.a.	6.78 ± 0.16 (-0.72 ± 0.08)	99 ± 1	8.06 ± 0.03 (0.84 ± 0.04)
6-naph	6.75 ± 0.09	n.a.	7.00 ± 0.12 (1.36 ± 0.03)	n.a.	-52 ± 3	6.04 ± 0.04
Iper-6-naph	6.76 ± 0.07	7.57 ± 0.06	7.00[a] (1.36)	n.a.	66 ± 2	8.08 ± 0.04
Isox-6-naph	7.46 ± 0.05	6.28 ± 0.44	7.43[b] (1.92 ± 0.22)	n.a.	13 ± 1	8.51 ± 0.18
6-phth	n.d.	n.a.	4.93 ± 0.02 (0.09 ± 0.01)	n.a.	-38 ± 2	5.37 ± 0.02
Iper-6-phth	n.d.	6.06 ± 0.04	4.93[a] (0.09)	n.a.	72 ± 2	7.72 ± 0.07
Isox-6-phth	n.d.	5.06 ± 0.05	4.93 [a] (0.09)	n.a.	37 ± 1	6.97 ± 0.11
8-naph	6.84 ± 0.04	n.a.	7.41 ± 0.33 (1.30 ± 0.05)	n.a.	n.d.	n.d.
Iper-8-naph	n.d.	n.d.	n.d.	n.d.	103 ± 2	9.15 ± 0.07
Isox-8-naph	n.d.	n.d.	n.d.	n.d.	74 ± 2	8.63 ± 0.06

Table 1: Pharmacological parameters of ligand binding to and activation of the M_2 receptor in membranes of CHO-hM_2 cells. $pEC_{50,diss}$: negative logarithm of the ligand concentration which half-maximally inhibits [^{3}H]NMS dissociation. pK_{active}, $pK_{inactive}$: negative logarithm of the equilibrium dissociation constants for the active binding pose and the purely allosteric inactive binding pose, respectively. α: cooperativity between [^{3}H]NMS and the respective ligand. pK: negative logarithm of the equilibrium dissociation constant calculated after curve fitting based on a four-parameter logistic function (4-PL function) and subsequent Cheng-Prusoff correction. E_{max}: maximal effect is reflected as the upper plateau of the corresponding concentration-effect curve relative to the upper plateau of the

acetylcholine concentration-effect curve. pEC_{50}: negative logarithm of the ligand concentration which elicits the half-maximal effect. n: slope. n.d.: not determined. n.a.: not applicable.
[a]: values were constrained to those obtained with the respective allosteric fragment. [b]: value was constrained to that obtained after curve fitting based on the allosteric ternary complex model.

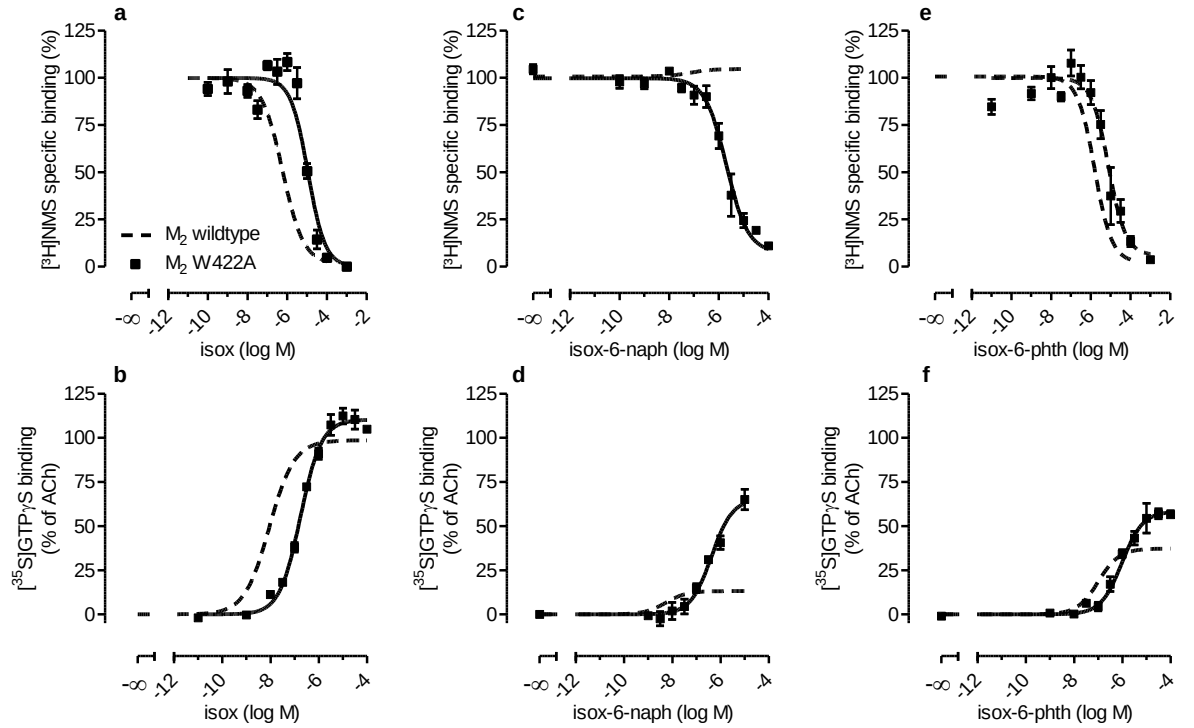

Figure 9: Allosteric loss-of-affinity receptor mutation promotes orthosteric [^{3}H]NMS displacement and receptor activation. (**a,c,e**) Equilibrium binding of indicated ligands to M_2 W422A mutant receptors stably expressed in live CHO-hM_2-W422A cells using [^{3}H]NMS as the radioactive probe. Total binding in the absence of test compounds was set to 100 %. Data points were fitted by a four-parameter logistic function and affinity values were calculated using subsequent Cheng-Prusoff correction (pK_i: isox = 5.28 ± 0.05; isox-6-naph = 6.06 ± 0.15; isox-6-phth = 5.32 ± 0.16). Data are means ± s.e.m. of 4 independent experiments conducted in triplicate. Binding curves of indicated ligands derived from equilibrium binding assays at the M_2 wildtype receptor are shown for comparison as dashed lines (for parameter values see **Table 2**). (**b,d,f**) [^{35}S]GTPγS binding to membranes of CHO-hM_2-W422A cells represents receptor-mediated G_i activation induced by the indicated ligands. Total [^{35}S]GTPγS binding in the absence of test compounds was set to 0 %; maximum ACh-induced [^{35}S]GTPγS binding was set to 100 % (pEC_{50}: isox = 6.77 ± 0.04; isox-6-naph = 6.38 ± 0.09; isox-6-phth = 6.02 ± 0.11; E_{Max}(%): isox = 100 ± 1; isox-6-naph = 66 ± 4; isox-6-phth = 58 ± 1). Data are means ± s.e.m. from 3-4 independent experiments conducted in triplicate. Concentration-effect curves of [^{35}S]GTPγS binding elicited by activation of M_2 wildtype receptors are shown for comparison as dashed lines (for parameter values see **Table 1**). Expression of M_2 wildtype and M_2 W422A mutant receptors was not significantly different (B_{max}-W422A = 78% of B_{max}-wildtype, P = 0.19, unpaired t-test).

Isox-6-naph's efficacy was rescued in the loss-of-affinity mutant M_2^{W422A}, recently identified as an allosteric key epitope[18,19]. At this mutant, isox-6-naph almost completely displaced [^{3}H]NMS, indicating a preference for the active pose and, in line with this, more efficaciously induced receptor activation than at the wild-type receptor (**Fig. 9**). The dependence of ligand efficacy on the orientation ratio was also confirmed in live Chinese hamster ovary (CHO)-hM_2 cells by assaying biological activity using DMR measurements[18,20,21] (**Fig. 10** and **Table 2**).

This demonstrated that the role of the orientation ratio for ligand efficacy is independent of the system.

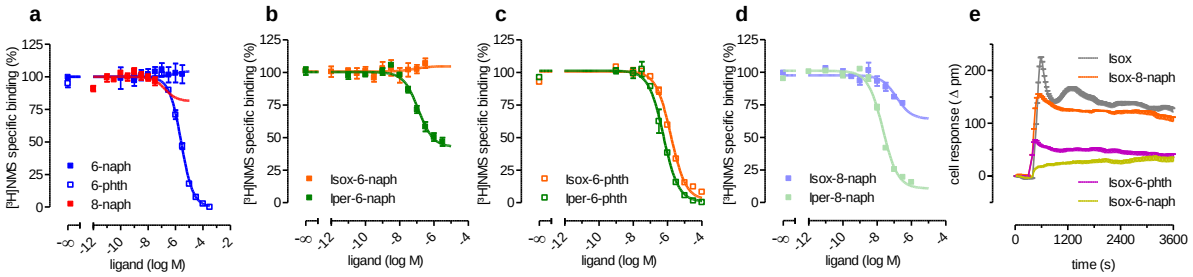

Figure 10: Ligand binding to and signaling of live CHO-hM$_2$ cells. Equilibrium binding of indicated ligands to M$_2$ receptors stably expressed in live CHO-hM$_2$ cells using [^{3}H]NMS as the radioactive probe. Total binding in the absence of test compounds was set to 100 %. Data points are fitted in the case of (**a**) by the allosteric ternary complex model and in the case of (**b-d**) by a model of bivalent ligand binding. Data are means ± s.e.m. of 3-11 independent experiments conducted in triplicate. (**e**) Shown are baseline-corrected DMR responses measured as wavelength shifts (Δ pm) and recorded over time after addition of indicated test compounds to CHO-hM$_2$ cells. Concentrations of ligands: isox 100 µM; isox-8-naph, isox-6-phth and isox-6-naph: 10 µM. Data are means and s.e.m. of one representative out of at least 4 independent experiments.

CHO-M_2 cells	[^{3}H]NMS binding				DMR
	Dissociation binding	Equilibrium binding			
Ligand	$pEC_{50,diss}$ ± s.e.m.	pK_{active} ± s.e.m.	$pK_{inactive}$ (α) ± s.e.m.	pK ± s.e.m.$_i$ (n ± s.e.m.)	% E_{max} (mean ± s.e.m.)
Acetylcholine	n.d.	n.a.	n.a.	6.24 ± 0.11	100 ± 3
Iperoxo	n.d.	n.a.	n.a.	7.95 ± 0.05 (-0.67 ± 0.04)	100 ± 3
Isox	n.d.	n.a.	n.a.	6.51 ± 0.04 (-0.82 ± 0.05)	103 ± 3
6-naph	6.09 ± 0.08	n.a.	6.04 ± 0.04 (1.08 ± 0.09)	n.a.	n.d.
Iper-6-naph	6.54 ± 0.11	6.64 ± 0.04	6.04[a] (1.08)	n.a.	58 ± 3[c]
Isox-6-naph	7.16 ± 0.05	n.c.	7.12[b] (1.12 ± 0.09)	n.a.	10 ± 2
6-phth	4.51 ± 0.09	n.a.	5.84 ± 0.04 (< 0.01)	n.a.	n.d.
Iper-6-phth	4.83 ± 0.07	6.37 ± 0.05	5.84[a] (< 0.01)	n.a.	89 ± 3[c]
Isox-6-phth	5.15 ± 0.05	5.62 ± 0.08	5.84[a] (< 0.01)	n.a.	22 ± 2
8-naph	6.69 ± 0.08	n.a.	6.84 ± 0.11 (0.71 ± 0.25)	n.a.	n.d.
Iper-8-naph	7.08 ± 0.08	7.85 ± 0.02	6.84[a] (0.71)	n.a.	105 ± 4[c]
Isox-8-naph	7.34 ± 0.03	6.40 ± 0.11	6.84[a] (0.71)	n.a.	57 ± 6

Table 2: Pharmacological parameters of ligand binding to and activation of the M_2 receptor in live CHO-hM_2 cells. $pEC_{50,diss}$: negative logarithm of the ligand concentration which half-maximally inhibits [^{3}H]NMS dissociation. pK_{active}, $pK_{inactive}$: negative logarithm of the equilibrium dissociation constants for the active binding mode and the purely allosteric inactive binding mode, respectively. α: cooperativity between [^{3}H]NMS and the respective ligand. pK: negative logarithm of the equilibrium dissociation constant calculated after curve fitting based on a four-parameter logistic function and subsequent Cheng-Prusoff correction. n: slope. E_{max}: maximal effect induced by ligand concentrations

of ligands sufficient to induce full receptor occupancy. Data were normalized to the maximal effect of 100 µM acetylcholine. n.d.: not determined. n.a.: not applicable. n.c.: fit did not converge.
[a]: values were constrained to those obtained with the respective allosteric fragment.
[b]: value was constrained to that obtained after curve fitting based on the allosteric ternary complex model.
[c]: data were taken from ref.18.

To probe the predictive power of the model of dynamic ligand binding, we replaced the allosteric 6-naph moiety with the 100-fold lower affinity inactive 6-phth (**8**) moiety (**Fig. 6** and **Table 1**), yielding the ligands iper-6-phth and isox-6-phth (**Fig. 3**). As expected, iper-6-phth and isox-6-phth had a lower receptor affinity (~1.5 log units) compared with their '6-naph' counterparts (**Fig. 11** and **Table 1**). As a consequence, the lower affinity of '6-phth' promoted binding of iper-6-phth and isox-6-phth in the active pose (**Fig. 8**). In line with this, isox-6-phth was more efficacious in stimulating a biological response than isox-6-naph (**Fig. 7c**). Iper-6-phth was only slightly more efficacious than iper-6-naph (**Fig. 7c**), indicating that the highly potent 'iper' moiety mediated optimal positioning of the bivalent ligand in the active pose, irrespective of the nature of the allosteric building block. The difference remaining between the maximum effects of the iper-6-x compounds and the 100% level of G_i activation (**Fig. 7d**) was due to the negative cooperativity of efficacy between the building blocks and, biologically, has been suggested to result from a reduced conformational freedom in the allosteric vestibule caused by the allosteric building block[18]. Thus, the degree of receptor activation was submaximal even at full occupancy in the active orientation (**Fig. 7d** and **Fig. 2**). In line with this, the group of bipharmacophoric probes containing a hexamethylene linker defined a sigmoidal orientation-effect relationship with a submaximal upper plateau (**Fig. 7d**).

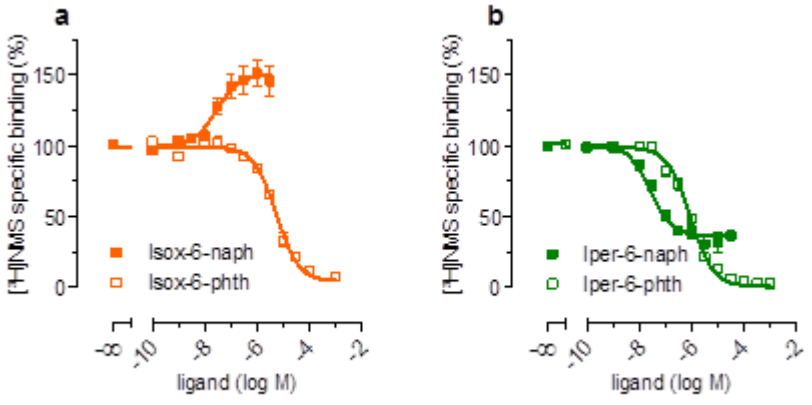

Figure 11: Binding topography of bi-pharmacophoric ligands consisting of the less-affine antagonistic moiety 6-phth. (**a-b**) Equilibrium binding of isox-6-phth (**a**) and iper-6-phth (**b**) to membranes of CHO-hM_2 cells using [^{3}H]NMS as an orthosteric probe. Total [^{3}H]NMS binding in the absence of test compounds was set to 100 %. Curve fitting was based on a model of bivalent ligand binding in case of isox-6-phth and iper-6-phth. Data are means ± s.e.m. from 4 independent experiments conducted in triplicate. Binding curves of isox-6-naph and iper-6-naph are shown again for comparison.

Ligands of an octamethylene linker type have a higher efficacy at M_2 receptors compared with ligands of the hexamethylene type[18]. Mechanistically, this is attributed to a less pronounced steric hindrance of activation-related conformational rearrangement[18]. In the present study, the octamethylene linker increased efficacy relative to the hexamethylene counterparts. However, as predicted by the difference in the orientation ratio, iper-8-naph (**9**) still displayed a higher level of receptor activation than isox-8-naph (**10**) (details on binding and functional experiments including the inactive fragment 8-naph (**11**) are in **Fig. 10** and **12** and **Tables 1** and **2**). This is in line with the concept of dynamic ligand binding and expands the range of achievable biological activity to full agonism (**Fig. 7d** and **Fig. 2**).

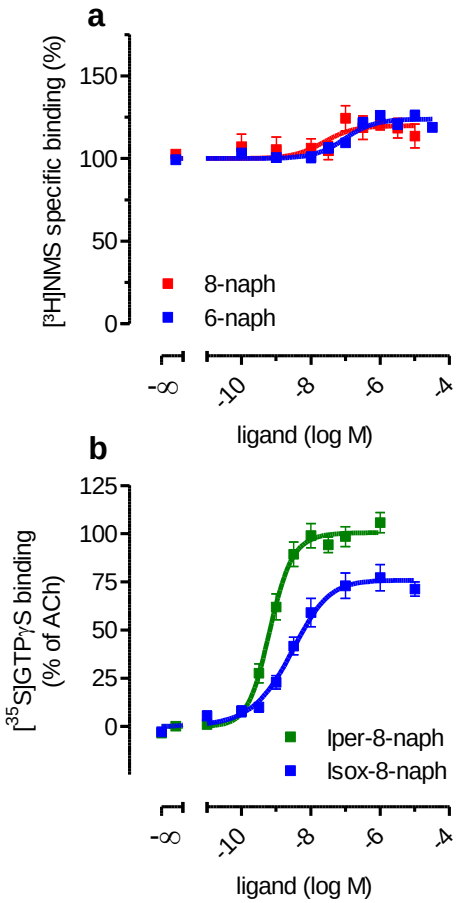

Figure 12: Binding of the allosteric inactive moiety 8-naph and receptor activation by bi-pharmacophoric ligands thereof. (**a**) Effect of 8-naph in membranes of CHO-hM_2 cells on orthosteric [^{3}H]NMS binding. Specific [^{3}H]NMS binding in the absence of test compound was set to 100 %. Curve fitting was based on the allosteric ternary complex model. Data are means ± s.e.m. from 4 independent experiments conducted in triplicate. The binding curve of 6-naph is shown for comparison. Both allosteric fragments did not differ neither in their affinity nor in their cooperativity with the orthosteric radioligand. (**b**) [^{35}S]GTPγS binding to membranes of CHO-hM_2 cells represents M_2 receptor-mediated G_i activation induced by the indicated bi-pharmacophoric ligands. Total [^{35}S]GTPγS binding in the absence of test compounds was set to 0 %; maximum ACh-induced [^{35}S]GTPγS binding was set to 100 %. Data are means ± s.e.m. from 7-9 independent experiments conducted in triplicate. Curve fitting was based on the operational model of agonism for dynamic ligands.

CHO-M_2 membranes	[^{3}H]NMS binding		[^{35}S]GTPγS binding		
	Equilibrium binding		Operational model		
Ligand	**pIC_{50} ± s.e.m.**	**pK_{obs} ± s.e.m.**	**pK_D ± s.e.m.**	**log τ_{dyn} ± s.e.m.**	**Δlog ε_{dyn} ± s.e.m.**
Iper-6-naph	7.39 ± 0.07	7.67 ± 0.13^{ns}	7.67^a	0.24 ± 0.03	-0.88 ± 0.04
Isox-6-naph	7.54 ± 0.17^b	7.46 ± 0.46^{ns}	7.46^a	-1.30 ± 0.09	-2.42 ± 0.10
Iper-6-phth	6.11 ± 0.04	6.09 ± 0.04^{ns}	6.09^a	1.04 ± 0.05	-0.08 ± 0.06
Isox-6-phth	5.32 ± 0.04	5.30 ± 0.05^{ns}	5.30^a	-0.09 ± 0.06	-1.21 ± 0.07

Table 3: Binding parameters, dynamic transduction coefficients and relative dynamic intrinsic efficacies of bi-pharmacophoric ligands. pIC_{50}: negative logarithm of the ligand concentration which half-maximally inhibits [^{3}H]NMS binding. Values were obtained by fitting the equilibrium binding curves with a four-parameter logistic function. pK_{obs}: negative logarithm of the observed equilibrium dissociation constant of dynamic ligands. Values were calculated according to equation 5 (main text) using the values compiled in **Table 1**. Note: the pIC_{50} and pK_{obs} are not significantly different from each other according to an unpaired t-test. pK_D: negative logarithm of the equilibrium dissociation constant of dynamic ligand-bound receptor complexes. pK_D represents the functional affinity of dynamic ligand and is shown in the **Note 1** to equal the pK_{obs} values. Therefore, for fitting the [^{35}S]GTPγS binding curves with equation 6 (main text) pK_D was constrained to the respective pK_{obs} values. log τ_{dyn} represents the dynamic transduction coefficient of dynamic ligands and was obtained by fitting the [^{35}S]GTPγS binding curves with equation 6 (main text). Δlog ε_{dyn} represents the relative dynamic intrinsic efficacy of the dynamic ligands and is system-independent. Δlog ε_{dyn} was calculated according to the following equation:

$$\log\left(\frac{\tau_{dyn}}{\tau_{ACh}}\right) = \log\left(\frac{\frac{\varepsilon_{MAX}\cdot f_{RAB}\cdot R_T}{K_E}}{\frac{\varepsilon_{ACh}\cdot R_T}{K_E}}\right) = \log\left(\frac{\varepsilon_{MAX}\cdot f_{RAB}}{\varepsilon_{ACh}}\right) = \log\left(\frac{\varepsilon_{dyn}}{\varepsilon_{ACh}}\right) = \Delta\log\varepsilon_{dyn}$$

log τ_{ACh} (1.12 ± 0.03) was determined by fitting the [^{35}S]GTPγS binding curves with the standard operational model of agonism[14]. ns: not significantly different. a: value was constrained to the respective pK_{obs} value. b: value represents the pEC_{50} as the equilibrium binding curve is upward-deflected and represents enhancement of [^{3}H]NMS binding.

3. Conclusion

Our findings revise the concept of partial agonism at GPCRs. We show that bipharmacophoric ligands dynamically switch between two distinct binding orientations, resulting in both active and inactive populations of receptors bound by a given ligand. This makes ligand efficacy at GPCRs predictable for what is to our knowledge the first time. It

allows generating libraries of agonists with various efficacies ranging from almost zero to full agonism. Using partial agonists with varying efficacies, the most efficient and safest level of receptor activation can be systematically elucidated. Thus, dynamic ligand binding in multiple orientations represents a new avenue of general and immediate applicability for the rational design of agonists with predictable efficacy at any GPCR.

Methods

Materials and buffers. Tissue culture media and assay reagents were purchased from Sigma-Aldrich (Taufkirchen, Germany) and Life Technologies (Darmstadt, Germany) and all laboratory reagents were from Sigma-Aldrich (Taufkirchen, Germany), unless specified otherwise. All of the purchased compounds were >99% purity. HEPES was purchased from AppliChem (Darmstadt, Germany) and Pertussis toxin (PTX) was purchased from Biotrend (Cologne, Germany). [^{3}H]NMS and [^{35}S]GTPγS were from PerkinElmer (Rodgau, Germany). Buffer A: 10 mM HEPES, 10 mM $MgCl_2$, 100 mM NaCl, pH 7.4; buffer B: Hank`s balanced salt solution (HBSS; Life technologies, Darmstadt, Germany), 20 mM HEPES, pH 7.0; buffer C: 150 mM NaCl, 10 mM HEPES, 2.5 mM KCl, 4 mM $CaCl_2$, 2 mM $MgCl_2$, 10 mM glucose, pH 7.3; buffer D: 144 mM NaCl, 10 mM HEPES, 5.4 mM KCl, 2 mM $CaCl_2$, 1 mM $MgCl_2$ pH 7.3.

Chemical synthesis of probes. Melting points were determined on a model B 540 Büchi or a Sanyo Gallenkamp melting point apparatus and are uncorrected. TLC analyses were performed on commercial silica gel 60 F254 aluminum sheets. ^{1}H NMR and ^{13}C NMR were recorded with a Varian Mercury 300 (^{1}H, 300.063 MHz; ^{13}C, 75.451 MHz) or a Bruker AV 400 (^{1}H, 400.132 MHz; ^{13}C, 100.613 MHz) spectrometer. The specific NMR assignments were unambiguously determined by using typical techniques including polarization transfer experiments (DEPT) and two-dimensional experiments, such as ^{1}H-^{1}H correlation (COSY) and ^{1}H-^{13}C-proton-carbon heteronuclear correlation (HMQC, HMBC). Chemical shifts (δ) are expressed in p.p.m., and coupling constants (*J*) in are expressed in Hertz. Abbreviations for data quoted are: s, singlet; t, triplet; m, multiplet; br, broad; br s, broad singlet. ESI mass spectra of the tested salts were recorded on a Varian 320 LC-MS/MS instrument. Data are reported as *m/z* of the corresponding positively charged molecular ions.

Iperoxo[22], Isox[23], 6-naph[17], 6-phth[17], iper-6-naph[17] and iper-6-phth[17], iper-8-naph[18], isox-6-naph[24], isox-6-phth[24], and 1,8-naphthalimidopropylamine (**12**)[24], have been resynthesized exactly as described previously.

The NMR spectroscopic features and the purity requirements of these known compounds matched those found in the literature. A schematic presentation of the synthetic route leading to compounds 8-naph and isox-8-naph is in **Figure 13**. Detailed information about the chemical syntheses and characterization of 8-bromo-*N*-(3-(1,3-dioxo-1*H*-benzo[de]isoquinolin-2(3*H*)-yl)-2,2-dimethylpropyl)-*N*,*N*-dimethyloctan-1-aminium bromide (**13**), 8-naph and isox-8-naph is provided in the **Note 2**.

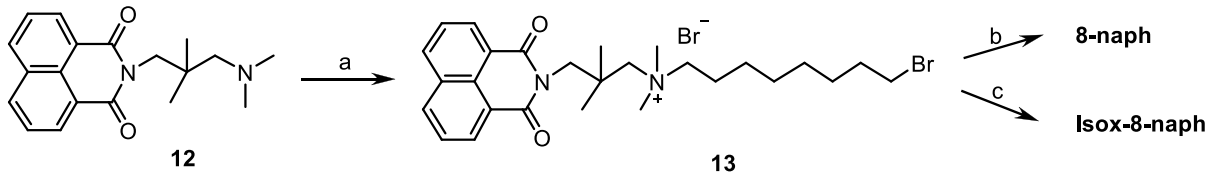

Figure 13: Reaction scheme for compounds 8-naph and isox-8-naph. (a) $Br(CH_2)_8Br$ (excess); (b) *N*,*N*-dimethylethylamine; (c) refluxing CH_3CN/base, 4-(isoxazol-3-yloxy)-*N*,*N*-dimethylbut-2-yn-1-amine.

Cell culture. Flp-In-Chinese hamster ovary cells (Flp-In-CHO) stably expressing the hM_2 receptor (CHO-hM_2 cells) or the hM_2^{W422A} mutant receptor (CHO-hM_2^{W422A} cells)[18] were cultured in Ham's nutrient mixture F-12 (HAM-F12) supplemented with 10% (v/v) FCS (FCS), 100 U/ml penicillin, 100 µg/ml streptomycin and 2 mM L-glutamine at 37 °C in a 5% CO_2 humidified atmosphere. HEK293 cells stably expressing the hM_2 receptor FRET-sensor were maintained in DMEM supplemented with 10% (v/v) FCS, 100 U/ml penicillin, 100 µg/ml streptomycin and 200 µg/ml G418 and cultured at 37 °C in a 7% CO_2 humidified atmosphere.

Radioligand binding experiments. Binding experiments using membranes of CHO-hM_2 cells were carried out in 96-well microtiter plates (ABgene, Germany) essentially as described previously[19,25]. Experiments were conducted in buffer A (supplemented with 100 µM GDP in case of equilibrium binding) at 30 °C using [^{3}H]NMS as the radioactive probe (2 nM for two-point kinetic dissociation and 0.2 nM for equilibrium binding experiments). Incubation time for equilibrium binding was 18 h and calculated as published elsewhere[19].

Binding experiments (dissociation and equilibrium) in live CHO-hM_2 cells and CHO-hM_2^{W422A} cells were conducted in buffer B exactly as described previously[18].

GTPγS binding experiments. Experiments were carried out in buffer A supplemented with 10 µM GDP using membranes of CHO-hM_2 cells and CHO-hM_2^{W422A} cells exactly as described previously[18].

DMR assay. A general protocol has been published recently[21]. DMR assays using live CHO-hM_2 cells were carried out in buffer B exactly as outlined elsewhere[18].

FlAsH labeling and single-cell FRET measurements. FlAsH-labeling was performed in buffer C as described previously[18, 26]. FRET measurements were essentially carried out in buffer D as recently outlined in detail[18]. HEK 293 cells stably expressing the hM_2 receptor FRET sensor were prestimulated with 10 µM iperoxo to induce a conformational change of the receptor protein. To determine the effects of the allosteric moieties 6-naph and 6-phth on receptor structure, prestimulated HEK293-hM_2 receptor FRET sensor cells were superfused with buffer D containing both 10 µM iperoxo and increasing concentrations of the respective allosteric fragment.

Calculations and data analysis. Data analysis in general was performed using Prism 5.01 (GraphPad Software, San Diego, CA).

Equilibrium binding data from ACh, iperoxo and isox were analyzed by a four-parameter logistic function yielding IC_{50} values, which were subsequently converted into apparent equilibrium dissociation constants, K_i, using the Cheng-Prusoff correction as described previously[17]. In case of the allosteric fragments 6-naph, 6-phth and 8-naph, the allosteric ternary complex model was applied, yielding parameters of affinity and cooperativity with the radioligand[17,27,28].

To analyze the equilibrium binding curves of the bipharmacophoric ligands to yield parameters for the affinities for the active as well as in the inactive pose, the following equation was used[17, 18,29] (derivation is in **Note 1**):

$$Y = \frac{[X]\cdot R_T}{[X] + K_X'} \tag{1}$$

where:

$$K_X' = K_X \cdot \frac{\left(1 + [AB]\cdot\left(\frac{K_A + K_B}{K_A \cdot K_B}\right)\right)}{\left(1 + \frac{\alpha'\cdot[AB]}{K_B}\right)} \tag{2}$$

Y represents the binding of the radioligand X (**Note 1**). $[X]$ and $[AB]$ denote the concentrations of the radioligand [^{3}H]NMS and the dynamic ligand AB, respectively. K_X is the equilibrium dissociation constant of the radioligand-receptor complex and reflects affinity of the radioligand ([^{3}H]NMS, K_X was set to 0.53 and 0.26 nM for CHO-hM_2 membranes and live cells, respectively). K_A and K_B are the equilibrium dissociation constants of the active and inactive dynamic ligand-receptor complexes, respectively, and are taken to reflect the

affinities of the dynamic ligand in the active and inactive pose, respectively. α' denotes the cooperativity between X and AB. R_T is the total number of receptors.

The orientation ratio R_{pose} was calculated as follows:

$$R_{pose} = -\log\left(\frac{K_A}{K_B}\right) = -\log\left(\frac{K_{active}}{K_{inactive}}\right) \quad (3)$$

Equilibrium binding curves of the bipharmacophoric ligands were additionally fitted by a four-parameter logistic function to yield values for the half-maximal inhibitory concentration (IC_{50}) of [^{3}H]NMS binding. The IC_{50} value is given by the following equation (derivation is in **Note 1**):

$$IC_{50} = \frac{K_A K_B([X] + K_X)}{K_X(K_A + K_B) + \alpha' K_A[X]} \quad (4)$$

In the presence of a very low concentration of X, the IC_{50} value approaches the observed dissociation constant of the dynamic ligand (derivation is in **Note 1**):

$$IC_{50} = \frac{K_A \cdot K_B}{K_A + K_B} = K_{obs} \quad (5)$$

[^{35}S]GTPγS binding data of all compounds were generally fitted by a four-parameter logistic function yielding parameter values for potency (pEC_{50}) and maximum effect (E_{MAX}). [^{35}S]GTPγS binding data of all bipharmacophoric compounds were additionally analyzed by the operational model of agonism for dynamic ligands (derivation is in **Note 1**):

$$E = \frac{E_{MAX}}{1 + \frac{([AB] + K_D)^n}{[AB]^n \cdot \tau_{dyn}^n}} \quad (6)$$

in which

$$K_D = \frac{K_A \cdot K_B}{K_A + K_B} = K_{obs} \quad (7)$$

and

$$\tau_{dyn} = \tau_{\max} \cdot f_{RAB} = \frac{\varepsilon_{\max} \cdot R_T}{K_E} \cdot \frac{K_B}{K_A + K_B} \quad (8)$$

E_{MAX} is the maximal response of the system reflected by the maximal effect of a full agonist, K_D is the affinity of the dynamic ligand from functional data and equals the observed dissociation constant K_{obs} obtained from binding data. K_A denotes the affinity of the ligand AB for the active pose; K_B denotes the affinity of the ligand AB for the inactive pose, τ_{dyn} represents the dynamic transduction coefficient of the ligand which is composed of $\tau_{\max}$ multiplied by the fraction of the ligand-receptor complexes in the active pose (f_{RAB}). $\tau_{\max}$ is the maximum transduction coefficient of the dynamic ligand at 100% occupancy of receptors in the active pose and is composed of the system-independent maximal intrinsic efficacy of the dynamic ligand ε_{MAX} and a system-dependent part R_T / K_E . K_E denotes the level of stimulus which elicits the half-maximal system response. n is the transducer slope. For fitting, K_D was constrained to the observed dissociation constant K_{obs} to yield dynamic transduction coefficients τ_{dyn} .

DMR recordings were solvent corrected. Quantification of probe-induced DMR signals was based on the signal's peak value (upward or downward deflected) between 500 s and 1,200 s and normalized on the peak value elicited by ACh, which was set 100%. Concentration-DMR curves of ACh, iperoxo and isox were fitted by the operational model of agonism[14], yielding parameter values K_A and τ to reflect affinity and efficacy of the respective agonist. Subsequent quantification of ligand bias was based on the use of a product of affinity and efficacy as described by Ehlert and co-workers[30,31]. Quantification was performed exactly as described previously[18].

Statistical analysis. Data are shown as mean ± s.e.m for *n* observations. Comparisons of groups were performed using one-way analysis of variance with Bonferroni's multiple comparison test.

Note 1

The binding model for dynamic ligands

Let AB be a bivalent ligand with two pharmacophores A and B . AB dynamically binds to a G protein-coupled receptor R to either stabilize the ligand receptor complexes $[RAB]$ or $[ABR]$ with the equilibrium dissociation constants K_{active} and $K_{inactive}$, respectively. In the

following theses constants are termed K_A and K_B, respectively. The equations are based on the following model which describes the aforementioned scenario.

$$[ABR] \rightleftharpoons AB + R \rightleftharpoons [RAB]$$

According to the law of mass action the concentrations of the ligand receptor complexes $[RAB]$ and $[ABR]$ are given as follows:

$$[RAB] = \frac{AB \cdot R}{K_A} \quad \textbf{(Equation 1)}$$

$$[ABR] = \frac{AB \cdot R}{K_B} \quad \textbf{(Equation 2)}$$

$$[ABR] = \frac{[RAB] \cdot K_A}{K_B} \quad \textbf{(Equation 3)}$$

The total concentration of receptors R_T is defined as follows:

$$R_T = R + [RAB] + [ABR] \quad \textbf{(Equation 4)}$$

Total binding of a dynamic ligand

The total binding of AB is given by:

$$\frac{[RAB]+[ABR]}{R_T} = \frac{\frac{[AB]\cdot[R]}{K_A} + \frac{[AB]\cdot[R]}{K_B}}{[R] + \frac{[AB]\cdot[R]}{K_A} + \frac{[AB]\cdot[R]}{K_B}} \quad \textbf{(Equation 5)}$$

Multiplying with $\frac{1}{[AB]\cdot[R]}$ yields:

$$\frac{[RAB]+[ABR]}{R_T} = \frac{\frac{1}{K_A} + \frac{1}{K_B}}{\frac{1}{[AB]} + \frac{1}{K_A} + \frac{1}{K_B}} \quad \textbf{(Equation 6)}$$

Rearranging yields the total binding $Y_{tot} = [RAB] + [ABR]$ of AB:

$$Y_{tot} = \frac{[AB] \cdot R_T}{[AB] + K_{obs}} \quad \textbf{(Equation 7)}$$

with the observed dissociation constant:

$$K_{obs} = \frac{K_A \cdot K_B}{K_A + K_B} \quad \textbf{(Equation 8)}$$

Fractional occupancies in the two binding modes

To determine the concentration-dependent fractional occupancy of a dynamic ligand AB in the binding mode $[RAB]$, one begins with:

$$\frac{[RAB]}{R_T} = \frac{\frac{[AB] \cdot [R]}{K_A}}{[R] + \frac{[AB] \cdot [R]}{K_A} + \frac{[AB] \cdot [R]}{K_B}} \quad \textbf{(Equation 9)}$$

Multiplying with $\frac{1}{[AB] \cdot [R]}$ yields:

$$\frac{[RAB]}{R_T} = \frac{\frac{1}{K_A}}{\frac{1}{[AB]} + \frac{1}{K_A} + \frac{1}{K_B}} \quad \textbf{(Equation 10)}$$

Rearranging yields:

$$\frac{[RAB]}{R_T} = \frac{[AB]}{[AB] \cdot \left(\frac{K_A + K_B}{K_B} \right) + K_A} \quad \textbf{(Equation 11)}$$

Dividing by $\frac{K_A + K_B}{K_B}$ gives the concentration-dependent fractional occupancy Y_{RAB} of AB in the binding mode $[RAB]$:

$$Y_{RAB} = \frac{f_{RAB} \cdot [AB] \cdot R_T}{[AB] + K_{obs}} \quad \textbf{(Equation 12)}$$

with $$f_{RAB} = \frac{K_B}{K_A + K_B} \quad \textbf{(Equation 13)}$$

where f_{RAB} represents the maximal fractional occupancy of AB in the binding mode $[RAB]$ at receptor saturation.

It can be shown that the concentration-dependent fractional occupancy Y_{ABR} of a dynamic ligand AB in the binding mode $[ABR]$ is given by:

$$Y_{ABR} = \frac{f_{ABR} \cdot [AB] \cdot R_T}{[AB] + K_{obs}} \quad \textbf{(Equation 14)}$$

$$f_{ABR} = \frac{K_A}{K_A + K_B} \quad \textbf{(Equation 15)}$$

with f_{ABR} representing the maximal fractional occupancy of AB in the binding mode $[ABR]$ at receptor saturation.

Note that both binding modes $[RAB]$ and $[ABR]$ have the same observed dissociation constant $K_{obs} = \frac{K_A \cdot K_B}{K_A + K_B}$.

Analysis of competition binding curves

The binding model described hereafter is analogous to the binding model for bivalent ligands which has been published recently[29]. Yet, to the best of our knowledge, a mathematical delineation of this model has not been reported until now.

Let AB be a bi-pharmacophoric ligand with pharmacophores A and B and X be an orthosteric radioligand. Let AB display a dynamic binding behavior: AB binds in orientation 1 with its pharmacophore A to the orthosteric site of a GPCR R to form active ligand-

receptor complexes $[RAB]$; alternatively AB binds in orientation 2 with its pharmacophore B either to the allosteric site of the X *-unoccupied* GPCR R to form inactive ligand-receptor complexes $[ABR]$ or to the allosteric site of the X *-occupied* GPCR R to form inactive ternary complexes $[ABRX]$. The figure illustrates the aforementioned scenario whereby K_A, K_B and K_X denote the equilibrium dissociation constants of the ligand-receptor species $[RAB]$, $[ABR]$ and $[RX]$, respectively and α denotes the cooperativity between AB and X.

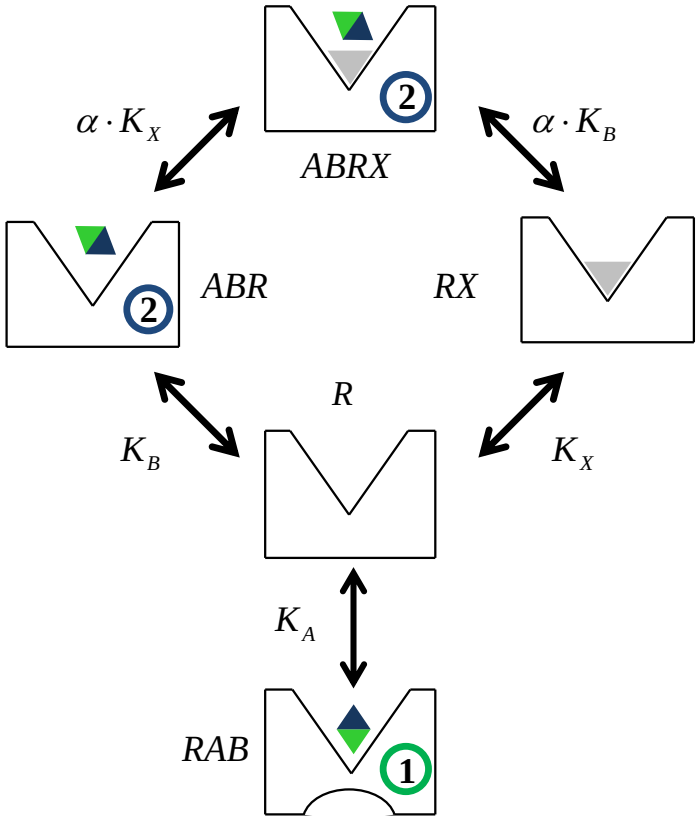

Figure 14: A model of dynamic ligand binding for bi-pharmacophoric, dualsteric ligands. Green: orthosteric moiety, blue: allosteric moiety. Grey triangle: orthosteric radioligand. The nomenclature of ligand/receptor-complexes and ligand orientations are indicated. Modified from ref 17.

According to the law of mass action the concentrations of the ligand-receptor species are given as follows:

$$[RX] = \frac{[R] \cdot [X]}{K_X} \qquad \textbf{(Equation 16)}$$

$$[RAB] = \frac{[R] \cdot [AB]}{K_A} \qquad \textbf{(Equation 17)}$$

$$[ABR] = \frac{[R] \cdot [AB]}{K_B} \quad \textbf{(Equation 18)}$$

$$[ABRX] = \frac{[RX] \cdot [AB]}{\alpha \cdot K_B} = \frac{[ABR] \cdot [X]}{\alpha \cdot K_X} \quad \textbf{(Equation 19)}$$

The total concentration of receptors R_T is defined as follows:

$$R_T = [R] + [RX] + [RAB] + [ABR] + [ABRX] \quad \textbf{(Equation 20)}$$

The binding of the orthosteric radioligand X in the presence of AB is given by the following equation:

$$\frac{[RX] + [ABRX]}{R_T} = \frac{[RX] + [ABRX]}{[R] + [RX] + [RAB] + [ABR] + [ABRX]} \quad \textbf{(Equation 21)}$$

Multiplying the numerator and denominator by $\frac{1}{[X] \cdot [R]}$ yields:

$$\frac{[RX] + [ABRX]}{R_T} = \frac{\frac{[RX]}{[X] \cdot [R]} + \frac{[ABRX]}{[X] \cdot [R]}}{\frac{[R]}{[X] \cdot [R]} + \frac{[RX]}{[X] \cdot [R]} + \frac{[RAB]}{[X] \cdot [R]} + \frac{[ABR]}{[X] \cdot [R]} + \frac{[ABRX]}{[X] \cdot [R]}} \quad \textbf{(Equation 22)}$$

Making the appropriate substitutions using **Equation 16**:

$$\frac{[RX] + [ABRX]}{R_T} = \frac{\frac{1}{K_X} + \frac{[ABRX]}{[X] \cdot [R]}}{\frac{1}{[X]} + \frac{1}{K_X} + \frac{[RAB]}{[X] \cdot [R]} + \frac{[ABR]}{[X] \cdot [R]} + \frac{[ABRX]}{[X] \cdot [R]}} \quad \textbf{(Equation 23)}$$

Making the following substitutions:

$[ABRX] = \frac{[RX] \cdot [AB]}{\alpha \cdot K_B}$; $[RX] = \frac{[R] \cdot [X]}{K_X}$; $[R] = \frac{[RAB] \cdot K_A}{[AB]}$; $[R] = \frac{[ABR] \cdot K_B}{[AB]}$ yields:

$$\frac{[RX] + [ABRX]}{R_T} = \frac{\frac{1}{K_X} + \frac{[AB]}{\alpha \cdot K_X \cdot K_B}}{\frac{1}{[X]} + \frac{1}{K_X} + \frac{[AB]}{[X] \cdot K_A} + \frac{[AB]}{[X] \cdot K_B} + \frac{[AB]}{\alpha \cdot K_X \cdot K_B}} \quad \textbf{(Equation 24)}$$

The equation simplifies to:

$$Y = \frac{[X] \cdot R_T}{[X] + K_X'} \qquad \textbf{(Equation 25)}$$

where:

$$K_X' = K_X \cdot \frac{\left(1 + [AB] \cdot \left(\frac{K_A + K_B}{K_A \cdot K_B}\right)\right)}{\left(1 + \frac{\alpha' \cdot [AB]}{K_B}\right)}$$

Here, Y denotes $[RX] + [ABRX]$. The transformation $\alpha' = \frac{1}{\alpha}$ is made to ensure that positive cooperativity is reflected by $\alpha' > 1$. **Equation 25** has previously been successfully applied to fit binding data of bi-pharmacophoric, dualsteric ligands[17].

Estimation of the IC_{50} of the dynamic ligand

In equilibrium binding experiments a fixed concentration of an orthosteric radioligand X and various concentrations of a dynamic competitor AB are applied. According to Ehlert[28] the fractional binding of X at a fixed concentration in the presence of increasing concentrations of a purely allosteric ligand A is:

$$\frac{Y}{Y_0} = \frac{[XR] + [XRA]}{[XR]} \qquad (\textbf{\textit{Equation A11}}, \text{ taken from ref. 28})$$

This equation can be transformed into **Equation 26** to display the fractional binding of X at a fixed concentration in the presence of increasing concentrations of a dynamic ligand AB is:

$$\frac{Y}{Y_0} = \frac{[RX] + [ABRX]}{[RX]} \qquad \textbf{(Equation 26)}$$

In this equation Y denotes the binding of X in the presence of AB while Y_0 denotes the binding of X in the absence of AB. Using **Equation 25**, **Equation 26** reduces to:

$$\frac{Y}{Y_0} = \frac{[X] + K_X}{[X] + K_X'} \qquad \textbf{(Equation 27)}$$

Substituting for K_X' using **Equation 25**, the fractional binding of X in the presence of AB is given by:

$$\frac{Y}{Y_0} = \frac{[X] + \frac{\alpha'[X][AB]}{K_B} + K_X + \frac{\alpha' K_X [AB]}{K_B}}{[X] + \frac{\alpha'[X][AB]}{K_B} + K_X + \frac{K_X[AB](K_A + K_B)}{K_A K_B}} \quad \textbf{(Equation 28)}$$

When $[AB]$ approaches infinity, the maximal fractional binding Y_{MAX} is represented by the following equation:

$$Y_{MAX} = \lim_{[AB]\to\infty} \frac{Y}{Y_0} = \frac{[X] + K_X}{[X] + \frac{K_X(K_A + K_B)}{\alpha' K_A}} \quad \textbf{(Equation 29)}$$

According to Ehlert[28] the concentration of an allosteric ligand $[A]$ which causes the half maximum effect on the binding of X (i.e. $IC_{50} = AB_{50}$) is represented by the following equation:

$$1 - \frac{Y}{Y_0} = \frac{(1 - Y_{MAX})}{2} \quad \textbf{(Equation 30)}$$

Equation 30 can also be applied to estimate the concentration of a dynamic ligand $[AB]$ which causes the half maximum effect on the binding of X. Substituting for $\frac{Y}{Y_0}$ and Y_{MAX} using **Equations 28** and **29**, respectively, and then solving for AB yields the IC_{50} of the dynamic ligand AB:

$$IC_{50} = AB_{50} = \frac{K_A K_B([X] + K_X)}{K_X(K_A + K_B) + \alpha' K_A [X]} \quad \textbf{(Equation 31)}$$

In the presence of a very low concentration of X, the IC_{50} value approaches the observed/apparent dissociation constant of the dynamic ligand (see above):

$$\lim_{[X]\to 0} IC_{50} = \frac{K_A \cdot K_B}{K_A + K_B} \quad \textbf{(Equation 32)}$$

The operational model of agonism for dynamic ligands

Let $[RAB]$ be active ligand-receptor complexes which elicit a cell response *via* signal transduction proteins. Further, let the stimulus (S) generated by a dynamic ligand AB be equivalent to the product of the fractional receptor occupancy in the active pose (Y_{RAB}) and the maximal intrinsic efficacy (ε_{MAX}) of the ligand[32].

$$S = \varepsilon_{MAX} \cdot Y_{RAB} \qquad \textbf{(Equation 33)}$$

Substituting Y_{RAB} using **Equations 12** and **8** yields:

$$S = \varepsilon_{MAX} \cdot \frac{f_{RAB} \cdot [AB] \cdot R_T}{[AB] + \frac{K_A \cdot K_B}{K_A + K_B}} \qquad \textbf{(Equation 34)}$$

A stimulus-response function according to Ehlert and colleagues[31] and similar to the operational model delineated by Black & Leff[14] is given by

$$E = \frac{E_{MAX} \cdot S}{K_E + S} \qquad \textbf{(Equation 35)}$$

where E is the measured response, E_{MAX} is the maximal response of the system and K_E denotes the level of stimulus which elicits the half maximal system response.

Substitution of **Equation 34** into **Equation 35** yields:

$$E = \frac{E_{MAX} \cdot \varepsilon_{MAX} \cdot \frac{f_{RAB} \cdot [AB] \cdot R_T}{[AB] + \frac{K_A \cdot K_B}{K_A + K_B}}}{K_E + \varepsilon_{MAX} \cdot \frac{f_{RAB} \cdot [AB] \cdot R_T}{[AB] + \frac{K_A \cdot K_B}{K_A + K_B}}} \qquad \textbf{(Equation 36)}$$

Divided by $\varepsilon_{MAX} \cdot \frac{f_{RAB} \cdot [AB] \cdot R_T}{[AB] + \frac{K_A \cdot K_B}{K_A + K_B}}$, **Equation 36** reduces to:

$$E = \frac{E_{MAX}}{\frac{K_E \cdot \left([AB] + \frac{K_A \cdot K_B}{K_A + K_B} \right)}{\varepsilon_{MAX} \cdot f_{RAB} \cdot [AB] \cdot R_T} + 1} \qquad \textbf{(Equation 37)}$$

Formation of the maximum transduction coefficient $\tau_{\max}$ ($\tau_{\max} = \frac{\varepsilon_{MAX} \cdot R_T}{K_E}$) at full occupancy of the ligand-receptor-complex in the active pose (RAB) yields an *operational model of agonism for dynamic ligands*:

$$E = \frac{E_{MAX}}{1 + \frac{([AB] + K_D)}{[AB] \cdot \tau_{dyn}}} \quad \textbf{(Equation 38)}$$

in which $$K_D = \frac{K_A \cdot K_B}{K_A + K_B} = K_{obs} \quad \textbf{(Equation 39)}$$

and $$\tau_{dyn} = \tau_{\max} \cdot f_{RAB} = \frac{\varepsilon_{MAX} \cdot R_T}{K_E} \cdot \frac{K_B}{K_A + K_B} \quad \textbf{(Equation 40)}$$

Note that the affinity K_D of the dynamic ligand from functional data equals the observed dissociation constant K_{obs} obtained from binding data.

$\tau_{\max}$ is the maximum transduction coefficient of the dynamic ligand at 100 % occupancy of receptors in the active pose (RAB) and is composed of the system-independent maximal intrinsic efficacy of the dynamic ligand ε_{MAX} and a system-dependent part $\frac{R_T}{K_E}$.

τ_{dyn} represents the dynamic transduction coefficient of the ligand which is composed of $\tau_{\max}$ multiplied by the fraction of the ligand-receptor complexes in the active pose (f_{RAB}).

A general logistic version of the operational model comprising a slope factor n can be applied in case of experimental curves that are steeper or flatter than 1:

$$E = \frac{E_{MAX}}{1 + \frac{([AB] + K_D)^n}{[AB]^n \cdot \tau_{dyn}^n}} \quad \textbf{(Equation 41)}$$

Note 2

Chemical syntheses and characterization

Synthesis of 8-Bromo-N-(3-(1,3-dioxo-1H-benzo[de]isoquinolin-2(3H)-yl)-2,2-dimethylpropyl)-N,N-dimethyloctan-1-aminium bromide (**13**)

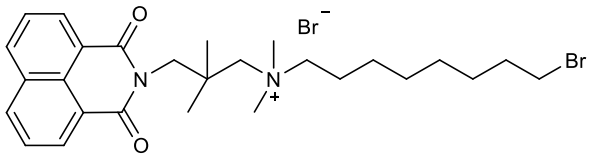

23 mmol of 1.8-naphthalimidopropylamine **12** and 228 mmol of 1.8-dibromooctane were heated in a microwave apparatus for 4 h (100 °C, 400 W, 4 h). After cooling the solid was filtered off, washed with petroleum ether and dried *in vacuo* to give **13** as a white salt in 9% yield. mp 138 – 142 °C. ^{1}H NMR (DMSO-d_6): 1.25 (s, 6H, C(C*H*$_3$)$_2$), 1.37 (m, 8H, $^{+}$N(CH$_2$)$_2$C*H*$_2$C*H*$_2$C*H*$_2$C*H*$_2$), 1.71 (m, 2H, $^{+}$NCH$_2$C*H*$_2$), 1.79 (m, 2 H, $^{+}$N(CH$_2$)$_6$C*H*$_2$), 3.16 (s, 6H, $^{+}$N(C*H*$_3$)$_2$), 3.38 (m, 2H, C*H*$_2$Br), 3.45 (s, 2H, $^{+}$NC*H*$_2$(CH$_2$)$_2$N$_{Naphth}$), 3.53 (t, 2H, $^{+}$NC*H*$_2$(CH$_2$)$_7$Br, *J* = 6.6), 4.13 (s, 2H, $^{+}$N(CH$_2$)$_2$C*H*$_2$N$_{Naphth}$), 7.89 (dd, 2H, arom., *J* = 7.6), 8.51 (m, 4H, arom.). ^{13}C NMR (DMSO-d_6): 21.9 ($^{+}$NCH$_2$*C*H$_2$), 25.5 (C(*C*H$_3$)$_2$), 25.6 (*C*(CH$_3$)$_2$), 27.4 ($^{+}$N(CH$_2$)$_4$*C*H$_2$*C*H$_2$), 27.7 ($^{+}$N(CH$_2$)$_2$*C*H$_2$), 28.3 ($^{+}$N(CH$_2$)$_3$*C*H$_2$), 32.1 ($^{+}$N(CH$_2$)$_6$*C*H$_2$), 35.2 ($^{+}$N*C*H$_2$), 49.1 ($^{+}$N(CH$_2$)$_2$*C*H$_2$N$_{Naphth}$), 51.9 (N(*C*H$_3$)$_2$), 67.6 (*C*H$_2$Br), 71.4 ($^{+}$N*C*H$_2$(CH$_2$)$_2$N$_{Naphth}$), 122.3 (C$_{Naphth}$), 127.3 (C$_{Naphth}$H), 127.4 (C$_{Naphth}$), 130.9 (C$_{Naphth}$H), 131.3 (C$_{Naphth}$), 134.3 (C$_{Naphth}$H), 164.6 (C=O). MS (ESI) *m/z* [M]$^{2+}$ Calcd for $C_{27}H_{38}BrN_2O_2^{+}$: 501.2. Found: 500.8.

Synthesis of N^1-(3-(1,3-Dioxo-1H-benzo[de]isoquinolin-2(3H)-yl)-2,2-dimethylpropyl)-N^8-ethyl-N^1,N^1,N^8,N^8-tetramethyloctane-1,8-diaminium **(8-naph) (11)**

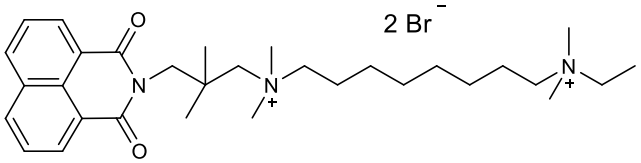

2 mmol of **13** and 4 mmol of *N*,*N*-dimethylethylamine were dissolved in acetonitrile (20 ml). To this solution a catalytic amount of KI/K_2CO_3 (1:1) was added and the reaction mixture was heated in a microwave apparatus for 3.4 h (80 °C, 500 W, 3.4 h). After cooling the solid was filtered off, washed with acetonitrile and dried *in vacuo* to give **8-naph** as a yellow salt in 41% yield. mp 170 – 175 °C. ^{1}H NMR (DMSO-d_6): 1.24 (s, 9H, C*H*$_3$/C(C*H*$_3$)$_2$), 1.30 (m, 8H, $^{+}$N(CH$_2$)$_2$C*H*$_2$C*H*$_2$C*H*$_2$C*H*$_2$), 1.69 (m, 4H, $^{+}$N(CH$_2$C*H*$_2$(CH$_2$)$_4$C*H*$_2$), 3.02 (s, 6H, $^{+}$N(C*H*$_3$)$_2$CH$_2$CH$_3$, 3.19 (s, 6H, $^{+}$N(C*H*$_3$)$_2$), 3.29 (m, 2H, $^{+}$N(CH$_2$)$_7$C*H*$_2$), 3.36 (m, 2H,

$^{+}NCH_2CH_3$), 3.47 (m, 4H, $N_{Naphth}(CH_2)_2CH_2{}^{+}NCH_2$), 4.12 (s, 2H, $N_{Naphth}CH_2$), 7.89 (t, 2H, arom., J = 7.6), 8.49 (m, 4H, arom.). ^{13}C NMR (DMSO-d_6): 7.8 ($^{+}NCH_2CH_3$), 21.5 ($C(CH_3)_2$), 21.9 ($^{+}NCH_2CH_2(CH_2)_4CH_2$), 25.4 ($C(CH_3)_2$), 25.5 ($^{+}N(CH_2)_5CH_2$), 25.6 ($^{+}N(CH_2)_2CH_3$), 28.1 ($^{+}N(CH_2)_3CH_2$), 28.2 ($^{+}N(CH_2)_4CH_2$), 48.8 ($N_{Naphth}CH_2$), 49.3 ($^{+}N(CH_3)_2CH_2CH_3$), 51.9 ($N(CH_3)_2$), 58.3 ($^{+}NCH_2CH_3$), 62.2 ($^{+}N(CH_2)_7CH_2$), 67.2 ($^{+}NCH_2$), 71.3 ($N_{Naphth}(CH_2)_2CH_2$), 122.1 ($C_{Naphth}$), 127.2 ($C_{Naphth}H$), 127.3 ($C_{Naphth}$), 130.8 ($C_{Naphth}H$), 131.2 ($C_{Naphth}$), 134.2 ($C_{Naphth}H$), 164.5 (C=O). MS (ESI) *m/z* $[M]^{2+}$ Calcd for $C_{31}H_{49}N_3O_2{}^{2+}$: 495.38. Found: 247.3.

Synthesis of N^1-(3-(1,3-dioxo-1H-benzo[de]isoquinolin-2(3H)-yl)-2,2-dimethylpropyl)-N^8-(4-(isoxazol-3-yloxy)but-2-ynyl)-N^1,N^1,N^8,N^8-tetramethyloctane-1,8-diaminium bromide **(Isox-8-naph) (10)**

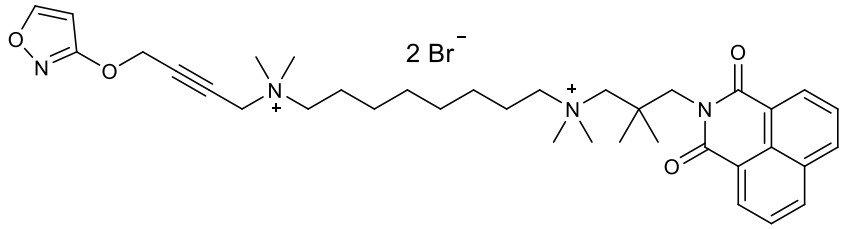

1 mmol of **13** and 1 mmol of 4-(isoxazol-3-yloxy)-*N*,*N*-dimethylbut-2-yn-1-amine were dissolved in acetonitrile (30 ml) and refluxed for 2-3 days in the presence of a catalytic amount of KI/K_2CO_3 (1:1). After the reaction was completed (TLC monitoring, eluent: 0.2 M aqueous NH_4NO_3/CH_3OH 2:3), a small amount of the solvent was evaporated. The obtained precipitate was filtered and recrystallized from acetonitrile and ethanol. The precipitate was filtered, washed with diethylether, and dried *in vacuo* to give the product **Isox-8-naph** as light brown powder in 68% yield. mp 166 °C. ^1H NMR (DMSO-d_6): 1.24 (s, 6H, $C(CH_3)_2$), 1.31 (br s, 8H, $^{+}N(CH_2)_2CH_2$ / $^{+}N(CH_2)_3CH_2$), 1.66 (br, 2H, $^{+}NCH_2CH_2$), 1.72 (br, 2H, $^{+}NCH_2CH_2$), 3.10 (s, 6H, $^{+}N(CH_3)_2$), 3.18 (s, 6H, $^{+}N(CH_3)_2$), 3.40 (br, 4H, $^{+}NCH_2$), 3.48 (s, 2H, $^{+}NCH_2$), 4.13 (s, 2H, $N_{Imide}CH_2$), 4.54 (s, 2H, $^{+}NCH_2C{\equiv}C$), 5.10 (s, 2H, $C{\equiv}CCH_2O$), 6.43 (d, 1H, CH_{4isox}, *J* = 1.8), 7.89 (m, 2H, arom.), 8.49 (m, 4H, arom.), 8.75 (d, 1H, CH_{5isox}, *J* = 2.0). ^{13}C NMR (DMSO-d_6): 21.9 / 22.2 ($^{+}NCH_2CH_2$ 2x), 25.7 ($C(CH_3)_2$ / $C(CH_3)_2$), 25.8 ($^{+}N(CH_2)_3CH_2$ 2x), 28.3 ($^{+}N(CH_2)_2CH_2$), 28.4 ($^{+}N(CH_2)_2CH_2$), 49.1 ($N_{Imide}CH_2$), 49.9 ($^{+}N(CH_3)_2$), 52.1 ($^{+}N(CH_3)_2$), 53.4 ($^{+}NCH_2C{\equiv}C$), 57.7 ($C{\equiv}CCH_2$), 63.2 ($^{+}NCH_2$), 67.5 ($^{+}NCH_2$), 71.7 (CH_2N^{+}), 76.6 ($C{\equiv}CCH_2O$), 86.2 ($^{+}NCH_2C{\equiv}C$), 96.2 (CH_{4isox}), 122.4 (C_{Naphth}), 127.4 (CH_{Naphth}), 127.6 (C_{Naphth}), 131.1 (CH_{Naphth}), 134.5 (C_{Naphth}), 134.5 (CH_{Naphth}), 162.2 (C_{isox}), 164.8 (C=O), 170.5 (CH_{5isox}). MS (ESI) *m/z* $[M]^{2+}$ Calcd for $C_{36}H_{50}N_4O_4{}^{2+}$: 600.4. Found: 300.4.

Acknowledgments

We thank Mechthild Kepe for excellent technical assistance and Corning Inc. for their support on the Epic system. A.B. is member of the graduate school Theoretical and Experimental Medicine at the University of Bonn. This work was funded by the Deutsche Forschungsgemeinschaft (DFG) by grants to K.M. (MO 821/2-1), U.H. (HO 1368/12-1), E.K. (KO 1583/3-1) and C.H. (SFB487 TPA1). B.C. is funded by the North-Rhine-Westphalia International Graduate Research School BIOTECH-PHARMA at the University of Bonn.

Author contributions

A.B. conceived the project, developed the mathematical framework for dynamic ligands, conducted all binding experiments in live CHO-M_2 and CHO-M_2 ^{W422A} cells, all [^{35}S]GTPγS binding experiments and DMR assays, and supervised experiments related to binding to membranes of CHO-hM_2 cells and to characterization of the allosteric fragments. B.C. characterized the allosteric fragments in binding and functional assays and conducted binding assays of the X-6-phth series in membranes of CHO-hM_2 cells. F.K. conducted binding assay of the X-6-naph series in membranes of CHO-hM_2 cells. R.M. synthesized and characterized '8-naph'. J.B. conducted FRET experiments. M.M. synthesized and characterized 'isox-8-naph'. C.D. provided isox and isox-6-phth. D.K. conducted all [^{35}S]GTPγS binding experiments to membranes of CHO-M_2 ^{W422A} cells. C.H. planned and supervised FRET experiments. U.H. planned and supervised chemical syntheses. C.T., M.D.A., C.H., and U.H. contributed to discussion. E.K. provided essential ideas. A.B. and K.M. made figures and wrote the manuscript. K.M. supervised the overall research.

Competing financial interests

The authors declare no competing financial interest.

References

1. Pierce, K.L., Premont, R.T. & Lefkowitz, R.J. *Nature Rev. Mol. Cell Biol.* **3,** 639–650 (2002).

2. Venkatakrishnan, A.J. *et al. Nature* **494,** 185–194 (2013).

3. Kenakin, T. *Nat. Rev. Drug Discov.* **1,** 103–110 (2002).

4. Kenakin, T. & Christopoulos, A. *Nat. Rev. Drug Discov.* **12,** 205–216 (2013).

5. Rosenbaum, D.M., Rasmussen, S.G.F. & Kobilka, B.K. *Nature* **459,** 356–363 (2009).

6. Warne, T. *et al. Nature* **469,** 241–244 (2011).

7. Swaminath, G. *et al. J. Biol. Chem.* **280,** 22165–22171 (2005).

8. Yao, X. *et al. Nat. Chem. Biol.* **2,** 417–422 (2006).

9. Kofuku, Y. *et al. Nat. Commun.* **3,** 1045 (2012).

10. Nikolaev, V.O., Hoffmann, C., Bünemann, M., Lohse, M.J. & Vilardaga, J.-P. *J. Biol. Chem*. **281,** 24506–24511 (2006).

11. Zürn, A. *et al*. *Mol. Pharmacol.* **75,** 534–541 (2009).

12. Kenakin, T. & Miller, L.J. *Pharmacol. Rev.* **62,** 265–304 (2010).

13. Nygaard, R. *et al. Cell* **152,** 532–542 (2013).

14. Black, J.W. & Leff, P. *Proc. R. Soc. Lond. B. Biol. Sci.* **220,** 141–162 (1983).

15. Bruning, J.B. *et al. Nature Chem. Biol.* **6,** 837–843 (2010).

16. Overington, J.P., Al-Lazikani, B. & Hopkins, A.L. *Nat. Rev. Drug Discov.* **5,** 993–996 (2006).

17. Antony, J. *et al. FASEB J.* **23,** 442–450 (2009).

18. Bock, A. *et al. Nature Commun.* **3,** 1044 (2012).

19. Prilla, S., Schrobang, J., Ellis, J., Höltje, H.-D. & Mohr, K. *Mol. Pharmacol*. **70,** 181–193 (2006).

20. Schröder, R. *et al. Nat. Biotechnol.* **28,** 943–949 (2010).

21. Schröder, R. *et al. Nat. Protoc.* **6,** 1748–1760 (2011).

22. Kloeckner, J., Schmitz, J. Holzgrabe, U. *Tetrahedr. Lett.* **51**, 3470-3472 (2010).

23. Dallanoce, C. *et al*. *Bioorg. Med. Chem.* **7**, 1539–1547 (1999).

24. Disingrini, T. *et al. J. Med. Chem*. **49**, 366-372 (2006).

25. Schrage, R. *et al. Br. J. Pharmacol.* **169,** 357–370 (2013).

26. Hoffmann, C. *et al. Nat. Methods* **2,** 171–176 (2005).

27. Jäger, D. *et al. J. Biol. Chem*. **282,** 34968–34976 (2007).

28. Ehlert, F.J. *Mol. Pharmacol*. **33**, 187-194 (1988).

29. May, L.T., Leach, K., Sexton P.M. & Christopoulos, A. *Annu. Rev. Pharmacol. Toxicol*. **47,** 1–51 (2007).

30. Ehlert, F.J., Griffin, M.T., Sawyer, G.W. & Bailon, R. *J. Pharmacol. Exp. Ther.* **289**, 981-992 (1999).

31. Griffin, M.T., Figueroa, K.W., Liller, S. & Ehlert, F.J. *J. Pharmacol. Exp. Ther.* **321**, 1193-1207 (2007).

32. Furchgott, R. F., *Adv. Drug. Res.* **3**, 21-55 (1966).

4. Synthesis of orthosteric/orthosteric hybrids to control partial agonism

1. Introduction

The G-protein coupled receptors (GPCRs) belong to one of the largest protein superfamily within most mammals and are organized in five main families, termed *Glutamate*, *Rhodopsin*, *Adhesion*, *Fizzled/Taste2,* and *Secretin* (GRAFS). All GPCRs share a common seven-transmembrane (7TM) topology.[1,2] They mediate cellular responses to a variety of extracellular signals like neurotransmitter, hormones and physical stimuli such as light.[3] Downstream signaling mediated by GPCRs is fundamental for most physiological processes, such as neurological, cardiovascular, endocrine or reproductive functions, making this superfamily an interesting target for therapeutic intervention.[1] Therefore, a detailed understanding of GPCR structures and function is unalterable. Recently, the muscarinic acetylcholine receptors (mAChR) were crystallized and their structure solved.[4-7] mAChRs are divided in five subtypes (M_1 – M_5) due to the diversity of their amino acid sequence. Iperoxo **1** (Figure 1, **A**), known as superagonist at the muscarinic receptors[8], was crystallized at the M_2 receptor. The x-ray structure indicates an interaction of iperoxo **1** at the orthosteric binding site and provides important insights into the activation mechanism.[6]

Agonists, binding to the orthosteric site, can be subdivided as full or partial agonists, depending on the degree of receptor activation. In contrast to classical full agonists, partial agonists are interesting drug candidates due to less mediated side effects. Well known partial agonists are salbutamol, a $ß_2$-sympathomimetic drug, or buprenorphine, acting in the treatment of bronchial asthma[9] and pain[10], respectively.

Beside agonists, also antagonists such as atropine **3** (isolated from belladonna plants) and scopolamine **4** (Figure 1, **A**) are known as drugs acting at the muscarinic orthosteric binding site. The orientation of the epoxide group in scopolamine forces another orientation of the tropane ring system in the orthosteric binding pocket in comparison to atropine.[11] Moreover, besides the orthosteric binding site many GPCRs also contain a topographically distinct allosteric binding site. Therefore, not only classical orthosteric drugs but also allosteric[12,13] and dualsteric[14-16] ligands can influence receptor function.

It is presumed that the design of dualsteric compounds can lead to drugs, addressing and stabilizing distinct receptor conformations in a predictable way. This concept is known as “dynamic ligand binding” describing the degree of GPCR activation (partial agonism) as well as biased agonism.[17] The M_2 selective bipharmacophoric ligand iper-6-naph **5** (Figure 1, **A**),

comprising of an orthosteric agonistic moiety (iper) and an allosteric inverse agonist (naph) linked via a hexamethylene chain was found to act as partial agonist. This orthosteric/allosteric hybrid is able to stabilize active receptor states in a dualsteric binding pose (i.e. bitopic orthosteric/allosteric) or can stabilize inactive receptor states in a purely allosteric binding pose. The degree of partial agonism depends on the level of binding and is defined as the relationship of active versus inactive receptor populations.[17] Due to dynamic ligand binding it is not compulsory to design orthosteric/allosteric bipharmacophoric ligands in order to generate partial agonism. This principle should also work with bipharmacophoric ligands consisting of orthosteric/orthosteric ligands providing that the two ligands differ in their intrinsic efficacy (agonist/antagonist) for receptor activation (Figure 1, **B**).

In this context, othosteric/orthosteric bipharmacophoric ligands were synthesized consisting of the orthosteric superagonist iperoxo[18] **1**, which activates all subtypes of the muscarinic receptor[19,20] or isoxazole[21] **2** and of an orthosteric antagonist, atropine **3** and scopolamine **4**, respectively. Both pharmacophores were linked by different alkyl chain length. Pharmacological investigations should provide information about the extent of partial agonism of the newly designed orthosteric/orthosteric hybrids.

2. Results and discussion

2.1 Chemistry

To obtain orthosteric/orthosteric hybrid compounds, the orthosteric agonist iperoxo or isoxazole was connected to an orthosteric antagonist, atropine and scopolamine, respectively. Commercially available atropine **3** was reacted with the corresponding dibromoalkane in acetonitrile at room temperature (C4, C6, and C8) or at 68 °C (C10) to yield the intermediates **6-C4** to **6-C10** in 43-89% yield. The reaction using 1,4-dibromobutane was carried out according to known procedure.[22] In analogy, for the synthesis of the scopolamine intermediates **7-C4** to **7-C10**, free scopolamine base **4** reacted with the corresponding dibromoalkane in acetonitrile at room temperature yielding **7-C4** to **7-C10** in 35-87%. These reactions last days to weeks and cannot be speeded up by heating up to 95 °C or using microwave assisted reactions. For the preparation of the final iperoxo/atropine hybrids **8-C4** to **8-C10**, isoxazole/atropine hybrids **10-C4** to **10-C10**, iperoxo/scopolamine hybrids **9-C4** to **9-C10**, and isoxazole/scopolamine hybrids **11-C4** to **11-C10**, the intermediates **6-Cn** and **7-Cn** were connected to the base of iperoxo **1**[18] and to the base of isoxazole **2**[19,21], respectively, in the presence of KI/K_2CO_3 in acetonitrile (Scheme 1).

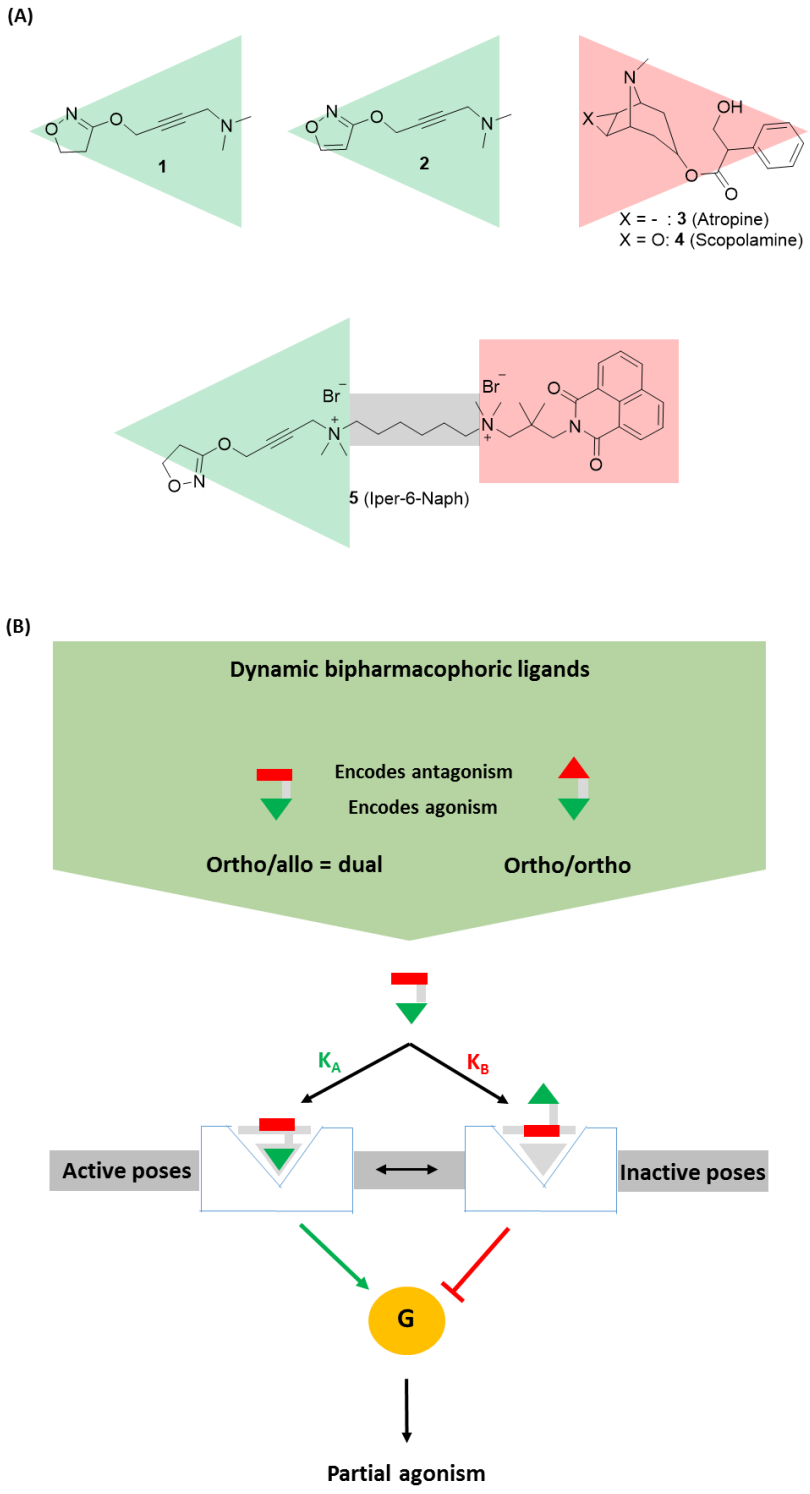

Figure 1: Concept of dynamic ligand binding. **(A)** Structures of orthosteric agonists' base of iperoxo **1** and base of isoxazole **2**, orthosteric antagonists' atropine **3**, scopolamine **4**, and dualsteric ligand iper-6-naph **5**. **(B)** Bipharmacophoric ligand binding to the receptor. Compounds consist either of ortho/allo ligands (green triangle and red rectangle) or ortho/ortho ligands (green and red triangle), linked to one agonistic (green) and one antagonistic (red) moiety. The dualsteric ligands can bind in two different binding poses: either in the active, stabilizing pose (activation of the G-protein) or in the inactive pose (no activation of the G-protein).[23] Abbreviations: allo, allosteric; dual, dualsteric; G, G-protein; ortho, orthosteric.

Scheme 1: Reaction scheme of the iperoxo/isoxazole-atropine/scopolamine hybrids **8-Cn**, **9-Cn**, **10-Cn**, and **11-Cn**.

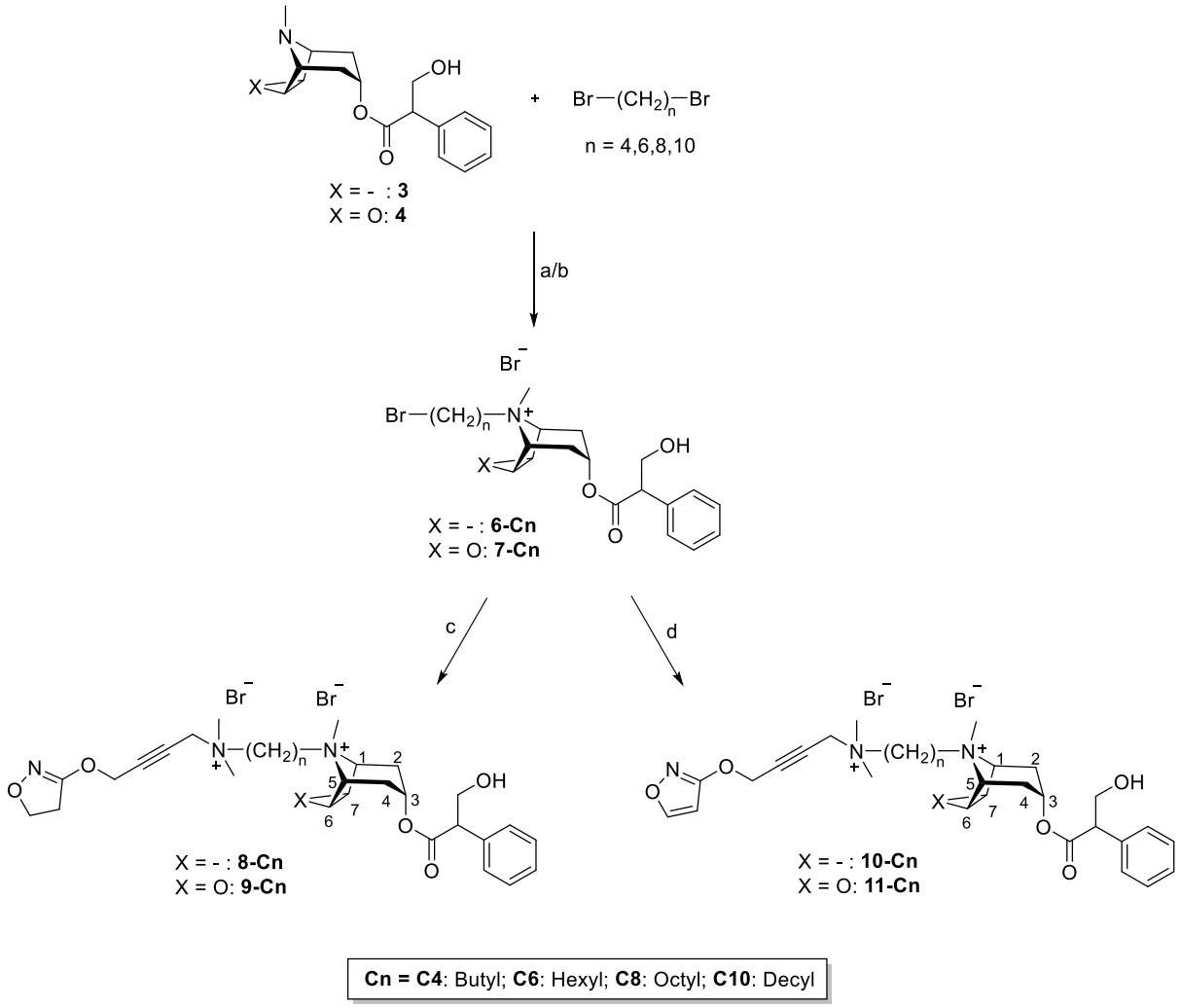

Reagents and conditions: a) CH_3CN, rt., 68 °C; b) CH_3CN, rt.; c) base of iperoxo **1**, KI/K_2CO_3, CH_3CN, 80 °C (microwave); d) base of isoxazole **2**, KI/K_2CO_3, CH_3CN, 80 °C (microwave).

Using only a 1:1 ratio of base of scopolamine **4** to 1,4-dibromobutane instead of an excess of the connecting chain led to the homodimeric side product **12** in 27% yield (Scheme 2).

Scheme 2: Reaction procedure of the scopolamine/scopolamine dimer **12**.

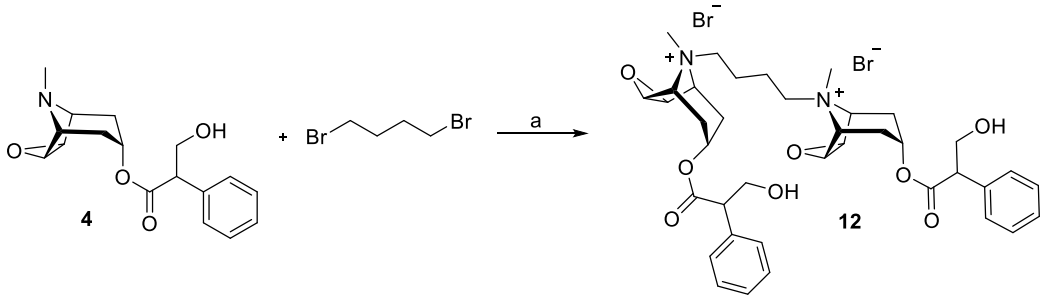

Reagents and conditions: a) CH_3CN, rt.

2.2 Stereochemistry

Tropine, a building block of atropine and scopolamine, respectively, are known to epimerize via inversion at the nitrogen atom in solution, resulting in either a *syn* or *anti* position of the methyl group.[24] By means of NMR spectroscopy, it was found out, that the tropine free base has a 20 time higher preference of the *anti p*osition of the methyl group which is in line with tropine-derivatives such as atropine.[25] However, in scopolamine an axial position of the methyl group is favored due to the repulsive interactions with the epoxy group (Figure 2).[26]

For docking and binding experiments the position of the methyl group as well as the position of the linker at the nitrogen atom is pivotal to know. Therefore, the herein synthesized final compounds were investigated in ^{1}H NMR and NOESY experiments. The latter utilizes the nuclear Overhauser effect NOE between the *N*-methyl and the tropine protons. The NOESY spectra confirm interactions between *N*-methyl hydrogens and the *exo* tropine protons at C-2 and C-4, concluding that the methyl group of the hybrid compounds are predominantly in *syn* and the alkyl chain linker moiety in *anti* position (Figure 2). This is in line with the results for dualsteric atropine and scopolamine related compounds found earlier by Schmitz et al.[11]

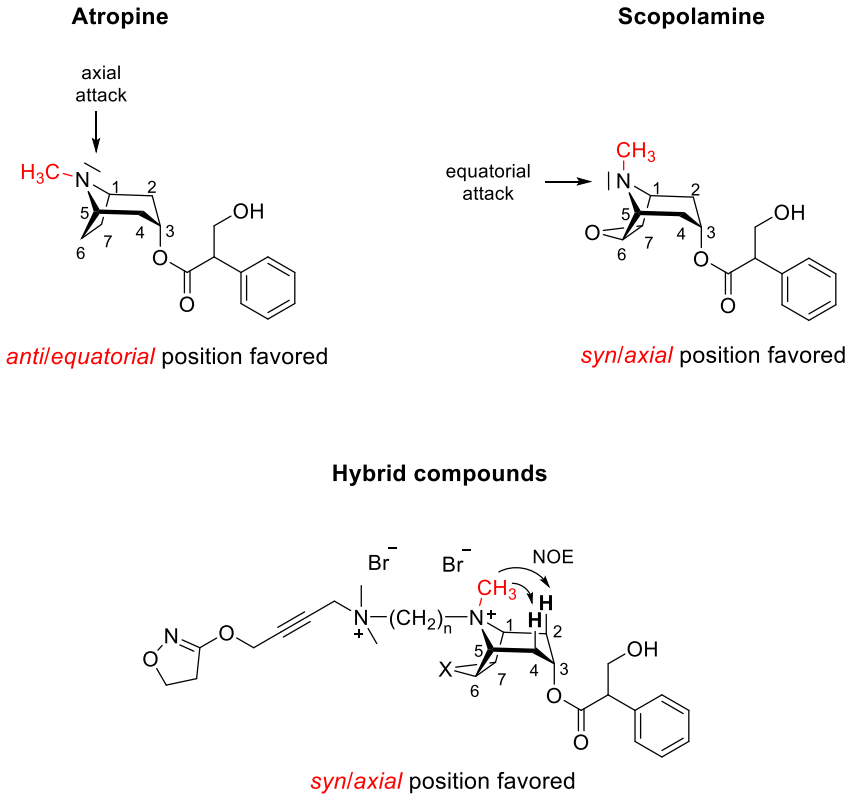

Figure 2: Depiction of the favored methyl group position *(syn* or *anti*) in atropine, scopolamine, and in the hybrid compounds, including nuclear Overhauser effect NOE interactions.

2.3 Pharmacology

The iperoxo/atropine hybrids **8-C4** to **8-C10** were investigated for their extent of partial agonism at the M_2 receptor in the working group of PD Dr. Tränkle and Prof. Dr. Mohr by Paul Bannenberg (Pharmacology and Toxicology, Institute of Pharmacy, University of Bonn, Germany). [^{35}S]GTPγS experiments as well as [^{3}H]NMS and [^{3}H]iperoxo radioligand binding experiments were performed on cell homogenates of CHO cells stably expressing M_2-mAChRs (CHO-hM_2).

2.3.1 [^{35}S]GTPγS binding measurements on the hM_2 receptor

[^{35}S]GTPγS experiments of iperoxo-C_n-atropine (**8-C4** to **8-C10**) (Figure 3, **A**) showed a linker chain length dependent degree of receptor activation. In general, the shorter the linker chain length, the higher the cell response. The short linked hybrids bind more probably with their agonistic moiety (iperoxo) to the receptor, whereas the long linked hybrids prefer binding with their inverse agonistic moiety (atropine), resulting in a lower upper plateau.

2.3.2 [^{3}H]NMS and [^{3}H]iperoxo binding experiments on the hM_2 receptor

Using [^{3}H]NMS in radioligand binding experiments of iperoxo-C_n-atropine (**8-C4** to **8-C10**), no influence on the binding affinity was observed, indicating that the agonistic and inverse agonistic part bind in the same ratio to the receptor. Using the radioligand [^{3}H]iperoxo, the binding of the agonistic moiety (iperoxo) is favoured, resulting in increased binding affinities (left shift of the binding curve) (Figure 3, **B**).

Taken together, the iperoxo-C_n-atropine hybrids show two different binding modes at the M_2 receptor depending on their linker chain length.

Further pharmacological investigations with respect to isoxazole/atropine hybrids, iperoxo/scopolamine hybrids, and isoxazole/scopolamine hybrids at the M_2 receptor are still in process.

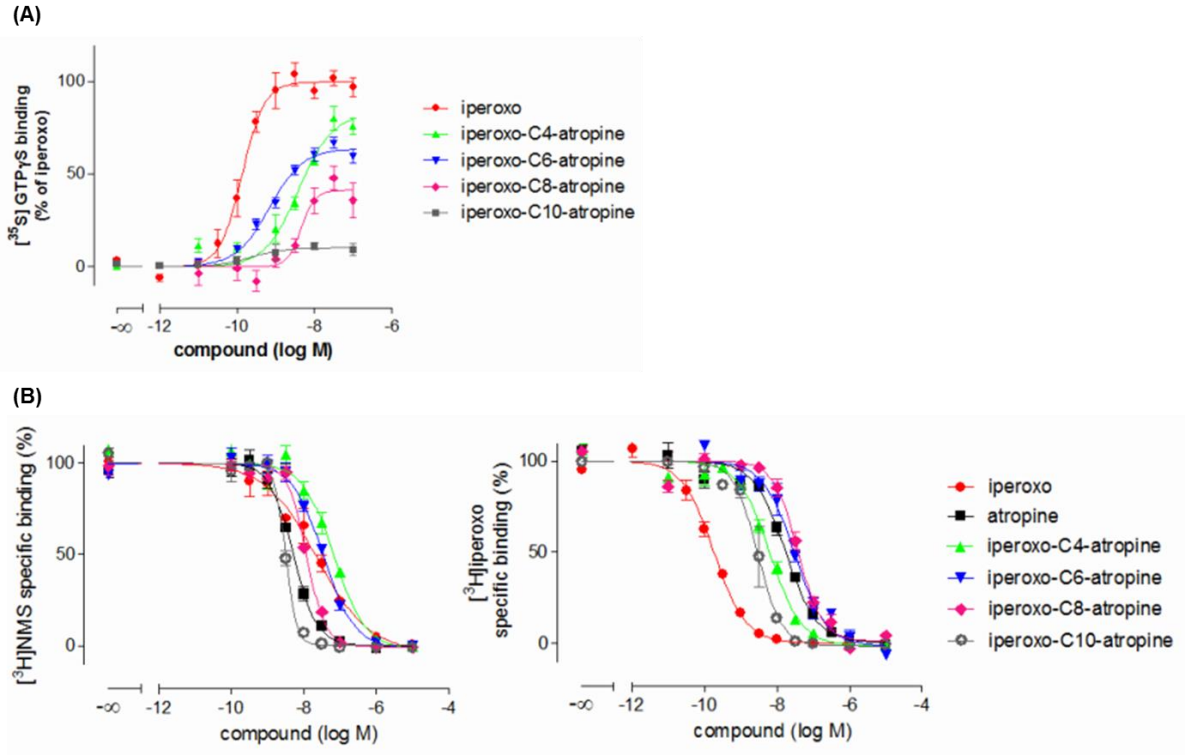

Figure 3: Radioligand binding studies. **(A)** M_2 receptor-mediated G_i protein activation reflected by [^{35}S]GTPγS binding in CHO-hM_2 cell homogenates. Maximum G_i protein activation by iperoxo was set to 100%. **(B)** [^{3}H]NMS and [^{3}H]iperoxo binding experiments in CHO-hM_2 homogenates. Upper plateau was set to 100%.

3. Material and methods

3.1 Chemistry

Chemicals were of analytical grade and purchased from Aldrich (Steinheim, Germany) and Merck (Darmstadt, Germany). Microwave provided reactions were accomplished on a MLS-rotaPREP instrument (Milestone, Leutkirch, Germany). Melting points were determined on a Stuart melting point apparatus SMP3 (Bibby Scientific, UK) and are uncorrected. FT-IR spectra were recorded on a Jasco FT-IR-6100 spectrometer (Gross-Umstadt, Germany) equipped with a diamond-ATR-unit. ^{1}H (400.132 MHz) and ^{13}C (100.613 MHz) NMR spectra were recorded on a Bruker AV 400 instrument (Bruker Biospin, Ettlingen, Germany). As internal standard, the signals of the deuterated solvent were used (DMSO-d_6: ^{1}H 2.50 ppm, ^{13}C 39.52 ppm). Abbreviation for data quoted are: s, singlet; d, doublet; t, triplet; q, quartet; m, multiplet; b, broad; dd, doublet of doublets; dt, doublet of triplets; tt, triplet of triplets; tq, triplet of quartets. Coupling constants (*J*) are given in Hz. NOESY experiments were acquired using the noesytp program on a Bruker Avance III 400 MHz spectrometer, with a mixing time of 1 s. The number of scans as well as the number of dummy scans was 16. The relaxation delay was 3 s, time domain size 2048, acquisition time 0.331776 s, the transmitter frequency offset 4.28 ppm, spectral width 7.71 ppm. ESI mass spectra of the novel compounds were measured on an Agilent LC/MSD Trap G2445D instrument (Waldbronn, Germany). Data are reported as mass-to-charge ratio (*m/z*) of the corresponding positively charged molecular ions. The purities of the new compounds **8-C4**, **10-C4**, **10-C8**, **10-C10**, **9-C10**, **11-C8** (confirming purity ≥90%) and **8-C6**, **8-C8**, **8-C10**, **10-C6**, **9-C4**, **9-C6**, **9-C8**, **11-C4**, **11-C6**, **11-C10**, **12** (confirming purity ≥95%) were measured on an Agilent 1100 series system with UV detector, using a C18 reversed-phase (Knauer, Germany) (150 x 4.6 mm) column. The mobile phase (MeOH/phosphate buffer = 70:30) was used at a flow rate of 1.5 mL/min, detecting at 210.0 nm. The synthesis of the base of iperoxo **1**[18,19] and the base of isoxazole **2**[19,21] were prepared according to literature known procedures.

3.1.1 General procedure for the synthesis of the atropine derivatives **6-C4**, **6-C6**, **6-C8**, and **6-C10**

Atropine **3** (1.50 g, 5.18 mmol) was dissolved with heating (60 °C) in 15 mL acetonitrile and treated with 1,4-dibromobutane (3.69 mL, 30.8 mmol), 1,6-dibromohexane (4.74 mL, 30.8 mmol), 1,8-dibromooctane (5.67 mL, 30.8 mmol), and 1,10-dibromodecane (13.8 mL, 61.6 mmol), respectively. The solution was held at room temperature for 3 d (C4), 7 d (C6 and C8) and at 68 °C for 3 d (C10). The crude products were purified as follows:

a) After addition of hexane (45 mL), a thick solid precipitated at the bottom of the flask. The solvent was decanted and the residue was dissolved in acetonitrile with heating. The solution was kept in the fridge overnight. The precipitate obtained was filtered and washed with acetonitrile to afford **6-C4** and **6-C8**.

b) The solution was added dropwise to heated *tert*-butylmethylether (50 °C). A white solid was obtained on the bottom of the flask. The solvent was decanted and the residue was dried *in vacuo* to obtain **6-C6**.

c) After addition of diethyl ether, a thick solid was built on the bottom of the flask. The solvent was decanted and the crude product was recrystallized several times in diethyl ether. The obtained white solid was dried *in vacuo* to afford **6-C10**.

(1R,3r,5S,8s)-8-(4-Bromobutyl)-3-((3-hydroxy-2-phenylpropanoyl)oxy)-8-methyl-8-azabicyclo[3.2.1]octan-8-ium bromide ***6-C4***

White, hygroscopic solid; yield 43%; mp 159.7-162.6 °C; IR (ATR): 3264, 2953, 2876, 1714, 1469, 1455, 1431 cm^{-1}; ^{1}H NMR (DMSO): 1.66-1,70 (m, 2H, **H**-2,$4_{eq.}$), 1.79-1.88 (m, 5H, Br-CH_2-C**H₂**/C**H₂**-CH_2-$^{+}NCH_3$/**H**-6,7), 2.09-2.22 (m, 3H, **H**-6,7), 2.54-2.58 (m, 2H, **H**-2,$4_{ax.}$), 3.04 (s, 3H, $^{+}$NC**H₃**), 3.21 (t, 2H, C**H₂**-$^{+}NCH_3$, *J* = 7.8), 3.58 (t, 2H, Br-C**H₂**, *J* = 6.4), 3.66-3.71 (m, 1H, C**H₂**-OH), 3.79-3.87 (m, 3H, C$\mathbf{H}_{phenyl}$/**H**-1,5), 3.95-4.01 (m, 1H, C**H₂**-OH), 5.00 (t, 1H, **H**-3, *J* = 5.4), 5.08 (t, 1H, O**H**, *J* = 5.2), 7.27-7.37 (m, 5H, C$\mathbf{H}_{phenyl}$). ^{13}C NMR (DMSO): 20.5, 24.0, 24.3, 29.0, 31.5, 31.6, 34.0, 40.1, 54.1, 59.3, 62.9, 63.4, 64.8, 65.0, 127.4, 128.1, 128.6, 136.1, 171.2.

(1R,3r,5S,8s)-8-(6-Bromohexyl)-3-((3-hydroxy-2-phenylpropanoyl)oxy)-8-methyl-8-azabicyclo[3.2.1]octan-8-ium bromide ***6-C6***

White, hygroscopic solid; yield 89%; mp 61.5-65.7 °C; IR (ATR): 3297, 2938, 2864, 1724, 1454, 1433 cm^{-1}; ^{1}H NMR (DMSO): 1.26-1.46 (m, 4H, Br-CH_2-CH_2-C**H₂**/C**H₂**-CH_2-CH_2-$^{+}NCH_3$), 1.61-1,69 (m, 3H, **H**-2,$4_{eq.}$/Br-CH_2-C**H**$_2$), 1.78-1.87 (m, 4H, Br-CH_2-C**H**$_2$/C**H₂**-CH_2-$^{+}NCH_3$/**H**-6,7), 2.06-2.26 (m, 3H, **H**-6,7), 2.54-2.59 (m, 2H, **H**-2,$4_{ax.}$), 3.03 (s, 3H, $^{+}$NC**H₃**), 3.15 (t, 2H, C**H₂**-$^{+}NCH_3$, *J* = 8.4), 3.54 (t, 2H, Br-C**H₂**, *J* = 6.4), 3.66-3.71 (m, 1H, C**H₂**-OH), 3.79-3.82 (m, 2H, **H**-1,5), 3.85-3.89 (m, 1H, C$\mathbf{H}_{phenyl}$), 3.95-4.01 (m, 1H, C**H₂**-OH), 5.00 (t, 1H, **H**-3, *J* = 5.6), 5.08 (t, 1H, O**H**, *J* = 5.6), 7.27-7.37 (m, 5H, C$\mathbf{H}_{phenyl}$). ^{13}C NMR (DMSO): 21.3, 24.0, 24.2, 24.8, 27.0, 31.5, 31.5, 31.8, 34.9, 54.1, 60.2, 62.8, 63.4, 64.5, 64.8, 127.3, 128.0, 128.5, 136.0, 171.1.

(1R,3r,5S,8s)-8-(8-Bromooctyl)-3-((3-hydroxy-2-phenylpropanoyl)oxy)-8-methyl-8-azabicyclo[3.2.1]octan-8-ium ***6-C8***

White, hygroscopic solid; yield 89%; IR (ATR): 3287, 2928, 2856, 1724, 1454, 1433 cm^{-1}; ^{1}H NMR (DMSO): 1.24-1.41 (m, 8H, Br-CH_2-CH_2-C**H₂**-C**H₂**/C**H₂**-C**H₂**-CH_2-CH_2-$^{+}NCH_3$), 1.60-1,69 (m, 3H, **H**-2,4$_{eq.}$/Br-CH_2-C**H**$_2$), 1.76-1.87 (m, 4H, Br-CH_2-C**H**$_2$/C**H₂**-CH_2-$^{+}NCH_3$/**H**-6,7), 2.09-2.26 (m, 3H, **H**-6,7), 2.54-2.58 (m, 2H, **H**-2,4$_{ax.}$), 3.03 (s, 3H, $^{+}$NC**H₃**), 3.15 (t, 2H, C**H₂**-$^{+}NCH_3$, *J* = 8.2), 3.53 (t, 2H, Br-C**H₂**, *J* = 6.6), 3.66-3.71 (m, 1H, C**H₂**-OH), 3.79-3.82 (m, 2H, **H**-1,5), 3.80-3.87 (m, 1H, C**H**$_{phenyl}$), 3.95-4.01 (m, 1H, C**H₂**-OH), 5.00 (t, 1H, **H**-3, *J* = 5.4), 5.08 (t, 1H, O**H**, *J* = 5.0), 7.26-7.37 (m, 5H, C**H**$_{phenyl}$). ^{13}C NMR (DMSO): 21.4, 24.0, 24.2, 25.6, 27.3, 27.7, 28.3, 31.5, 31.5, 32.0, 35.1, 40.0, 54.1, 60.3, 62.8, 63.4, 64.5, 64.8, 127.3, 128.0, 128.5, 136.0, 171.1.

(1R,3r,5S,8s)-8-(10-Bromodecyl)-3-((3-hydroxy-2-phenylpropanoyl)oxy)-8-methyl-8-azabicyclo[3.2.1]octan-8-ium bromide ***6-C10***

White, hygroscopic solid; yield 73%; IR (ATR): 3291, 2926, 2854, 1725, 1454, 1433 cm^{-1}; ^{1}H NMR (DMSO): 1.23-1.39 (m, 12H, Br-CH_2-CH_2-C**H₂**-C**H₂**-C**H₂**/C**H₂**-C**H₂**-C**H₂**-CH_2-CH_2-$^{+}NCH_3$), 1.58-1,69 (m, 3H, **H**-2,4$_{eq.}$/Br-CH_2-C**H**$_2$), 1.75-1.87 (m, 4H, Br-CH_2-C**H**$_2$/C**H₂**-CH_2-$^{+}NCH_3$/**H**-6,7), 2.06-2.25 (m, 3H, **H**-6,7), 2.52-2.59 (m, 2H, **H**-2,4$_{ax.}$), 3.03 (s, 3H, $^{+}$NC**H₃**), 3.13-3.17 (m, 2H, C**H₂**-$^{+}NCH_3$), 3.52 (t, 2H, Br-C**H₂**, *J* = 6.8), 3.66-3.70 (m, 1H, C**H₂**-OH), 3.78-3.89 (m, 3H, **H**-1,5/C**H**$_{phenyl}$), 3.96-4.00 (m, 1H, C**H₂**-OH), 5.00 (t, 1H, **H**-3 *J* = 5.6), 7.26-7.37 (m, 5H, C**H**$_{phenyl}$). ^{13}C NMR (DMSO): 21.5, 24.0, 24.2, 25.7, 27.4, 27.9, 28.4, 28.6, 28.6, 31.5, 31.5, 32.1, 35.1, 40.0, 54.1, 60.3, 62.8, 63.4, 64.5, 64.8, 127.3, 128.0, 128.5, 136.0, 171.1.

3.1.2 General procedure for the synthesis of the scopolamine derivatives **7-C4**, **7-C6**, **7-C8**, and **7-C10**

The free base of scopolamine **4** was achieved by solving scopolamine hydrobromide trihydrate in water and addition of 1 M aqueous sodium hydroxide solution to adjust a pH value of 11. This solution was extracted with dichloromethane. The combined organic phases were dried over Na_2SO_4. The solvent was evaporated *in vacuo* to obtain the free base of scopolamine as a white viscous oil.

The base of scopolamine **4** (1.76 g, 5.79 mmol) was dissolved with heating (60 °C) in 20 mL acetonitrile and treated with 1,4-dibromobutane (4.69 mL, 39.1 mmol), 1,6-dibromohexane (3.79 mL, 24.6 mmol), 1,8-dibromooctane (7.25 mL, 39.4 mmol), and 1,10-dibromodecane

(8.85 mL, 39.4 mmol), respectively. The solution was stirred at room temperature for 34 d in a sealed pressure tube. A fine white precipitate was obtained. This suspension was dropwise added to cold diethylether and the suspension was kept in the fridge overnight. A white precipitate is obtained at the bottom of the flask. The solvent was decanted and the residue was dried *in vacuo* to obtain the desired compounds.

(1R,2R,4S,5S,7s,9S)-9-(4-Bromobutyl)-7-(((S)-3-hydroxy-2-phenylpropanoyl)oxy)-9-methyl-3-oxa-9-azatricyclo[3.3.1.0^{2,4}]nonan-9-ium bromide ***7-C4***

White, hygroscopic solid; yield 87%; IR (ATR): 3330, 3057, 2958, 2878, 1724, 1466, 1453, 1435 cm^{-1}; ^{1}H NMR (DMSO): 1.73-1.82 (m, 4H, Br-CH_2-C**H$_2$**/C**H$_2$**-CH_2-$^{+}$NCH_3), 1.91-1.95 (m, 2H, **H**-2,4$_{eq.}$), 2.57-2.68 (m, 2H, **H**-2,4$_{ax.}$), 3.04 (s, 3H, $^{+}$NC**H$_3$**), 3.53-3.59 (m, 4H, C**H$_2$**-$^{+}$NCH_3/Br-C**H$_2$**), 3.66-3.79 (m, 3H, **H**-6,7/C**H$_2$**-OH), 3.94-4.01 (m, 2H, C**H**$_{phenyl}$/C**H$_2$**-OH), 4.17 (d, 1H, **H**-1,5, *J* = 2.4), 4.21 (d, 1H, **H**-1,5, *J* = 2.4), 5.02 (t, 1H, **H**-3, *J* = 6.0), 5.11 (t, 1H, O**H**, *J* = 5.2), 7.26-7.35 (m, 5H, C**H**$_{phenyl}$). ^{13}C NMR (DMSO): 20.7, 28.1, 28.8, 33.8, 44.4, 53.4, 53.6, 54.0, 62.0, 62.8, 62.8, 63.0, 66.8, 127.3, 128.1, 128.4, 136.0, 170.8.

(1R,2R,4S,5S,7s,9S)-9-(6-Bromohexyl)-7-(((S)-3-hydroxy-2-phenylpropanoyl)oxy)-9-methyl-3-oxa-9-azatricyclo[3.3.1.0^{2,4}]nonan-9-ium bromide ***7-C6***

White, hygroscopic solid; yield 73%; IR (ATR): 3330, 3058, 2936, 2863, 1725, 1467, 1454, 1436 cm^{-1}; ^{1}H NMR (DMSO): 1.19-1.27 (m, 2H, Br-CH_2-CH_2-C**H$_2$**), 1.37-1.44 (m, 2H, C**H$_2$**-CH_2-CH_2-$^{+}$NCH_3), 1.63-1.94 (m, 6H, **H**-2,4$_{eq.}$/Br-CH_2-C**H$_2$**/C**H$_2$**-CH_2-$^{+}$NCH_3), 2.55-2.66 (m, 2H, **H**-2,4$_{ax.}$), 3.02 (s, 3H, $^{+}$NC**H$_3$**), 3.49-3.55 (m, 4H, Br-C**H$_2$**/C**H$_2$**-$^{+}$NCH_3), 3.66-3.80 (m, 3H, **H**-6,7/C**H$_2$**-OH), 3.94-4.00 (m, 2H, C**H**$_{phenyl}$/C**H$_2$**-OH), 4.16 (d, 1H, **H**-1,5, *J* = 2.4), 4.20 (d, 1H, **H**-1,5, *J* = 2.4), 5.02 (t, 1H, **H**-3, *J* = 6.0), 5.11 (t, 1H, O**H**, *J* = 5.2), 7.27-7.36 (m, 5H, C**H**$_{phenyl}$). ^{13}C NMR (DMSO): 21.6, 24.6, 26.9, 28.1, 31.7, 34.9, 44.3, 53.5, 53.6, 54.0, 62.1, 62.7, 62.9, 62.8, 67.7, 127.4, 128.1, 128.5, 136.0, 170.8.

(1R,2R,4S,5S,7s,9S)-9-(8-Bromooctyl)-7-(((S)-3-hydroxy-2-phenylpropanoyl)oxy)-9-methyl-3-oxa-9-azatricyclo[3.3.1.0^{2,4}]nonan-9-ium bromide ***7-C8***

White, hygroscopic solid; yield 56%; IR (ATR): 3304, 2928, 2856, 1725, 1454, 1436 cm^{-1}; ^{1}H NMR (DMSO): 1.20-1.22 (m, 2H, Br-CH_2-CH_2-C**H$_2$**), 1.27-1.30 (m, 4H, Br-CH_2-CH_2-CH_2-C**H$_2$**/C**H$_2$**-CH_2-CH_2-CH_2-$^{+}$NCH_3), 1.34-1.39 (m, 2H, C**H$_2$**-CH_2-$^{+}$NCH_3), 1.63-1.94 (m, 6H, **H**-2,4$_{eq.}$/Br-CH_2-C**H$_2$**/C**H$_2$**-CH_2-CH_2-$^{+}$NCH_3), 2.57-2.67 (m, 2H, **H**-2,4$_{ax.}$), 3.04 (s, 3H, $^{+}$NC**H$_3$**), 3.50-3.54 (m, 4H, Br-C**H$_2$**/C**H$_2$**-$^{+}$NCH_3), 3.66-3.80 (m, 3H, **H**-6,7/C**H$_2$**-OH), 3.94-3.99 (m, 2H,

C**H**$_{phenyl}$/C**H$_2$**-OH), 4.18 (d, 1H, **H**-1,5, *J* = 2.4), 4.22 (d, 1H, **H**-1,5 *J* = 2.4), 5.03 (t, 1H, **H**-3, *J* = 6.0), 5.11 (t, 1H, O**H**, *J* = 5.4), 7.26-7.34 (m, 5H, C**H**$_{phenyl}$). ^{13}C NMR (DMSO): 21.6, 25.4, 27.2, 27.6, 28.1, 28.1, 32.0, 35.1, 44.3, 53.4, 53.6, 54.0, 62.0, 62.7, 62.8, 67.7, 127.3, 128.1, 128.4, 136.0, 170.8.

(1R,2R,4S,5S,7s,9S)-9-(10-Bromodecyl)-7-(((S)-3-hydroxy-2-phenylpropanoyl)oxy)-9-methyl-3-oxa-9-azatricyclo[3.3.1.0^{2,4}]nonan-9-ium bromide ***7-C10***

Transparent, hygroscopic solid; yield 35%; IR (ATR): 3337, 2925, 2854, 1726, 1467, 1454, 1436 cm^{-1}; ^{1}H NMR (DMSO): 1.16-1.22 (m, 2H, Br-CH$_2$-CH$_2$-C**H$_2$**), 1.23-1.30 (m, 8H, Br-CH$_2$-CH$_2$-CH$_2$-CH$_2$-C**H$_2$**/C**H$_2$**-CH$_2$-CH$_2$-CH$_2$-CH$_2$-$^+$NCH$_3$), 1.34-1.39 (m, 2H, C**H$_2$**-CH$_2$-$^+$NCH$_3$), 1.62-1.94 (m, 6H, **H**-2,4$_{eq.}$/Br-CH$_2$-C**H$_2$**/C**H$_2$**-CH$_2$-CH$_2$-$^+$NCH$_3$), 2.57-2.67 (m, 2H, **H**-2,4$_{ax.}$), 3.04 (s, 3H, $^+$NC**H$_3$**), 3.50-3.55 (m, 4H, Br-C**H$_2$**/C**H$_2$**-$^+$NCH$_3$), 3.66-3.81 (m, 3H, **H**-6,7/C**H$_2$**-OH), 3.94-3.99 (m, 2H, C**H**$_{phenyl}$/C**H$_2$**-OH), 4.19 (d, 1H, **H**-1,5, *J* = 2.5), 4.23 (d, 1H, **H**-1,5, *J* = 2.4), 5.03 (t, 1H, **H**-3, *J* = 5.8), 5.11 (dd, 1H, O**H**, *J* = 4.7 Hz, *J* = 5.8 Hz), 7.26-7.34 (m, 5H, C**H**$_{phenyl}$). ^{13}C NMR (DMSO): 21.6, 25.5, 27.4, 27.9, 28.1, 28.3, 28.6, 28.5, 32.1, 35.1, 44.3, 53.4, 53.6, 54.0, 62.0, 62.7, 62.8, 67.7, 127.3, 128.1, 128.4, 136.0, 170.8.

3.1.3 General procedure for the synthesis of the atropine/iperoxo hybrids **8-C4**, **8-C6**, **8-C8**, and **8-C10**, atropine/isoxazole hybrids **10-C4**, **10-C6**, **10-C8**, and **10-C10**, scopolamine/iperoxo hybrids **9-C4**, **9-C6**, **9-C8**, and **9-C10**, and scopolamine/isoxazole hybrids **11-C4**, **11-C6**, **11-C8**, and **11-C10**

To a solution of 1 equiv of **6-C4**, **6-C6**, **6-C8**, **6-C10**, **7-C4**, **7-C6**, **7-C8**, and **7-C10** in 10-15 mL acetonitrile, 2 equiv of the base of iperoxo **1**[18,19] and of the base of isoxazole **2**,[19,21] respectively, and a catalytic amount of KI/K_2CO_3 (1:1) were added. The reaction mixture was heated in the microwave (500 W, 80 °C) for 8 h. After cooling to room temperature the surplus of KI/K_2CO_3 was filtered and the solvent was evaporated to half volume. After addition of diethyl ether the solution was kept in the fridge overnight. An oily precipitate was built at the bottom of the flask. The solvent was decanted and the residue was dried *in vacuo*. If the product was still not pure, the residue was dissolved in acetonitrile and recrystallized in diethyl ether.

(1R,3r,5S,8s)-8-(4-((4-((4,5-Dihydroisoxazol-3-yl)oxy)but-2-yn-1-yl)dimethylammonio)butyl)-3-((3-hydroxy-2-phenylpropanoyl)oxy)-8-methyl-8-azabicyclo[3.2.1]octan-8-ium bromide ***8-C4***

Yellow, hygroscopic solid; yield 14%; IR (ATR): 3386, 2956, 1723, 1625, 1468, 1434, 140 cm^{-1}; ^{1}H NMR (DMSO): 1.67-1.89 (m, 7H, **H**-2,4$_{eq.}$/**H**-6,7/$^+$N(CH$_3$)$_2$-CH$_2$-C**H$_2$**/C**H$_2$**-CH$_2$-

$^{+}NCH_3$), 2.10-2.29 (m, 3H, **H**-6,7), 2.55-2.60 (m, 2H, **H**-2,$4_{ax.}$), 2.97-3.14 (m, 11H, $^{+}N(C\mathbf{H_3})_2$/$^{+}NC\mathbf{H_3}$/**H**-$4_{2\text{-isox}}$), 3.22-3.26 (m, 2H, $C\mathbf{H_2}$-$^{+}NCH_3$), 3.44 (t, 2H, $^{+}N(CH_3)_2$-$C\mathbf{H_2}$, *J* = 7.6), 3.67-3.72 (m, 1H, $C\mathbf{H}_2OH$), 3.79-3.83 (m, 2H, **H**-1,5), 3.89-3.90 (m, 1H, $C\mathbf{H}_{phenyl}$), 3.96-4.02 (m, 1H, $C\mathbf{H}_2OH$), 4.33 (t, 2H, **H**-$5_{2\text{-isox}}$, *J* = 9.6), 4.53 (s, 2H, ^{+}N-$C\mathbf{H_2}$-C≡), 4.95 (s, 2H, ≡C-$C\mathbf{H_2}$-O), 5.01 (t, 1H, **H**-3, *J* = 5.4), 5.08 (t, 1H, O**H**, *J* = 5.2), 7.27-7.37 (m, 5H, $C\mathbf{H}_{phenyl}$). ^{13}C NMR (DMSO): 18.8, 19.1, 23.9, 24.2, 31.4, 31.5, 32.2, 40.1, 49.7, 53.6, 54.0, 57.2, 59.4, 62.3, 62.8, 63.3, 64.8, 65.0, 69.5, 76.0, 86.0, 127.3, 128.0, 128.5, 136.0, 166.7, 171.1. MS (ESI) m/z $[M+H]^{2+}$ Calcd for $C_{30}H_{45}N_3O_5^{2+}$: 262.7. Found: 263.5. HPLC purity 91.1%. Impurity: traces of the base of iperoxo **1**.

(1R,3r,5S,8s)-8-(6-((4-((4,5-Dihydroisoxazol-3-yl)oxy)but-2-yn-1-yl)dimethylammonio)hexyl)-3-((3-hydroxy-2-phenylpropanoyl)oxy)-8-methyl-8-azabicyclo[3.2.1]octan-8-ium bromide ***8-C6***

Yellow, hygroscopic solid; yield 37%; IR (ATR): 3385, 2940, 1723, 1625, 1468, 1434, 1400 cm^{-1}; ^{1}H NMR (DMSO): 1.29-1.37 (m, 4H, $^{+}N(CH_3)_2$-CH_2-CH_2-$C\mathbf{H_2}$/$C\mathbf{H_2}$-CH_2-CH_2-$^{+}NCH_3$), 1.67-1,88 (m, 7H, **H**-$2,4_{eq.}$/**H**-6,7/$^{+}N(CH_3)_2$-CH_2-$C\mathbf{H_2}$/$C\mathbf{H_2}$-CH_2-$^{+}NCH_3$), 2.07-2.23 (m, 3H, **H**-6,7), 2.53-2.60 (m, 2H, **H**-2,$4_{ax.}$), 2.95-3.05 (m, 11H, $^{+}N(C\mathbf{H_3})_2$/$^{+}NC\mathbf{H_3}$/**H**-$4_{2\text{-isox}}$), 3.13-3.20 (m, 2H, $C\mathbf{H_2}$-$^{+}NCH_3$), 3.34-3.39 (m, 2H, $^{+}N(CH_3)_2$-$C\mathbf{H_2}$), 3.67-3.72 (m, 1H, $C\mathbf{H_2}$-OH), 3.79-3.82 (m, 2H, **H**-1,5), 3.87-3.88 (m, 1H, $C\mathbf{H}_{phenyl}$), 3.96-4.02 (m, 1H, $C\mathbf{H_2}$-OH), 4.32 (t, 2H, **H**-$5_{2\text{-isox}}$, *J* = 9.6), 4.49 (s, 2H, ^{+}N-$C\mathbf{H_2}$-C≡), 4.94 (s, 2H, ≡C-$C\mathbf{H_2}$-O), 5.01 (t, 1H, **H**-3 *J* = 5.4), 5.08 (t, 1H, O**H**, *J* = 5.2), 7.27-7.37 (m, 5H, $C\mathbf{H}_{phenyl}$). ^{13}C NMR (DMSO): 21.3, 21.5, 25.1, 25.1, 31.5, 31.5, 32.2, 40.1, 49.7, 53.2, 54.1, 57.1, 59.5, 62.9, 62.9, 63.4, 64.6, 64.8, 69.5, 76.1, 85.9, 127.3, 128.0, 128.5, 136.0, 166.6, 171.1. MS (ESI) m/z $[M]^{+}$ Calcd for $C_{32}H_{49}N_3O_5^{2+}$: 277.7. Found: 277.7. HPLC purity 95.9%.

(1R,3r,5S,8s)-8-(8-((4-((4,5-Dihydroisoxazol-3-yl)oxy)but-2-yn-1-yl)dimethylammonio)octyl)-3-((3-hydroxy-2-phenylpropanoyl)oxy)-8-methyl-8-azabicyclo[3.2.1]octan-8-ium bromide ***8-C8***

Yellow, hygroscopic solid; yield 6%; IR (ATR): 3394, 2929, 2858, 1724, 1625, 1466, 1434 cm^{-1}; ^{1}H NMR (DMSO): 1.22-1.42 (m, 8H, $^{+}N(CH_3)_2$-CH_2-CH_2-$C\mathbf{H_2}$-$C\mathbf{H_2}$/$C\mathbf{H_2}$-$C\mathbf{H_2}$-CH_2-CH_2-$^{+}NCH_3$), 1.59-1,88 (m, 7H, **H**-$2,4_{eq.}$/**H**-6,7/$^{+}N(CH_3)_2$-CH_2-$C\mathbf{H_2}$/$C\mathbf{H_2}$-CH_2-$^{+}NCH_3$), 2.08-2.22 (m, 3H, **H**-6,7), 2.54-2.60 (m, 2H, **H**-2,$4_{ax.}$), 2.93-3.09 (m, 11H, $^{+}N(C\mathbf{H_3})_2$/$^{+}NC\mathbf{H_3}$/**H**-$4_{2\text{-isox}}$), 3.12-3.15 (m, 2H, $C\mathbf{H_2}$-$^{+}NCH_3$), 3.33-3.36 (m, 2H, $^{+}N(CH_3)_2$-$C\mathbf{H_2}$), 3.67-3.72 (m, 1H, $C\mathbf{H_2}$-OH), 3.78-3.82 (m, 2H, **H**-1,5), 3.84-3.86 (m, 1H, $C\mathbf{H}_{phenyl}$), 3.95-4.02 (m, 1H, $C\mathbf{H_2}$-OH), 4.32 (t, 2H, **H**-$5_{2\text{-isox}}$, *J* = 9.6), 4.44 (s, 2H, ^{+}N-$C\mathbf{H_2}$-C≡), 4.94 (s, 2H, ≡C-$C\mathbf{H_2}$-O), 5.00 (t, 1H, **H**-3, *J* = 5.4), 5.08 (t, 1H, O**H**, *J* = 5.2), 7.27-7.37 (m, 5H, $C\mathbf{H}_{phenyl}$). ^{13}C NMR (DMSO): 21.5, 21.7, 24.0, 24.2, 25.5, 25.6, 28.2, 28.3, 31.5, 31.5, 32.2, 40.0, 49.7, 53.2, 54.1, 57.1, 60.3, 62.9,

63.0, 63.4, 64.6, 64.8, 69.5, 76.1, 85.9, 127.3, 128.0, 128.5, 136.0, 166.6, 171.1. MS (ESI) m/z $[M+H]^{2+}$ Calcd for $C_{34}H_{53}N_3O_5^{2+}$: 291.7. Found: 291.7. HPLC purity 99.3%.

(1R,3r,5S,8s)-8-(10-((4-((4,5-Dihydroisoxazol-3-yl)oxy)but-2-yn-1-yl)dimethylammonio)decyl)-3-((3-hydroxy-2-phenylpropanoyl)oxy)-8-methyl-8-azabicyclo[3.2.1]octan-8-ium bromide ***8-C10***

Yellow, hygroscopic solid; yield 17%; IR (ATR): 3289, 2926, 2856, 1724, 1625, 1466, 1434 cm^{-1}; ^1H NMR (DMSO): 1.23-1.34 (m, 12H, $^+N(CH_3)_2$-CH_2-CH_2-C**H₂**-C**H₂**-C**H₂**/C**H₂**-C**H₂**-C**H₂**-CH_2-$^+NCH_3$), 1.65-1,87 (m, 7H, **H**-2,$4_{eq.}$/**H**-6,7/$^+N(CH_3)_2$-CH_2-C**H₂**/C**H₂**-CH_2-$^+NCH_3$), 2.07-2.21 (m, 3H, **H**-6,7), 2.52-2.58 (m, 2H, **H**-2,$4_{ax.}$), 2.94-3.09 (m, 11H, $^+N(C\mathbf{H_3})_2$/$^+NC\mathbf{H_3}$/**H**-$4_{2\text{-isox}}$), 3.14-3.18 (m, 2H, C**H₂**-$^+NCH_3$), 3.35-3.39 (m, 2H, $^+N(CH_3)_2$-C**H₂**), 3.66-3.71 (m, 1H, C**H₂**-OH), 3.79-3.82 (m, 2H, **H**-1,5), 3.87-3.89 (m, 1H, C$\mathbf{H}_{phenyl}$), 3.95-4.01 (m, 1H, C**H₂**-OH), 4.32 (t, 2H, **H**-$5_{2\text{-isox}}$, *J* = 9.6), 4.50 (s, 2H, $^+$N-C**H₂**-C≡), 4.94 (s, 2H, ≡C-C**H₂**-O), 5.01 (t, 1H, **H**-3, *J* = 5.6), 5.08 (t, 1H, O**H**, *J* = 5.2), 7.27-7.37 (m, 5H, C$\mathbf{H}_{phenyl}$). ^{13}C NMR (DMSO): 21.5, 21.7, 24.0, 24.2, 25.6, 25.8, 28.3, 28.5, 28.6, 28.6, 31.5, 31.5, 32.2, 40.0, 49.7, 53.2, 54.1, 57.1, 60.3, 62.9, 63.0, 63.4, 64.5, 64.8, 69.5, 76.1, 85.8, 127.3, 128.0, 128.5, 136.0, 166.6, 171.1. MS (ESI) m/z $[M+H]^{2+}$ Calcd for $C_{36}H_{57}N_3O_5^{2+}$: 305.7. Found: 305.9. HPLC purity 100.0%.

(1R,3r,5S,8s)-3-((3-Hydroxy-2-phenylpropanoyl)oxy)-8-(4-((4-(isoxazol-3-yloxy)but-2-yn-1-yl)dimethylammonio)butyl)-8-methyl-8-azabicyclo[3.2.1]octan-8-ium bromide ***10-C4***

Brown, hygroscopic solid; yield 60%; IR (ATR): 3312, 2955, 1721, 1578, 1482, 1429 cm^{-1}; ^1H NMR (DMSO): 1.67-1.88 (m, 7H, **H**-2,$4_{eq.}$/**H**-6,7/$^+N(CH_3)_2$-CH_2-C**H₂**/C**H₂**-CH_2-$^+NCH_3$), 2.09-2.26 (m, 3H, **H**-6,7), 2.50-2.60 (m, 2H, **H**-2,$4_{ax.}$), 3.08-3.15 (m, 9H, $^+N(C\mathbf{H_3})_2$/$^+NC\mathbf{H_3}$), 3.26-3.28 (m, 2H, C**H₂**-$^+NCH_3$), 3.44-3.48 (m, 2H, $^+N(CH_3)_2$-C**H₂**), 3.67-3.71 (m, 1H, C**H₂**-OH), 3.79-3.83 (m, 2H, **H**-1,5), 3.90-3.91(m, 1H, C$\mathbf{H}_{phenyl}$), 3.96-4.01 (m, 1H, C**H₂**-OH), 4.56 (s, 2H, $^+$N-C**H₂**-C≡), 5.01 (t, 1H, **H**-3, *J* = 5.2), 5.12 (br, 2H, O**H**/≡C-C**H₂**-O), 6.45 (d, 1H, **H**-4_{isox}, *J* = 1.6), 7.27-7.37 (m, 5H, C$\mathbf{H}_{phenyl}$), 8.75 (d, 1H, **H**-5_{isox}, *J* = 1.6). ^{13}C NMR (DMSO): 18.8, 19.1, 23.9, 24.2, 31.5, 31.5, 40.1, 49.7, 53.6, 54.0, 57.6, 59.4, 62.3, 62.8, 63.3, 64.8, 65.0, 76.3, 86.1, 96.0, 127.3, 128.0, 128.5, 136.1, 162.0, 170.3, 171.1. MS (ESI) m/z $[M-2Br^-]^{2+}$ Calcd for $C_{30}H_{43}N_3O_5^{2+}$: 262.7. Found: 263.5. HPLC purity 91.7%. Impurity: traces of the base of isoxazole **2**.

(1R,3r,5S,8s)-3-((3-Hydroxy-2-phenylpropanoyl)oxy)-8-(6-((4-(isoxazol-3-yloxy)but-2-yn-1-yl)dimethylammonio)hexyl)-8-methyl-8-azabicyclo[3.2.1]octan-8-ium bromide ***10-C6***

Brown, hygroscopic solid; yield 50%; IR (ATR): 3319, 2924, 1723, 1577, 1482, 1428 cm^{-1}; ^1H NMR (DMSO): 1.30 (br, 4H, $^+N(CH_3)_2$-CH_2-CH_2-C**H₂**/C**H₂**-CH_2-CH_2-$^+NCH_3$), 1.66-1.87 (m, 7H, **H**-2,$4_{eq.}$/**H**-6,7/$^+N(CH_3)_2$-CH_2-C**H₂**/C**H₂**-CH_2-$^+NCH_3$), 2.12-2.24 (m, 3H, **H**-6,7), 2.55-2.60 (m, 2H, **H**-2,$4_{ax.}$), 3.07-3.11 (m, 9H, $^+N(CH_3)_2$/$^+NCH_3$), 3.17-3.21 (m, 2H, C**H₂**-$^+NCH_3$), 3.37-3.41 (m, 2H, $^+N(CH_3)_2$-C**H₂**), 3.66-3.70 (m, 1H, C**H₂**-OH), 3.79-3.86 (m, 2H, **H**-1,5), 3.91-3.92 (m, 1H, CH_{phenyl}), 3.95-4.00 (m, 1H, C**H₂**-OH), 4.55 (s, 2H, ^+N-C**H₂**-C≡), 5.01 (t, 1H, **H**-3, *J* = 5.5), 5.11 (br, 2H, O**H**/≡C-C**H₂**-O), 6.45 (d, 1H, **H**-4_{isox}, *J* = 1.8), 7.26-7.36 (m, 5H, CH_{phenyl}), 8.76 (d, 1H, **H**-5_{isox}, *J* = 1.8). ^{13}C NMR (DMSO): 21.2, 21.5, 24.0, 24.2, 25.0, 25.0, 31.5, 31.5, 40.1, 49.7, 53.2, 54.0, 57.5, 60.1, 62.8, 63.4, 64.6, 64.8, 76.3, 85.9, 96.0, 127.3, 128.0, 128.5, 136.0, 162.0, 170.3, 171.1. MS (ESI) m/z $[M\text{-}2Br^-]^{2+}$ Calcd for $C_{32}H_{47}N_3O_5^{2+}$: 276.7. Found: 277.2. HPLC purity 95.9%.

(1R,3r,5S,8s)-3-((3-Hydroxy-2-phenylpropanoyl)oxy)-8-(8-((4-(isoxazol-3-yloxy)but-2-yn-1-yl)dimethylammonio)octyl)-8-methyl-8-azabicyclo[3.2.1]octan-8-ium bromide ***10-C8***

Brown, hygroscopic solid; yield 63%; IR (ATR): 3294, 2925, 2858, 1724, 1577, 1482, 1428 cm^{-1}; ^1H NMR (DMSO): 1.23-1.30 (m, 8H, $^+N(CH_3)_2$-CH_2-CH_2-C**H₂**-C**H₂**/C**H₂**-C**H₂**-CH_2-CH_2-$^+NCH_3$), 1.65-1.90 (m, 7H, **H**-2,$4_{eq.}$/**H**-6,7/$^+N(CH_3)_2$-CH_2-C**H₂**/C**H₂**-CH_2-$^+NCH_3$), 2.08-2.25 (m, 3H, **H**-6,7), 2.54-2.59 (m, 2H, **H**-2,$4_{ax.}$), 2.96-3.10 (m, 9H, $^+N(CH_3)_2$/$^+NCH_3$), 3.16-3.20 (m, 2H, C**H₂**-$^+NCH_3$), 3.34-3.40 (m, 2H, $^+N(CH_3)_2$-C**H₂**), 3.66-3.71 (m, 1H, C**H₂**-OH), 3.79-3.82 (m, 2H, **H**-1,5), 3.88-3.90 (m, 1H, CH_{phenyl}), 3.95-4.01 (m, 1H, C**H₂**-OH), 4.52 (s, 2H, ^+N-C**H₂**-C≡), 5.01 (t, 1H, **H**-3, *J* = 5.5), 5.07-5.10 (m, 2H, O**H**/≡C-C**H₂**-O), 6.44 (d, 1H, **H**-4_{isox}, *J* = 1.8), 7.26-7.37 (m, 5H, CH_{phenyl}), 8.75 (d, 1H, **H**-5_{isox}, *J* = 1.8). ^{13}C NMR (DMSO): 21.5, 21.7, 24.0, 24.2, 25.4, 25.6, 28.1, 28.2, 31.5, 31.5, 40.1, 49.7, 53.1, 54.1, 57.4, 60.2, 62.8, 62.9, 63.4, 64.5, 64.8, 76.3, 85.9, 95.9, 127.3, 128.0, 128.5, 136.0, 162.0, 170.3, 171.1. MS (ESI) m/z $[M\text{-}2Br^-]^{2+}$ Calcd for $C_{34}H_{51}N_3O_5^{2+}$: 290.9. Found: 290.9. HPLC purity 93.6%. Impurity: traces of the base of iperoxo **1**.

(1R,3r,5S,8s)-3-((3-Hydroxy-2-phenylpropanoyl)oxy)-8-(10-((4-(isoxazol-3-yloxy)but-2-yn-1-yl)dimethylammonio)decyl)-8-methyl-8-azabicyclo[3.2.1]octan-8-ium bromide ***10-C10***

Brown, hygroscopic solid; yield 52%; IR (ATR): 3274, 2925, 2854, 1725, 1577, 1482 cm^{-1}; ^1H NMR (DMSO): 1.23-1.27 (m, 12H, $^+N(CH_3)_2$-CH_2-CH_2-C**H₂**-C**H₂**-C**H₂**/C**H₂**-C**H₂**-C**H₂**-CH_2-CH_2-$^+NCH_3$), 1.65-1.87 (m, 7H, **H**-2,$4_{eq.}$/**H**-6,7/N$(CH_3)_2$-CH_2-C**H₂**/C**H₂**-CH_2-$^+NCH_3$), 2.06-2.26 (m, 3H, **H**-6,7), 2.52-2.59 (m, 2H, **H**-2,$4_{ax.}$), 2.95-3.09 (m, 9H, $^+N(CH_3)_2$/$^+NCH_3$), 3.15-3.19 (m,

2H, C**H₂**-$^{+}$NCH$_3$), 3.33-3.38 (m, 2H, $^{+}$N(CH$_3$)$_2$-C**H₂**), 3.66-3.71 (m, 1H, C**H₂**-OH), 3.79-3.82 (m, 2H, **H**-1,5), 3.88-3.89 (m, 1H, C**H**$_{phenyl}$), 3.95-4.01 (m, 1H, C**H₂**-OH), 4.52 (s, 2H, $^{+}$N-C**H₂**-C≡), 5.01 (t, 1H, **H**-3, *J* = 5.5), 5.07-5.10 (m, 2H, O**H**/≡C-C**H₂**-O), 6.43 (d, 1H, **H**-4$_{isox}$, *J* = 1.8), 7.26-7.37 (m, 5H, C**H**$_{phenyl}$), 8.75 (d, 1H, **H**-5$_{isox}$, *J* = 1.8). ^{13}C NMR (DMSO): 21.5, 21.7, 24.0, 24.2, 25.5, 25.7, 28.3, 28.5, 28.6, 28.6, 31.5, 31.5, 40.0, 49.7, 53.1, 54.1, 57.4, 60.3, 62.8, 63.0, 63.4, 64.5, 64.7, 76.3, 85.9, 95.9, 127.3, 128.0, 128.5, 136.0, 162.0, 170.3, 171.1. MS (ESI) m/z [M-2Br^{-}]$^{2+}$ Calcd for $C_{36}H_{55}N_3O_5^{2+}$: 304.7. Found: 304.9. HPLC purity 93.3%. Impurity: traces of the base of isoxazole **2**.

(1R,2R,4S,5S,7s,9S)-9-(4-((4-((4,5-Dihydroisoxazol-3-yl)oxy)but-2-yn-1-yl)dimethylammonio)butyl)-7-(((S)-3-hydroxy-2-phenylpropanoyl)oxy)-9-methyl-3-oxa-9-azatricyclo[3.3.1.0^{2,4}]nonan-9-ium bromide ***9-C4***

Brown, hygroscopic solid; yield 55%; IR (ATR): 3371, 2951, 1723, 1625, 1436, 1401 cm^{-1}; ^{1}H NMR (DMSO): 1.68-1.97 (m, 6H, **H**-2,4$_{eq.}$/$^{+}$N(CH$_3$)$_2$-CH$_2$-C**H₂**/C**H₂**-CH$_2$-$^{+}$NCH$_3$), 2.59-2.70 (m, 2H, **H**-2,4$_{ax.}$), 3.01-3.16 (m, 11H, $^{+}$N(C**H₃**)$_2$/$^{+}$NC**H₃**/**H**-4$_{2\text{-}isox}$), 3.40-3.51 (m, 2H, $^{+}$N(CH$_3$)$_2$-C**H₂**), 3.59-3.61 (m, 2H, C**H₂**-$^{+}$NCH$_3$), 3.69-3.81 (m, 3H, **H**-6,7/C**H₂**-OH), 3.95-4.03 (m, 2H, C**H**$_{phenyl}$/C**H₂**-OH), 4.22 (d, 1H, **H**-1,5, *J* = 2.4), 4.27 (d, 1H, **H**-1,5, *J* = 2.0), 4.33 (t, 2H, **H**-5$_{2\text{-}isox}$, *J* = 9.6), 4.55 (br, 2H, $^{+}$N-C**H₂**-C≡), 4.95 (s, 2H, ≡C-C**H₂**-O), 5.04 (t, 1H, **H**-3, *J* = 5.8), 5.11 (br, 1H, O**H**), 7.26-7.34 (m, 5H, C**H**$_{phenyl}$). ^{13}C NMR (DMSO): 19.0, 19.1, 28.1, 32.2, 44.5, 49.7, 53.4, 53.6, 53.6, 54.0, 57.2, 62.0, 62.2, 62.8, 62.9, 63.0, 63.1, 66.8, 69.5, 76.1, 86.0, 127.3, 128.1, 128.4, 136.0, 166.7, 170.8. MS (ESI) m/z [M]$^{+}$ Calcd for $C_{30}H_{43}N_3O_6^{2+}$: 270.7. Found: 270.6. HPLC purity 98.6%.

(1R,2R,4S,5S,7s,9S)-9-(6-((4-((4,5-Dihydroisoxazol-3-yl)oxy)but-2-yn-1-yl)dimethylammonio)hexyl)-7-(((S)-3-hydroxy-2-phenylpropanoyl)oxy)-9-methyl-3-oxa-9-azatricyclo[3.3.1.0^{2,4}]nonan-9-ium bromide ***9-C6***

Brown, hygroscopic solid; yield 52%; IR (ATR): 3357, 2940, 2875, 1724, 1625, 1436, 1400 cm^{-1}; ^{1}H NMR (DMSO): 1.23-1.28 (m, 4H, $^{+}$N(CH$_3$)$_2$-CH$_2$-CH$_2$-C**H₂**/C**H₂**-CH$_2$-CH$_2$-$^{+}$NCH$_3$), 1.70-1.95 (m, 6H, **H**-2,4$_{eq.}$/$^{+}$N(CH$_3$)$_2$-CH$_2$-C**H₂**/C**H₂**-CH$_2$-$^{+}$NCH$_3$), 2.59-2.68 (m, 2H, **H**-2,4$_{ax.}$), 3.00-3.18 (m, 11H, $^{+}$N(C**H₃**)$_2$/$^{+}$NC**H₃**/**H**-4$_{2\text{-}isox}$), 3.36-3.40 (m, 2H, $^{+}$N(CH$_3$)$_2$-C**H₂**), 3.51-3.55 (m, 2H, C**H₂**-$^{+}$NCH$_3$), 3.67-3.81 (m, 3H, **H**-6,7/C**H₂**-OH), 3.95-4.04 (m, 2H, C**H**$_{phenyl}$/C**H₂**-OH), 4.20 (d, 1H, **H**-1,5, *J* = 2.4), 4.24 (d, 1H, **H**-1,5, *J* = 2.0), 4.33 (t, 2H, **H**-5$_{2\text{-}isox}$, *J* = 9.6), 4.51 (br, 2H, $^{+}$N-C**H₂**-C≡), 4.94 (s, 2H, ≡C-C**H₂**-O), 5.04 (t, 1H, **H**-3, *J* = 5.9), 5.12 (br, 1H, O**H**), 7.26-7.36 (m, 5H, C**H**$_{phenyl}$). ^{13}C NMR (DMSO): 21.5, 21.5, 25.0, 25.1, 28.1, 32.2, 44.3, 49.7, 53.4, 53.6, 54.0, 57.2, 62.0, 62.7, 62.8, 62.9, 67.5, 69.5, 76.1, 85.9, 127.3, 128.1,

128.4, 136.0, 166.6, 170.8. MS (ESI) m/z $[M\text{-}2Br^-]^{2+}$ Calcd for $C_{32}H_{47}N_3O_6^{2+}$: 284.7. Found: 284.8. HPLC purity 96.4%.

(1R,2R,4S,5S,7s,9S)-9-(8-((4-((4,5-Dihydroisoxazol-3-yl)oxy)but-2-yn-1-yl)dimethylammonio)octyl)-7-(((S)-3-hydroxy-2-phenylpropanoyl)oxy)-9-methyl-3-oxa-9-azatricyclo[3.3.1.0^{2,4}]nonan-9-ium bromide ***9-C8***

Brown, hygroscopic solid; yield 43%; IR (ATR): 3373, 2929, 2858, 1725, 1625, 1436, 1399 cm^{-1}; ^1H NMR (DMSO): 1.21-1.31 (m, 8H, $^+N(CH_3)_2$-CH_2-CH_2-C**H$_2$**-C**H$_2$**/C**H$_2$**-C**H$_2$**-CH_2-CH_2-$^+NCH_3$), 1.68-1.94 (m, 6H, **H**-2,4$_{eq.}$/$^+N(CH_3)_2$-CH_2-C**H$_2$**/C**H$_2$**-CH_2-$^+NCH_3$), 2.57-2.67 (m, 2H, **H**-2,4$_{ax.}$), 2.99-3.21 (m, 11H, $^+N(C$**H$_3$**$)_2$/^+NC**H$_3$**/**H**-4$_{2\text{-isox}}$), 3.36-3.41 (m, 2H, $^+N(CH_3)_2$-C**H$_2$**), 3.51-3.55 (m, 2H, C**H$_2$**-$^+NCH_3$), 3.67-3.80 (m, 3H, **H**-6,7/C**H$_2$**-OH), 3.94-4.03 (m, 2H, C**H**$_{phenyl}$/C**H$_2$**-OH), 4.22 (d, 2H, **H**-1,5, *J* = 17.4), 4.32 (d, 1H, **H**-5$_{2\text{-isox}}$, *J* = 9.6), 4.51 (br, 2H, ^+N-C**H$_2$**-C≡), 4.94 (s, 2H, ≡C-C**H$_2$**-O), 5.03 (t, 1H, **H**-3, *J* = 5.9), 5.11 (br, 1H, O**H**), 7.26-7.36 (m, 5H, C**H**$_{phenyl}$). ^{13}C NMR (DMSO): 21.6, 21.7, 25.4, 25.4, 25.4, 28.0, 28.1, 32.2, 44.4, 49.7, 53.2, 53.4, 53.6, 54.0, 57.2, 62.1, 62.7, 62.8, 62.8, 63.0, 67.7, 69.5, 76.1, 85.8, 127.3, 128.1, 128.4, 136.0, 166.6, 170.8. MS (ESI) m/z $[M\text{-}2Br^-]^{2+}$ Calcd for $C_{34}H_{51}N_3O_6^{2+}$: 298.7. Found: 298.8. HPLC purity 97.8%.

(1R,2R,4S,5S,7s,9S)-9-(10-((4-((4,5-Dihydroisoxazol-3-yl)oxy)but-2-yn-1-yl)dimethylammonio)decyl)-7-(((S)-3-hydroxy-2-phenylpropanoyl)oxy)-9-methyl-3-oxa-9-azatricyclo[3.3.1.0^{2,4}]nonan-9-ium bromide ***9-C10***

Brown, hygroscopic solid; yield 32%; IR (ATR): 3343, 2925, 2856, 1725, 1625, 1436, 1400 cm^{-1}; ^1H NMR (DMSO): 1.20-1.28 (m, 12H, $^+N(CH_3)_2$-CH_2-CH_2-C**H$_2$**-C**H$_2$**-C**H$_2$**/C**H$_2$**-C**H$_2$**-C**H$_2$**-CH_2-CH_2-$^+NCH_3$), 1.66-1.94 (m, 6H, **H**-2,4$_{eq.}$/$^+N(CH_3)_2$-CH_2-C**H$_2$**, C**H$_2$**-CH_2-$^+NCH_3$), 2.57-2.70 (m, 2H, **H**-2,4$_{ax.}$), 2.99-3.15 (m, 11H, $^+N(C$**H$_3$**$)_2$/^+NC**H$_3$**/**H**-4$_{2\text{-isox}}$), 3.35-3.39 (m, 2H, $^+N(CH_3)_2$-C**H$_2$**), 3.49-3.55 (m, 2H, C**H$_2$**-$^+NCH_3$), 3.66-3.82 (m, 3H, **H**-6,7/C**H$_2$**-OH), 3.94-4.00 (m, 2H, C**H**$_{phenyl}$/C**H$_2$**-OH), 4.18 (d, 1H, **H**-1,5, *J* = 2.3), 4.22 (d, 1H, **H**-1,5, *J* = 2.3), 4.32 (t, 2H, **H**-5$_{2\text{-isox}}$, *J* = 9.6), 4.50 (br, 2H, ^+N-C**H$_2$**-C≡), 4.94 (s, 2H, ≡C-C**H$_2$**-O), 5.03 (t, 1H, **H**-3, *J* = 5.9), 5.11 (t, 1H, O**H**, *J* = 5.0), 7.26-7.34 (m, 5H, C**H**$_{phenyl}$). ^{13}C NMR (DMSO): 21.7, 25.5, 25.6, 28.1, 28.3, 28.4, 28.6, 32.2, 44.3, 49.7, 53.2, 53.4, 53.6, 54.0, 57.1, 62.1, 62.7, 62.8, 63.0, 67.7, 69.5, 76.1, 85.8, 127.3, 128.1, 128.4, 136.0, 166.6, 170.8. MS (ESI) m/z $[M\text{-}2Br^-]^{2+}$ Calcd for $C_{36}H_{55}N_3O_6^{2+}$: 312.7. Found: 312.8. HPLC purity 93.7%. Impurity: traces of the base of iperoxo **1**.

(1R,2R,4S,5S,7s,9S)-7-(((S)-3-Hydroxy-2-phenylpropanoyl)oxy)-9-(4-((4-(isoxazol-3-yloxy)but-2-yn-1-yl)dimethylammonio)butyl)-9-methyl-3-oxa-9-azatricyclo[3.3.1.$0^{2,4}$]nonan-9-ium bromide ***11-C4***

White, hygroscopic solid; yield 55%; IR (ATR): 3329, 2932, 1723, 1578, 1481 cm^{-1}; ^{1}H NMR (DMSO): 1.67-1.97 (m, 6H, **H**-2,4$_{eq.}$/$^{+}N(CH_3)_2$-CH_2-C**H$_2$**/C**H$_2$**-CH_2-$^{+}NCH_3$), 2.59-2.69 (m, 2H, **H**-2,4$_{ax.}$), 3.06-3.11 (m, 9H, $^{+}N(CH_3)_2$/$^{+}NCH_3$), 3.35-3.41 (m, 2H, $^{+}N(CH_3)_2$-C**H$_2$**), 3.56-3.59 (m, 2H, C**H$_2$**-$^{+}NCH_3$), 3.67-3.81 (m, 3H, **H**-6,7/C**H$_2$**-OH), 3.94-4.03 (m, 2H, C**H**$_{phenyl}$/C**H$_2$**-OH), 4.19 (d, 1H, **H**-1,5, *J* = 2.0), 4.24 (d, 1H, **H**-1,5, *J* = 2.4), 4.50 (br, 2H, $^{+}$N-C**H$_2$**-C≡), 5.04 (t, 1H, **H**-3, *J* = 6.0), 5.10-5.12 (m, 3H, O**H**/≡C-C**H$_2$**-O), 6.44 (d, 1H, **H**-4$_{isox}$, *J* = 2.0), 7.27-7.35 (m, 5H, C**H**$_{phenyl}$), 8.75 (d, 1H, **H**-5$_{isox}$, *J* = 2.0). ^{13}C NMR (DMSO): 19.0, 19.1, 28.1, 44.4, 49.7, 53.4, 53.6, 53.6, 54.0, 57.4, 62.0, 62.3, 62.8, 62.9, 63.1, 66.8, 76.2, 86.1, 96.0, 127.3, 128.1, 128.4, 136.0, 162.0, 170.3, 170.8. MS (ESI) m/z $[M]^{2+}$ Calcd for $C_{30}H_{41}N_3O_6^{2+}$: 269.7. Found: 269.6. HPLC purity 95.0%.

(1R,2R,4S,5S,7s,9S)-7-(((S)-3-Hydroxy-2-phenylpropanoyl)oxy)-9-(6-((4-(isoxazol-3-yloxy)but-2-yn-1-yl)dimethylammonio)hexyl)-9-methyl-3-oxa-9-azatricyclo[3.3.1.$0^{2,4}$]nonan-9-ium bromide ***11-C6***

Brown, hygroscopic solid; yield 22%; IR (ATR): 3338, 2931, 2869, 1724, 1578, 1481 cm^{-1}; ^{1}H NMR (DMSO): 1.24-1.25 (m, 4H, $^{+}N(CH_3)_2$-CH_2-CH_2-C**H$_2$**/C**H$_2$**-CH_2-CH_2-$^{+}NCH_3$), 1.67-1.96 (m, 6H, **H**-2,4$_{eq.}$/$^{+}N(CH_3)_2$-CH_2-C**H$_2$**/C**H$_2$**-CH_2-$^{+}NCH_3$), 2.58-2.68 (m, 2H, **H**-2,4$_{ax.}$), 3.05-3.07 (m, 9H, $^{+}N(CH_3)_2$/$^{+}NCH_3$), 3.34-3.41 (m, 2H, $^{+}N(CH_3)_2$-C**H$_2$**), 3.51-3.55 (m, 2H, C**H$_2$**-$^{+}NCH_3$), 3.67-3.80 (m, 3H, **H**-6,7/C**H$_2$**-OH), 3.94-4.01 (m, 2H, C**H**$_{phenyl}$/C**H$_2$**-OH), 4.18 (d, 1H, **H**-1,5, *J* = 2.0), 4.22 (d, 1H, **H**-1,5, *J* = 2.4), 4.47 (br, 2H, $^{+}$N-C**H$_2$**-C≡), 5.03 (t, 1H, **H**-3, *J* = 5.8), 5.10 (br, 2H, ≡C-C**H$_2$**-O), 6.44 (d, 1H, **H**-4$_{isox}$, *J* = 1.6 Hz), 7.27-7.34 (m, 5H, C**H**$_{phenyl}$), 8.75 (d, 1H, **H**-5$_{isox}$, *J* = 1.6). ^{13}C NMR (DMSO): 21.5, 25.0, 25.1, 28.1, 44.3, 49.7, 53.2, 53.5, 53.6, 54.0, 57.4, 62.0, 62.7, 62.8, 62.9, 62.8, 67.5, 76.2, 86.0, 96.0, 127.3, 128.1 128.4, 136.0, 162.0, 170.3, 170.8. MS (ESI) m/z $[M]^{+}$ Calcd for $C_{32}H_{45}N_3O_6^{2+}$: 283.7. Found: 283.7. HPLC purity 97.9%.

(1R,2R,4S,5S,7s,9S)-7-(((S)-3-Hydroxy-2-phenylpropanoyl)oxy)-9-(8-((4-(isoxazol-3-yloxy)but-2-yn-1-yl)dimethylammonio)octyl)-9-methyl-3-oxa-9-azatricyclo[3.3.1.$0^{2,4}$]nonan-9-ium bromide ***11-C8***

Brown, hygroscopic solid; yield 62%; IR (ATR): 3321, 2925, 2858, 1725, 1578, 1482 cm^{-1}; ^{1}H NMR (DMSO): 1.21-1.29 (m, 8H, $^{+}N(CH_3)_2$-CH_2-CH_2-C**H$_2$**-C**H$_2$**/C**H$_2$**-C**H$_2$**-CH_2-CH_2-$^{+}NCH_3$), 1.65-1.95 (m, 6H, **H**-2,4$_{eq.}$/$^{+}N(CH_3)_2$-CH_2-C**H$_2$**/C**H$_2$**-CH_2-$^{+}NCH_3$), 2.57-2.67 (m, 2H, **H**-2,4$_{ax.}$), 3.04-3.08 (m, 9H, $^{+}N(CH_3)_2$/$^{+}NCH_3$), 3.34-3.37 (m, 2H, $^{+}N(CH_3)_2$-C**H$_2$**), 3.51-3.55 (m, 2H, C**H$_2$**-

$^{+}NCH_3$), 3.66-3.80 (m, 3H, **H**-6,7/C**H$_2$**-OH), 3.94-4.00 (m, 2H, C**H**$_{phenyl}$/C**H$_2$**-OH), 4.18 (d, 1H, **H**-1,5, *J* = 2.0), 4.22 (d, 1H, **H**-1,5, *J* = 2.1), 4.49 (br, 2H, $^{+}$N-C**H$_2$**-C≡), 5.03 (t, 1H, **H**-3, *J* = 5.9), 5.10 (br, 3H, ≡C-C**H$_2$**-O/CH_2-O**H**), 6.43 (d, 1H, **H**-4$_{isox}$, *J* = 1.8), 7.27-7.34 (m, 5H, C**H**$_{phenyl}$), 8.74 (d, 1H, **H**-5$_{isox}$, *J* = 1.8). ^{13}C NMR (DMSO): 21.6, 21.7, 25.4, 28.1, 28.1, 44.3, 49.7, 53.1, 53.4, 53.6, 54.0, 57.4, 62.0, 62.7, 62.8, 63.0, 67.7, 76.3, 85.9, 96.0, 127.3, 128.1, 128.4, 136.0, 162.0, 170.3, 170.8. MS (ESI) m/z $[M]^+$ Calcd for $C_{34}H_{49}N_3O_6^{2+}$: 297.7. Found: 297.7. HPLC purity 94.1%. Impurity: traces of the base of isoxazole **2**.

(1R,2R,4S,5S,7s,9S)-7-(((S)-3-Hydroxy-2-phenylpropanoyl)oxy)-9-(10-((4-(isoxazol-3-yloxy)but-2-yn-1-yl)dimethylammonio)decyl)-9-methyl-3-oxa-9-azatricyclo[3.3.1.0^{2,4}]nonan-9-ium bromide ***11-C10***

Beige, hygroscopic solid; yield 39%; IR (ATR): 3341, 2925, 2854, 1725, 1578, 1482 cm^{-1}; ^{1}H NMR (DMSO): 1.20-1.27 (m, 12H, $^{+}N(CH_3)_2$-CH_2-CH_2-C**H$_2$**-C**H$_2$**-C**H$_2$**/C**H$_2$**-C**H$_2$**-C**H$_2$**-CH_2-CH_2-CH_2-$^{+}NCH_3$), 1.62-1.94 (m, 6H, **H**-2,4$_{eq.}$/$^{+}N(CH_3)_2$-CH_2-C**H$_2$**/C**H$_2$**-CH_2-$^{+}NCH_3$), 2.56-2.67 (m, 2H, **H**-2,4$_{ax}$), 3.03-3.07 (m, 9H, $^{+}N(CH_3)_2$/$^{+}NCH_3$), 3.34-3.41 (m, 4H, $^{+}N(CH_3)_2$-C**H$_2$**), 3.50-3.54 (m, 2H, C**H$_2$**-$^{+}NCH_3$), 3.67-3.80 (m, 3H, **H**-6,7/C**H$_2$**-OH), 3.94-4.00 (m, 2H, C**H**$_{phenyl}$/C**H$_2$**-OH), 4.17 (d, 1H, **H**-1,5, *J* = 2.4), 4.21 (d, 1H, **H**-1,5, *J* = 2.4), 4.47 (br, 2H, $^{+}$N-C**H$_2$**-C≡), 5.03 (t, 1H, **H**-3, *J* = 6.0), 5.10 (br, 3H, ≡C-C**H$_2$**-O/CH_2-O**H**), 6.43 (d, 1H, **H**-4$_{isox}$, *J* = 2.0), 7.27-7.34 (m, 5H, C**H**$_{phenyl}$), 8.74 (d, 1H, **H**-5$_{isox}$, *J* = 2.0). ^{13}C NMR (DMSO): 21.7, 25.5, 28.1, 28.3, 28.4, 28.6, 44.3, 49.7, 53.1, 53.6, 53.6, 54.0, 57.4, 62.0, 62.7, 62.8, 63.0, 67.7, 76.3, 85.9, 95.9, 127.3, 128.1, 128.4, 136.0, 162.0, 170.3, 170.8. MS (ESI) m/z $[M]^+$ Calcd for $C_{36}H_{53}N_3O_6^{2+}$: 311.7. Found: 311.7. HPLC purity 96.0%.

3.1.4 Procedure for the Synthesis of the Scopolamine dimer (1*R*,2*R*,4*S*,5*S*,7*S*,9*S*)-7-(((*S*)-3-Hydroxy-2-phenylpropanoyl)oxy)-9-(4-((1*R*,2*R*,4*S*,5*S*,7*R*,9*R*)-7-(((*S*)-3-hydroxy-2-phenylpropanoyl)oxy)-9-methyl-3-oxa-9-azatricyclo[3.3.1.0^{2,4}]nonan-9-ium-9-yl)butyl)-9-methyl-3-oxa-9-azatricyclo[3.3.1.0^{2,4}]nonan-9-ium bromide **12**

The free base of scopolamine **4** (3.11 g, 10.3 mmol) was dissolved with heating to 60 °C in 20 mL acetonitrile and treated with 1,4-dibromobutane (1.23 mL, 10.3 mmol). The solution was stirred at room temperature for 29 d in a sealed pressure tube. A fine white precipitate was obtained. The solid was filtered, washed with acetonitrile and dried *in vacuo* to obtain **12**.

White powder; yield 27%; mp 207-209 °C; IR (ATR): 3263, 3057, 2972, 2931, 1718, 1468, 1448, 1431 cm^{-1}; ^{1}H NMR (DMSO): 1.62-1,68 (m, 4H, C**H$_2$**-CH_2-$^{+}NCH_3$), 1.76-1.83 (m, 2H, **H**-

2,4$_{eq.}$), 1.91-1.95 (m, 2H, **H**-2,4$_{eq.}$), 2.58-2.68 (m, 4H, **H**-2,4$_{ax.}$), 3.07 (s, 6H, $^{+}$NC**H$_3$**), 3.54-3.57 (m, 4H, C**H$_2$**-$^{+}$NCH$_3$), 3.67-3.71 (dd, 2H, C**H**$_{phenyl}$, *J* = 5.6, *J* = 10), 3.76-3.81 (m, 4H, C**H$_2$**-OH/**H**-6,7), 3.95-4.05 (m, 4H, C**H$_2$**-OH/**H**-6,7), 4.21 (d, 2H, **H**-1,5, *J* = 2.0), 4.26 (d, 2H, **H**-1,5, *J* = 2.0), 5.03 (t, 2H, **H**-3, *J* = 6.0), 5.11 (br, 2H, O**H**), 7.26-7.34 (m, 10H, C**H**$_{phenyl}$). ^{13}C NMR (DMSO): 19.6, 28.7, 45.0, 54.0, 54.2, 54.7, 62.6, 63.4, 63.6, 67.4, 127.9, 128.7, 129.0, 136.6, 171.4. MS(ESI): m/z [M-2Br^{-}]$^{2+}$ Calcd for $C_{38}H_{50}N_2O_8^{2+}$: 331.2. Found: 331.7. HPLC purity 95.1%.

References

[1] Fredriksson, R., Lagerström, M. C., Lundin, L. G., and Schiöth, H. B. (2003) The G-protein-coupled receptors in the human genome form five main families. Phylogenetic analysis, paralogon groups, and fingerprints, *Mol. Pharmacol. 63*, 1256-1272.

[2] Gloriam, D. E., Fredriksson, R., and Schiöth, H. B. (2007) The G protein-coupled receptor subset of the rat genome, *BMC Genomics 8*, 338.

[3] Lagerström, M. C., and Schiöth, H. B. (2008) Structural diversity of G protein-coupled receptors and significance for drug discovery, *Nat. Rev. Drug. Discov. 7*, 339-357.

[4] Haga, K., Kruse, A. C., Asada, H., Yurugi-Kobayashi, T., Shiroishi, M., Zhang, C., Weis, W. I., Okada, T., Kobilka, B. K., Haga, T., and Kobayashi, T. (2012) Structure of the human M2 muscarinic acetylcholine receptor bound to an antagonist, *Nature 482*, 547-551.

[5] Thal, D. M., Sun, B., Feng, D., Nawaratne, V., Leach, K., Felder, C. C., Bures, M. G., Evans, D. A., Weis, W. I., Bachhawat, P., Kobilka, T. S., Sexton, P. M., Kobilka, B. K., and Christopoulos, A. (2016) Crystal structures of the M1 and M4 muscarinic acetylcholine receptors, *Nature 531*, 335-340.

[6] Kruse, A. C., Ring, A. M., Manglik, A., Hu, J., Hu, K., Eitel, K., Hübner, H., Pardon, E., Valant, C., Sexton, P. M., Christopoulos, A., Felder, C. C., Gmeiner, P., Steyaert, J., Weis, W. I., Garcia, K. C., Wess, J., and Kobilka, B. K. (2013) Activation and allosteric modulation of a muscarinic acetylcholine receptor, *Nature 504*, 101-106.

[7] Kruse, A. C., Hu, J., Pan, A. C., Arlow, D. H., Rosenbaum, D. M., Rosemond, E., Green, H. F., Liu, T., Chae, P. S., Dror, R. O., Shaw, D. E., Weis, W. I., Wess, J., and Kobilka, B. K. (2012) Structure and dynamics of the M3 muscarinic acetylcholine receptor, *Nature 482*, 552-556.

[8] Schrage, R., Seemann, W. K., Kloeckner, J., Dallanoce, C., Racke, K., Kostenis, E., De Amici, M., Holzgrabe, U., and Mohr, K. (2013) Agonists with supraphysiological efficacy at the muscarinic M2 ACh receptor, *Br. J. Pharmacol. 169*, 357-370.

[9] Bremner, P., Siebers, R., Crane, J., Beasley, R., and Burgess, C. (1996) Partial vs Full β-Receptor Agonism, *Chest 109*, 957-962.

[10] Sorge, J., and Sittl, R. (2004) Transdermal buprenorphine in the treatment of chronic pain: results of a phase III, multicenter, randomized, double-blind, placebo-controlled study, *Clin. Ther. 26*, 1808-1820.

[11] Schmitz, J., van der Mey, D., Bermudez, M., Klöckner, J., Schrage, R., Kostenis, E., Tränkle, C., Wolber, G., Mohr, K., and Holzgrabe, U. (2014) Dualsteric muscarinic antagonists--orthosteric binding pose controls allosteric subtype selectivity, *J. Med. Chem. 57*, 6739-6750.

[12] Christopoulos, A. (2014) Advances in G protein-coupled receptor allostery: from function to structure, *Mol. Pharmacol. 86*, 463-478.

[13] Wootten, D., Christopoulos, A., and Sexton, P. M. (2013) Emerging paradigms in GPCR allostery: implications for drug discovery, *Nat. Rev. Drug. Discov. 12*, 630-644.

[14] Bock, A., and Mohr, K. (2013) Dualsteric GPCR targeting and functional selectivity: the paradigmatic M(2) muscarinic acetylcholine receptor, *Drug Discov. Today Technol. 10*, e245-252.

[15] Lane, J. R., Sexton, P. M., and Christopoulos, A. (2013) Bridging the gap: bitopic ligands of G-protein-coupled receptors, *Trends Pharmacol. Sci. 34*, 59-66.

[16] Valant, C., Robert Lane, J., Sexton, P. M., and Christopoulos, A. (2012) The best of both worlds? Bitopic orthosteric/allosteric ligands of g protein-coupled receptors, *Annu. Rev. Pharmacol. Toxicol. 52*, 153-178.

[17] Bock, A., Chirinda, B., Krebs, F., Messerer, R., Batz, J., Muth, M., Dallanoce, C., Klingenthal, D., Tränkle, C., Hoffmann, C., De Amici, M., Holzgrabe, U., Kostenis, E., and Mohr, K. (2014) Dynamic ligand binding dictates partial agonism at a G protein-coupled receptor, *Nat. Chem. Biol. 10*, 18-20.

[18] Kloeckner, J., Schmitz, J., and Holzgrabe, U. (2010) Convergent, short synthesis of the muscarinic superagonist iperoxo, *Tetrahedron Lett. 51*, 3470-3472.

[19] Dallanoce, C., Conti, P., De Amici, M., De Micheli, C., Barocelli, E., Chiavarini, M., Ballabeni, V., Bertoni, S., and Impicciatore, M. (1999) Synthesis and functional characterization of novel derivatives related to oxotremorine and oxotremorine-M, *Bioorg. Med. Chem. 7*, 1539-1547.

[20] Barocelli, E., Ballabeni, V., Bertoni, S., Dallanoce, C., De Amici, M., De Micheli, C., and Impicciatore, M. (2000) New analogues of oxotremorine and oxotremorine-M - Estimation of their in vitro affinity and efficacy at muscarinic receptor subtypes, *Life Sci. 67*, 717-723.

[21] Disingrini, T., Muth, M., Dallanoce, C., Barocelli, E., Bertoni, S., Kellershohn, K., Mohr, K., De Amici, M., and Holzgrabe, U. (2006) Design, synthesis, and action of oxotremorine-related hybrid-type allosteric modulators of muscarinic acetylcholine receptors, *J. Med. Chem. 49*, 366-372.

[22] Makarevich, I. F., and Gubin, Y. I. (2006) Quaternary salts of alkaloids, *Chemistry of Natural Compounds 42*, 473-476.

[23] Bock, A., Kostenis, E., Tränkle, C., Lohse, M. J., and Mohr, K. (2014) Pilot the pulse: controlling the multiplicity of receptor dynamics, *Trends Pharmacol. Sci. 35*, 630-638.

[24] Glaser, R., Peng, Q. J., and Perlin, A. S. (1988) Stereochemistry of the N-Methyl Group in Salts of Tropane Alkaloids, *J. Org. Chem. 53*, 2172-2180.

[25] Closs, G. L. (1959) The Configurational Equilibrium of the N-Methyl Group in Some Tropane Deuteriohalides1, *J. Am. Chem. Soc. 81*, 5456-5461.

[26] Fodor, G., Chastain, R. V., Frehel, D., Copper, M. J., Mandava, N., and Gooden, E. L. (1971) Stereochemistry of tropane quaternization, *J. Am. Chem. Soc. 93*, 403-413.

5. Synthesis and signaling studies of quaternary iperoxo- and acetylcholine related homodimers on the M_2 muscarinic receptor

1. Introduction

The muscarinic acetylcholine receptor (mAChR), belonging to rhodopsin-like (Family A) G protein-coupled receptors (GPCR), is subdivided in five subtypes (M_1 - M_5) and plays a key role in regulating the activity of many peripheral and central nervous system functions. These subtypes differ in their location and physiological function. The M_2 muscarinic acetylcholine receptor is widely expressed in the central nervous system and in the body periphery, but particularly in the heart and in smooth muscle tissues. Therefore, the M_2 receptor is an interesting target for the reduction of heart rate and smooth muscle contraction.[1] M_2 receptors preferentially activate the $G_{i/o}$ family of G-proteins, resulting in the inhibition of adenylate cyclase (AC), followed by the reduction of cyclic AMP (cAMP) concentration and a decrease in neurotransmitter release via the blockage of voltage-gated calcium channels.[2] Nevertheless, using high agonist concentrations, G_s-protein activation is also possible besides the $G_{i/o}$-protein activation.[3-5] The endogenous ligand acetylcholine binds to the designated “orthosteric site”. Iperoxo[6] is known as a very potent orthosteric ligand for the M_2 receptor, having higher efficacy for receptor activation than the endogenous ligand acetylcholine (Figure 1).[7] However, the high homology found in the M_1 - M_5 orthosteric binding site is challenging for the development of subtype-selective muscarinic agonists and antagonists. Besides an orthosteric binding site there is a topographically distinct less conserved allosteric binding site which is far less conserved throughout the muscarinic receptors and, thus, a promising target for developing subtype-selective allosteric modulators.[8] To combine the advantages of high receptor activation and subtype-selectivity, the concept of hybrid molecules was developed. Here, two distinct pharmacological active moieties, orthoster and alloster, are connected by different linker length, which exhibit novel and improved pharmacological properties.[9,10] These bivalent ligands can simultaneously bind to the orthosteric and the allosteric binding site of G protein-coupled muscarinic acetylcholine receptors.[11,12] Several examples of dualsteric ligands have been reported in literature such as for hybrid 1 (Figure 1), consisting of the superagonist iperoxo[6] binding to the orthosteric and a phthalimid moiety related to W84[13,14] addressing the allosteric site. This dualsteric molecule shows subtype selectivity and affinity concerning the M_2 receptor as well as biased signaling for the G_i pathway.[12,15,16]

In earlier studies, several muscarinic homobivalent ligands, carrying two identical pharmacophoric units have been investigated such as the dimers of the agonist xanomeline[17] or carbachol[18] as well as of the M_2 selective antagonist methoctramine[19]. Depending on the pharmacophoric structure and the linker these compounds showed different potencies, affinities and intrinsic activities, as the homodimerization resulted not always in increased affinity or potency. Furthermore, Bock et al. described the concept of dynamic bipharmacophoric ligands, consisting of two pharmacophores (e.g. orthoster/orthoster) linked via alkyl chains of variable lengths, to control and fine-tune partial agonism at the muscarinic M_2 receptor.[20]

The question arises, if dualsteric compounds such as hybrid 1 (Figure 1) must necessarily consist of an allosteric and an orthosteric moiety or if also the connection of two orthosteric units are sufficient for receptor activation. Gaussian accelerated molecular dynamics (GaMD) simulations of the superagonist iperoxo bound to the orthosteric binding site of the muscarinic M_2 receptor confirmed that iperoxo is able to dissociate from the orthosteric binding site and visits the ECL2/ECL3 of the allosteric binding site.[21] On this basis, it was of interest to see the effect of homodimerization of the M_2 superagonist iperoxo[7] and of the endogenous ligand acetylcholine. The idea was that these homodimers could possibly bind to the two distinct binding sites, orthosteric and allosteric, in the same receptor or to two orthosteric sites of dimeric receptors. Therefore, a set of quaternary homodimers consisting either of the agonist iperoxo or acetylcholine linked by alkyl chains of variable length were synthesized. The iperoxo related compound as well as the acetylcholine related compounds were tested for their M_2 affinity in binding studies. The iperoxo-dimer with a C_6 linker was compared to iper-6-phth (hybrid 1) in order to proof the relevance of the allosteric and antagonistic building block phthalimide in hybrid 1 for selective signaling. Furthermore, the mediated effect of the iperoxo related compounds and of the acetylcholine related compounds, including special focus on the influence of alkyl chain elongation, will be compared.

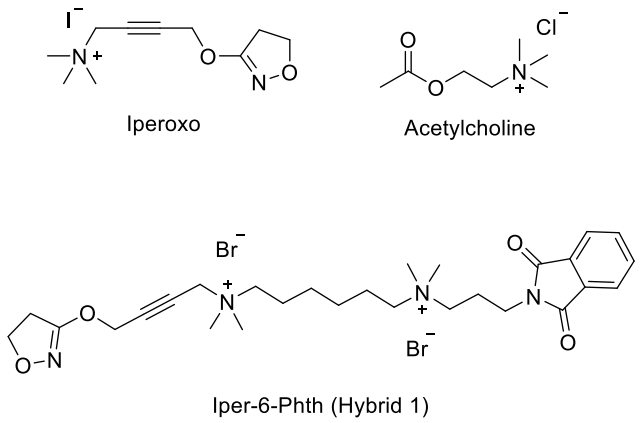

Figure 1: Structures of iperoxo, acetylcholine, and the dualsteric (orthosteric/allosteric) agonist hybrid 1.

2. Results and discussion

2.1 Chemistry

The syntheses of the quaternary iperoxo- and acetylcholine dimers (**3-C4** to **3-C10** and **5-C4** to **5-C10**) were accomplished by the reaction of iperxo-base **1**[6] and 2-dimethylaminoethyl acetate **4**, respectively, with the corresponding dibromoalkanes **2-C4** to **2-C10** (Scheme 1). The syntheses were carried out in a microwave assisted reaction by addition of a catalytic amount of KI/K_2CO_3 in refluxing acetonitrile to afford the compounds **3-C4** to **3-C10** and **5-C4** to **5-C10** in 15-96% and 53-87% yield, respectively.

Scheme 1: Synthesis of the quaternary iperoxo- and acetylcholine-dimers.

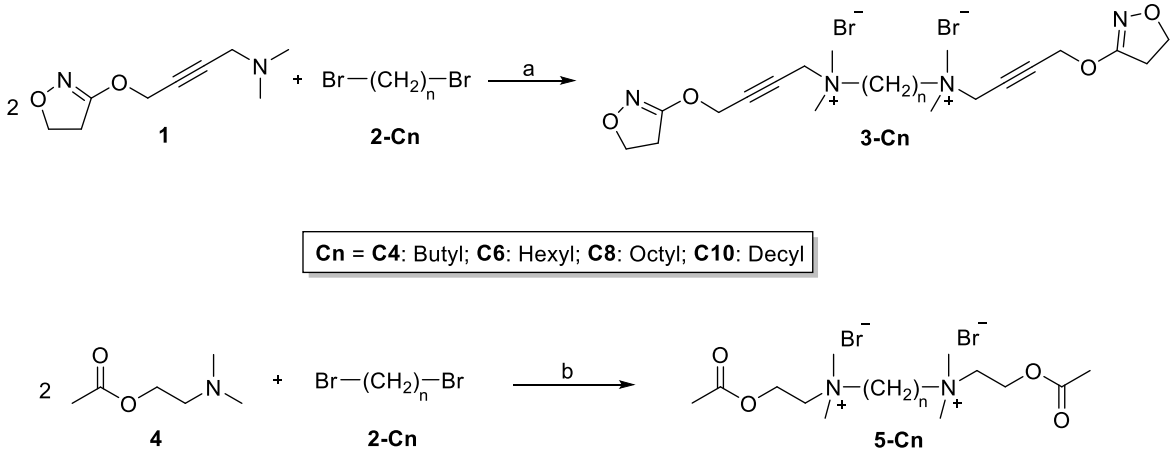

Reagents and conditions: a) KI/K_2CO_3, CH_3CN, 70 °C (microwave); b) KI/K_2CO_3, CH_3CN, 100 °C (microwave).

2.2 Pharmacology

The compounds were investigated for their ligand-receptor interactions in living chinese hamster CHO-hM_2 ovary cells and in membrane homogenates for signaling studies.[1] [^{35}S]GTPγS binding in membrane suspension of CHO-hM_2 cells, reflecting the replacement of GDP by GTP at G-protein α subunits as an effect of receptor activation by an agonist, was used. Agonists investigated on CHO-hM_2 cells preferentially activate the G_i pathway.[22] Pretreatment of CHO-hM_2 cells with PTX suppresses G_i activation, which results exclusively in the activation of the G_s pathway. The concentration of intracellular cAMP formation is measured.

2.2.1 [^{35}S]GTPγS binding measurements on the hM_2 receptor

First, the G_i activation caused by iperoxo and their derivatives iper-6-iper **3-C6** and iper-6-phth was investigated in order to prove the relevance of the allosteric moiety phthalimide in the dualsteric compound iper-6-phth for selective signaling. Iperoxo induced the maximum effect. Interestingly, both, iperoxo-dimer and -hybrid, displayed the same but lower effect of some 65%, indicating that the phthalimide moiety of iper-6-phth is not essential for G_i activation but the second part of the molecule hinders full activation (Figure 2A).

Both acetylcholine derivatives (ACh-4-ACh **5-C4** and ACh-6-ACh **5-C6**) displayed a strong loss of potency in comparison to acetylcholine (Figure 2B), depending on the length of the middle chain. In principle, the shorter the linker the weaker is the effect. Whereas ACh-8-ACh **5-C8** and ACh-10-ACh **5-C10** can be regarded as partial agonists (Figure 2C), the dimers with a C_6 and C_4 linker are inactive. The much higher potency of the iperoxo derivatives in comparison to the acetylcholine derivatives concerning the G_i pathway might be explained by the fact that iperoxo shows a 100-fold higher potency (pEC_{50} = 8.99 ± 0.04) than the endogenous agonist acetylcholine (pEC_{50} = 7.02 ± 0.03) (Table 1).

Taken together, dimerization of the agonist results in a loss of potency concerning the G_i pathway.

[1] The experiments were gratefully performed in the working group of PD Dr. Tränkle and Prof. Dr. Mohr by Anna Krüger (Pharmacology and Toxicology, Institute of Pharmacy, University of Bonn, Germany)

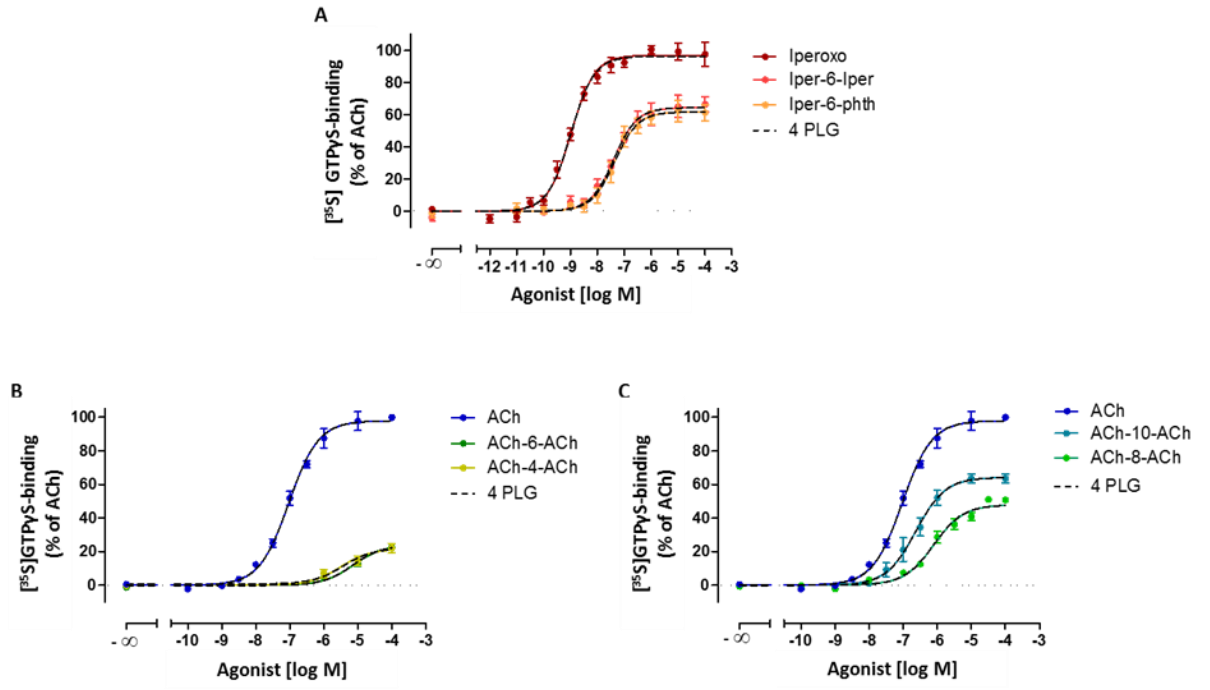

Figure 2: M_2 receptor-mediated G_i protein activation reflected by [^{35}S]GTPγS binding to membranes of CHO-hM_2 cells. (**A**) Activation through iperoxo and iperoxo derivatives. (**B**) Activation through acetylcholine and middle chain-elongated acetylcholine derivatives. (**C**) Activation through acetylcholine and long chain-elongated acetylcholine derivatives. Curves are fitted with the operational model (coloured) and with the four-parameter-logistic equation (4 PLC, black). Data are fitted according to the maximum effect of acetylcholine (100 µM).

2.2.2 cAMP-formation measurements on CHO-hM_2-cells

In cAMP measurements the concentration of intracellular cAMP formation, induced by ligand binding to the receptor followed by G-protein activation, is measured. Thus, the measurement gives information about the extent of G_s protein activation caused by ligand binding. Pretreatment of CHO-hM_2 cells with pertussis toxin (PTX) silenced G_i- and vice versa disclosed G_s coupling.

Iper-6-iper **3-C6** showed a 6.5-time higher maximum effect than iper-6-phth (Figure 3A). Whereas the dimers with C_4 and C_6 linker showed no cAMP-formation, acetylcholine-dimers with a longer middle chain mediate a larger effect (Figure 3B). ACh-8-ACh **5-C8** and ACh-10-ACh **5-C10** mediated weak partial agonism, almost similar to the one obtained for iper-6-phth (Figure 3C, Table 1).

In summary, no acetylcholine-dimer could reach the high maximum effect of the iperoxo-dimer on the G_s pathway.

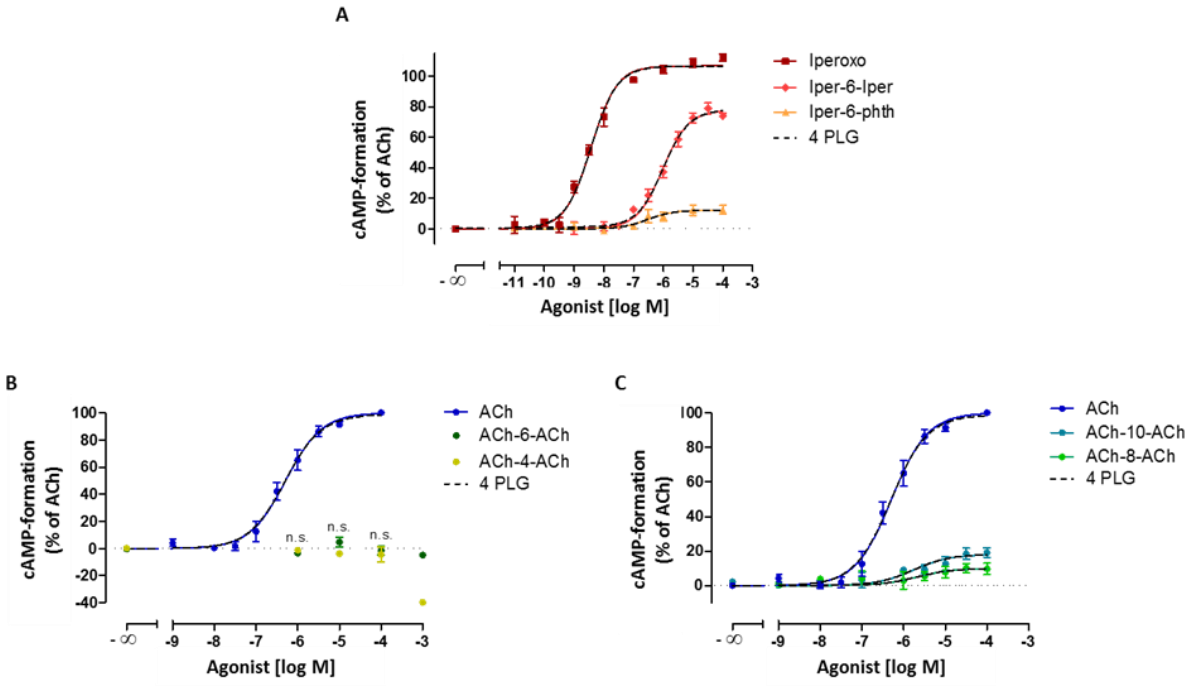

Figure 3: M_2 receptor-mediated G_s protein activation reflected by cAMP-formation in live CHO-hM_2 cells. (**A**) Activation through iperoxo and iperoxo derivatives. (**B**) Activation through acetylcholine and middle chain-elongated acetylcholine derivatives. Data are means ±s.e.m. from at least three independent experiments conducted in triplicates. For 10^{-3} M only one experiment in triplicate was conducted. n.s.: not significantly different from zero. (**C**) Activation through acetylcholine and long chain-elongated acetylcholine derivatives. Curves are fitted with the operational model (coloured) and with the four-parameter-logistic equation (4 PLC, black). Data are fitted according to the maximum effect of acetylcholine (100 µM).

2.2.3 Characterization of signaling pathway activation induced by G_i- and G_s-proteins

The investigated substances showed greater pEC_{50}-values for the G_i pathway compared to the G_s pathway, only the value for ACh-8-ACh **5-C8** was not significantly different from the value obtained out of the G_i activation (Figure 4A). The maximum effect (E_{max}) was also stronger on the G_i pathway in contrast to the G_s pathway. Exceptions are iperoxo and iper-6-iper **3-C6**, which resulted in higher maximum effects on the G_s pathway (Figure 4B).

Furthermore, the transduction coefficient $\log(\tau/K_A)$ was calculated in order to eliminate system bias and focus on ligand bias. Due to the obtained results, it could be clarified that iper-6-iper **3-C6** also has a selectivity on the G_i pathway. Among the acetylcholine derivatives, ACh-10-ACh **5-C10** was found to display the largest specificity with respect to pathway signaling (Figure 5A, 5B).

Table 1: Functional parameters of the investigated muscarinic agonists on hM_2-receptors. Potencies (pEC_{50}) and maximum effects (E_{max}) of the investigated agonists out of [^{35}S]GTPγS binding experiments (G_i activation) and cAMP experiments (G_s activation). E_{max} data are means ±s.e.m. and fitted according to the maximum effect of acetylcholine (100 µM).

Compound	G_i-activation		G_s-activation	
	pEC_{50}	% E_{max}	pEC_{50}	% E_{max}
Iperoxo	8.99 ± 0,04	97 ± 2	8.43 ± 0,04	106 ± 2
Iper-6-Iper	7.39 ± 0,08	65 ± 2	6.02 ± 0,05	78 ± 2
Iper-6-phth	7.35 ± 0,09	62 ± 3	6.51 ± 0,29	12 ± 2
Acetylcholin	7.02 ± 0,03	98 ± 2	6.30 ± 0,05	99 ± 3
ACh-10-ACh	6.62 ± 0,07	64 ± 2	5.76 ± 0,25	18 ± 2
ACh-8-ACh	6.10 ± 0,06	48 ± 2	5.67 ± 0,45	11 ± 2
ACh-6-ACh	5.13 ± 0,15	24 ± 2	-	n.s.
ACh-4-ACh	5.50 ± 0,23	22 ± 2	-	n.s.

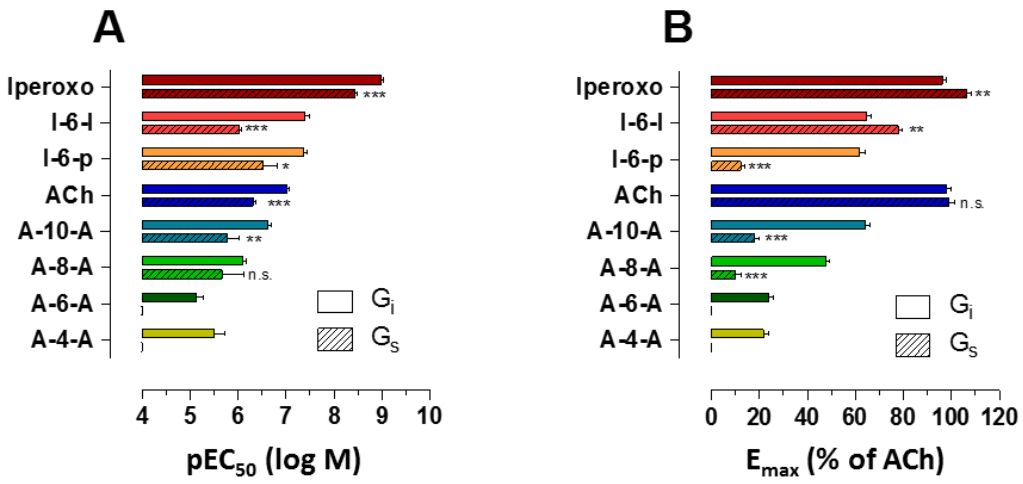

Figure 4: Potencies (**A**) and maximum effects (**B**) of the investigated muscarinic agonists on hM_2-receptors. Data are means ±s.e.m. *: P<0.05; **: P<0.01; ***: P<0.001; n.s.: not significantly different from the value obtained out of the G_i activation (t-test).

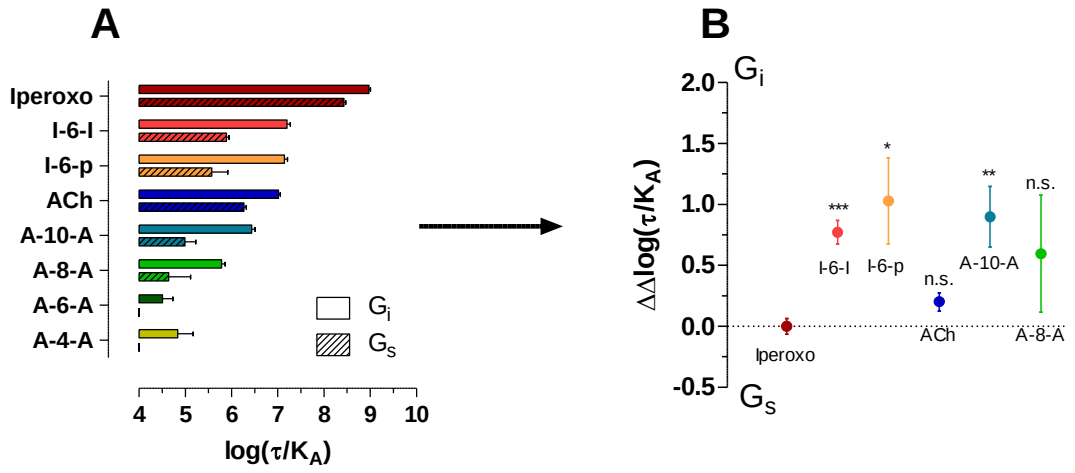

Figure 5: log(τ/K_A)-values (**A**) and ΔΔlog(τ/K_A)-values (**B**) of the investigated muscarinic agonists. Data are means ±s.e.m. *: P<0.05; **: P<0.01; ***: P<0.001; n.s.: not significantly different from the reference agonists (t-test).

Further details concerning pharmacological investigations of the compounds can be found in the appendix as well as in the master thesis of Anna Krüger (Pharmacology and Toxicology, Institute of Pharmacy, University of Bonn, Germany).

3. Discussion

The scope of this study was to examine the relevance of the allosteric moiety in the dualsteric iperoxo related hybrid 1 for G-protein activation. Iperoxo- and acetylcholine dimers were investigated on their ability for G_i and G_s pathway activation in comparison to the homomers and to the iperoxo-related hybrid 1. It is well known that the dualsteric compound iper-6-phth (hybrid 1), consisting of the superagonist iperoxo[6] binding to the orthosteric and a phthalimid moiety related to W84[13,14] addressing the allosteric site, induces an agonistic effect on the muscarinic M_2 receptor.[12] The relevance of the allosteric moiety phthalimide in the dualsteric compound iper-6-phth for selective signaling was of interest. Therefore, the two iperoxo derivatives iper-6-iper **3-C6** and iper-6-phth were investigated and were found to activate the G_i pathway in a similar manner, whereas only a weak G_s activation was caused by both compounds which was expected. Both compounds displayed specificity according to signaling pathway. This effect was higher for iper-6-phth, because iper-6-iper **3-C6** is also a strong partial agonist on the G_s pathway. It is known that the specificity according to signaling pathway for iper-6-phth is caused by dualsteric binding.[15] Here, the strong agonistic effect of iperoxo results in G_i protein activation and reduction of G_s protein activation. Furthermore, binding of the phthalimide moiety in the allosteric vestibule results in restricted movement of

the receptor.[15] Consequently, a specific conformation of the receptor is stabilized, which favours G_i activation.[15]

Another aspect is the correlation between the size of the substituents and their selectivity: the larger the substituent, the stronger the selectivity.[23] The second iperoxo moiety is smaller than the phthalimide moiety, resulting in weaker selectivity for iper-6-iper **3-C6**. The smaller iperoxo moiety is not sufficient for the reduction of the maximum effect on the G_s pathway. However, due to the strong decrease of potency, iper-6-iper **3-C6** also results in selectivity. Furthermore, in contrast to the heterobivalent ligand iper-6-phth, iper-6-iper **3-C6** consists of two identical pharmacophoric moieties. Therefore, the orientation of the homobivalent ligand in the receptor is the same, because one iperoxo moiety out of two is always located next to the orthosteric binding pocket. The insertion of a second iperoxo moiety resulted not in higher potency values on the G_i pathway for iper-6-iper **3-C6** in comparison to iper-6-phth. Consequently, the inhibition effect for the activation of the orthosteric binding pocket is not stronger influenced by the phthalimide moiety than by the iperoxo moiety. Notable in both compounds the second part of the molecule might be crucial for hindrance of full receptor activation resulting in partial agonism for iper-6-iper **3-C6** and iper-6-phth.

Next, iper-6-iper **3-C6** and ACh-6-ACh **5-C6** were investigated in order to prove the relevance of iperoxo in the dualsteric compounds. The values found for ACh-6-ACh **5-C6** are lower in comparison to iper-6-iper **3-C6** and iper-6-phth, respectively. So, the activation of G_i proteins was weak for ACh-6-ACh **5-C6** and G_s proteins could not be activated at all (Figure 2B, Figure 3B). A possible reason for these results is the fact that iperoxo, known as superagonist at the M_2 muscarinic receptor, is found to be 100 times more potent than the endogenous ligand acetylcholine.[7] Therefore, the potency mediated by the iperoxo moiety in the compound iper-6-iper **3-C6** is sufficient for the generation of strong partial agonism on both signaling pathways. However, the acetylcholine consisting compound ACh-6-ACh **5-C6** could only mediate weak partial agonism on the G_i pathway.

Another aspect is, that the binding of ACh-6-ACh **5-C6** cannot be only bitopic but also purely allosteric. In earlier studies computational simulations confirmed the binding and dissociation of the orthosteric GPCR ligand tiotropium to an experimentally validated allosteric site of the M_3 muscarinic receptor.[24] On this basis, during the binding process of ACh-6-ACh **5-C6** into the deep lying orthosteric binding site of the M_2 receptor, a purely allosteric interaction of ACh-6-ACh **5-C6** could also be possible because for bitopic binding the ligand has to overcome the energy barrier between the extracellular vestibule and the orthosteric binding pocket.[24]

The extent of G-protein activation depends on the dimension of agonist-induced conformational transitions of the inner loop region. Earlier studies showed, that dualsteric compounds having a C_6 alkyl linker chain length restricted inner loop region dynamics. However, longer middle chain elongation shifted the second moiety further outward into the allosteric region. Consequently, a orthosteric agonist like intracellular loop rearrangement was possible resulting in greater G-protein activation.[15] In order to clarify the effect of the extension of the alkyl chain of the herein synthesized compounds, ACh-8-ACh **5-C8** and ACh-10-ACh **5-C10** were studied. On the G_i pathway a correlation between the alkyl chain length and the obtained effect could be found: the longer the alkyl chain, the greater the potency and maximum effect. The higher flexibility of the long alkyl chain compounds resulted in greater effects because the receptor is less restricted in its mobility.[15] However, the activation of the G_s signaling pathway by longer chain acetylcholine derivatives remained still weak. This results in a significant selectivity for the G_i pathway concerning ACh-10-ACh **5-C10**.

Matucci et al.[18] reported about homodimerization of two carbachol units resulting in derivatives which lost agonistic activity in comparison to carbachol alone. Kinetic binding studies revealed that compounds having a long-elongated methylene linker are able to slow the rate of dissociation of NMS, suggesting a bitopic behavior. These findings were also underlined by docking simulations.[18] Besides simultaneous orthosteric/allosteric binding within one receptor, the C10 alkyl chain elongated homodimers could possibly, due to their long and flexible linker length, bridge dimeric receptors by binding into the two respective orthosteric sites. For clarification if the iperoxo- as well as the acetylcholine dimers are able to bind also dualsteric to the receptor or even to two orthosteric sites in a dimeric receptor further radio ligand binding studies and molecular docking simulations are necessary.

Kruse et al. described the orthosteric agonist iperoxo bound to the active state of the M_2 muscarinic acetylcholine receptor, resulting in an outward movement at the intracellular site of TM6. Simultaneously, an inward movement in the orthosteric site was observable leading to cation-π-interactions between Tyr $104^{3.33}$, Tyr $403^{6.51}$ and Tyr $426^{7.39}$. The so induced closure of the aromatic lid over the agonist, separating the orthosteric from the allosteric site, resulted in full receptor activation. This tyrosine lid formation seems to be essential for agonist binding and activation in muscarinic receptors.[25] It is conceivable, that the additional second moiety in the investigated dimers, which is oriented to the allosteric site, hinders the closure of the tyrosine lid which results in restricted receptor movement and therefore less receptor activation. Earlier studies showed that even the elongation of iperoxo by a hexamethylen chain is sufficient for reduced efficiency on the G_i as well as on the G_s

pathway in comparison to iperoxo alone.[15] On the basis of the herein synthesized dimers it has been demonstrated that partial agonism can be rationally designed.

4. Methods

4.1 Chemistry

Chemicals were of analytical grade and purchased from Aldrich (Steinheim, Germany) and Merck (Darmstadt, Germany). Microwave provided reactions were accomplished on a MLS-rotaPREP instrument (Milestone, Leutkirch, Germany). Melting points were determined on a Stuart melting point apparatus SMP3 (Bibby Scientific, UK) and are uncorrected. IR analysis was carried out on a Jasco FT-IR-6100 spectrometer (Gross-Umstadt, Germany) equipped with a diamond-ATR-unit. Wavelengths are labeled as $\tilde{\nu}$. ^{1}H (400.132 MHz) and ^{13}C (100.613 MHz) NMR spectra were recorded on a Bruker AV 400 instrument (Bruker Biospin, Ettlingen, Germany). As internal standard, the signals of the deuterated solvent was used (DMSO-d_6: ^{1}H 2.50 ppm, ^{13}C 39.52 ppm). Abbreviation for data quoted are: s, singlet; d, doublet; t, triplet; q, quartet; m, multiplet; b, broad; dd, doublet of doublets; dt, doublet of triplets; tt, triplet of triplets; tq, triplet of quartets. Coupling constants (*J*) are given in Hz. ESI mass spectra of the novel compounds were measured on an Agilent LC/MSD Trap G2445D instrument (Waldbronn, Germany). Data are reported as mass-to-charge ratio (*m/z*) of the corresponding positively charged molecular ions. The purities of the final new compounds were determined using qNMR and were found to be ≥90% (**3-C8** and **3-C10**) and ≥95% (for all other new compounds). 1,2,4,5-Tetrachloro-3-nitrobenzene (Sigma Aldrich, Steinheim, Germany) was chosen as internal standard. qNMR data were acquired at 90° pulse tip angles with recovery delays of 60 s and acquisition time of 3.7 s in a non-spinning mode at a calibrated probe temperature of 300 K. Sixteen scans of 64 K data points for FID were acquired with a spectral width of 8012 Hz (16 ppm). Manuel phase and baseline correction were performed prior to integration. Preliminary data processing was carried out with Bruker software, TOPSPIN 3.0.

4.1.1 General procedure for the synthesis of the homobivalente quaternary iperoxo dimers **3-C4**, **3-C6**, **3-C8**, and **3-C10**

To a solution of 2 equiv of iperoxo base[6] in 10 mL acetonitrile, 1 equiv of the corresponding bromoalkane **2-C4**, **2-C6**, **2-C8**, and **2-C10** and a catalytic amount of KI/K_2CO_3 (1:1) were added. The reaction mixture was heated in the microwave (500 W, 70 °C) for 2-3 h. After cooling to room temperature the surplus of KI/K_2CO_3 was filtered off and the solvent was

evaporated to half of the volume. The solution was kept in the fridge overnight. The precipitate obtained was filtered, washed with Et_2O and dried *in vacuo*.

N^1,N^4-Bis(4-((4,5-dihydroisoxazol-3-yl)oxy)but-2-yn-1-yl)-N^1,N^1,N^4,N^4-tetramethylbutane-1,4-diaminium bromide ***3-C4***

Light, yellow solid; yield 69%; mp 184.8-186.5 °C; IR (ATR): 3003, 2911, 2853, 1626, 1480, 1437, 1399, 1335, 1251 cm^{-1}; ^1H NMR (DMSO): 2.73-2.77 (m, 4H, ^+N-CH_2-C**H_2**), 3.03 (t, 4H, **H**-$4_{2\text{-isox}}$, *J* = 9.6), 3.12 (s, 12H, $^+N(CH_3)_2$), 3.44-3.48 (m, 4H, ^+N-C**H_2**), 4.33 (t, 4H, **H**-$5_{2\text{-isox}}$, *J* = 9.6), 4.53 (s, 4H, ≡C-C**H_2**-N^+), 4.95 (s, 4H, O-C**H_2**-C≡). ^{13}C NMR (DMSO): 19.1, 32.2, 49.7, 53.6, 57.2, 62.2, 69.6, 76.0, 86.1, 166.7. MS (ESI) m/z $[M]^{2+}$ Calcd for $C_{22}H_{36}N_4O_4^{2+}$: 210.1 Found: 210.1. qNMR purity 95.9%.

N^1,N^6-Bis(4-((4,5-dihydroisoxazol-3-yl)oxy)but-2-yn-1-yl)-N^1,N^1,N^6,N^6-tetramethylhexane-1,6-diaminium bromide ***3-C6***

Light, yellow solid; yield 49%; mp 156.4-159.3 °C; IR (ATR): 3004, 2952, 2928, 2871, 1625, 1484, 1442, 1422, 1400, 1343, 1333, 1279, 1248 cm^{-1}; ^1H NMR (DMSO): 1.32-1.37 (m, 4H, ^+N-CH_2-CH_2-C**H_2**), 1.69-1.78 (m, 4H, ^+N-CH_2-C**H_2**), 3.03 (t, 4H, **H**-$4_{2\text{-isox}}$, *J* = 9.6), 3.11 (s, 12H, $^+N(CH_3)_2$), 3.36-3.40 (m, 4H, ^+N-C**H_2**), 4.33 (t, 4H, **H**-$5_{2\text{-isox}}$, *J* = 9.6), 4,50 (s, 4H, ≡C-C**H_2**-N^+), 4.94 (s, 4H, O-C**H_2**-C≡). ^{13}C NMR (DMSO): 21.6, 25.1, 32.2, 49.7, 53.3, 57.1, 62.9, 69.5, 76.1, 85.9, 166.6. MS (ESI) m/z $[M]^{2+}$ Calcd for $C_{24}H_{40}N_4O_4^{2+}$: 224.2 Found: 224.1. qNMR purity 95.9%.

N^1,N^8-Bis(4-((4,5-dihydroisoxazol-3-yl)oxy)but-2-yn-1-yl)-N^1,N^1,N^8,N^8-tetramethyloctane-1,8-diaminium bromide ***3-C8***

Light, yellow solid; yield 15%; mp 169.8-174.2 °C; IR (ATR): 3000, 2954, 2925, 2863, 1632, 1488, 1468, 1396, 1344, 1269, 1244 cm^{-1}; ^1H NMR (DMSO): 1.29-1.32 (m, 8H, ^+N-CH_2-CH_2-C**H_2**-C**H_2**), 1.64-1.72 (m, 4H, ^+N-CH_2-C**H_2**), 3.02 (t, 4H, **H**-$4_{2\text{-isox}}$, *J* = 9.6), 3.10 (s, 12H, $^+N(CH_3)_2$), 3.39-3.41 (m, 4H, ^+N-C**H_2**), 4.32 (t, 4H, **H**-$5_{2\text{-isox}}$, *J* = 9.6), 4,51 (s, 4H, ≡C-C**H_2**-N^+), 4.93 (s, 4H, O-C**H_2**-C≡).^{13}C NMR (DMSO): 21.7, 25.5, 28.1, 32.2, 49.7, 53.2, 57.2, 63.0, 69.5, 76.1, 85.9, 166.7. MS (ESI) m/z $[M]^{2+}$ Calcd for $C_{26}H_{44}N_4O_4^{2+}$: 238.2 Found: 238.1. qNMR purity 90.5%.

N^1,N^{10}-Bis(4-((4,5-dihydroisoxazol-3-yl)oxy)but-2-yn-1-yl)-N^1,N^1,N^{10},N^{10}-tetramethyldecane-1,10-diaminium bromide ***3-C10***

Light, yellow solid; yield 36%; mp 160.7-165.5 °C; IR (ATR): 3001, 2912, 2853, 1627, 1480, 1467, 1435, 1404, 1336, 1252 cm^{-1}; ^{1}H NMR (DMSO): 1.30 (s, 12H, $^+$N-CH_2-CH_2-C**H_2**-C**H_2**-C**H_2**), 1.62-1.72 (m, 4H, $^+$N-CH_2-C**H_2**), 3.02 (t, 4H, **H**-$4_{2\text{-isox}}$, *J* = 9.2), 3.09 (s, 12H, $^+$N(C**H_3**)$_2$), 3.36-3.38 (m, 4H, $^+$N-C**H_2**), 4.32 (t, 4H, **H**-$5_{2\text{-isox}}$, *J* = 9.2), 4,51 (s, 4H, ≡C-C**H_2**-N^+), 4.93 (s, 4H, O-C**H_2**-C≡). ^{13}C NMR (DMSO): 21.7, 25.6, 28.3, 28.6, 32.2, 49.7, 53.2, 57.1, 63.0, 69.5, 76.1, 85.8, 166.6. MS (ESI) m/z $[M]^{2+}$ Calcd for $C_{28}H_{48}N_4O_4^{2+}$: 252.2 Found: 252.2. qNMR purity 91.8%.

4.1.2 General procedure for the synthesis of the homobivalente quaternary acetylcholine dimers **5-C4**, **5-C6**, **5-C8**, and **5-C10**

2 equiv of 2-dimethylaminoethyl acetate **4** and 1 equiv of the corresponding bromoalkane **2-C4**, **2-C6**, **2-C8**, and **2-C10** were dissolved in 10 mL acetonitrile. A catalytic amount of KI/K_2CO_3 (1:1) was added and the reaction mixture was heated in the microwave (400 W, 100 °C) for 4 h. After cooling to room temperature the surplus of KI/K_2CO_3 was filtered off and the solvent was evaporated to half of the volume. The solution was kept in the fridge overnight. The precipitate obtained was filtered, washed with acetonitrile and dried *in vacuo*.

N^1,N^4-Bis(2-acetoxyethyl)-N^1,N^1,N^4,N^4-tetramethylbutane-1,4-diaminium bromide ***5-C4***

White solid; yield 83%; mp 215.6-218.1 °C; IR (ATR): 3008, 2991, 2960, 1739, 1494, 1474, 1455, 1442, 1349, 1217, 1049, 1039 cm^{-1}; ^{1}H NMR (DMSO): 1.39-1.57 (m, 4H, $^+$N(CH_3)$_2$-CH_2-C**H_2**), 2.08 (s, 6H, C**H_3**), 3.11 (s, 12H, $^+$N(C**H_3**)$_2$), 3.42-3.45 (m, 4H, $^+$N(CH_3)$_2$-C**H_2**), 3.66-3.68 (m, 4H, O-CH_2-C**H_2**), 4.43-4.45 (m, 4H, O-C**H_2**). ^{13}C NMR (DMSO): 19.0, 20.7, 50.6, 57.4, 61.5, 62.9. MS (ESI) m/z $[M]^{2+}$ Calcd for $C_{16}H_{34}N_2O_4^{2+}$: 159.1 Found: 159.1. qNMR purity 95.9%.

N^1,N^6-Bis(2-acetoxyethyl)-N^1,N^1,N^6,N^6-tetramethylhexane-1,6-diaminium bromide ***5-C6***

White solid; yield 86%; mp 121.7-124.9 °C; IR (ATR): 3004, 2948, 2924, 2865, 1738, 1481, 1427, 1375, 1359, 1230, 1039 cm^{-1}; ^{1}H NMR (DMSO): 1.32-1.38 (m, 4H, $^+$N(CH_3)$_2$-CH_2-CH_2-C**H_2**), 1.68-1.76 (m, 4H, $^+$N(CH_3)$_2$-CH_2-C**H_2**), 2.06 (s, 6H, C**H_3**), 3.12 (s, 12H, $^+$N(C**H_3**)$_2$), 3.38-3.42 (m, 4H, $^+$N(CH_3)$_2$-C**H_2**), 3.67-3.69 (m, 4H, O-CH_2-C**H_2**), 4.41-4.44 (m, 4H, O-C**H_2**). ^{13}C

NMR (DMSO): 20.6, 21.5, 25.1, 50.5, 57.4, 61.3, 63.6, 169.8. MS (ESI) m/z $[M]^{2+}$ Calcd for $C_{18}H_{38}N_2O_4^{2+}$: 173.1 Found: 173.1. qNMR purity 96.8%.

N^1,N^8-Bis(2-acetoxyethyl)-N^1,N^1,N^8,N^8-tetramethyloctane-1,8-diaminium bromide ***5-C8***

White solid; yield 87%; mp 175.6-177.8 °C; IR (ATR): 3053, 3005, 2985, 2947, 2924, 2865, 1740, 1497, 1476, 1455, 1421, 1409, 1372, 1227, 1038 cm^{-1}; ^1H NMR (DMSO): 1.27-1.34 (m, 8H, $^+N(CH_3)_2$-CH_2-CH_2-C**H_2**-C**H_2**), 1.64-1.72 (m, 4H, $^+N(CH_3)_2$-CH_2-C**H_2**), 2.06 (s, 6H, C**H_3**), 3.09 (s, 12H, ^+N(C**H_3**$)_2$), 3.36-3.39 (m, 4H, $^+N(CH_3)_2$-C**H_2**), 3.64-3.67 (m, 4H, O-CH_2-C**H_2**), 4.41-4.43 (m, 4H, O-C**H_2**). ^{13}C NMR (DMSO): 20.6, 21.7, 25.6, 28.2, 50.5, 57.4, 61.2, 63.8, 169.8. MS (ESI) m/z $[M]^{2+}$ Calcd for $C_{20}H_{42}N_2O_4^{2+}$: 187.2 Found: 187.2. qNMR purity 95.6%.

N^1,N^{10}-Bis(2-acetoxyethyl)-N^1,N^1,N^{10},N^{10}-tetramethyldecane-1,10-diaminium bromide ***5-C10***

White solid; yield 53%; mp 107.1-116.3 °C; IR (ATR): 3004, 2980, 2944, 2923, 2858, 1741, 1496, 1479, 1426, 1409, 1371, 1358, 1223, 1041 cm^{-1}; ^1H NMR (DMSO): 1.22-1.36 (m, 12H, $^+N(CH_3)_2$-CH_2-CH_2-C**H_2**-C**H_2**-C**H_2**), 1.61-1.71 (m, 4H, $^+N(CH_3)_2$-CH_2-C**H_2**), 2.05 (s, 6H, C**H_3**), 3.08 (s, 12H, ^+N(C**H_3**$)_2$), 1.35-1.38 (m, 4H, $^+N(CH_3)_2$-C**H_2**), 3.63-3.66 (m, 4H, O-CH_2-C**H_2**), 4.40-4.43 (m, 4H, O-C**H_2**). ^{13}C NMR (DMSO): 20.6, 21.7, 25.7, 28.4, 28.7, 50.5, 57.4, 61.2, 63.8, 169.8. MS (ESI) m/z $[M]^{2+}$ Calcd for $C_{22}H_{46}N_2O_4^{2+}$: 201.2 Found: 201.2. qNMR purity 95.9%.

References

[1] Wess, J. (2004) Muscarinic acetylcholine receptor knockout mice: novel phenotypes and clinical implications, *Annu. Rev. Pharmacol. Toxicol. 44*, 423-450.

[2] Davie, B. J., Christopoulos, A., and Scammells, P. J. (2013) Development of M1 mAChR allosteric and bitopic ligands: prospective therapeutics for the treatment of cognitive deficits, *ACS Chem. Neurosci. 4*, 1026-1048.

[3] Griffin, M. T., Figueroa, K. W., Liller, S., and Ehlert, F. J. (2007) Estimation of agonist activity at G protein-coupled receptors: analysis of M2 muscarinic receptor signaling through Gi/o,Gs, and G15, *J. Pharmacol. Exp. Ther. 321*, 1193-1207.

[4] Michal, P., El-Fakahany, E. E., and Dolezal, V. (2007) Muscarinic M2 receptors directly activate Gq/11 and Gs G-proteins, *J. Pharmacol. Exp. Ther. 320*, 607-614.

[5] Kenakin, T. (2013) New concepts in pharmacological efficacy at 7TM receptors: IUPHAR review 2, *Br. J. Pharmacol. 168*, 554-575.

[6] Kloeckner, J., Schmitz, J., and Holzgrabe, U. (2010) Convergent, short synthesis of the muscarinic superagonist iperoxo, *Tetrahedron Lett. 51*, 3470-3472.

[7] Schrage, R., Seemann, W. K., Kloeckner, J., Dallanoce, C., Racke, K., Kostenis, E., De Amici, M., Holzgrabe, U., and Mohr, K. (2013) Agonists with supraphysiological efficacy at the muscarinic M2 ACh receptor, *Br. J. Pharmacol. 169*, 357-370.

[8] Kruse, A. C., Kobilka, B. K., Gautam, D., Sexton, P. M., Christopoulos, A., and Wess, J. (2014) Muscarinic acetylcholine receptors: novel opportunities for drug development, *Nat. Rev. Drug. Discov. 13*, 549-560.

[9] Mohr, K., Schmitz, J., Schrage, R., Tränkle, C., and Holzgrabe, U. (2013) Molecular alliance-from orthosteric and allosteric ligands to dualsteric/bitopic agonists at G protein coupled receptors, *Angew. Chem. Int. Ed. Engl. 52*, 508-516.

[10] Valant, C., Robert Lane, J., Sexton, P. M., and Christopoulos, A. (2012) The best of both worlds? Bitopic orthosteric/allosteric ligands of g protein-coupled receptors, *Annu. Rev. Pharmacol. Toxicol. 52*, 153-178.

[11] Disingrini, T., Muth, M., Dallanoce, C., Barocelli, E., Bertoni, S., Kellershohn, K., Mohr, K., De Amici, M., and Holzgrabe, U. (2006) Design, synthesis, and action of oxotremorine-related hybrid-type allosteric modulators of muscarinic acetylcholine receptors, *J. Med. Chem. 49*, 366-372.

[12] Antony, J., Kellershohn, K., Mohr-Andra, M., Kebig, A., Prilla, S., Muth, M., Heller, E., Disingrini, T., Dallanoce, C., Bertoni, S., Schrobang, J., Tränkle, C., Kostenis, E., Christopoulos, A., Holtje, H. D., Barocelli, E., De Amici, M., Holzgrabe, U., and Mohr, K. (2009) Dualsteric GPCR targeting: a novel route to binding and signaling pathway selectivity, *FASEB J. 23*, 442-450.

[13] Mohr, K., Tränkle, C., and Holzgrabe, U. (2003) Structure/Activity Relationships of M 2 Muscarinic Allosteric Modulators, *Receptors Channels 9*, 229-240.

[14] Mohr, M., Heller, E., Ataie, A., Mohr, K., and Holzgrabe, U. (2004) Development of a new type of allosteric modulator of muscarinic receptors: hybrids of the antagonist AF-DX 384 and the hexamethonio derivative W84, *J. Med. Chem. 47*, 3324-3327.

[15] Bock, A., Merten, N., Schrage, R., Dallanoce, C., Batz, J., Kloeckner, J., Schmitz, J., Matera, C., Simon, K., Kebig, A., Peters, L., Müller, A., Schrobang-Ley, J., Tränkle, C., Hoffmann, C., De Amici, M., Holzgrabe, U., Kostenis, E., and Mohr, K. (2012) The allosteric vestibule of a seven transmembrane helical receptor controls G-protein coupling, *Nat. Commun. 3*, 1044.

[16] Bock, A., Chirinda, B., Krebs, F., Messerer, R., Batz, J., Muth, M., Dallanoce, C., Klingenthal, D., Tränkle, C., Hoffmann, C., De Amici, M., Holzgrabe, U., Kostenis, E., and Mohr, K. (2014) Dynamic ligand binding dictates partial agonism at a G protein-coupled receptor, *Nat. Chem. Biol. 10*, 18-20.

[17] Rajeswaran, W. G., Cao, Y., Huang, X. P., Wroblewski, M. E., Colclough, T., Lee, S., Liu, F. H., Nagy, P. I., Ellis, J., Levine, B. A., Nocka, K. H., and Messer, W. S. (2001) Design, synthesis, and biological characterization of bivalent 1-methyl-1,2,5,6-tetrahydropyridyl-1,2,5-thiadiazole derivatives as selective muscarinic agonists, *J. Med. Chem. 44*, 4563-4576.

[18] Matucci, R., Nesi, M., Martino, M. V., Bellucci, C., Manetti, D., Ciuti, E., Mazzolari, A., Dei, S., Guandalini, L., Teodori, E., Vistoli, G., and Romanelli, M. N. (2016) Carbachol dimers as homobivalent modulators of muscarinic receptors, *Biochem. Pharmacol. 108*, 90-101.

[19] Melchiorre, C., Cassinelli, A., and Quaglia, W. (1987) Differential blockade of muscarinic receptor subtypes by polymethylene tetraamines. Novel class of selective antagonists of cardiac M-2 muscarinic receptors, *J. Med. Chem. 30*, 201-204.

[20] Bock, A., Kostenis, E., Tränkle, C., Lohse, M. J., and Mohr, K. (2014) Pilot the pulse: controlling the multiplicity of receptor dynamics, *Trends Pharmacol. Sci. 35*, 630-638.

[21] Miao, Y., and McCammon, J. A. (2016) Graded activation and free energy landscapes of a muscarinic G-protein–coupled receptor, *PNAS Early Edition*, 1-6.

[22] Milligan, G. (2003) Principles: Extending the utility of [35S]GTPγS binding assays, *Trends Pharmacol. Sci. 24*, 87-90.

[23] Bock, A., and Mohr, K. (2013) Dualsteric GPCR targeting and functional selectivity: the paradigmatic M(2) muscarinic acetylcholine receptor, *Drug Discov. Today Technol. 10*, e245-252.

[24] Kruse, A. C., Hu, J., Pan, A. C., Arlow, D. H., Rosenbaum, D. M., Rosemond, E., Green, H. F., Liu, T., Chae, P. S., Dror, R. O., Shaw, D. E., Weis, W. I., Wess, J., and Kobilka, B. K. (2012) Structure and dynamics of the M3 muscarinic acetylcholine receptor, *Nature 482*, 552-556.

[25] Kruse, A. C., Ring, A. M., Manglik, A., Hu, J. X., Hu, K., Eitel, K., Hübner, H., Pardon, E., Valant, C., Sexton, P. M., Christopoulos, A., Felder, C. C., Gmeiner, P., Steyaert, J., Weis, W. I., Garcia, K. C., Wess, J., and Kobilka, B. K. (2013) Activation and allosteric modulation of a muscarinic acetylcholine receptor, *Nature 504*, 101-106.

6. Synthesis of tertiary iperoxo- and acetylcholine related homodimers as tools for the design of bias agonism

Beside the synthesis of the quaternary iperoxo- and acetylcholine related homodimers (see chapter 5) also tertiary homodimeric analogs with varying alkyl chain length were synthesized. These tertiary homodimers should act as tools for the design of bias agonism. Additionally, such tertiary ligands could be interesting drugable compounds due to their ability of passing the blood-brain-barrier.

1. Synthesis of tertiary iperoxo related homodimers

For the synthesis of tertiary iperoxo dimers, 4-((4,5-dihydroisoxazol-3-yl)oxy)-*N*,*N*-dimethylbut-2-yn-1-amine (base of iperoxo) was tried to react either with methylamine hydrochloride in methanol or in methanol by the addition of $AlMe_3$, which should activate the amine by complex formation *in situ*. However, the base of iperoxo proved to be unreactive (Scheme 1).

Scheme 1: Synthetic approaches for the synthesis of tertiary iperoxo-dimers.

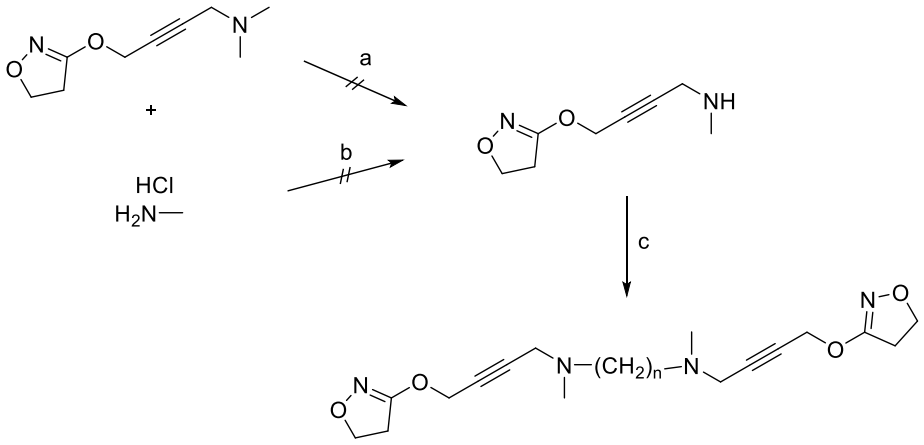

Reagents and conditions: a) MeOH, 5 h, reflux; b) $AlMe_3$, MeOH, 30 min 0 °C, 5 h reflux; c) KI/K_2CO_3, CH_3CN, rt.

In another synthetic approach modified halogenated iperoxo **4** was achieved via the reaction of 3-nitro-4,5-dihydroisoxazole[1,2] **2** with 2-butyne-1,4-diol **1** and sodium hydride in THF, according to the procedure previously described.[3,4] Further reaction with thionyl chloride in pyridine and benzene/dichloromethane led to the halogenated compound **4** in 78% yield.

Finally, the tertiary iperoxo dimers **6-C4** to **6-C8** were achieved by means of 2 equiv **4** with the corresponding *N*,*N*-dimethylalkane-diamines **5-C4** to **5-C8** in the presence of catalytic amounts of KI/K_2CO_3 in acetonitrile (Scheme 2). The tertiary iperoxo dimers **6-C4** to **6-C8** were obtained in 21-52% yield. **6-C6** and **6-C8** were then converted into the corresponding oxalate, or pretreated with hydrochloric acid yielding the ammonium salts **6-C6 oxalate** and **6-C8 hydrochlorate**.

Scheme 2: Synthesis of tertiary iperoxo-dimers **6-C4** to **6-C8** and of the corresponding salts **6-C6 oxalate** and **6-C8 hydrochlorate**.

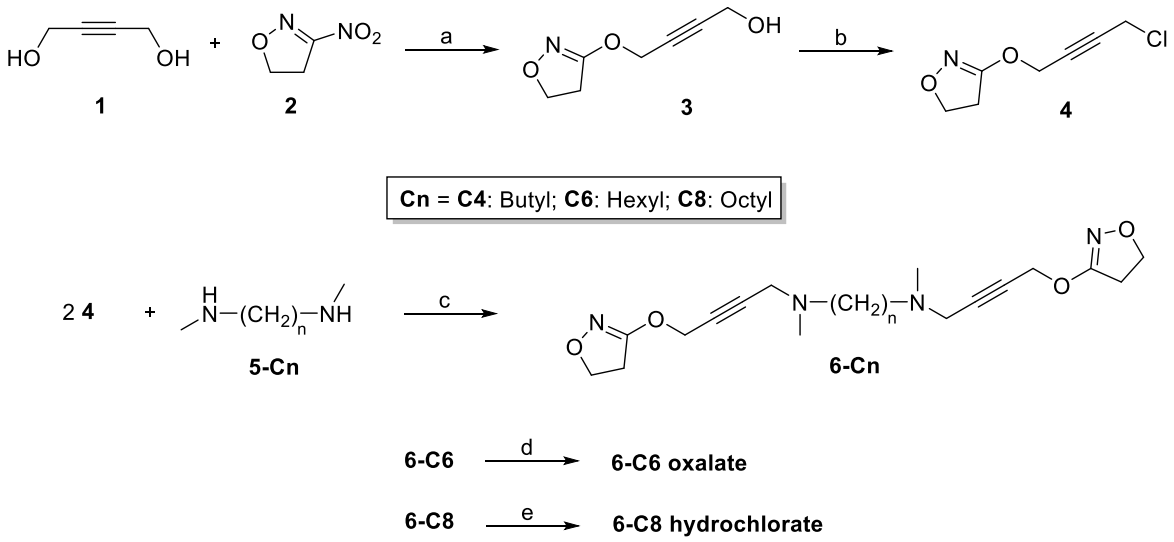

Reagents and conditions: a) NaH (60% suspension), THF, 1 h rt., 3 h reflux; b) $SOCl_2$, pyridine, benzene/CH_2Cl_2, rt.; c) KI/K_2CO_3, CH_3CN, rt.; d) oxalic acid, *t*BME; e) ethereal HCl (1M), *t*BME.

2. Synthesis of tertiary acetylcholine related homodimers

For the synthesis of tertiary acetylcholine-dimers, 2-(methylamino)ethanol was reacted with di-*tert*-butyl dicarbonate in order to protect the amine function, resulting in 84% of the intermediate. Further reaction with acetic anhydride under basic conditions yielded the esterified intermediate in 96%. Deprotection of the BOC-group was not successful by using HCl (4N) in ethyl acetate for 2 h and TFA:CH_2Cl_2 (1:1) for varied reaction times, respectively. The addition of HCl (5-6N) in isopropanol led to 2-(methylamino)ethyl acetate hydrochloride in 37% yield. Further reaction with 1,6-dibromohexane under basic conditions in a microwave assisted reaction did not result in the tertiary acetylcholine-dimer (Scheme 3).

Scheme 3: Synthetic approaches for the synthesis of tertiary acetylcholine-dimers.

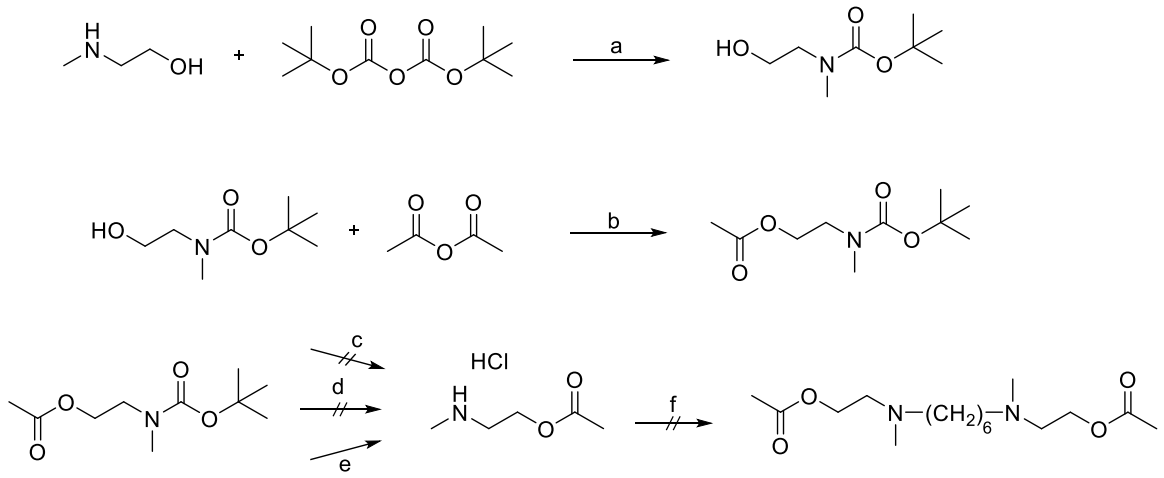

Reagents and conditions: a) ethyl acetate, 1.5 h, ice-cooling; b) pyridine, 4-dimethylaminopyridine, 2 h, rt.; c) HCl (4N) in ethyl acetate, 2 h, rt.; d) TFA:CH_2Cl_2 (1:1), 20-90 min, rt.; e) HCl (5-6N) in isopropanol, 20 min, rt.; f) $Br(CH_2)_6Br$, KI/K_2CO_3, CH_3CN, 100 °C (microwave).

In further attempts, tertiary acetylcholine dimers **8-C4** to **8-C8** were produced by reacting 2 equiv of 2-bromoethylacetate **7** with 1 equiv of the corresponding *N*,*N*`-dimethylalkane-diamines **5-C4** to **5-C8** in the presence of catalytic amounts of KI/K_2CO_3 in acetonitrile (Scheme 4). The tertiary acetylcholine-dimers **8-C4** to **8-C8** could be isolated in 11-27% yield. Due to the instability of the tertiary amine compounds, **8-C6** and **8-C8** were further converted into their corresponding oxalate salts **8-C6 oxalate** and **8-C8 oxalate**.

Scheme 4: Synthesis of tertiary acetylcholine-dimers **8-C4** to **8-C8** and of the corresponding salts **8-C6 oxalate** and **8-C8 oxalate**.

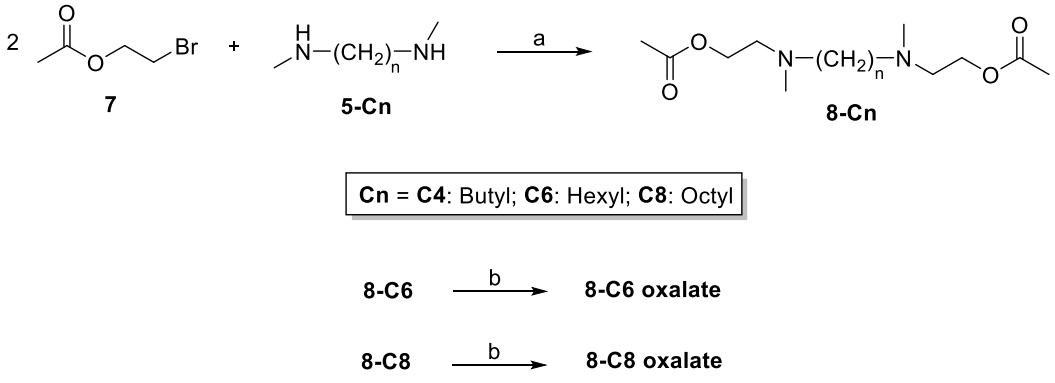

Reagents and conditions: a) KI/K_2CO_3, CH_3CN, rt.; b) oxalic acid, *t*BME.

The elementary analysis (C, H, N) of the salts **6-C6 oxalate**, **6-C8 hydrochlorate**, **8-C6 oxalate**, and **8-C8 oxalate** were measured and found to be > ±0.3 in comparison to the theoretical values. This is due to the very hygroscopic salts, resulting in greater mass and therefore in small deviations between the theoretical and experimental values.

The pharmacological investigations (performed in the working group of PD Dr. Tränkle and Prof. Dr. Mohr, Pharmacology and Toxicology, Institute of Pharmacy, University of Bonn, Germany) of the tertiary iperoxo- and acetylcholine related homodimers concerning their extent on bias agonism at the M_2 receptor are still in process.

3. Methods

Chemicals were of analytical grade and purchased from Aldrich (Steinheim, Germany) and Merck (Darmstadt, Germany). TLC analyses were performed on commercial silica gel 60 F_{254} aluminum sheets (Macherey-Nagel, Düren, Germany); spots were further evidenced by spraying with Ninhydrin reagent[5] for tertiary amines. For manual column chromatography, silica gel 60, 230-400 mesh (Merck, Darmstadt, Germany) was used. Column chromatography was also performed on an Interchim Puri Flash 430 (Ultra Performance Flash Purification) instrument (Montluçon, France) connected to an Interchim Flash ELSD, using a silica column (25 g – 30 µm) (Interchim, Montluçon, France). Melting points were determined on a Stuart melting point apparatus SMP3 (Bibby Scientific, UK) and are uncorrected. IR analysis was carried out on a Jasco FT-IR-6100 spectrometer (Gross-Umstadt, Germany) equipped with a diamond-ATR-unit. Wavelengths are labeled as ṽ. ^{1}H (400.132 MHz) and ^{13}C (100.613 MHz) NMR spectra were recorded on a Bruker AV 400 instrument (Bruker Biospin, Ettlingen, Germany). As internal standard, the signals of the deuterated solvents were used (DMSO-d_6: ^{1}H 2.50 ppm, ^{13}C 39.52 ppm; $CDCl_3$: ^{1}H 7.26 ppm, ^{13}C 77.16 ppm). Abbreviation for data quoted are: s, singlet; d, doublet; t, triplet; q, quartet; m, multiplet; b, broad; dd, doublet of doublets; dt, doublet of triplets; tt, triplet of triplets; tq, triplet of quartets. Coupling constants (*J*) are given in Hz. ESI mass spectra of the novel compounds were measured on an Agilent LC/MSD Trap G2445D instrument (Waldbronn, Germany). Data are reported as mass-to-charge ratio (*m/z*) of the corresponding positively charged molecular ions. Microanalyses (C, H, N) were carried out on a CHNS-932 apparatus (Leco, Mönchengladbach, Germany). The purities of the final new compounds were determined using qNMR and were found to be ≥90% (**6-C8**) and ≥95% (for all other new compounds). 1,2,4,5-Tetrachloro-3-nitrobenzene (Sigma Aldrich, Steinheim, Germany) was chosen as internal standard. qNMR data were acquired at 90° pulse tip angles with recovery

delays of 60 s and acquisition time of 3.7 s in a non-spinning mode at a calibrated probe temperature of 300 K. Sixteen scans of 64 K data points for FID were acquired with a spectral width of 8012 Hz (16 ppm). Manuel phase and baseline correction were performed prior to integration. Preliminary data processing was carried out with Bruker software, TOPSPIN 3.0.

3.1 Synthesis of 3-((4-Chlorobut-2-yn-1-yl)oxy)-4,5-dihydroisoxazole **4**

A. 2-Butyne-1,4-diol **1** 1.52 g (17.7 mmol) was suspended in 20 mL of dry THF under argon atmosphere. Then, sodium hydride 0.70 g (18.0 mmol, 60% suspension in paraffin) was added and the reaction mixture stirred at room temperature for 1 h. 3-Nitro-4,5-dihydroisoxazole[1] **2** 2.04 g (18.0 mmol) dissolved in 10 mL of dry THF was added dropwise and refluxed for 3 h. Then, deionized water was added to the mixture and extracted with chloroform. The combined organic layers were dried over anhydrous Na_2SO_4, filtered and the solvent removed *in vacuo*. The crude product was purified via column chromatography (100% $CHCl_3$, then 100% MeOH) to yield 32% of **3** as yellow oil.

4-((4,5-Dihydroisoxazol-3-yl)oxy)but-2-yn-1-ol ***3***: $C_7H_9NO_3$; M = 155.15 g/mol; yield 32%.

The spectroscopic data are in accordance with the literature.[3,4]

B. **3** 0.80 g (5.16 mmol) was dissolved in 2 mL benzene and 2 mL dichloromethane. To this solution pyridine 0.46 mL (5.70 mmol) was added followed by thionyl chloride 0.40 mL (5.51 mmol) at 0 °C. The reaction mixture was stirred at room temperature for 20.5 h. The reaction mixture was quenched with ice cold water, extracted with ethyl acetate (three times), and the combined organic layers were washed with $NaHCO_3$ solution, water and brine. The organic phases were dried over anhydrous Na_2SO_4 and concentrated under reduced pressure. The product was obtained as brown oil.

3-((4-Chlorobut-2-yn-1-yl)oxy)-4,5-dihydroisoxazole ***4***: $C_7H_8ClNO_2$; M = 173.60 g/mol; yield 78%.

The spectroscopic data are in accordance with the literature.[4]

3.2 General procedure for the synthesis of the homobivalente tertiary iperoxo dimers **6-C4**, **6-C6**, and **6-C8**

2 equiv of **4** and 1 equiv of the corresponding *N*,*N*`-dimethylalkane-diamine **5-C4**, **5-C6**, and **5-C8** were dissolved in dry acetonitrile (20 mL), respectively. After addition of K_2CO_3 1.00 g (7.24 mmol) and a catalytic amount of KI, the reaction mixture was stirred at room temperature overnight. The surplus of KI/K_2CO_3 was filtered off. The filtrate was diluted in chloroform and extracted with aqueous $NaHCO_3$-solution (3%). The combined organic phases were tried over Na_2SO_4, filtered and the solvent was removed *in vacuo*. The crude product was purified by silica gel column chromatography (CH_2Cl_2/MeOH = 2:1; colored by ninhydrin reagent) providing the target compounds.

N^1,N^4-Bis(4-((4,5-dihydroisoxazol-3-yl)oxy)but-2-yn-1-yl)-N^1,N^4-dimethylbutane-1,4-diamine ***6-C4***

Yellowish oil; $C_{20}H_{30}N_4O_4$; M = 390.48 g/mol; yield 27%; R_f = 0.42 (CH_2Cl_2/MeOH = 2:1); IR (ATR): 2938, 2801, 2796, 1625, 1402, 1339, 961, 929, 862 cm^{-1}; ^{1}H NMR ($CDCl_3$): 1.46-1.50 (m, 4H, N(CH_3)-CH_2-C**H_2**), 2.30 (s, 6H, N(C**H_3**)), 2.42 (t, 4H, N(CH_3)-C**H_2**), *J* = 6.8), 2.99 (t, 4H, **H**-$4_{2\text{-isox}}$, *J* = 9.6), 3.39 (t, 4H, ≡C-C**H_2**-N(CH_3), *J* = 1.8), 4.41 (t, 4H, **H**-$5_{2\text{-isox}}$, *J* = 9.6), 4.79 (t, 4H, O-C**H_2**-C≡, *J* = 1.8). ^{13}C NMR ($CDCl_3$): 25.4, 33.1, 41.8, 45.9, 55.7, 58.2, 69.8, 78.7, 83.2, 167.0. MS (ESI) m/z $[M]^+$ Calcd for $C_{20}H_{31}N_4O_4^+$: 391.2 Found: 391.1. MS (ESI) m/z $[M]^{2+}$ Calcd for $C_{20}H_{32}N_4O_4^{2+}$: 196.1 Found: 196.1. qNMR purity 97.5%.

N^1,N^6-Bis(4-((4,5-dihydroisoxazol-3-yl)oxy)but-2-yn-1-yl)-N^1,N^6-dimethylhexane-1,6-diamine ***6-C6***

Brownish oil; $C_{22}H_{34}N_4O_4$; M = 418.53 g/mol; yield 21%; R_f = 0.72 (CH_2Cl_2/MeOH = 2:1); IR (ATR): 2937, 2928, 2871, 1624, 1407, 1339, 964, 928, 858 cm^{-1}; ^{1}H NMR ($CDCl_3$): 1.33-1.37 (m, 4H, N(CH_3)-CH_2-CH_2-C**H_2**), 1.49-1.53 (m, 4H, N(CH_3)-CH_2-C**H_2**), 2.37 (s, 6H, NC**H_3**), 2.49 (t, 4H, N(CH_3)-C**H_2**, *J* = 7.4), 2.99 (t, 4H, **H**-$4_{2\text{-isox}}$, *J* = 9.6), 3.46 (s, 4H, ≡C-C**H_2**-N(CH_3)), 4,42 (t, 4H, **H**-$5_{2\text{-isox}}$, *J* = 9.6), 4.79 (t, 4H, O-C**H_2**-C≡, *J* = 1.8). ^{13}C NMR ($CDCl_3$): 27.1, 27.1, 33.1, 41.6, 45.7, 55.7, 58.0, 69.8, 77.2, 166.9. MS (ESI) m/z $[M]^{2+}$ Calcd for $C_{22}H_{36}N_4O_4^{2+}$: 210.1 Found: 210.1. qNMR purity 95.5%.

N^1,N^8-Bis(4-((4,5-dihydroisoxazol-3-yl)oxy)but-2-yn-1-yl)-N^1,N^8-dimethyloctane-1,8-diamine ***6-C8***

Brownish oil; $C_{24}H_{38}N_4O_4$; M = 446.58 g/mol; yield 52%; R_f = 0.83 (CH_2Cl_2/MeOH = 2:1); IR (ATR): 2929, 2855, 2797, 1625, 1402, 1339, 963, 930, 863 cm^{-1}; ^1H NMR ($CDCl_3$): 1.31-1.35 (m, 8H, $N(CH_3)$-CH_2-CH_2-C**H_2**-C**H_2**), 1.48-1.51 (m, 4H, $N(CH_3)$-CH_2-C**H_2**), 2.37 (s, 6H, $N(C$**H_3**$)$), 2.48 (t, 4H, $N(CH_3)$-C**H_2**, *J* = 7.6), 2.99 (t, 4H, **H**-$4_{2\text{-isox}}$, *J* = 9.6), 3.46 (s, 4H, ≡C-C**H_2**-$N(CH_3)$), 4,42 (t, 4H, **H**-$5_{2\text{-isox}}$, *J* = 9.6), 4.80 (t, 4H, O-C**H_2**-C≡, *J* = 1.8). ^{13}C NMR ($CDCl_3$): 27.1, 27.2, 29.3, 33.1, 41.6, 45.7, 55.8, 58.1, 69.8, 77.3, 166.9. MS (ESI) m/z $[M]^{2+}$ Calcd for $C_{24}H_{40}N_4O_4^{2+}$: 224.2 Found: 224.1. qNMR purity 91.8%.

3.3 Synthesis of N^1,N^6-Bis(4-((4,5-dihydroisoxazol-3-yl)oxy)but-2-yn-1-yl)-N^1,N^6-dimethylhexane-1,6-diaminium carboxyformate **6-C6 oxalate**

To a stirred solution of 1 equiv of **6-C6** in *tert*-butylmethylether (3 mL) was added dropwise 2 equiv of oxalic acid. The precipitate obtained was filtered, washed with chloroform and dried *in vacuo* to yield the oxalate salt **6-C6 oxalate** in 26% as light yellow solid.

$C_{26}H_{38}N_4O_{12}$; M = 598.60 g/mol; mp 135.0-140.4 °C; IR (ATR): 3010, 2969, 2913, 2358, 1733, 1627, 1408, 1336, 1186, 975, 927, 856 cm^{-1}; ^1H NMR (DMSO): 1.28-1.32 (m, 4H, $^+N(CH_3)$-CH_2-CH_2-C**H_2**), 1.49-1.51 (m, 4H, $^+N(CH_3)$-CH_2-C**H_2**), 2.50 (s, 6H, ^+NC**H_3**), 2.70 (t, 4H, $^+N(CH_3)$-C**H_2**, *J* = 4.9), 2.99 (t, 4H, **H**-$4_{2\text{-isox}}$, *J* = 9.4), 3.78 (s, 4H, ≡C-C**H_2**-$^+N(CH_3)$), 4.31 (t, 4H, **H**-$5_{2\text{-isox}}$, *J* = 9.4), 4,84 (s, 4H, O-C**H_2**-C≡). ^{13}C NMR (DMSO): 24.9, 25.9, 32.3, 41.6, 44.6, 54.5, 57.4, 69.5, 162.7, 166.7. MS (ESI) m/z $[M]^{2+}$ Calcd for $C_{22}H_{36}N_4O_4^{2+}$: 210.1 Found: 210.1. qNMR purity 98.8%. Anal. Calcd for $C_{26}H_{38}N_4O_{12}$ (598.25): C, 45.17; H, 5.48; N, 7.80. Found: C, 46.17; H, 5.86; N, 7.98.

3.4 Synthesis of N^1,N^8-Bis(4-((4,5-dihydroisoxazol-3-yl)oxy)but-2-yn-1-yl)-N^1,N^8-dimethyloctane-1,8-diaminium chloride 5.5 hydrate **6-C8 hydrochlorate**

To a stirred solution of 1 equiv of **6-C8** in *tert*-butylmethylether (3 mL) was added dropwise 2 equiv of ethereal HCl-solution (1M). The precipitate obtained was filtered, washed with chloroform and dried *in vacuo* to yield the hydrochloric acid salt **6-C8 hydrochlorate** in 90% as brown solid.

$C_{24}H_{51}Cl_2N_4O_{9.5}$; M = 618.59 g/mol; IR (ATR): 2934, 2900, 2500, 1700, 1626, 1400, 1338, 1165, 968, 928 cm^{-1}; ^1H NMR (DMSO): 1.24-1.34 (m, 8H, $^+N(CH_3)$-CH_2-CH_2-C**H_2**-C**H_2**), 1.60-1.70 (m, 4H, $^+N(CH_3)$-CH_2-C**H_2**), 2.75 (s, 6H, $^+N(C$**H_3**$)$), 2.99-3.09 (m, 8H, **H**-$4_{2\text{-isox}}$, $^+N(CH_3)$-C**H_2**), 4.16 (s, 4H, ≡C-C**H_2**-$^+N(CH_3)$), 4.32 (t, 4H, **H**-$5_{2\text{-isox}}$, *J* = 9.6), 4,89 (s, 4H, O-C**H_2**-C≡),

11.04 (br, 2H, $^{+}N(CH_3)$**H**). ^{13}C NMR (DMSO): 23.3, 25.8, 28.1, 32.2, 41.6, 44.0, 54.1, 57.2, 69.6, 166.7. MS (ESI) m/z $[M]^{2+}$ Calcd for $C_{24}H_{40}N_4O_4^{2+}$: 224.2 Found: 224.1. Anal. Calcd for $C_{24}H_{51}Cl_2N_4O_{9.5}$ (617.30): C, 46.60; H, 8.31; N, 9.06. Found: C, 47.38; H, 7.03; N, 9.18.

3.5 General procedure for the synthesis of the homobivalente tertiary acetylcholine dimers **8-C4**, **8-C6**, and **8-C8**

2 equiv of 2-bromoethylacetate and 1 equiv of corresponding *N*,*N*`-dimethylalkane-diamine **5-C4**, **5-C6**, and **5-C8** were dissolved in dry acetonitrile (20 mL), respectively. After addition of K_2CO_3 1.00 g (7.24 mmol) and a catalytic amount of KI, the reaction mixture was stirred at room temperature overnight. The surplus of KI/K_2CO_3 was filtered off. The filtrate was diluted in chloroform and extracted with aqueous $NaHCO_3$-solution (3%). The combined organic phases were dried over Na_2SO_4, filtered and the solvent was removed *in vacuo*. The residue was kept in the fridge until an oil precipitates on the bottom of the flask. The surplus was decanted off and dried *in vacuo*.

*(Butane-1,4-diylbis(methylazanediyl))bis(ethane-2,1-diyl) diacetate **8-C4***

Brown oil; $C_{14}H_{28}N_2O_4$; M = 288.38 g/mol; yield 11%; IR (ATR): 2946, 2780, 2789, 1736, 1457, 1370, 1230, 1038 cm^{-1}; ^1H NMR (DMSO): 1.35-1.38 (m, 4H, $N(CH_3)$-CH_2-C**H₂**), 1.99 (s, 6H, C**H₃**), 2.16 (s, 6H, N(C**H₃**)), 2.31 (t, 4H, $N(CH_3)$-C**H₂**, *J* = 6.6), 2.52 (t, 4H, O-CH_2-C**H₂**, *J* = 6.0), 4.06 (t, 4H, O-C**H₂**, *J* = 5.8). ^{13}C NMR (DMSO): 20.7, 24.3, 42.1, 55.2, 57.0, 61.7, 170.3. MS (ESI) m/z $[M]^+$ Calcd for $C_{14}H_{29}N_2O_4^+$: 289.2. Found: 289.1. qNMR purity 99.1%.

*(Hexane-1,6-diylbis(methylazanediyl))bis(ethane-2,1-diyl) diacetate **8-C6***

Transparent oil; $C_{16}H_{32}N_2O_4$; M = 316.44 g/mol; yield 27%; IR (ATR): 2934, 2852, 2788, 1737, 1456, 1369, 1230, 1038 cm^{-1}; ^1H NMR (DMSO): 1.22-1.26 (m, 4H, $N(CH_3)$-CH_2-CH_2-C**H₂**), 1.33-1.38 (m, 4H, $N(CH_3)$-CH_2-C**H₂**), 1.99 (s, 6H, C**H₃**), 2.16 (s, 6H, N(C**H₃**)), 2.29 (t, 4H, $N(CH_3)$-C**H₂**, *J* = 7.2), 2.52 (t, 4H, O-CH_2-C**H₂**, *J* = 5.4), 4.05 (t, 4H, O-C**H₂**, *J* = 6.0). ^{13}C NMR (DMSO): 20.7, 26.6, 26.7, 42.1, 55.1, 57.1, 61.6, 170.2. MS (ESI) m/z $[M]^+$ Calcd for $C_{16}H_{33}N_2O_4^+$: 317.3. Found: 317.1. qNMR purity 97.6%.

(Octane-1,8-diylbis(methylazanediyl))bis(ethane-2,1-diyl) diacetate ***8-C8***

Brown oil; $C_{18}H_{36}N_2O_4$; M = 344.49 g/mol; yield 25%; IR (ATR): 2928, 2859, 2790, 1733, 1610, 1469, 1370, 1230, 1038 cm^{-1}; ^1H NMR (DMSO): 1.23-1.28 (m, 8H, $N(CH_3)$-CH_2-CH_2-C**H₂**-C**H₂**), 1.34-1.39 (m, 4H, $N(CH_3)$-CH_2-C**H₂**), 1.98 (s, 6H, C**H₃**), 2.14 (s, 6H, N(C**H₃**)), 2.28 (t, 4H, $N(CH_3)$-C**H₂**, *J* = 7.2), 2.50 (t, 4H, O-CH_2-C**H₂**, *J* = 6.2), 4.04 (t, 4H, O-C**H₂**, *J* = 5.8). ^{13}C NMR (DMSO): 20.7, 26.6, 26.7, 28.9, 42.1, 55.2, 57.2, 61.7, 170.2. MS (ESI) m/z $[M]^+$ Calcd for $C_{18}H_{37}N_2O_4^+$: 345.3. Found: 345.1. qNMR purity 95.3%.

3.6 General procedure for the preparation of the oxalic acid salts **8-C6 oxalate** and **8-C8 oxalate**

To a stirred solution of 1 equiv of **8-C6** and **8-C8** in *tert*-butylmethylether (3 mL) was added dropwise 2 equiv of oxalic acid, respectively. The precipitate obtained was filtered, washed with chloroform and dried *in vacuo* to yield the desired oxalate salts **8-C6 oxalate** and **8-C8 oxalate**.

N^1,N^6-Bis(2-acetoxyethyl)-N^1,N^6-dimethylhexane-1,6-diaminium carboxyformate ***8-C6 oxalate***

Light yellow solid; $C_{20}H_{36}N_2O_{12}$; M = 496.51 g/mol; yield 58%; mp 170.4-177.2 °C; IR (ATR): 3002, 2941, 2865, 2649, 1738, 1708, 1633, 1222, 1072, 1038, 980, 934, 910 cm^{-1}; ^1H NMR (DMSO): 1.28-1.32 (m, 4H, $^+N(CH_3)$-CH_2-CH_2-C**H₂**), 1.56-1.59 (m, 4H, $^+N(CH_3)$-CH_2-C**H₂**), 2.04 (s, 6H, C**H₃**), 2.65 (s, 6H, N(C**H₃**)), 2.90 (t, 4H, $^+N(CH_3)$-C**H₂**, *J* = 8.0), 3.18 (t, 4H, O-CH_2-C**H₂**, *J* = 5.2), 4.27 (t, 4H, O-C**H₂**, *J* = 5.4). ^{13}C NMR (DMSO): 20.6, 23.6, 25.6, 39.7, 53.6, 55.6, 58.9, 165.1, 170.2. MS (ESI) m/z $[M]^{2+}$ Calcd for $C_{16}H_{34}N_2O_4^{2+}$: 159.1 Found 159.1. qNMR purity 97.0%. Anal. Calcd for $C_{20}H_{36}N_2O_{12}$ (496.23): C, 48.38; H, 7.31; N, 5.64. Found: C, 47.62; H, 7.25; N, 5.46.

N^1,N^8-Bis(2-acetoxyethyl)-N^1,N^8-dimethyloctane-1,8-diaminium carboxyformate ***8-C8 oxalate***

White solid; $C_{22}H_{40}N_2O_{12}$; M = 524.56 g/mol; yield 71%; mp 140.4-143.7 °C; IR (ATR): 3015, 2929, 2858, 2694, 1732, 1717, 1635, 1474, 1388, 1364, 1228, 1069, 1034, 944 cm^{-1}; ^1H NMR (DMSO): 1.22-1.31 (m, 8H, $^+N(CH_3)$-CH_2-CH_2-C**H₂**-C**H₂**), 1.55-1.62 (m, 4H, $^+N(CH_3)$-CH_2-C**H₂**), 2.04 (s, 6H, C**H₃**), 2.69 (s, 6H, $^+$NC**H₃**), 2.96 (t, 4H, $^+N(CH_3)$-C**H₂**, *J* = 8.0), 3.24 (t, 4H, O-CH_2-C**H₂**, *J* = 5.2), 4,29 (t, 4H, O-C**H₂**, *J* = 5.2). ^{13}C NMR (DMSO): 20.6, 23.5, 25.9, 28.3, 39.7, 53.4, 55.5, 58.6, 163.8, 170.1. MS (ESI) m/z $[M]^{2+}$ Calcd for $C_{18}H_{38}N_2O_4^{2+}$: 173.1

Found: 173.1. qNMR purity 95.3%. Anal. Calcd for $C_{22}H_{40}N_2O_{12}$ (524.26): C, 50.37; H, 7.69; N, 5.34. Found: C, 49.40; H, 7.98; N, 5.52.

References

[1] Kloeckner, J., Schmitz, J., and Holzgrabe, U. (2010) Convergent, short synthesis of the muscarinic superagonist iperoxo, *Tetrahedron Lett. 51*, 3470-3472.

[2] Wade, P. A. (1978) Synthesis of 3-Substituted 2-Isoxazolines and 5,6-Dihydro-1,2,4h-Oxazines, *J. Org. Chem. 43*, 2020-2023.

[3] Dallanoce, C., Conti, P., De Amici, M., De Micheli, C., Barocelli, E., Chiavarini, M., Ballabeni, V., Bertoni, S., and Impicciatore, M. (1999) Synthesis and functional characterization of novel derivatives related to oxotremorine and oxotremorine-M, *Bioorg. Med. Chem. 7*, 1539-1547.

[4] De Amici, M., Conti, P., Fasoli, E., Barocelli, E., Ballabeni, V., Bertoni, S., Impicciatore, M., Roth, B. L., Ernsberger, P., and De Micheli, C. (2003) Synthesis and in vitro pharmacology of novel heterocyclic muscarinic ligands, *Il Farmaco 58*, 739-748.

[5] Friedman, M., and Williams, L. D. (1974) Stoichiometry of formation of Ruhemann's purple in the ninhydrin reaction, *Bioorg. Chem. 3*, 267-280.

7. Novel bipharmacophoric inhibitors of the cholinesterases with affinity to the muscarinic receptors M_1 and M_2

Messerer, R., Dallanoce, C., Matera, C., Wehle, S., Flammini, L., Chirinda, B., Bock, A., Irmen, M., Tränkle, C., Barocelli, E., Decker, M., Sotriffer, C., De Amici, M., Holzgrabe, U.

Manuscript in preparation (unpublished)

Abstract

A set of hybrid compounds composed of the fragment of allosteric modulators of the muscarinic receptor, i.e. W84 and naphmethonium, and the well known AChE inhibitor tacrine on the one hand, and the skeletons of the orthosteric muscarinic agonists, iperoxo and isox, respectively, on the other hand were synthesized. The two molecular moieties were connected *via* a polymethylene linker of varying length. These bipharmacophoric compounds were investigated for inhibition of AChE (from electric eel) and BChE (from equine serum), as well as on human ChEs *in vitro* and compared to previously synthesized dimeric inhibitors. Among the studied hybrids, compound **10-C10**, characterized by a 10 carbon alkylene linker connecting tacrine and iperoxo, proved to be the most potent inhibitor with the highest pIC_{50} values of 9.81 (AChE from electric eel) and 8.75 (BChE from equine serum), respectively. Docking experiments with compounds **10-C10**, **7b-C10**, and **7a-C10** helped to interpret the experimental inhibitory power towards AChE, which is affected by the nature of the allosteric molecular moiety, with the tacrine-containing hybrid being much more active than the naphthalimido- and phthalimido-containing analogs. Furthermore, the most active AChE inhibitors were found to have affinity at M_1 and M_2 muscarinic receptors. Since **10-C10** showed almost no cytotoxicity, it emerged as a promising lead structure for the development of an anti-Alzheimer drug.

Abbreviations:

ACh, acetylcholine; AChE, acetylcholinesterase, AD, Alzheimer Disease; ATC, Acetylthiocholine; BChE, Butyrylcholinesterase; BTC, Butyrylthiocholine; CAS, catalytic active site; DTNB, Dithionitrobenzoic acid; GPCR, G protein-coupled receptor; M_1, muscarinic acetylcholine receptor subtype 1; M_2, muscarinic acetylcholine receptor subtype 2; RMSD, root mean square deviation; PAS, peripheral anionic site.

1. Introduction

Alzheimer's disease (AD) is one of the most prominent neurodegenerative diseases affecting worldwide about 9% of the population aged over 65 and 26% of the people older than 85.[1] Due to the rising number of patients,[2] in the future there is an urgent need for the development of new, highly effective drugs against AD. Beside other strategies, today's pharmacotherapy of AD is essentially based on the cholinergic hypothesis since the concentration of ACh is decreased in the brain leading to the loss of cognitive functions. The main therapeutic approach is to inhibit acetylcholinesterase (AChE), an enzyme responsible for the rapid hydrolysis of ACh,[3] and the butyrylcholinesterase (BChE), an enzyme with structural features very similar to those of AChE.[4-6] Indeed, high levels of BChE were found to influence Aβ aggregation during the early stages of senile plaque formation.[7] Therefore, concurrent inhibition of both BChE and AChE may have clinical benefits in the treatment of AD symptoms.[7] Tacrine (Figure 1), donepezil, galantamine, and rivastigmine are well known ChE inhibitors for AD therapy.[8] Nevertheless, the clinical effectiveness of AChEIs in AD therapy is still under debate[9] and the use of tacrine is currently limited due to its serious hepatotoxicity.[10] As a consequence, tacrine has recently been used for the development of hybrid molecules[11-15] in order to combine its potent AChE inhibition with other favorable pharmacological benefits, such as reduced hepatotoxicity. In particular, bis(7)tacrine dimer **9-C7** (Figure 2) was found to address both sites of the enzyme, the catalytic active site (CAS) as well as the peripheral anionic site (PAS), resulting in 1000-fold higher AChE inhibitory potency than tacrine.[16]

In addition, agonists of the muscarinic receptor, especially of the M_1 subtype, have gained great interest in the development of anti-Alzheimer drugs, because muscarinic M_1 agonists can directly stimulate neurotransmission. Recently, so-called dualsteric ligands, combining the moieties of allosteric modulators such as W84 **4** and naphmethonium **5** (Figure 1) and the superagonist iperoxo[17] **2** (Figure 1) were tested for their anticholinesterase activity and found to be moderate inhibitors of the rat brain cholinesterase.[18] Aiming at compounds with improved anticholinesterase activity for both AChE and BChE combined with affinity to the M_1 and M_2 receptor, this small set of compounds was extended by using polymethylene linker chains of different length and by linkage of the phthalyl moiety to the agonist isox **3**[19-21] (Figure 2). Furthermore, tacrine and iperoxo were combined within one molecule leading to new hybrid molecules (Figure 2). The entire set of compounds was tested for its anticholinesterase activity and affinity to the M_2 and in part the M_1 muscarinic receptor, in order to find out whether hybrid compounds can serve as a strategy for the development of anti-Alzheimer drugs.

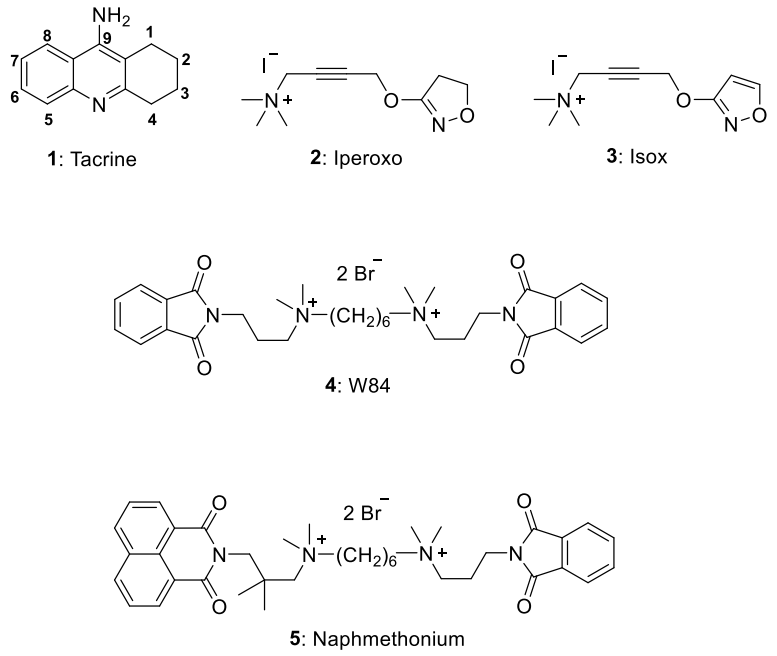

Figure 1: Structures of tacrine **1**, iperoxo **2**, isox **3**, W84 **4**, and naphmethonium **5**.

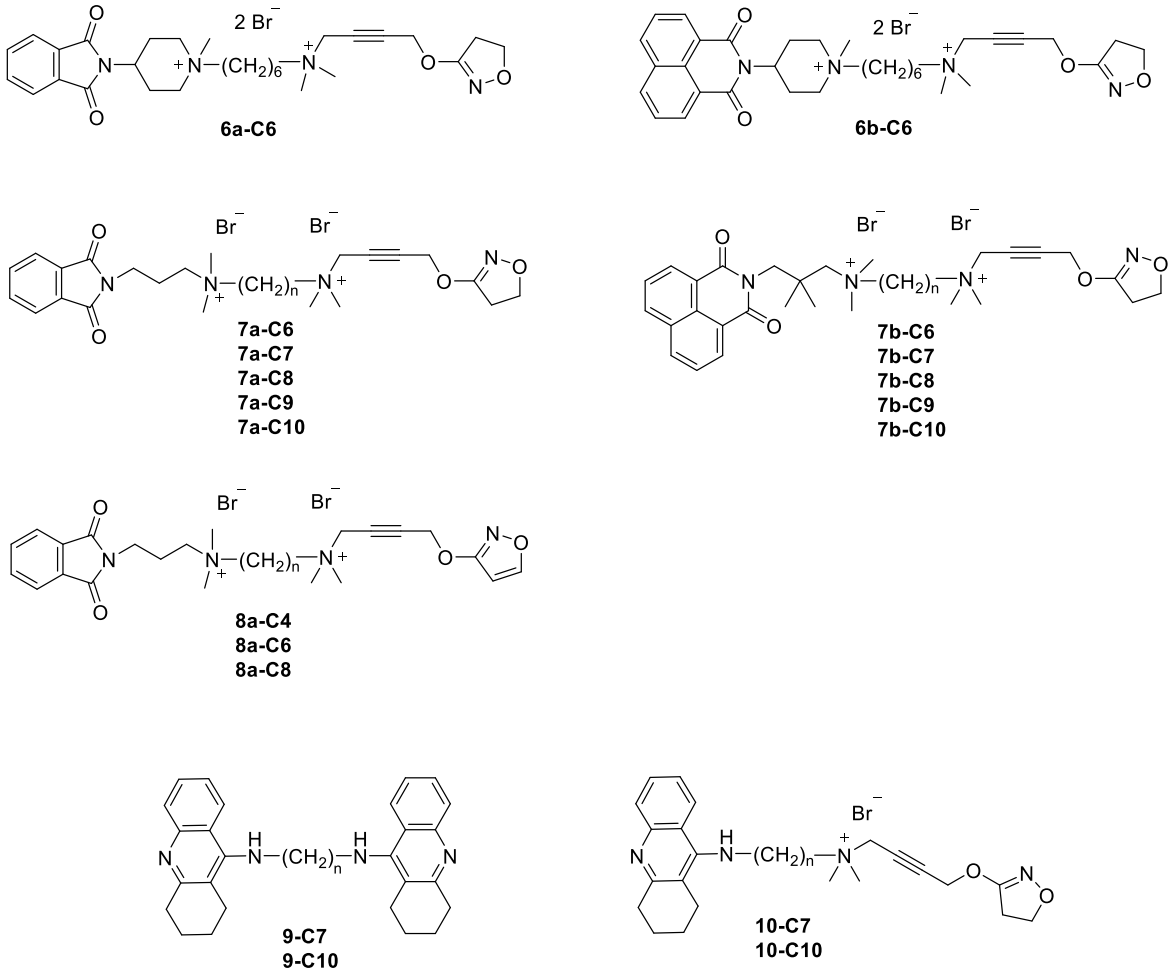

Figure 2: Structures of the different hybrid sets and tacrine dimers investigated in this study.

2. Results and discussion

2.1 Chemistry

The synthesis of the iperoxo related bisquaternary ligands **7a-C7/C8**[18,22], **7b-C7/C8**[18,22], **6a/b-C6**[18], and isoxazole derivative **8a-C6**[19] as well as the synthesis of the homodimeric tacrine hybrids **9-C7/C10**[23] were accomplished according to previously described procedures (Scheme 1). In brief, phthalimidopropylamine **11a**[19] and 1,8-naphthalimidopropylamine **11b**[19], respectively, were reacted with a large excess of commercially available dibromoalkanes in refluxing acetonitrile (Scheme 1). The monoquaternary intermediates were obtained in 57-98% yield. Subsequent reaction with a slight excess of iperoxo-base **2**[17,20] and 4-(isoxazol-3-yloxy)-*N*,*N*-dimethylbut-2-yn-1-amine **3**[19], respectively, in refluxing acetonitrile afforded the desired compounds **7a-C9**, **7a-C10**, **7b-C9**, and **7b-C10** in 88-95% and **8a-C4**, and **8a-C8** in 53% and 63% yield, respectively.

Scheme 1: a) CH_3CN, reflux.

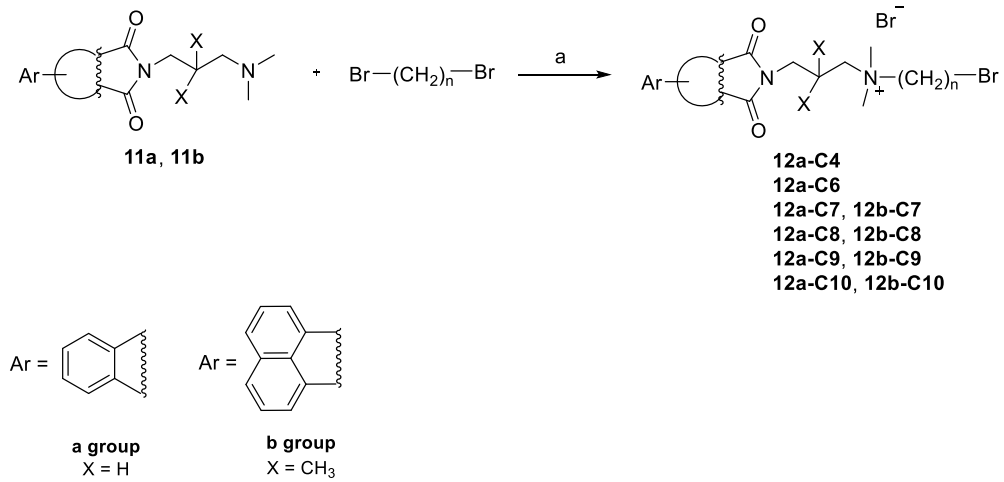

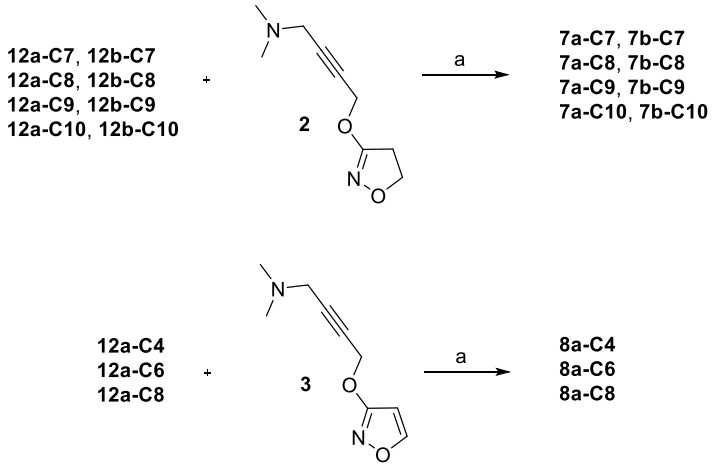

For preparation of the two tacrine-containing hybrid molecules, tacrine **1**[24] was treated with a large excess of commercially available 1,7-dibromoheptane and 1,10-dibromodecane to obtain the known intermediates **13-C7**[25] and **13-C10**[24]. Subsequent addition of two equivalents of iperoxo-base **2**[17,20], in acetonitrile in a microwave assisted reaction yielded the target compounds **10-C7** and **10-C10** (Scheme 2).

Scheme 2: a) KOH, CH_3CN, rt; b) KI/K_2CO_3, CH_3CN, 80 °C (microwave).

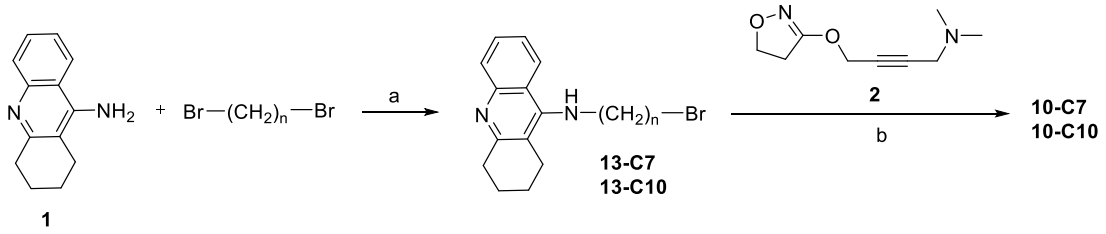

2.2 Pharmacology

The compounds were evaluated towards the BChE (E.C.3.1.1.8) from equine serum, the hBChE (E.C.3.1.1.8) from human serum as well as the AChE (E.C.3.1.1.7) from electric eel, and the hAChE (E.C.3.1.1.7), a recombinant expressed in HEK 293 cells (see Table 1). The compounds containing a naphthyl moiety (**7b-C7** and **7b-C8**) were reported in literature to exhibit higher anticholinesterase activity toward the cholinesterase from rat brain homogenates than the hybrids comprising a phthalyl moiety (**7a-C7** and **7a-C8**) (Table 1).[18] These findings could also be confirmed using the other AChEs and BChEs. With regard to the linker length, a longer linker resulted in higher anticholinesterase activity, with **7a-C10** and **7b-C10** having the highest inhibitory potency (pIC_{50} (BChE) = 5.37 and 6.99 and pIC_{50} (AChE) = 5.26 and 6.50, respectively). In contrast, compounds linked to isox **3** (**8a-C4**, **8a-C6**, and **8a-C8**) as well as the hybrids containing a more rigid allosteric fragment (**6a-C6** and **6b-C6**) showed moderate cholinesterase inhibition.

Tacrine is known as a potent anticholinesterase inhibitor.[26] Replacing the naphthyl moiety of hybrid **7b-C10** with tacrine **10-C10** resulted in excellent inhibitory activity for both AChE (pIC_{50} = 9.81) and BChE (pIC_{50} = 8.75), with an increased potency compared to that of monomeric tacrine **1** (Table 1). A similar inhibitory activity was found towards hChEs, where it exhibited about 1.5-2 log unit higher potency than **7b-C10** and tacrine **1**. Moreover, the hybrid **10-C10** is as active as the previously reported dimers **9-C7** and **9-C10** (Figure 2).[16,23,27,28] A shorter linker length (**10-C7**) decreased the inhibitory activity slightly (Table 1).

Table 1: In vitro cholinesterase activity, cytotoxicity, and logP values of the investigated compounds.

Compound	BChE[a] pIC_{50} [M][b]	AChE[c] pIC_{50} [M][b]	hBChE[d] pIC_{50} [M][b]	hAChE[e] pIC_{50} [M][b]	Cytotoxicity HEP G2 IC_{50} [µM]	logP[f]
1	8.57	7.60	n.d.	n.d.	111 (±2.28)	n.d.
6a-C6	4.97	5.62	n.d.	n.d.	n.d.	0.84
6b-C6	6.07	5.98	n.d.	n.d.	n.d.	1.54
7a-C7	5.19	4.83	n.d.	n.d.	n.d.	0.79
7a-C8	5.13	4.89	n.d.	n.d.	n.d.	0.78
7a-C9	4.88	4.80	n.d.	n.d.	n.d.	0.79
7a-C10	5.37	5.26	5.71	4.88	n.d.	0.80
7b-C7	6.69	6.04	n.d.	n.d.	n.d.	1.70
7b-C8	6.46	6.10	n.d.	n.d.	n.d.	1.61
7b-C9	6.49	6.44	n.d.	n.d.	n.d.	1.69
7b-C10	6.99	6.50	6.58	5.97	n.d.	1.77
8a-C4	4.07	19.12 % inhib. at 100 µM	n.d.	n.d.	n.d.	1.55
8a-C6	4.41	32.91 % inhib. at 100 µM	n.d.	n.d.	n.d.	0.99
8a-C8	5.10	4.17	n.d.	n.d.	n.d.	0.83
9-C7	9.14	10.48	n.d.	n.d.	< 1.38 (±0.08)	n.d.
9-C10	9.34	9.00	n.d.	n.d.	< 1.25 (±0.00)	n.d.
10-C7	8.29	8.76	8.34	8.70	> 160 (±0.00)	2.05
10-C10	8.75	9.81	8.74	8.75	32.2 (±0.41)	3.28
13-C7	6.58	9.40	n.d.	n.d.	n.d.	n.d.
13-C10	8.06	9.25	n.d.	n.d.	n.d.	n.d.

[a] BChE from equine serum (E.C.3.1.1.8). [b] pIC_{50} (SE) values are the negative logarithm of the concentration causing half-maximal inhibition of cholinesterase activity. [c] AChE from electric eel (E.C.3.1.1.7). [d] hBChE from human serum (E.C.3.1.1.8). [e] hAChE, a recombinant expressed in HEK 293 cells. [f] For logP-calculation see Table 4 and Table 5. n.d.: not determined.

Since the hybrids **7a-C6** and **7b-C6** were found to have comparable binding affinity measures regarding the M_1 and M_2 receptor[29] and because tacrine, an allosteric modulator, is known for its M_2 receptor subtype selectivity (over M_1 and M_3)[30] the compounds **7a/b-C10** and **10-C7/C10** were tested for their affinity to the M_2 receptor, representatively (see Table 2). In other words, the M_2 receptor was chosen foremost instead of M_1 to offer the tacrine moiety the highest propensity to bind allosterically to the M receptor. Firstly, the allosterically retarding action of selected compounds on the kinetics of [^{3}H]NMS dissociation from M_2 receptors was checked and quantified in order to calculate the incubation time needed for reaching binding equilibrium in the presence of a given test compound (cf. Table 2 and Detailed Experimental Procedures). Thereafter, in equilibrium binding experiments all compounds were found to show almost the same high affinity measures $\log IC_{50}$ in orthosterically unliganded M_2 receptors in the nanomolar range of concentration, suggesting that the iperoxo part of the hybrids is occupying the orthosteric binding site of M_2 (cf. high affinity of iperoxo reference[31]). Thus, the tacrine moiety of **10-C7/C10**, even in M_2 receptors, was not able to hinder the iperoxo moiety from governing the high affinity binding of the hybrids to the orthosteric site. The inhibition of orthosteric ligand dissociation by the hybrids (Figure 3A) revealed their affinities $\log K_{X,diss}$ at the allosteric site of M_2 receptors to be lower than at orthosterically unliganded receptors throughout (Table 2) which is in line with downward directed inhibition curves at the orthosterically unliganded receptor and binding equilibrium (see above and Figure 3B). The compounds **7b-C10** and **10-C10** had equal $\log K_{X,diss}$ values in NMS-occupied M_2 receptors suggesting the tacrine moiety to equal the naphmethonium moiety regarding their contribution to allosteric binding of these otherwise identical hybrids (Table 2). Finally, the selected tacrine hybrids **10-C7** and **10-C10** were studied in NMS liganded and unliganded M_1 receptors and yielded qualitatively a very similar picture, with the exception that the dissociation of [^{3}H]NMS from M_1 receptors was maximally retarded 5 fold by **10-C10** (equivalent to a reduction of k_{-1} to 20 percent, cf. Figure 4A). This value of **10-C10**, nevertheless, was reached in a concentration dependent fashion and thus documented the possibility of a purely allosteric binding pose also of this hybrid at M_1 receptors (cf. Figure 4A). That being said, quantitatively, the individual affinity measures of **10-C7** and **10-C10** dropped between 3-8 fold (Figure 4 and Table 3) compared to M_2 receptors (Figure 3 and Table 2). The extent of decreased binding affinity of these hybrids at *orthosterically unliganded* M_1 receptor could be explained by the 10 fold loss of iperoxo affinity compared to M_2 receptors reported recently,[32] whereas the twofold affinity loss reported for tacrine alone in the literature is too small to explain it.[30] The ratios of affinity measures calculated based on receptor occupancy with or without NMS differed at M_2 receptors for **10-C7** (104-fold) compared to **10-C10** (20-fold) (cf. Table 2) whereas the corresponding ratios calculated at M_1 receptors for **10-C7** (79-fold) and **10-C10** (55-fold),

were similar (cf. Table 3). Taken together, **10-C7** and **10-C10** showed slightly attenuated affinity measures in M_1 compared to M_2 receptors but qualitatively similar receptor affinity binding profiles.

Future studies will explore how these high affinity muscarinic hybrids interact with M_1 receptors in the context of AD.

Table 2: Numerical estimates of parameters from binding experiments characterizing the interaction of the test compounds with the inverse orthosteric agonist NMS at muscarinic M_2 receptors.

	[^{3}H]NMS-dissociation kinetics		[^{3}H]NMS-equilibrium binding	
Compound	Log$K_{X,diss}$ X➔NMS-M_2	n slope	logIC_{50} X➔M_2	n slope
10-C7	-6.36* ±0.04	-1.17 ±0.14	-8.38 ±0.08	-0.63 ±0.05**
10-C10	-6.94 ±0.04	-0.67 ±0.05**	-8.24* ±0.09	-0.98 ±0.16
7b-C10	-7.18* ±0.05	-0.77 ±0.08	-8.53 ±0.04	-0.76 ±0.05**
7a-C10	-5.57* ±0.07	-0.88 ±0.13	-8.42 ±0.05	-0.63 ±0.04**
7a-C6	-4.93*, § ± 0.03	-0.89 ±0.05	-6.03* ±0.02	-0.98 ±0.05

log$K_{X,diss}$, log binding constant of the allosteric agent X for NMS-bound receptors measured as the concentration of the test compound ligand that reduces the dissociation rate constant of [^{3}H]NMS dissociation by 50%; n: slope factor of the curve; logIC_{50}: log concentration of the test compound X reducing the specific binding of the orthosteric radioligand [^{3}H]NMS in the absence of X by 50%. The data shown are mean values ± S.E.M. of three to four experiments carried out in duplicate (dissociation) or triplicate (equilibrium binding). *, value was determined with curve slope fixed to unity; **, value deviates significantly from unity (F-test, P<0.05). §, value was taken from Bock et al. 2014. For further details see references Fang et al. 2010 and detailed pharmacological procedures.

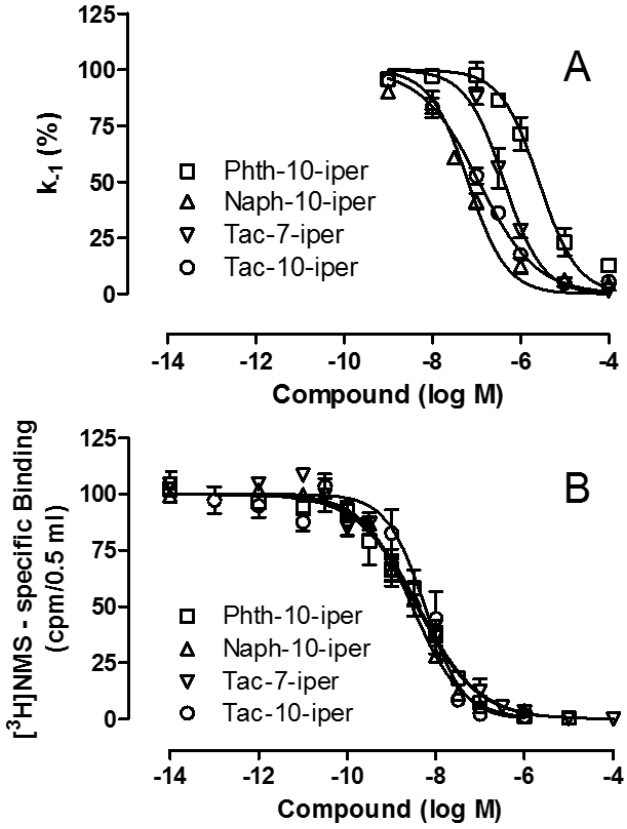

Figure 3: (**A**) Retardation of NMS dissociation expressed as concentration-effect curves of selected test-compounds on the dissociation rate constant k_{-1} of the radioligand [^{3}H]NMS to determine $\log K_{X,diss}$ as an affinity measure of the test compounds at M_2 receptors that are orthosterically blocked by NMS. (**B**) Test-compound induced inhibition of specific [^{3}H]NMS (0.2 nM) equilibrium binding to estimate corresponding affinity measures at orthosterically unliganded M_2 receptors. Curves were obtained by logistic curve fitting. The data illustrated are mean values ± S.E.M. of three to four experiments carried out as (**A**) duplicate or (**B**) triplicate determinations.

Table 3: Numerical estimates of parameters from binding experiments characterizing the interaction of selected test compounds with the inverse orthosteric agonist NMS at muscarinic M_1 receptors.

	[^{3}H]NMS-dissociation kinetics		[^{3}H]NMS-equilibrium binding	
Compound	$LogK_{X,diss}$ X➔NMS-M_1	n slope	$logIC_{50}$ X➔M_1	n slope
10-C7	-5.59* ±0.08	-0.81 ±0.12	-7.49* ±0.06	-0.98 ±0.14*
10-C10	-5.98*,§ ±0.11	-0.89§ ±0.20	-7.72* ±0.05	-1.05 ±0.11

$logK_{X,diss}$, log binding constant of the allosteric agent X for NMS-bound receptors measured as the concentration of the test compound ligand that reduces the dissociation rate constant of [^{3}H]NMS dissociation by 50%; n: slope factor of the curve; $logIC_{50}$: log concentration of the test compound X reducing the specific binding of the orthosteric radioligand [^{3}H]NMS in the absence of X by 50%. The data shown are mean values ± S.E.M. of three to four experiments carried out in duplicate (dissociation) or quadruplicate (equilibrium binding). *, value was determined with curve slope fixed to unity; §, values derived with bottom plateau significantly different from zero (F-test, $P<0.05$). For further details see references Fang et al. 2010 and detailed pharmacological procedures.

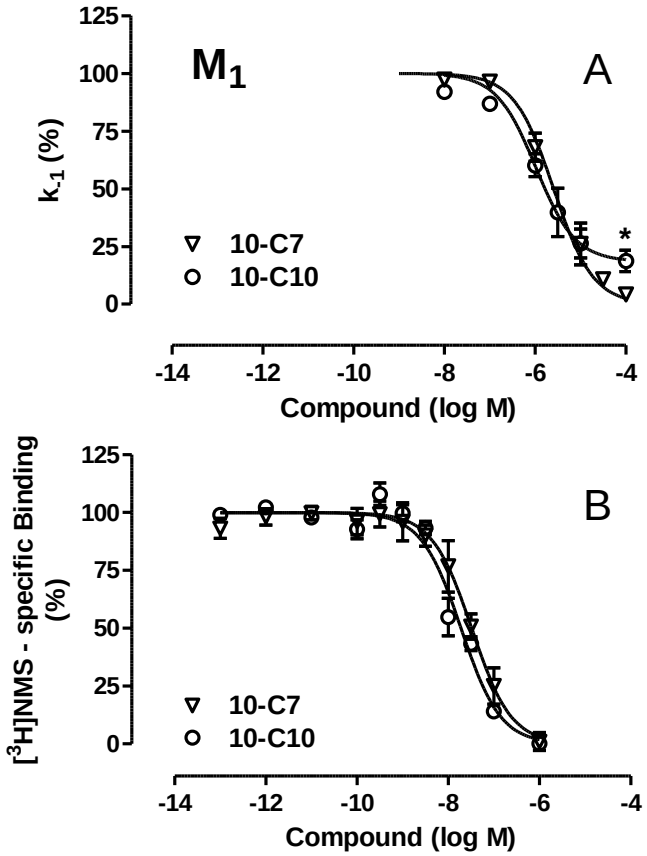

Figure 4: (**A**) Retardation of NMS dissociation expressed as concentration-effect curves of selected test-compounds on the dissociation rate constant k_{-1} of the radioligand [^{3}H]NMS to determine $\log K_{X,diss}$ as an affinity measure of the test compounds at M_1 receptors that are orthosterically blocked by NMS. (**B**) Test-compound induced inhibition of specific [^{3}H]NMS (0.2 nM) equilibrium binding to estimate corresponding affinity measures at orthosterically unliganded M_1 receptors. Curves were obtained by logistic curve fitting. The data illustrated are mean values ± S.E.M. of three to four experiments carried out as (**A**) duplicate or (**B**) quadruplicate determinations.*, bottom plateau deviates significantly from zero (F-Test, P< 0.05).

2.3 Cytotoxicity

The use of tacrine in the treatment of Alzheimer`s disease is currently limited due to its serious hepatotoxicity.[10,13] Interestingly, the combination of tacrine with iperoxo through a heptyl or decyl linker chain (**10-C7** and **10-C10**) resulted in a lower cytotoxicity towards HEPG2 cells than the dimers **9-C7** and **9-C10** (Table 1). Especially the cytotoxicity of the most potent hybrid **10-C7** is very low, which makes it an interesting lead compound.

2.4 Physicochemical properties

The logP value (octanol-water partition coefficient) is a measure of lipophilicity and enables to some degree prediction of permeability across biological membranes *in vitro* and *in vivo*.[33] Therefore, the lipophilicity of the novel hybrid compounds was determined by the using a RP (reversed phase) HPLC method reported earlier.[34] LogP values ranged from 0.78 to 3.28 (Table 1, 4, and 5) and hint to good oral bioavailability.[35] Hybrids containing a phthalyl moiety are more hydrophilic (logP = 0.78 – 1.55) than their naphthyl analogs (logP = 1.54 – 3.28). Not surprisingly, the longer the chain length the greater the lipophilicity. The two tacrine-linked hybrids **10-C7** (logP 2.05) and **10-C10** (logP 3.28) share a similar overall lipophilic molecular skeleton like their phthalyl and naphthyl analogs, even though they possess only one permanently charged nitrogen.

Table 4: Experimentally determined logk` and calculated logP values of selected reference substances.

Reference substance	logk`	logP[36]
Biphenyl	1.08	4.01
Ethylbenzene	0.87	3.15
Chlorobenzene	0.62	2.89
Toluene	0.66	2.73
Benzene	0.41	2.13
2-Phenylethanol	-0.01	1.36
Acetanilide	-0.22	1.00
2-Butanone	-0.35	0.30

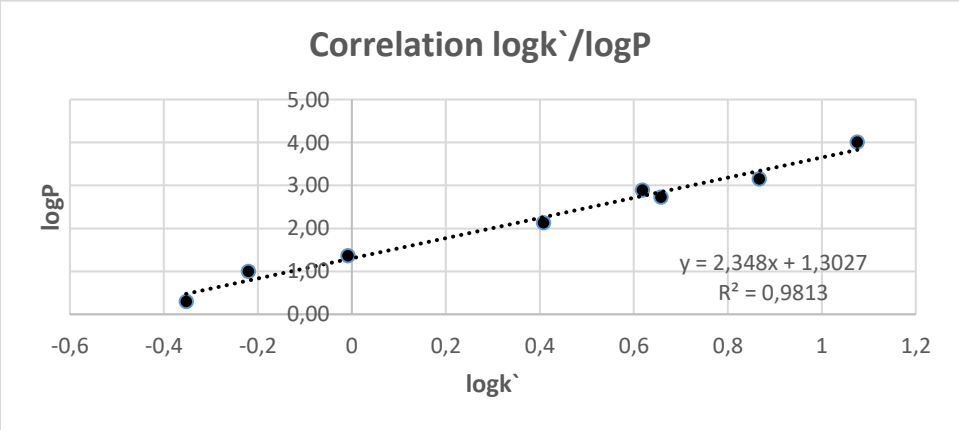

Table 5: Experimentally determined k` and logk` values and calculated logP values of the hybrid compounds.

Compound	k`	logk`	logP
7a-C7	0.60	-0.22	0.79
7a-C8	0.60	-0.22	0.78
7a-C9	0.60	-0.22	0.79
7a-C10	0.61	-0.21	0.80
8a-C4	1.27	0.11	1.55
8a-C6	0.74	-0.13	0.99
8a-C8	0.63	-0.20	0.83
6a-C6	0.63	-0.20	0.84
6b-C6	1.26	0.10	1.54
7b-C7	1.47	0.17	1.70
7b-C8	1.35	0.13	1.61
7b-C9	1.46	0.16	1.69
7b-C10	1.58	0.20	1.77
10-C10	6.96	0.84	3.28
10-C7	2.08	0.32	2.05

2.5 Computational studies

Tacrine and bis-tacrine derivatives belong to the most active inhibitors of AChE, displaying one-digit nanomolar IC_{50} values.[23,37-39] Crystal structures of these ligands in complex with AChE show conserved binding modes of the tacrine pharmacophore in the catalytic active site (CAS).[40-42] This conserved binding mode was also assumed for the tacrine scaffold of **10-C10** as well as for the naphthyl moiety of **7b-C10** and the phthalyl moiety of **7a-C10**, the most promising hybrid derivatives endowed with anticholinesterase activity. Docking studies for these large compounds were performed using a scaffold match constraint to reduce the search space and obtain more consistent poses. The selected representative poses of the three ligands show a similar orientation of the CAS-binding motif and of the iperoxo-motif, which is placed in the peripheral anionic site (PAS) (Figure 5). For **10-C10**, a hydrogen-bond distance of 2.7 Å between the tacrine unit and the His440 backbone is observed; further stabilization might occur through π-π interactions with Trp84 and Phe330 (at 4.5 and 3.5 Å,

respectively; Figure 5a). While the decamethylene linker spans the AChE binding gorge, the quaternary ammonium group is placed at the entrance of the binding site where it is rather solvent exposed. The iperoxo-motif refolds back and is localized in the PAS region. Similar interaction possibilities were found for **7b-C10** and **7a-C10** (Figure 5b).

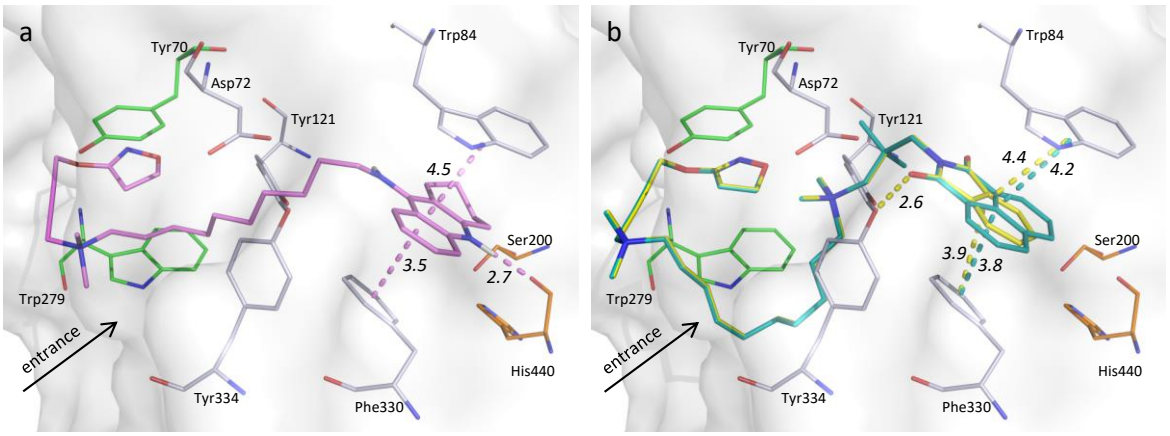

Figure 5: a) Docking solution of **10-C10** (pink), with the interaction distances shown in the CAS (orange) and the iperoxo-motif in the PAS (green). b) Docking solution of **7b-C10** (blue) and **7a-C10** (yellow) with their interaction distances. Distances were measured between the geometric centers of the interacting units and are given in italic numbers, with the unit Å omitted for clarity. The figure was generated with PyMol (The PyMOL Molecular Graphics System, version 1.8.0.5, Schrödinger, LLC).

Besides rather unspecific hydrophobic interactions, a hydrogen bond interaction between one of the carbonyl-oxygens and Tyr334 is observed for **7b-C10** and **7a-C10** (2.6 Å distance in both cases). The extended decamethylene linker protrudes to the enzyme surface. The additional permanently charged nitrogen atom, which represents the major difference between **7b-C10** and **7a-C10** on the one hand and **10-C10** on the other, is placed between Tyr121 and Asp72 in the middle of the AChE gorge (Figure 6).

Given the similar binding modes, the question arises why **7b-C10** shows a remarkably lower affinity than **10-C10**. An obvious hypothesis is that the additional quaternary ammonium group causes this difference, presumably because of a much higher desolvation penalty in comparison to the uncharged alkylene chain. A 3D-RISM analysis carried out with MOE[43] supports this assumption: relevant unfavorable contributions (depicted in red in Figure 7) to the solvation free energy of binding appear around the ammonium group of **7b-C10**, but not in the corresponding area of **10-C10** (Figure 7).

As the docking pose of **7a-C10** and **7b-C10** is virtually identical in the linker region, the same unfavorable contributions of the quaternary nitrogen can be assumed for **7a-C10**.

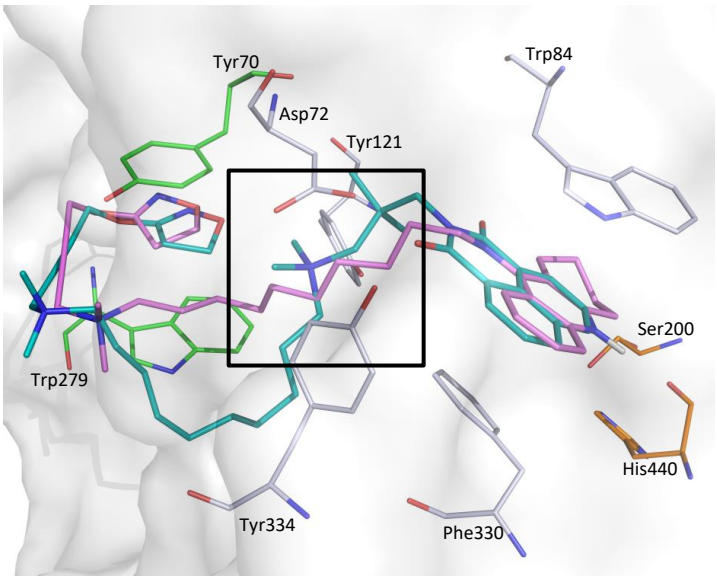

Figure 6: Overlap of the docking solutions of **10-C10** (pink) and **7b-C10** (blue), highlighting the main difference in the linker region (box). The figure was generated with PyMol (The PyMOL Molecular Graphics System, version 1.8.0.5, Schrödinger, LLC).

In addition to this qualitative representation of (de-)solvation contributions to the binding free energy, solvation free energies were calculated with the quantum chemical SMD method for tetramethylammonium and *n*-propane as the two fragment molecules representing the different linkers in **7b-C10** (ammonium) and **10-C10** (alkylene chain).[44] Using *n*-octanol as the dielectric medium mimicking the protein environment, a desolvation free energy of -3.26 kcal/mol was obtained for propane (as expected, propane favors an apolar environment), whereas a value of +0.92 kcal/mol was calculated for tetramethylammonium. Accordingly, a free energy difference of 4.18 kcal/mol (in favor of propane, viz. **10-C10**) may arise due to the different solvation properties. This estimate would be perfectly in line with the affinity difference between **10-C10** and **7b-C10**, which should be around 4.5 kcal/mol based on the difference in IC_{50}.

In summary, although all three ligands are likely to display a similar orientation in the AChE binding site, the extra charge incorporated by the quaternary nitrogen in the linker of **7b-C10** and **7a-C10** appears to be rather unfavorable and is most probably the main reason for the relatively low IC_{50} values of **7b-C10** and **7a-C10** in comparison to **10-C10**.

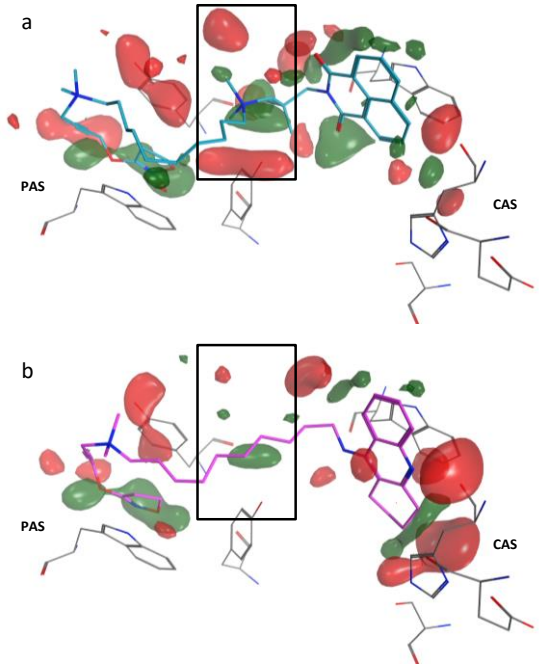

Figure 7: Depiction of 3D-RISM computed $\Delta G_{binding}$ solvation contributions for a) **7b-C10** and b) **10-C10** (red = unfavorable and green = favorable contribution), contoured at an iso-level of 1 kcal/mol Å^3. The figure was generated with MOE 2016.05.

3. Conclusion

In summary, a set of hybrid compounds was investigated which incorporates one moiety (phthalyl, naphthyl, tacrine) that binds to the catalytic active site and another moiety (iperoxo **2**, isox **3**) that addresses the peripheral anionic site of cholinesterases. The two pharmacophoric groups were connected by a polymethylene chain of varying length. The compounds were evaluated for their anticholinesterase activity and the results indicated that both, the nature of the two moieties as well as the length of the alkylene chain are crucial for their potency. Naphthyl-related hybrids (**b** series) were found to be more active than the corresponding W84-related analogs (**a** series). Additionally, the longer the alkylene chain length the higher the observed IC_{50} values. Compounds bearing longer linker length fit better into the binding gorge of the enzyme and therefore result in higher activity. Computational studies supported these experimental findings. The ten-methylene chain exactly covers the distance between PAS and CAS of the cholinesterase, engendering a simultaneous block of the enzyme activity. Notably, the additional quaternary ammonium group in the naphmethonium- and W84-related dual derivatives resulted in an unfavorable higher desolvation penalty in comparison to the uncharged alkylene chain present in the tacrine-related hybrids. In addition, the most potent ChE inhibitors show high affinity to muscarinic M_1 and M_2 receptors and thus have possibly a dual mechanism of action. Moreover, the most potent compound showed a low cytotoxicity.

Structural variations of the hybrid compounds, especially with regard to optimization of the linker, without quaternary ammonium groups in order to obtain tertiary amines, are however, necessary in the light of drug development studies and are in progress.

4. Experimental section

4.1 Chemistry

Melting points were determined on a B540 Büchi apparatus (Flawil, Switzerland) as well as on a Stuart melting point apparatus SMP3 (Bibby Scientific, UK) and are uncorrected. ^{1}H (400.132 MHz) and ^{13}C (100.613 MHz) NMR spectra were recorded on a Bruker AV 400 instrument (Bruker Biospin, Ettlingen, Germany) or on a Varian Mercury 300 (^{1}H, 300.063; ^{13}C, 75.451 MHz) spectrometer (Darmstadt, Germany). As internal standard, the signals of the deuterated solvents were used (DMSO-d_6: ^{1}H 2.50 ppm, ^{13}C 39.52 ppm; $CDCl_3$: ^{1}H 7.26 ppm, ^{13}C 77.16 ppm). Abbreviation for data quoted are: s, singlet; d, doublet; t, triplet; q, quartet; m, multiplet; b, broad; dd, doublet of doublets; dt, doublet of triplets; tt, triplet of triplets; tq, triplet of quartets. Coupling constants (*J*) are given in Hz. TLC analyses were performed on commercial silica gel 60 F_{254} aluminum sheets and on pre-coated TLC-plates Alox-25/UV_{254} (Macherey-Nagel, Düren, Germany); spots were further evidenced by spraying with a dilute alkaline potassium permanganate solution and with Dragendorff reagent,[45,46] for tertiary amines. For column chromatography, silica gel 60, 230-400 mesh (Merck, Darmstadt, Germany) and aluminium oxide 90 basic (Macherey Nagel, Düren, Germany) was used. Column chromatography was also performed on an Interchim Puri Flash 430 (Ultra Performance Flash Purification) instrument (Montluçon, France) connected to an Interchim Flash ELSD. Used columns are: Silica 25 g – 30 µm, Alox-B 40 g – 32/63 µm, Alox-B 25 g – 32/63 µm (Interchim, Montluçon, France). ESI mass spectra of the compounds were obtained on an Agilent LC/MSD Trap G2445D instrument (Waldbronn, Germany) and on a Varian 320 LC-MS/MS instrument (Darmstadt, Germany). Data are reported as mass-to-charge ratio (*m/z*) of the corresponding positively charged molecular ions. Microwave supported reactions were carried out on a MLS-rotaPREP instrument (Milestone, Leutkirch, Germany). Chemicals were of analytical grade and purchased from Aldrich (Steinheim, Germany), Merck (Darmstadt, Germany), PerkinElmer Life Sciences (Homburg, Germany) and Sigma Chemicals (München, Germany). The purity of final compounds **7a-C9**, **7a-C10**, **8a-C4**, **8a-C8**, **7b-C9**, and **7b-C10** was determined using an Agilent Technologies 1220 Infinity LC HPLC instrument (Waldbronn, Germany). The HPLC analyses were performed on a LiChrosher® 100 RP-8 analytical column (250 x 4.6 mm; 5.0 µm; Bischoff). The injection volume of the sample was 10 µL. The mobile phase consisted of (A) 50 mM potassium

phosphate buffer (pH 3) and (B) acetonitrile (A/B 30:70) and was isocratically delivered at a flow rate of 1 ml/min. All final compounds tested for biological activity showed ≥ 95% purity (detection by UV absorption at 210 nm). Purities of target compounds **10-C7** and **10-C10** were determined using capillary electrophoresis and were found to be ≥ 95%. The CE measurements were performed by means of a Beckman Coulter P/ACE System MDQ (Fullerton, CA, USA), equipped with a diode array detector measuring at wavelengths of 210 nm and 254 nm. A fused silica capillary (effective length 50.0 cm, total length 60.2 cm, inner diameter 50 µm) was used for the separation. A new capillary was conditioned by rinsing for 30 min with 0.1 mol/L NaOH, 2 min with H_2O, 10 min with 0.1 mol/L HCl and 2 min with H_2O. Before each run the capillary was rinsed for 2 min with H_2O and 5 min with the running buffer. All rinsing steps were performed with a pressure of 30.0 psi. The samples were injected with a pressure of 0.5 psi for 5.0 s at the anodic side of the capillary. The capillary was kept at 25 °C and a voltage of +25 kV was applied. A 50 mM aqueous sodium borate, pH 10.5, was prepared as running buffer, using ultrapure Milli-Q water (Millipore, Milford, MA, USA). The aqueous solutions were filtered through a 0.22 µm pore-size CME (cellulose mix ester) filter (Carl Roth GmbH, Karlsruhe, Germany).

Tacrine **1**[24], the two bistacrines **9-C7**/**C10**[23], phthalimidopropylamine **11a**[19], naphthalimidopropylamine **11b**[19], Δ^2-isoxazolinyl tertiary base **2**[17,20], isoxazole tertiary amine **3**[19,20], and the bisquaternary ligands **7a-C7**, **6a-C6**, **6b-C6**, **7b-C7**[18], **7a-C8**, **7b-C8**[22], and **8a-C6**[19] were prepared according to previously reported procedures. The synthesis of the intermediates **13-C7** and **13-C10** were carried out according to ref[24,25].

4.1.1 General procedure for the synthesis of phthalimido monoquaternary bromides **12a-C4**, **12a-C8**, **12a-C9**, and **12a-C10**

To a stirred solution of phthalimidopropylamine **11a** (1 equiv) in acetonitrile, the suitable alkyl dibromide (10 equiv) was added and the reaction was refluxed for 3 days. After the reaction was completed (TLC monitoring, eluent a: CH_2Cl_2/MeOH = 9:1; eluent b: 0.2 M aqueous KNO_3/MeOH = 2:3), about one-half of the solvent was evaporated under reduced pressure and diethyl ether was added. The solvent was decanted off and the residue was repeatedly washed with diethyl ether providing the desired monoquaternary intermediates.

4-Bromo-N-[3-(1,3-dioxoisoindolin-2-yl)propyl]-N,N-dimethylbutan-1-aminium bromide ***12a-C4***

Phthalimidopropylamine **11a** (1.00 g, 4.31 mmol) and 1,4-dibromobutane **12-C4** (5.1 mL, 43.1 mmol) in acetonitrile (15 mL) were used as reactants to give **12a-C4** (1.12 g, 57% yield).

Compound **12a-C4**: Brownish solid (from 2-propanol/diethyl ether); mp 178-181 °C; R_f = 0.52 (SiO_2, 0.2 M aqueous KNO_3/MeOH = 2:3); ^{1}H NMR ($CDCl_3$): δ 1.83-2.06 (m, 4H, $^+$N-CH_2-C**H₂**-C**H₂**), 2.18-2.38 (m, 2H, N_{pht}-CH_2-C**H₂**), 3.22-3.53 (m, 2H, C**H₂**-Br), 3.42 (s, 6H, $^+$N(C**H₃**)$_2$), 3.61-3.73 (m, 2H, C**H₂**-N$^+$), 3.74-3.82 (m, 2H, $^+$N-C**H₂**), 3.86 (t, 2H, N_{pht}-C**H₂**, *J* = 6.6), 7.63-7.78 (m, 2H, arom.), 7.79-7.87 (m, 2H, arom.). ^{13}C NMR ($CDCl_3$): δ 21.6, 22.8, 29.1, 33.2, 35.2, 51.6 (2C), 61.8, 63.3, 123.6 (2C), 131.9 (2C), 134.5 (2C), 168.4 (2C). MS (ESI) *m/z* [M]$^+$ Calcd for $C_{17}H_{24}BrN_2O_2^+$: 367.1 Found: 367.1.

4-Bromo-N-[3-(1,3-dioxoisoindolin-2-yl)propyl]-N,N-dimethylbutan-1-aminium bromide ***12a-C8***

Phthalimidopropylamine **11a** (1.00 g, 4.31 mmol) and 1,8-dibromooctane **12-C8** (7.9 mL, 43.1 mmol) in acetonitrile (15 mL) were used as reactants to give **12a-C8** (1.48 g, 68% yield).

Compound **12a-C8**: White solid (from 2-propanol/diethyl ether); mp 149-153 °C; R_f = 0.66 (SiO_2, 0.2 M aqueous KNO_3/MeOH = 2:3); ^{1}H NMR ($CDCl_3$): δ 1.12-1.28 (m, 8H, $^+$N-CH_2-CH_2-C**H₂**-C**H₂**-C**H₂**-C**H₂**), 1.61-1.65 (m, 2H, $^+$N-CH_2-C**H₂**), 1.67-1.72 (m, 2H, C**H₂**-CH_2-Br), 2.10-2.18 (m, 2H, N_{pht}-CH_2-C**H₂**), 3.27 (t, 2H, C**H₂**-Br, *J* = 6.6), 3.31 (s, 6H, $^+$N(C**H₃**)$_2$), 3.45-3.51 (m, 2H, $^+$N-C**H₂**), 3.58-3.65 (m, 2H, C**H₂**-N$^+$), 3.71 (t, N_{pht}-C**H₂**, *J* = 6.3), 7.59-7.63 (m, 2H, arom.), 7.66-7.69 (m, 2H, arom.). ^{13}C NMR ($CDCl_3$): δ 22.6, 22.9, 26.2, 28.0, 28.5, 29.1, 32.7, 34.3, 35.1, 51.5 (2C), 61.5, 64.5, 123.6 (2C), 131.9 (2C), 134.5 (2C), 168.3 (2C). MS (ESI) *m/z* [M]$^+$ Calcd for $C_{21}H_{32}BrN_2O_2^+$: 423.2 Found: 423.2.

9-Bromo-N-[3-(1,3-dioxoisoindolin-2-yl)propyl]-N,N-dimethylnonan-1-aminium bromide ***12a-C9***

Phthalimidopropylamine **11a** (180 mg, 0.78 mmol) and 1,9-dibromononane **12-C9** (1.6 mL, 7.75 mmol) in acetonitrile (12 mL) were used as reactants to give **12a-C9** (394 mg, 98% yield).

Compound **12a-C9**: Yellow foamy solid; R_f = 0.47 (SiO_2, CH_2Cl_2/MeOH = 9:1); ^{1}H NMR ($CDCl_3$): δ 1.17-1.29 (m, 10H, $^+$N-CH_2-CH_2-C**H₂**-C**H₂**-C**H₂**-C**H₂**-C**H₂**), 1.55-1.68 (m, 2H, $^+$N-CH_2-C**H₂**), 1.68-1.77 (m, 2H, C**H₂**-CH_2-Br), 2.13-2.18 (m, 2H, N_{pht}-CH_2-C**H₂**), 3.30 (t, 2H, C**H₂**-Br, *J* = 6.6), 3.34 (s, 6H, $^+$N(C**H₃**)$_2$), 3.46-3.51 (m, 2H, $^+$N-C**H₂**), 3.62-3.67 (m, 2H, C**H₂**-N$^+$), 3.73 (t, 2H, N_{pht}-C**H₂**, *J* = 6.6), 7.62-7.66 (m, 2H, arom.), 7.67-7.71 (m, 2H, arom.). ^{13}C NMR ($CDCl_3$): δ 22.7, 23.0, 26.3, 28.2, 28.7, 29.2, 29.3, 32.9, 34.4, 35.2, 51.5 (2C), 61.5, 64.5, 123.6 (2C), 131.9 (2C), 134.5 (2C), 168.4 (2C). MS (ESI) *m/z* [M]$^+$ Calcd for $C_{22}H_{34}BrN_2O_2^+$: 437.2 Found: 437.2.

10-Bromo-N-[3-(1,3-dioxoisoindolin-2-yl)propyl]-N,N-dimethyldecan-1-aminium bromide ***12a-C10***

Phthalimidopropylamine **11a** (223 mg, 0.96 mmol) and 1,10-dibromodecane **12-C10** (2.2 mL, 9.60 mmol) in acetonitrile (12 mL) were used as reactants to give **12a-C10** (445 mg, 87% yield).

Compound **12a-C10**: Yellow foamy solid; R_f = 0.39 (SiO_2, CH_2Cl_2/MeOH = 9:1); ^{1}H NMR ($CDCl_3$): δ 1.26-1.39 (m, 12H, $^+$N-CH_2-CH_2-C**H₂**-C**H₂**-C**H₂**-C**H₂**-C**H₂**-C**H₂**), 1.62-1.73 (m, 2H, $^+$N-CH_2-C**H₂**), 1.75-1.85 (m, 2H, C**H₂**-CH_2-Br), 2.16-2.26 (m, 2H, N_{pht}-CH_2-C**H₂**), 3.37 (t, 2H, C**H₂**-Br, *J* = 6.9), 3.41 (s, 6H, $^+$N(C**H₃**)$_2$), 3.49-3.55 (m, 2H, $^+$N-C**H₂**), 3.65-3.71 (m, 2H, C**H₂**-N^+), 3.80 (t, 2H, N_{pht}-C**H₂**, *J* = 6.6), 7.68-7.72 (m, 2H, arom.), 7.75-7.79 (m, 2H, arom.). ^{13}C NMR ($CDCl_3$): δ 22.7, 23.0, 26.4, 28.3, 28.8, 29.3, 29.4 (2C), 33.0, 34.4, 35.2, 51.6 (2C), 61.6, 64.6, 123.7 (2C), 132.0 (2C), 134.6 (2C), 168.4 (2C). MS (ESI) *m/z* $[M]^+$ Calcd for $C_{23}H_{36}BrN_2O_2^+$: 451.2 Found: 451.2.

4.1.2 General procedure for the synthesis of 1,8-Naphthalimido monoquaternary bromides **12b-C9** and **12b-C10**

To a stirred solution of 1,8-naphthalimidopropylamine **11b** (1 equiv) in acetonitrile, the suitable alkyl dibromide (10 equiv) was added and the reaction was refluxed for 5 days. After the reaction was completed (TLC monitoring, eluent a: CH_2Cl_2/MeOH = 9:1; eluent b: 0.2 M aqueous KNO_3/MeOH = 2:3), about one-half of the solvent was evaporated under reduced pressure and diethyl ether was added. The solvent was decanted off and the residue was repeatedly washed with diethyl ether providing the desired monoquaternary intermediates.

9-Bromo-N-[3-(1,3-dioxo-1H-benzo[de]isoquinolin-2(3H)-yl)-2,2-dimethylpropyl]-N,N-dimethylnonan-1-aminium bromide ***12b-C9***

1,8-Naphthalimidopropylamine **11b** (180 mg, 0.58 mmol) and 1,9-dibromononane **12-C9** (1.2 mL, 5.80 mmol) in acetonitrile (12 mL) were used as reactants to give **12b-C9** (335 mg, 97% yield).

Compound **12b-C9**: White solid (from diethyl ether); mp 143 °C; R_f = 0.42 (SiO_2, CH_2Cl_2/MeOH = 9:1); ^{1}H NMR (CD_3OD): δ 1.32-1.58 (m, 10H, $^+$N-CH_2-CH_2-C**H₂**-C**H₂**-C**H₂**-C**H₂**-C**H₂**), 1.38 (s, 6H, C(C**H₃**)$_2$), 1.78-1.85 (m, 4H, $^+$N-CH_2-C**H₂**-$(CH_2)_5$-C**H₂**), 3.34 (s, 6H, $^+$N(C**H₃**)$_2$), 3.40 (t, 2H, C**H₂**-Br, *J* = 6.6), 3.49-3.52 (m, 2H, $^+$N-C**H₂**), 3.55 (s, 2H, C**H₂**-N^+), 4.21 (s, 2H, N_{napht}-C**H₂**), 7.71 (t, 2H, arom., *J* = 7.4), 8.23 (d, 2H, arom., *J* = 8.3), 8.38 (d, 2H, arom., *J* = 7.2). ^{13}C NMR (CD_3OD): δ 22.8, 25.5 (2C), 26.2, 28.0, 28.5, 29.0, 29.1, 32.8 (2C),

33.6, 39.3, 52.3 (2C), 68.8, 72.5, 122.1 (2C), 127.1, 127.8, 131.3 (2C), 131.7 (2C), 134.6 (2C), 165.2 (2C). MS (ESI) *m/z* $[M]^+$ Calcd for $C_{28}H_{40}BrN_2O_2^+$: 517.2 Found: 517.2.

10-Bromo-N-[3-(1,3-dioxo-1H-benzo[de]isoquinolin-2(3H)-yl)-2,2-dimethylpropyl]-N,N-dimethyldecan-1-aminium bromide ***12b-C10***

1,8-Naphthalimidopropylamine **11b** (200 mg, 0.64 mmol) and 1,10-dibromodecane **12-C10** (1.5 mL, 6.44 mmol) in acetonitrile (12 mL) were used as reactants to give **12b-C10** (240 mg, 61% yield).

Compound **12b-C10**: Brownish solid (from diethyl ether); mp 145 °C; R_f = 0.67 (SiO_2, CH_2Cl_2/MeOH = 9:1); ^{1}H NMR ($CDCl_3$): δ 1.19 (s, 6H, C(C**H$_3$**)$_2$), 1.26-1.37 (m, 12H, $^+$N-CH_2-CH_2-C**H$_2$**-C**H$_2$**-C**H$_2$**-C**H$_2$**-C**H$_2$**-CH_2), 1.70-1.79 (m, 4H, $^+$N-CH_2-C**H$_2$**-$(CH_2)_6$-C**H$_2$**), 3.31 (t, 2H, C**H$_2$**-Br, *J* = 6.9), 3.54 (s, 6H, $^+$N(C**H$_3$**)$_2$), 3.65 (s, 2H, C**H$_2$**-N^+), 3.71-3.76 (m, 2H, $^+$N-C**H$_2$**), 4.28 (s, 2H, N_{napht}-C**H$_2$**), 7.69 (t, 2H, arom., *J* = 7.7), 8.19 (d, 2H, arom., *J* = 8.3), 8.45 (d, 2H, arom., *J* = 7.4). ^{13}C NMR ($CDCl_3$): δ 23.4, 26.4, 26.8 (2C), 28.3, 28.8, 29.4 (2C), 32.9, 34.4 (2C), 39.4, 48.3, 53.2 (2C), 68.4, 72.1, 122.2 (2C), 127.3 (2C), 128.2, 131.7, 132.0 (2C), 134.8 (2C), 165.3 (2C). MS (ESI) *m/z* $[M]^+$ Calcd for $C_{29}H_{42}BrN_2O_2^+$: 529.2 Found: 529.2.

4.1.3 General procedure for the synthesis of phthal-isox-hybrids **8a-C4** and **8a-C8**

To a stirred solution of the bromo intermediate (1 equiv) in acetonitrile, the isoxazole tertiary amine **3** (1.5 equiv) was added and the reaction was refluxed for 2 days. After the reaction was completed (TLC monitoring, eluent 0.2 M aqueous KNO_3/MeOH = 2:3), about one-half of the solvent was evaporated under reduced pressure and the residual solid obtained was collected by filtration and purified through crystallization providing the desired target compounds.

N^1-(3-(1,3-Dioxoisoindolin-2-yl)propyl)-N^4-(4-(isoxazol-3-yloxy)but-2-yn-1-yl)-N^1,N^1,N^4,N^4-tetramethylbutane-1,4-diaminium bromide ***8a-C4***

N-(4-Bromo-butyl)-phthalimidopropyl-dimethylammonium bromide **12a-C4** (1.00 g, 2.23 mmol) and tertiary amine **3** (603 mg, 3.35 mmol) in acetonitrile (20 mL) were used as reactants to give **8a-C4** (743 mg, 53% yield).

Compound **8a-C4**: Colorless solid (from 2-propanol/diethyl ether); mp 193-195 °C; R_f = 0.4 (SiO_2, 0.2 M aqueous KNO_3/MeOH = 2:3); ^{1}H NMR (CD_3OD): δ 1.83-1.92 (m, 4H, $^+$N-CH_2-C**H$_2$**-C**H$_2$**-CH_2-N^+), 2.16-2.27 (m, 2H, N_{pht}-CH_2-C**H$_2$**), 3.13 (s, 6H, $^+$N(C**H$_3$**)$_2$), 3.19 (s, 6H,

$^{+}$N(C**H$_3$**)$_2$), 3.42-3.57 (m, 6H, N_{pht}-CH_2-CH_2-C**H$_2$**-N^+-C**H$_2$**-CH_2-CH_2-C**H$_2$**-N^+), 3.82 (t, 2H, N_{pht}-C**H$_2$**, *J* = 6.3), 4.43 (s, 2H, $^{+}$N-C**H$_2$**-C≡), 5.06 (s, 2H, ≡C-C**H$_2$**-O), 6.18 (d, 1H, **H**-4_{isox}, *J* = 1.7), 7.81-7.89 (m, 4H, arom.), 8.44 (s, 1H, **H**-5_{isox}, *J* = 1.7). ^{13}C NMR (CD_3OD): *δ* 19.4, 19.6, 22.0, 34.6, 50.0 (4C), 54.2, 57.2, 62.1, 63.0, 63.2, 75.2, 86.7, 95.7, 122.9 (2C), 131.9 (2C), 134.1 (2C), 161.3, 168.4 (2C), 170.8. MS (ESI) *m/z* $[M]^+$ Calcd for $C_{26}H_{36}BrN_4O_4^+$: 549.2 Found: 549.2.

N^1-(3-(1,3-Dioxoisoindolin-2-yl)propyl)-N^8-(4-(isoxazol-3-yloxy)but-2-yn-1-yl)-N^1,N^1,N^8,N^8-tetramethyloctane-1,8-diaminium bromide ***8a-C8***

N-(8-Bromo-octyl)-phthalimidopropyl-dimethylammonium bromide **12a-C8** (1.00 g, 1.98 mmol) and tertiary amine **3** (536 mg, 2.97 mmol) in acetonitrile (20 mL) were used as reactants to give **8a-C8** (854 mg, 63% yield).

Compound **8a-C8**: White solid (from 2-propanol/diethyl ether); mp 190-191 °C; R_f = 0.42 (SiO_2, 0.2 M aqueous KNO_3/MeOH = 2:3); ^{1}H NMR (CD_3OD): *δ* 1.36-1.44 (m, 8H, $^{+}$N-CH_2-CH_2-C**H$_2$**-C**H$_2$**-C**H$_2$**-C**H$_2$**), 1.73-1.85 (m, 4H, $^{+}$N-CH_2-**CH_2**-$(CH_2)_4$-**CH_2**-CH_2-N^+), 2.15-2.25 (m, 2H, N_{pht}-CH_2-C**H$_2$**), 3.14 (s, 6H, $^{+}$N(C**H$_3$**)$_2$), 3.22 (s, 6H, $^{+}$N(C**H$_3$**)$_2$), 3.36-3.41 (m, 2H, $^{+}$N-C**H$_2$**-$(CH_2)_7$), 3.46-3.51 (m, 4H, C**H$_2$**-$^{+}$N-$(CH_2)_7$-C**H$_2$**-N^+), 3.81 (t, 2H, N_{pht}-C**H$_2$**, *J* = 6.6), 4.49 (s, 2H, $^{+}$N-C**H$_2$**-C≡), 5.06 (s, 2H, ≡C-C**H$_2$**-O), 6.21 (d, 1H, **H**-4_{isox}, *J* = 1.4), 7.80-7.88 (m, 4H, arom.), 8.48 (s, 1H, **H**-5_{isox}, *J* = 1.4). ^{13}C NMR (CD_3OD): *δ* 22.2, 22.3, 22.4, 24.2, 25.8, 25.9, 28.5, 34.7, 50.1 (4C), 53.9, 57.3, 63.6, 64.2, 64.4, 75.7, 86.6, 95.9, 123.1 (2C), 132.2 (2C), 134.4 (2C), 161.5, 168.6 (2C), 171.0. MS (ESI) *m/z* $[M]^+$ Calcd for $C_{30}H_{44}BrN_4O_4^+$: 603.3 Found: 603.3.

4.1.4 General procedure for the synthesis of phthal-iper-hybrids **7a-C9** and **7a-C10**

To a stirred solution of the bromo intermediate (1 equiv) in acetonitrile, the Δ^2-isoxazolinyl tertiary amine **2** (1.5 equiv) was added and the reaction was refluxed for 5 days. After the reaction was completed (TLC monitoring, eluent 0.2 M aqueous KNO_3/MeOH = 2:3), about one-half of the solvent was evaporated under reduced pressure and diethyl ether (5 mL) was added. The solvent was decanted off and the residue was repeatedly washed with diethyl ether providing the desired target compounds.

*N^1-(4-((4,5-Dihydroisoxazol-3-yl)oxy)but-2-yn-1-yl)-N^9-(3-(1,3-dioxoisoindolin-2-yl)propyl)-N^1,N^1,N^9,N^9-tetramethylnonane-1,9-diaminium bromide **7a-C9***

N-(9-Bromo-nonyl)-phthalimidopropyl-dimethylammonium bromide **12a-C9** (330 mg, 0.64 mmol) and tertiary amine **2** (174 mg, 0.95 mmol) in acetonitrile (10 mL) were used as reactants to give **7a-C9** (405 mg, 91% yield).

Compound **7a-C9**: Yellow, very hygroscopic solid (from diethyl ether); R_f = 0.4 (SiO_2, CH_2Cl_2/MeOH = 8:2); ^{1}H NMR (CD_3OD): δ 1.31-1.44 (m, 10H, $^+$N-CH_2-CH_2-C**H₂**-C**H₂**-C**H₂**-C**H₂**-C**H₂**), 1.70-1.88 (m, 4H, $^+$N-CH_2-C**H₂**-$(CH_2)_5$-C**H**$_2$), 2.15-2.25 (m, 2H, N_{pht}-CH_2-C**H₂**), 3.03 (t, 2H, **H**-$4_{2\text{-isox}}$, *J* = 9.6), 3.13 (s, 6H, $^+$N(C**H₃**)$_2$), 3.24 (s, 6H, $^+$N(C**H₃**)$_2$), 3.34-3.40 (m, 2H, $^+$N-C**H₂**-$(CH_2)_8$), 3.45-3.54 (m, 4H, C**H₂**-$^+$N-$(CH_2)_8$-C**H₂**-N^+), 3.81 (t, 2H, N_{pht}-C**H₂**, *J* = 6.6), 4.39 (t, 2H, **H**-$5_{2\text{-isox}}$, *J* = 9.6), 4.50 (s, 2H, $^+$N-C**H₂**-C≡), 4.92 (s, 2H, ≡C-C**H₂**-O), 7.81-7.89 (m, 4H, arom.). ^{13}C NMR (CD_3OD): δ 22.2, 22.4, 22.5, 26.0 (2C), 28.7, 28.9, 32.6 (2C), 34.8, 50.1 (4C), 54.1, 57.3, 61.7, 64.3 (2C), 70.1, 75.6, 86.5, 123.1 (2C), 132.2 (2C), 134.4 (2C), 167.5, 168.6 (2C). MS (ESI) *m/z* $[M]^{2+}$ Calcd for $C_{31}H_{48}N_4O_4^{2+}$: 270.2 Found: 270.0.

*N^1-(4-((4,5-Dihydroisoxazol-3-yl)oxy)but-2-yn-1-yl)-N^{10}-(3-(1,3-dioxoisoindolin-2-yl)propyl)-N^1,N^1,N^{10},N^{10}-tetramethyldecane-1,10-diaminium bromide **7a-C10***

N-(10-Bromo-decyl)-phthalimidopropyl-dimethylammonium bromide **12a-C10** (420 mg, 0.79 mmol) and tertiary amine **2** (216 mg, 1.20 mmol) in acetonitrile (8 mL) were used as reactants to give **7a-C10** (496 mg, 88% yield).

Compound **7a-C10**: Brownish, very hygroscopic solid (from diethyl ether); R_f = 0.3 (SiO_2, CH_2Cl_2/MeOH = 9:1). ^{1}H-NMR (CD_3OD): δ 1.32-1.44 (m, 12H, $^+$N-CH_2-CH_2-C**H₂**-C**H₂**-C**H₂**-C**H₂**-C**H₂**-C**H₂**), 1.70-1.86 (m, 4H, $^+$N-CH_2-C**H₂**-$(CH_2)_6$-C**H**$_2$), 2.16-2.26 (m, 2H, N_{pht}-CH_2-C**H₂**), 3.03 (t, 2H, **H**-$4_{2\text{-isox}}$, *J* = 9.6), 3.14 (s, 6H, $^+$N(C**H₃**)$_2$), 3.25 (s, 6H, $^+$N(C**H₃**)$_2$), 3.33-3.38 (m, 2H, $^+$N-C**H₂**-$(CH_2)_9$), 3.41-3.50 (m, 4H, C**H₂**-$^+$N-$(CH_2)_9$-C**H₂**-N^+), 3.81 (t, 2H, N_{pht}-C**H₂**, *J* = 6.3), 4.39 (t, 2H, **H**-$5_{2\text{-isox}}$, *J* = 9.6), 4.51 (s, 2H, $^+$N-C**H₂**-C≡), 4.92 (s, 2H, ≡C-C**H₂**-O), 7.81-7.88 (m, 4H, arom.). ^{13}C NMR (CD_3OD): δ 22.2, 22.4, 22.6, 26.1, 26.2, 28.9, 28.9, 29.1, 32.6 (2C), 34.8, 50.2 (2C), 50.4 (2C), 54.1, 57.3, 61.7, 64.4, 64.5, 70.1, 75.7, 86.4, 123.2 (2C), 132.2 (2C), 134.5 (2C), 167.5, 168.7 (2C). MS (ESI) *m/z* $[M]^{2+}$ Calcd for $C_{32}H_{50}N_4O_4^{2+}$: 277.2 Found: 277.0.

4.1.5 General procedure for the synthesis of naphthal-iper-hybrids **7b-C9** and **7b-C10**

To a stirred solution of bromo intermediate (1 equiv) in acetonitrile, Δ^2-isoxazolinyl tertiary amine **2** (1.5 equiv) was added and the reaction was refluxed for 3 days. After the reaction was completed (TLC monitoring, eluent 0.2 M aqueous KNO_3/MeOH = 2:3), about one-half of the solvent was evaporated under reduced pressure and diethyl ether was added. The solvent was decanted off and the residue was repeatedly washed with diethyl ether providing the desired target compounds.

N^1-(4-((4,5-Dihydroisoxazol-3-yl)oxy)but-2-yn-1-yl)-N^9-(3-(1,3-dioxo-1H-benzo[de]isoquinolin-2(3H)-yl)-2,2-dimethylpropyl)-N^1,N^1,N^9,N^9-tetramethylnonane-1,9-diaminium bromide ***7b-C9***

N-(9-Bromo-nonyl)-1,8-naphthalimidopropyl-dimethylammonium bromide **12b-C9** (242 mg, 0.41 mmol) and tertiary amine **2** (111 mg, 0.61 mmol) in acetonitrile (3 mL) were used as reactants to give **7b-C9** (300 mg, 95% yield).

Compound **7b-C9**: Yellow solid; mp 185 °C; R_f = 0.59 (SiO_2, CH_2Cl_2/MeOH = 9:1); ^{1}H NMR (CD_3OD): δ 1.32 (s, 6H, C(C**H₃**)$_2$), 1.36-1.46 (m, 10H, $^+$N-CH_2-CH_2-C**H₂**-C**H₂**-C**H₂**-C**H₂**-C**H₂**), 1.74-1.82 (m, 4H, $^+$N-CH_2-C**H₂**-$(CH_2)_5$-C**H**$_2$), 3.01 (t, 2H, **H**-$4_{2\text{-isox}}$, *J* = 9.6), 3.24 (s, 6H, $^+$N(C**H₃**)$_2$), 3.33 (s, 6H, $^+$N(C**H₃**)$_2$), 3.48-3.54 (m, 4H, $^+$N-C**H₂**-$(CH_2)_7$-C**H₂**-N^+), 3.56 (s, 2H, C**H₂**-N^+), 4.25 (s, 2H, N_{napht}-C**H₂**), 4.37 (t, 2H, **H**-$5_{2\text{-isox}}$, *J* = 9.6), 4.50 (s, 2H, $^+$N-C**H₂**-C≡), 4.90 (s, 2H, ≡C-C**H₂**-O), 7.77 (t, 2H, arom., *J* = 7.7), 8.31 (d, 2H, arom., *J* = 8.3), 8.45 (d, 2H, arom., *J* = 7.2). ^{13}C NMR (CD_3OD): δ 22.5, 22.8, 25.5, 26.0, 26.1, 28.7, 28.8, 28.9, 32.6 (2C), 39.4, 50.1 (2C), 52.2 (2C), 54.1, 57.3, 64.3, 68.8 (2C), 70.1, 72.6, 75.6, 86.5, 122.2 (2C), 127.1 (2C), 127.9, 131.3 (2C), 131.8, 134.6 (2C), 165.4 (2C), 167.5. MS (ESI) *m/z* $[M]^{2+}$ Calcd for $C_{37}H_{54}N_4O_4^{2+}$: 309.2 Found: 309.2.

N^1-(4-((4,5-Dihydroisoxazol-3-yl)oxy)but-2-yn-1-yl)-N^{10}-(3-(1,3-dioxo-1H-benzo[de]isoquinolin-2(3H)-yl)-2,2-dimethylpropyl)-N^1,N^1,N^{10},N^{10}-tetramethyldecane-1,10-diaminium bromide ***7b-C10***

N-(10-Bromo-decyl)-1,8-naphthalimidopropyl-dimethylammonium bromide **12b-C10** (175 mg, 0.29 mmol) and tertiary amine **2** (78 mg, 0.43 mmol) in acetonitrile (6 mL) were used as reactants to give **7b-C10** (211 mg, 93% yield).

Compound **7b-C10**: Brownish solid; mp 186 °C; R_f = 0.2 (SiO_2, CH_2Cl_2/MeOH = 9:1); ^{1}H NMR (CD_3OD): δ 1.33 (s, 6H, C(C**H₃**)$_2$), 1.37-1.46 (m, 12H, $^+$N-CH_2-CH_2-C**H₂**-C**H₂**-C**H₂**-C**H₂**-C**H₂**-C**H₂**), 1.77-1.85 (m, 4H, $^+$N-CH_2-C**H₂**-$(CH_2)_6$-C**H**$_2$), 3.01 (t, 2H, **H**-$4_{2\text{-isox}}$, *J* = 9.6), 3.21 (s,

6H, $^{+}N(CH_3)_2$), 3.31 (s, 6H, $^{+}N(CH_3)_2$), 3.45-3.51 (m, 4H, ^{+}N-CH_2-$(CH_2)_8$-CH_2-N^{+}), 3.55 (s, 2H, CH_2-N^{+}), 4.28 (s, 2H, N_{napht}-CH_2), 4.38 (t, 2H, **H**-$5_{2\text{-isox}}$, J = 9.6), 4.46 (s, 2H, ^{+}N-CH_2-C≡), 4.90 (s, 2H, ≡C-CH_2-O), 7.81 (t, 2H, arom., J = 8.0), 8.35 (d, 2H, arom., J = 8.3), 8.52 (d, 2H, arom., J = 7.2). ^{13}C NMR (CD_3OD): δ 22.5, 22.8, 25.4, 26.1, 26.2, 28.9, 29.0, 29.1 (2C), 32.5 (2C), 39.3, 50.1 (2C), 52.2 (2C), 54.0, 57.2, 64.3, 68.8 (2C), 70.0, 72.6, 75.5, 86.4, 122.3 (2C), 127.1 (2C), 128.0, 131.4 (2C), 132.0, 134.6 (2C), 165.5 (2C), 167.5. MS (ESI) *m/z* $[M]^{2+}$ Calcd for $C_{38}H_{56}N_4O_4^{2+}$: 316.2 Found: 316.4.

4.1.6 General procedure for the synthesis of the tac-iper-hybrids **10-C7** and **10-C10**

To a solution of given amounts of intermediate bromide in 15 mL of acetonitrile 2 equiv of the Δ^2-isoxazolinyl tertiary amine **2** and a catalytic amount of KI/K_2CO_3 (1:1) were added. The reaction mixture was heated in the microwave (500 W, 80 °C) for 4 h. After cooling to room temperature the surplus of KI/K_2CO_3 was filtered and the filtrate was concentrated *in vacuo*. The residue obtained was purified via column chromatography (Alox, CH_2Cl_2/MeOH = 9:1) providing the target compounds.

*N-(4-((4,5-Dihydroisoxazol-3-yl)oxy)but-2-yn-1-yl)-N,N-dimethyl-7-((1,2,3,4-tetrahydroacridin-9-yl)amino)heptan-1-aminium bromide **10-C7***

N-(7-Bromoheptyl)-1,2,3,4-tetrahydroacridin-9-amine **13-C7** (300 mg, 0.80 mmol) reacted with tertiary amine **2** (291 mg, 1.60 mmol) to obtain the target compound **10-C7** (188 mg, 42% yield).

Compound **10-C7**: Yellowish, hygroscopic solid; R_f = 0.42 (Alox, CH_2Cl_2:MeOH = 9:1); ^{1}H NMR (DMSO): 1.23-1.29 (m, 6H, NH-CH_2-CH_2-CH_2-CH_2-CH_2), 1.54-1.65 (m, 4H, CH_2-CH_2-N^{+}/ NH-CH_2-CH_2), 1.81-1.86 (m, 4H, C2-H_2/C3-H_2), 2.71 (t, 2H, C1-H_2, J = 5.9), 2.90 (t, 2H, C4-H_2, J = 6.2), 2.99 (t, 2H, **H**-$4_{2\text{-isox}}$, J = 9.6), 3.04 (s, 6H, $^{+}N(CH_3)_2$), 3.27-3.34 (m, 2H, CH_2-N^{+}), 3.38-3.43 (m, 2H, NHCH_2), 4.29 (t, 2H, **H**-$5_{2\text{-isox}}$ J = 9.6), 4.41 (br, 2H, ^{+}N-CH_2-C≡), 4.92 (br, 2H, ≡C-CH_2-O), 5.41 (t, 1H, N**H**, J = 6.1), 7.34 (ddd, 1H, C7-**H**, J = 1.3, J = 6.8, J = 8.2), 7.52 (ddd, 1H, C6-**H**, J = 1.3, J = 6.8, J = 8.3), 7.70 (dd, 1H, C5-**H**, J = 1.0, J = 8.4), 8.11 (d, 1H, C8-**H**, J = 8.1). ^{13}C NMR (DMSO): 21.6, 22.4, 22.6, 25.0, 25.5, 26.0, 28.1, 30.4, 32.1, 33.4, 47.8, 49.7, 53.2, 57.1, 63.1, 69.5, 76.0, 85.9, 115.7, 120.1, 122.9, 123.1, 127.8, 128.1, 146.7, 150.3, 157.8, 166.6. MS (ESI) m/z $[M]^{+}$ Calcd for $C_{29}H_{41}N_4O_2^{+}$: 477.3 Found: 477.4.

N-(4-((4,5-Dihydroisoxazol-3-yl)oxy)but-2-yn-1-yl)-N,N-dimethyl-10-((1,2,3,4-tetrahydroacridin-9-yl)amino)decan-1-aminium bromide ***10-C10***

N-(10-Bromodecyl)-1,2,3,4-tetrahydroacridin-9-amine **13-C10** (305 mg, 0.73 mmol) reacted with tertiary amine **1** (266 mg, 1.46 mmol) to obtain the target compound **10-C10** (44.0 mg, 10% yield).

Compound **10-C10**: Brown, hygroscopic solid; R_f = 0.41 (Alox, CH_2Cl_2:MeOH = 9:1); ^{1}H NMR (DMSO): 1.21-1.24 (m, 12H, NH-CH_2-CH_2-C**H$_2$**-C**H$_2$**-C**H$_2$**-C**H$_2$**-C**H$_2$**-C**H$_2$**), 1.51-1.58 (m, 2H, NH-CH_2-C**H$_2$**), 1.62-1.65 (m, 2H, C**H$_2$**-CH_2-N^+), 1.81-1.84 (m, 4H, C2-**H$_2$**/C3-**H$_2$**), 2.70 (t, 2H, C1-**H$_2$**, *J* = 5.9), 2.90 (t, 2H, C4-**H$_2$**, *J* = 6.1), 3.00 (t, 2H, **H**-$4_{2\text{-isox}}$, *J* = 9.6), 3.06 (s, 6H, $^+$N(C**H$_3$**)$_2$), 3.29-3.33 (m, 2H, C**H$_2$**-N^+), 3.38-3.44 (m, 2H, NH-C**H$_2$**), 4.30 (t, 2H, **H**-$5_{2\text{-isox}}$, *J* = 9.6), 4.42 (s, 2H, $^+$N-C**H$_2$**-C≡), 4.93 (s, 2H, ≡C-C**H$_2$**-O), 5.47 (br, 1H, N**H**), 7.34 (ddd, 1H, C7-**H**, *J* = 1.2, *J* = 6.8, *J* = 8.1), 7.51-7.55 (m, 1H, C6-**H**), 7.70 (dd, 1H, C5-**H**, *J* = 1.0, *J* = 8.4), 8.11 (d, 1H, C8-**H**, *J* = 8.1). ^{13}C NMR (DMSO): 21.7, 22.3, 22.6, 24.9, 25.5, 26.1, 28.3, 28.5, 28.6, 28.7, 30.4, 32.1, 33.1, 47.7, 49.7, 53.2, 57.1, 63.1, 69.5, 76.0, 85.9, 115.5, 119.9, 123.0, 123.1, 128.0, 147.2, 150.5, 157.4, 166.6. MS (ESI) m/z $[M]^+$ Calcd for $C_{32}H_{47}N_4O_2^+$: 519.4. Found: 519.5.

4.2 Pharmacology

4.2.1 AChE/BChE inhibition

The determination of IC_{50} values for AChE and BChE inhibition by all the compounds was performed according to the known procedure based on the Ellman assay.[47] AChE (E.C.3.1.1.7, from electric eel) and BChE (E.C.3.1.1.8, from equine serum) were purchased from Sigma Aldrich (Steinheim, Germany). hAChE, (E.C.3.1.1.7, a recombinant expressed in HEK 293 cells) was obtained from Sigma Aldrich (Steinheim, Germany) and hBChE (E.C.3.1.1.8, from human serum) was kindly donated by Dr. Oksana Lockridge (University of Nebraska Medical Center). DTNB (Ellman's reagent), ATC and BTC iodides were obtained from Fluka (Buchs, Switzerland). For buffer preparation, 2.40 g of potassium dihydrogen phosphate were dissolved in 500 ml of water and adjusted with a NaOH-solution (0.1 M) to pH = 8.0. Enzyme solutions were prepared with buffer to give 2.5 units/ml and stabilized with 2 mg albumin bovine (SERVA, Heidelberg, Germany) per ml of enzyme solution. 396 mg of DTNB were dissolved in 100 ml of buffer to give a 10 mM solution (0.3 mM in assay). The stock solutions of the test compounds were prepared either in pure puffer (**1**, **9-C7**, and **9-C10**), in a 50%/50% mixture of buffer/ethanol (**7a-C10**, **8a-C6**, **6b-C6**, **7b-C8**, **7b-C9**, **7b-C10**, **10-C10**, and **10-C7**) or in pure ethanol (**7a-C7**, **7a-C8**, **7a-C9**, **8a-C4**, **8a-C8**, **6a-C6**, **7b-C7**, **13-C7**, and **13-C10**) with a concentration of 33.3 mM (1 mM in assay) and step wise

diluted with ethanol to a concentration of 33.3 nM (1 nM in assay). The highest concentration of the test compounds applied in the assay was 10^{-3} M (the amount of EtOH in the stock solution did not influence enzyme activity in the assay). The assay was performed at 25 °C according to the following procedure: A cuvette containing 1.5 ml of buffer, 50 µL of DTNB solution, 50 µL of the respective enzyme and 50 µL of the test compound solution was incubated for 4.5 min. Then the reaction was started by addition of 10 µL of the substrate solution (ATC/BTC). The solution was mixed immediately and incubated for further 2.5 min. Then the absorption was measured at 412 nm with a Shimadzu UVmini-1240 spectrophotometer (Duisburg, Germany). To measure full enzyme activity, 50 µL of buffer replaced the test compound solution. For determining the blank value, additionally 50 µL of buffer replaced the enzyme solution. Each test compound concentration was measured in triplicate. The enzyme activity in percentage was plotted against the logarithm of the compound concentrations from which the IC_{50} values were calculated by the software GraphPad Prism.

4.2.2 M_2- and M_1-receptor binding measurements

Cell culture and preparation of membranes. Chinese hamster ovary cells (CHO-cells) endowed with the human M_2- or M_1-receptor gene by stable transfection were generously provided by Dr. N. J. Buckley, University of Leeds, U.K.. Cells were cultured and processed as reported earlier.[48] The membrane pellets obtained were washed twice in 20 mM HEPES, 0.1 mM Na_4EDTA, pH 7.4, 4 °C ('storage buffer') and the final pellets were stored as a membrane suspension in storage buffer at -80 °C. The Lowry method was applied to determine protein content which amounted to 3.8 mg/ml membrane suspension.

Binding experiments. [^{3}H]NMS filtration binding experiments were carried out as described previously.[49] In 1.2 ml 96-deep well microplates (Abgene House, Epsom, U.K.), membranes were added to 400 µl of incubation buffer (10 mM HEPES, 10 mM $MgCl_2$, and 100 mM NaCl, pH 7.4, at 30 °C). In [^{3}H]NMS equilibrium binding experiments 0.2 nM [^{3}H]NMS and 25-40 µg protein/ml membranes were applied. Nonspecific [^{3}H]NMS binding was estimated in the presence of 1 µM atropine and did not exceed 5% of total radioligand binding. Under control conditions specific binding of [^{3}H]NMS was characterized by a negative log equilibrium dissociation constant, $\log KD,M_2 = -9.12 \pm 0.10$ and $\log KD,M_1 = -9.42 \pm 0.04$ (mean ± S.E.M., n = 6). In homologous and heterologous competition experiments with [^{3}H]NMS the incubation time amounted to 2 h and 2-4 h, respectively. In order to calculate the incubation time necessary to equilibrate [^{3}H]NMS binding in the presence of an allosteric test compound the following equation was used:

$$t_{0.5_{obs}} = t_{0.5_{off}} \cdot \left(1 + \frac{1}{K_{X,diss}} \cdot [X]\right) \quad (1)$$

$t_{0.5obs}$ is an estimate of [^{3}H]NMS association half-life time in the presence of the allosteric test compound X, $t_{0.5off}$ is the half-life time of [^{3}H]NMS dissociation in the absence of allosteric modulator ($t_{0.5off,M2}$ = 2.1 ± 0.03, means ± S.E.M., n=12; $t_{0.5off,M1}$ = 7.4 ± 0.54, means ± S.E.M., n=12), and $K_{X,diss}$ indicates the modulator concentration at which the half-life time of [^{3}H]NMS dissociation is doubled. Equilibrium was assumed to be reached after 5 x $t_{0.5obs}$.

In dissociation experiments, membranes were incubated with [^{3}H]NMS for 30 minutes (M_2) or 60 minutes (M_1) at 30 °C. Then, aliquots of this mixture were added to excess unlabelled ligand in buffer over a total period of 120 min followed by simultaneous filtration of all samples. In order to determine the effect of the test compounds on the dissociation of [^{3}H]NMS, dissociation was measured by addition of 1 µM atropine in combination with the respective test compounds. Three-point kinetic experiments were performed in analogy to two-point kinetic experiments[50] with measurements of [^{3}H]NMS binding at t) 0,5 t) 5 min and t) 8 min at M_2 and 0,5 t) 14 min and t) 17 min at M_1 receptors.

Receptor bound radioligand was separated by filtration on a Tomtech 96-well Mach III Harvester (Wallac®) using glass fibre filtermats (Filtermat A®, Wallac, Turku, Finland) which had been pretreated with 0.2 % polyethyleneimine (M_2: 0.2%, M_1:0.1%). The filtration was followed by two rapid washing steps (Aqua purificata, at 4 °C) whereafter the filtermats were dried for 3 min at 400 W in a microwave oven. Finally, scintillation wax (Meltilex® A, Wallac, Turku, Finland) was melted for 1 min at 90 °C onto the filtermat using a Dri-Block® DB-2A (Techne, Duxford Cambridge, U.K.). After placing the filters in sample bags (Wallac, Turku, Finland) filter bound radioactivity was measured using a Microbeta Trilux-1450 scintillation counter (Wallac, Turku, Finland).

Data analysis. Computer-aided, non-linear regression analysis using Prism 5.03 (GraphPad Software®, San Diego, CA, U.S.A.) was applied to analyse the binding data from individual experiments. [^{3}H]NMS dissociation data were analysed assuming a monoexponential decay. The ability of the allosteric agents to retard [^{3}H]NMS dissociation were expressed as the % reduction of the apparent rate constant k_{-1} for [^{3}H]NMS dissociation. The concentration-effect curves (CEC) for the reduction of the [^{3}H]NMS dissociation rate constant k_{-1} and of [^{3}H]NMS specific binding by the test compounds were fitted to a four parameter logistic function. The upper plateau was the value of k_{-1} measured in the absence of test compound and was fixed at 100%, whereas the log inflection point ($logIC_{50}$) and slope factors n were set as variables. The bottom plateau was checked whether it, as a variable, yielded a significantly better fit compared with it being fixed at 0%. Finally, we tested whether the slope factors of the curves

were different from unity. In all statistical comparisons an F-test was applied and $P < 0.05$ was chosen as the level of statistical significance. Applying the four parameter logistic function the $logIC_{50}$-values were estimated with n constrained to -1 if the observed slope factors did not differ significantly from unity. The inflection point of a CEC for the retarding action of the test compound on radioligand dissociation stands for an *effect* and thus was designated $logK_{x,diss.}$ In homologous competition binding experiments, the K_D value for the radioligand was calculated according to DeBlasi et al.[51] In heterologous competition binding experiments, performed in parallel under identical experimental conditions with respect to membranes, radioligand-affinity and -concentration, the $logIC_{50}$ values for the hybrid compounds were taken to reflect a model-independent measure of binding affinity and were used for comparisons.

4.3 Cytotoxicity

The compounds to be tested were solubilised and serially diluted in DMSO. 1×10^5 HEPG2 (ATCC) cells/ml were incubated in a volume of 200 µL in 96-well cell culture plates in RPMI medium (Gibco) with 10% FCS (PAA) without phenol red with serial compound dilutions at 37 °C and 5% CO_2 for 72 h. The final concentration of DMSO was 1%. After 24 h of incubation, 10% of an AlamarBlue solution (Trinova) was added. The IC_{50}-value was calculated with the respect to controls without compounds from the absorbance values measured at 550 nm using 630 nm as reference wavelength.

4.4 LogP determination by means of RP HPLC[34]

The partition coefficients of the compounds **7a-C7**, **7a-C8**, **7a-C9**, **7a-C10**, **8a-C4**, **8a-C6**, **8a-C8**, **6a-C6**, **6b-C6**, **7b-C7**, **7b-C8**, **7b-C9**, **7b-C10**, **10-C10**, and **10-C7** were determined by RP chromatography using methanol/phosphate buffer 70:30 as eluent. The phosphate buffer was prepared by dissolving aqueous potassium dihydrogen phosphate solution (0.02 M) and addition of aqueous sodium hydroxide solution (0.1 M) adjusting a pH-value of 7.4. Liquid chromatography was conducted on an Agilent 1100 series system using a C18 reversed-phase (Knauer, Germany) (150 x 4.6 mm) column. The mobile phase (MeOH/phosphate buffer = 70/30) was used at a flow rate of 1.5 ml/min. The chromatographic systems were calibrated with solutes (2-butanon, acetanilide, 2-phenylethanol, benzene, toluene, chlorobenzene, ethylbenzene, biphenyl) for which an experimental octanol/water partition coefficient was available.[36] The testing compounds **7a-C7**, **7a-C8**, **7a-C9**, **7a-C10**, **8a-C4**, **8a-C6**, **8a-C8**, **6a-C6**, **6b-C6**, **7b-C7**, **7b-C8**, **7b-C9**, **7b-C10**, **10-C10**, and **10-C7** were dissolved

in MeOH (100 µg/ml). Experiments were run in triplicate. The peak maxima were measured at 254 nm. Capacity ratio was calculated using the following equation: $k' = (t_r - t_o)/t_o$. t_r is the average retention time of the analyte and t_o is the average retention time of the solvent. A linear regression was performed for the *logk`/logP* data of the reference compounds to obtain a correlation equation ($y = 2.348x + 1.3027$; $R^2 = 0.9813$) which was used for the calculation of the logP values of the compounds (Table 4 and Table 5).

4.5 Computational studies

Docking studies were performed according to a previously developed protocol for bis-tacrine compounds.[39] Briefly, the *Tc*AChE crystal structure with PDB-ID 2CKM was chosen due to its high resolution of 2.15 Å.[40,52] This isoform is complexed with a bis-tacrine ligand; accordingly, the PAS-forming residues Tyr70 and Trp279 show a parallel orientation with the second tacrine unit binding between them in a sandwich-type π-π interaction. This particular orientation of the PAS residues is not present in any hAChE crystal structure known to date. However, a reorientation of the amino acids according to an induced-fit process seems reasonable also for other isoforms of AChE.

Although the inhibition data were obtained with *ee*AChE, a *Tc*AChE crystal structure was used for the docking studies because of the much higher resolution in comparison to the low-resolution (> 4.20 Å) structure of *ee*AChE. Both isoforms show high homologies with respect to the 6AChE (Table 6).

Docking settings were previously reported by Chen *et al*.[39] Briefly, Gold 5.2.2[53,54], was used with 4˙000˙000 as number of operations and the scoring function ASP,[55] generating 50 poses for **7b-C10** and **10-C10**. The protonation of the protein and the ligands was performed at pH = 8, which reflects Ellman assay conditions. Ligand protonation states were calculated using MoKa,[56] which indicated a protonated acridinic nitrogen of the tacrine moiety.

Following the approach of Chen *et al*., a scaffold match constraint was used for docking of **10-C10**.[39] A representative binding pose was identified as top ASP-pose (score: 85.50), which also yielded the best DSX score (─183.41). The scaffold of **7b-C10** was extracted from the second-best pose (ASP) due to its large overlap with the tacrine scaffold. In a docking using this scaffold, the second best ranked ASP-pose (score: 76.71) was also the top-pose in rescoring with DSX (─181.81) and thus chosen as representative binding pose. **7a-C10** was created through a modeling approach by elimination and addition of the required atoms in the **7b-C10** docking solution (rank 1, ASP) according to the protocol used by Sawatzky *et al*.[57] The isoindoline-dione motif was minimized to an RMSD-gradient of 0.001 kcal/mol·Å to

achieve planarity, by keeping all other atoms fixed. The so designed ligand was locally minimized in the binding site using MinMuDS[58] with CSD-potentials (final DSX score: –153.39).[59]

A 3D-RISM calculation was performed with default settings in MOE 2016.05,[43] using the **7b-C10** and **10-C10** docking poses and 2CKM binding site atoms within 8 Å around the ligand.

Solvation free energies were calculated with the SMD method, a parameterized SCRF-based solvation model developed by Truhlar and coworkers, which is based on the quantum mechanical charge density of the solute molecule interacting with a continuum description of the solvent.[44] The tetramethylammonium and n-propane model compounds were built and preminimized (with MMFF94s) in MOE. The quantum chemical calculations with the SMD solvation model were carried out with Gaussian09 Revision C.01[60] at the HF/6-31G* level of theory (full geometry optimization). Instead of calculating the transfer free energies from the gas phase to water (which leads to overestimation of the desolvation penalties,[61] in particular for charged compounds), the transfer free energies from water (ε = 78.3553) to *n*-octanol (ε = 9.8629) (obtained from SCRF/SMD calculations with water and *n*-octanol as solvents, respectively) were used to estimate the desolvation free energy.

Sequence alignment

The identity and homology between *ee*AChE and hAChE amounts to 88% and 93%, respectively. Therefore, *ee*AChE can be used to replace hAChE in enzyme kinetic measurements. *Tc*AChE shows an identity and homology of about 57% and 73%, respectively, to both *ee*AChE and hAChE. The binding site of these three isoforms is highly conserved, with the replacement of Phe330 in *ee*AChE and *Tc*AChE by Tyr337 in hAChE as the main difference. Thus, *Tc*AChE can savely be used as model system for docking studies even though enzyme kinetic data may be obtained with other AChE isoforms.

Table 6: Sequence alignment of electric eel, torpedo californica, and human AChE with identity (left) and homology (right).

	Identity [%]			**Homology [%]**		
	*Tc*AChE	*ee*AChE	hAChE	*Tc*AChE	*ee*AChE	hAChE
*Tc*AChE	100	57.7	56.5	100	73.4	73.8
*ee*AChE	-	100	88.0	-	100	93.0
hAChE	-	-	100	-	-	100

Method:

Pairwise sequence alignment was carried out with the Needle program, using the EBLOSUM62 matrix of EMBOSS v.6.3.1.[62] The PDB-IDs 4EY7 (human),[63] 1C2O (electric eel)[64] and 2CKM (torpedo californica)[40] were taken for comparison.

Acknowledgements

Thanks are due to the German Academic National Foundation (Studienstiftung des deutschen Volkes) for awarding a Ph.D. scholarship to S. Wehle. The skillful technical assistance of Mechthild Kepe, Iris Jusen, and Matthias Hoffmann is gratefully acknowledged. We also thank the Institute for Molecular Infection Biology of the University of Würzburg (Germany) for evaluation of the cytotoxicity.

References

[1] (2014) Deutsche Alzheimer Gesellschaft, Factsheet "Das Wichtigste 1 – Die Häufigkeit von Demenzerkrankungen".

[2] Ballard, C., Gauthier, S., Corbett, A., Brayne, C., Aarsland, D., and Jones, E. (2011) Alzheimer's disease, *The Lancet 377*, 1019-1031.

[3] Soreq, H., and Seidman, S. (2001) Acetylcholinesterase--new roles for an old actor, *Nat. Rev. Neurosci. 2*, 294-302.

[4] Nicolet, Y., Lockridge, O., Masson, P., Fontecilla-Camps, J. C., and Nachon, F. (2003) Crystal structure of human butyrylcholinesterase and of its complexes with substrate and products, *J. Biol. Chem. 278*, 41141-41147.

[5] Giacobini, E. (2004) Cholinesterase inhibitors: new roles and therapeutic alternatives, *Pharmacol. Res. 50*, 433-440.

[6] Tasker, A., Perry, E. K., and Ballard, C. G. (2005) Butyrylcholinesterase: impact on symptoms and progression of cognitive impairment, *Expert Rev. Neurother. 5*, 101-106.

[7] Geula, C., and Darvesh, S. (2004) Butyrylcholinesterase, cholinergic neurotransmission and the pathology of Alzheimer's disease, *Drugs Today 40*, 711-721.

[8] Grimmer, T., and Kurz, A. (2006) Effects of Cholinesterase Inhbititors on Behavioural Disturbances in Alzheimer`s Disease, *Drugs Aging 23*, 957-967.

[9] Munoz-Torrero, D. (2008) Acetylcholinesterase Inhibitors as Disease-Modifying Therapies for Alzheimers Disease, *Curr. Med. Chem. 15*, 2433-2455.

[10] Watkins, P. B., Zimmerman, H. J., Knapp, M. J., Gracon, S. I., and Lewis, K. W. (1994) Hepatotoxic effects of tacrine administration in patients with Alzheimer's disease, *JAMA 271*, 992-998.

[11] Lange, J. H., Coolen, H. K., van der Neut, M. A., Borst, A. J., Stork, B., Verveer, P. C., and Kruse, C. G. (2010) Design, synthesis, biological properties, and molecular modeling investigations of novel tacrine derivatives with a combination of acetylcholinesterase inhibition and cannabinoid CB1 receptor antagonism, *J. Med. Chem. 53*, 1338-1346.

[12] Fang, L., Jumpertz, S., Zhang, Y., Appenroth, D., Fleck, C., Mohr, K., Tränkle, C., and Decker, M. (2010) Hybrid molecules from xanomeline and tacrine: enhanced tacrine actions on cholinesterases and muscarinic M1 receptors, *J. Med. Chem. 53*, 2094-2103.

[13] Chen, X., Zenger, K., Lupp, A., Kling, B., Heilmann, J., Fleck, C., Kraus, B., and Decker, M. (2012) Tacrine-silibinin codrug shows neuro- and hepatoprotective effects in vitro and pro-cognitive and hepatoprotective effects in vivo, *J. Med. Chem. 55*, 5231-5242.

[14] Carreiras, M. C., Soriano, E., and Marco, J. L. (2013) Multipotent 1,8-naphthyridines, as new tacrine analogues, for the treatment of Alzheimer's disease, *From Bioactive Heterocycles* 1-17.

[15] Romero, A., Cacabelos, R., Oset-Gasque, M. J., Samadi, A., and Marco-Contelles, J. (2013) Novel tacrine-related drugs as potential candidates for the treatment of Alzheimer's disease, *Bioorg. Med. Chem. Lett. 23*, 1916-1922.

[16] Pang, Y. P., Hong, F., Quiram, P., Jelacic, T., and Brimijoin, S. (1997) Synthesis of alkylene linked bis-THA and alkylene linked benzyl-THA as highly potent and selective inhibitors and molecular probes of acetylcholinesterase, *J Chem Soc Perk T 1*, 171-176.

[17] Kloeckner, J., Schmitz, J., and Holzgrabe, U. (2010) Convergent, short synthesis of the muscarinic superagonist iperoxo, *Tetrahedron Lett. 51*, 3470-3472.

[18] Matera, C., Flammini, L., Quadri, M., Vivo, V., Ballabeni, V., Holzgrabe, U., Mohr, K., De Amici, M., Barocelli, E., Bertoni, S., and Dallanoce, C. (2014) Bis(ammonio)alkane-type agonists of muscarinic acetylcholine receptors: synthesis, in vitro functional characterization, and in vivo evaluation of their analgesic activity, *Eur. J. Med. Chem. 75*, 222-232.

[19] Disingrini, T., Muth, M., Dallanoce, C., Barocelli, E., Bertoni, S., Kellershohn, K., Mohr, K., De Amici, M., and Holzgrabe, U. (2006) Design, synthesis, and action of oxotremorine-related hybrid-type allosteric modulators of muscarinic acetylcholine receptors, *J. Med. Chem. 49*, 366-372.

[20] Dallanoce, C., Conti, P., De Amici, M., De Micheli, C., Barocelli, E., Chiavarini, M., Ballabeni, V., Bertoni, S., and Impicciatore, M. (1999) Synthesis and functional characterization of novel derivatives related to oxotremorine and oxotremorine-M, *Bioorg. Med. Chem. 7*, 1539-1547.

[21] Barocelli, E., Ballabeni, V., Bertoni, S., De Amici, M., and Impicciatore, M. (2001) Evidence for specific analgesic activity of a muscarinic agonist selected among a new series of acetylenic derivatives, *Life Sci. 68*, 1775-1785.

[22] Bock, A., Merten, N., Schrage, R., Dallanoce, C., Batz, J., Kloeckner, J., Schmitz, J., Matera, C., Simon, K., Kebig, A., Peters, L., Müller, A., Schrobang-Ley, J., Tränkle, C., Hoffmann, C., De Amici, M., Holzgrabe, U., Kostenis, E., and Mohr, K. (2012) The allosteric vestibule of a seven transmembrane helical receptor controls G-protein coupling, *Nat. Commun. 3*, 1044.

[23] Carlier, P. R., Han, Y. F., Chow, E. S.-H., Li, C. P.-L., Wang, H., Lieu, T. X., Wong, H. S., and Pang, Y. P. (1999) Evaluation of Short-tether Bis-THA AChE Inhibitors. A Further Test of the Dual Binding Site Hypothesis, *Bioorg. Med. Chem. 7*, 351-357.

[24] Sun, Y., Chen, J., Chen, X., Huang, L., and Li, X. (2013) Inhibition of cholinesterase and monoamine oxidase-B activity by Tacrine-Homoisoflavonoid hybrids, *Bioorg. Med. Chem. 21*, 7406-7417.

[25] Camps, P., Formosa, X., Munoz-Torrero, D., Petrignet, J., Badia, A., and Clos, M. V. (2005) Synthesis and pharmacological evaluation of huprine-tacrine heterodimers: subnanomolar dual binding site acetylcholinesterase inhibitors, *J. Med. Chem. 48*, 1701-1704.

[26] Levy, R. (1987) Tetrahydroaminoacridine and Alzheimer's disease, *Lancet 1*, 322.

[27] Wang, H., Carlier, P. R., Ho, W. L., Wu, D. C., Lee, N. T., Li, C. P., Pang, Y. P., and Han, Y. F. (1999) Effects of bis(7)-tacrine, a novel anti-Alzheimer`s agent, on rat brain AChE, *Neuroreport 10*, 789-793.

[28] Han, Y. F., Li, C. P., Chow, E., Wang, H., Pang, Y. P., and Carlier, P. R. (1999) Dual-site binding of bivalent 4-aminopyridine- and 4-aminoquinoline-based AChE inhibitors: contribution of the hydrophobic alkylene tether to monomer and dimer affinities, *Bioorg. Med. Chem. 7*, 2569-2575.

[29] Antony, J., Kellershohn, K., Mohr-Andra, M., Kebig, A., Prilla, S., Muth, M., Heller, E., Disingrini, T., Dallanoce, C., Bertoni, S., Schrobang, J., Tränkle, C., Kostenis, E., Christopoulos, A., Holtje, H. D., Barocelli, E., De Amici, M., Holzgrabe, U., and Mohr, K. (2009) Dualsteric GPCR targeting: a novel route to binding and signaling pathway selectivity, *FASEB J. 23*, 442-450.

[30] Kiefer-Day, J. S., Campbell, H. E., Towles, J., and el-Fakahany, E. E. (1991) Muscarinic subtype selectivity of tetrahydroaminoacridine: possible relationship to its capricious efficacy, *Eur. J. Pharmacol. 203*, 421-423.

[31] Schrage, R., Seemann, W. K., Kloeckner, J., Dallanoce, C., Racke, K., Kostenis, E., De Amici, M., Holzgrabe, U., and Mohr, K. (2013) Agonists with supraphysiological efficacy at the muscarinic M2 ACh receptor, *Br. J. Pharmacol. 169*, 357-370.

[32] Schrage, R., Holze, J., Klöckner, J., Balkow, A., Klause, A. S., Schmitz, A. L., De Amici, M., Kostenis, E., Tränkle, C., Holzgrabe, U., and Mohr, K. (2014) New insight into active muscarinic receptors with the novel radioagonist [(3)H]iperoxo, *Biochem. Pharmacol. 90*, 307-319.

[33] Nakao, K., Fujikawa, M., Shimizu, R., and Akamatsu, M. (2009) QSAR application for the prediction of compound permeability with in silico descriptors in practical use, *J. Comput. Aided Mol. Des. 23*, 309-319.

[34] Alptüzün, V., Prinz, M., Hörr, V., Scheiber, J., Radacki, K., Fallarero, A., Vuorela, P., Engels, B., Braunschweig, H., Erciyas, E., and Holzgrabe, U. (2010) Interaction of (benzylidene-hydrazono)-1,4-dihydropyridines with ß-amyloid, acetylcholine, and butyrylcholine esterases, *Bioorg. Med. Chem. 18*, 2049-2059.

[35] Lipinski, C. A., Lombardo, F., Dominy, B. W., and Feeney, P. J. (2001) Experimental and computational approaches to estimate solubility and permeability in drug discovery and development settings, *Adv. Drug Deliv. Rev. 46*, 3-26.

[36] Hansch, C., Leo, A., and Hoekman, D. (1995) *Exploring QSAR: Volume 2: Hydrophobic, Electronic and Steric Constants, American Chemical Society*, Waschington DC.

[37] Doucet-Personeni, C., Bentley, P. D., Fletcher, R. J., Kinkaid, A., Kryger, G., Pirard, B., Taylor, A., Taylor, R., Taylor, J., Viner, R., Silman, I., Sussman, J. L., Greenblatt, H. M., and Lewis, T. (2001) A structure-based design approach to the development of novel, reversible AChE inhibitors, *J. Med. Chem. 44*, 3203-3215.

[38] Carlier, P. R., Du, D. M., Han, Y., Liu, J., and Pang, Y. P. (1999) Potent, easily synthesized huperzine A-tacrine hybrid acetylcholinesterase inhibitors, *Bioorg. Med. Chem. Lett. 9*, 2335-2338.

[39] Chen, X., Wehle, S., Kuzmanovic, N., Merget, B., Holzgrabe, U., Konig, B., Sotriffer, C. A., and Decker, M. (2014) Acetylcholinesterase Inhibitors with Photoswitchable Inhibition of ß-Amyloid Aggregation, *ACS Chem. Neurosci. 5*, 377-389.

[40] Rydberg, E. H., Brumshtein, B., Greenblatt, H. M., Wong, D. M., Shaya, D., Williams, L. D., Carlier, P. R., Pang, Y. P., Silman, I., and Sussman, J. L. (2006) Complexes of alkylene-linked tacrine dimers with *Torpedo californica* acetylcholinesterase: Binding of bis(5)-tacrine produces a dramatic rearrangement in the active-site gorge, *J. Med. Chem. 49*, 5491-5500.

[41] Harel, M., Schalk, I., Ehret-Sabatier, L., Bouet, F., Goeldner, M., Hirth, C., Axelsen, P. H., Silman, I., and Sussman, J. L. (1993) Quaternary ligand binding to aromatic residues in the active-site gorge of acetylcholinesterase, *Proc. Natl. Acad. Sci. U. S. A. 90*, 9031-9035.

[42] Bissantz, C., Kuhn, B., and Stahl, M. (2010) A medicinal chemist's guide to molecular interactions, *J. Med. Chem. 53*, 5061-5084.

[43] Chemical Computing Group, Molecular Operating Environment (MOE), 2016.05, 1010 Sherbooke St. West, Suite No. 910, Montreal, QC, H3A 2R7, Canada.

[44] Marenich, A. V., Cramer, C. J., and Truhlar, D. G. (2009) Universal solvation model based on solute electron density and on a continuum model of the solvent defined by the bulk dielectric constant and atomic surface tensions, *J. Phys. Chem. B 113*, 6378-6396.

[45] Dragendorff, G. (1872) Beiträge zur gerichtlichen Chemie einzelner organischer Gifte. Untersuchungen aus dem pharmaceutischen Institute in Dorpat, p 312, Verlag der Kaiserlichen Hochbuchhandlung Heinrich Schmitzdorff (Karl Böttger), Sankt Petersburg.

[46] Nayeem AA, K. A., Rahman MS, Rahman M. (2011) Evaluation of phytochemical and pharmacological properties of Mikania cordata (Asteraceae) leaves, *J. Pharmacognosy Phytother. 3*, 118-123.

[47] Ellman, G. L., Courtney, K. D., Andres, V., Jr., and Feather-Stone, R. M. (1961) A new and rapid colorimetric determination of acetylcholinesterase activity, *Biochem. Pharmacol. 7*, 88-95.

[48] Tränkle, C., Weyand, O., Voigtlander, U., Mynett, A., Lazareno, S., Birdsall, N. J., and Mohr, K. (2003) Interactions of orthosteric and allosteric ligands with [3H]dimethyl-W84 at the common allosteric site of muscarinic M2 receptors, *Mol. Pharmacol. 64*, 180-190.

[49] Tränkle, C., Dittmann, A., Schulz, U., Weyand, O., Buller, S., Johren, K., Heller, E., Birdsall, N. J., Holzgrabe, U., Ellis, J., Holtje, H. D., and Mohr, K. (2005) Atypical muscarinic allosteric modulation: cooperativity between modulators and their atypical binding topology in muscarinic M2 and M2/M5 chimeric receptors, *Mol. Pharmacol. 68*, 1597-1610.

[50] Kostenis, E., and Mohr, K. (1996) Two-point kinetic experiments to quantify allosteric effects on radioligand dissociation, *Trends Pharmacol. Sci. 17*, 280-283.

[51] Deblasi, A., Oreilly, K., and Motulsky, H. J. (1989) Calculating Receptor Number from Binding Experiments Using Same Compound as Radioligand and Competitor, *Trends Pharmacol. Sci. 10*, 227-229.

[52] Bernstein, F. C., Koetzle, T. F., Williams, G. J. B., Meyer, E. F., Brice, M. D., Rodgers, J. R., Kennard, O., Shimanouchi, T., and Tasumi, M. (1977) The protein data bank: A computer-based archival file for macromolecular structures, *J. Mol. Biol. 112*, 535-542.

[53] CCDCSoftware. GOLDSUITE 5.2, www.ccdc.cam.ac.uk.

[54] Verdonk, M. L., Cole, J. C., Hartshorn, M. J., Murray, C. W., and Taylor, R. D. (2003) Improved protein-ligand docking using GOLD, *Proteins 52*, 609-623.

[55] Mooij, W. T., and Verdonk, M. L. (2005) General and targeted statistical potentials for protein-ligand interactions, *Proteins 61*, 272-287.

[56] Milletti, F., Storchi, L., Sforna, G., and Cruciani, G. (2007) New and original pKa prediction method using grid molecular interaction fields, *J. Chem. Inf. Model. 47*, 2172-2181.

[57] Sawatzky, E., Wehle, S., Kling, B., Wendrich, J., Bringmann, G., Sotriffer, C. A., Heilmann, J., and Decker, M. (2016) Discovery of Highly Selective and Nanomolar Carbamate-Based Butyrylcholinesterase Inhibitors by Rational Investigation into Their Inhibition Mode, *J. Med. Chem. 59*, 2067-2082.

[58] Spitzmüller, A., Velec, H. F. G., and Klebe, G. (2011) MiniMuDS: A New Optimizer using Knowledge-Based Potentials Improves Scoring of Docking Solutions, *J. Chem. Inf. Model. 51*, 1423-1430.

[59] Neudert, G., and Klebe, G. (2011) DSX: a knowledge-based scoring function for the assessment of protein-ligand complexes, *J. Chem. Inf. Model. 51*, 2731-2745.

[60] Frisch, M. J., Trucks, G. W., Schlegel, H. B., Scuseria, G. E., Robb, M. A., Cheeseman, J. R., Scalmani, G., Barone, V., Mennucci, B., Petersson, G. A., Nakatsuji, H., Caricato, M., Li, X., Hratchian, H. P., Izmaylov, A. F., Bloino, J., Zheng, G., Sonnenberg, J. L., Hada, M., Ehara, M., Toyota, K., Fukuda, R., Hasegawa, J., Ishida, M., Nakajima, T., Honda, Y., Kitao, O., Nakai, H., Vreven, T., Montgomery, J. A., Jr., Peralta, J. E., Ogliaro, F., Bearpark, M., Heyd, J. J., Brothers, E., Kudin, K. N., Staroverov, V. N., Kobayashi, R., Normand, J., Raghavachari, K., Rendell, A., Burant, J. C., Iyengar, S. S., Tomasi, J., Cossi, M., Rega, N., Millam, J. M., Klene, M., Knox, J. E., Cross, J. B., Bakken, V., Adamo, C., Jaramillo, J., Gomperts, R., Stratmann, R. E., Yazyev, O., Austin, A. J., Cammi, R., Pomelli, C., Ochterski, J. W., Martin, R. L., Morokuma, K., Zakrzewski, V. G., Voth, G. A., Salvador, P., Dannenberg, J. J., Dapprich, S., Daniels, A. D., Farkas, Ö., Foresman, J. B., Ortiz, J. V., Cioslowski, J., and Fox, D. J., Gaussian 09 Revision C.01, Gaussian, Inc., Wallingford CT.

[61] Mysinger, M. M., and Shoichet, B. K. (2010) Rapid context-dependent ligand desolvation in molecular docking, *J. Chem. Inf. Model. 50*, 1561-1573.

[62] Rice, P., Longden, I., and Bleasby, A. (2000) EMBOSS: The European molecular biology open software suite, *Trends Genet. 16*, 276-277.

[63] Cheung, J., Rudolph, M. J., Burshteyn, F., Cassidy, M. S., Gary, E. N., Love, J., Franklin, M. C., and Height, J. J. (2012) Structures of human acetylcholinesterase in complex with pharmacologically important ligands, *J. Med. Chem. 55*, 10282-10286.

[64] Bourne, Y., Grassi, J., Bougis, P. E., and Marchot, P. (1999) Conformational flexibility of the acetylcholinesterase tetramer suggested by X-ray crystallography, *J. Biol. Chem. 274*, 30370-30376.

D. Discussion

The ability of bipharmacophoric ligands to bind simultaneously to the orthosteric and allosteric site within one receptor opens the way towards subtype-selective GPCR-targeting ligands as well as signaling bias resulting in reduced side effects. The development of the "dynamic ligand binding" concept offers new perspectives concerning the binding character of dualsteric ligands. Such bipharmacophoric ligands, consisting of an orthosteric agonistic moiety and an allosteric inverse agonistic moiety linked via variable linker chain length, behave as dynamic ligands, switching between two different orientations. The ratio of active, characterized by an dualsteric binding pose, versus inactive states, characterized by a purely allosteric binding pose, defines the extent of partial agonism.[1] In order to generate and fine-tune partial agonism it is not compulsory to design orthosteric/allosteric bipharmacophoric ligands. This concept can further be extended to bipharmacophoric ligands consisting of orthosteric/orthosteric or allosteric/allosteric moieties by assuming that the two moieties differ in their affinity and intrinsic efficacy for receptor activation.[2] These concepts pave the way for the design of new partial agonists.

In this context, the aim of the study performed here was the design, synthesis and pharmacological investigation of new dualsteric compounds for muscarinic acetylcholine receptors. Depending on the composition of the hybrids, these ligands should act as partial agonists with different outcome or as full agonists, depending on their structure-activity relationship.

On this basis, two orthosteric ligands, having different binding affinities to the orthosteric binding site were connected via alkyl chains of different length. As antagonist atropine and scopolamine, respectively, and as agonists iperoxo and isoxazole, respectively, were used (Figure 1). The four sets of hybrid compounds were built by means of the reaction of atropine or the free base of scopolamine to the corresponding dibromoalkane chain followed by coupling of the base of iperoxo and the base of isoxazole, respectively. Such designed hybrid compounds are helpful tools for the rational design of partial agonism in future.

Furthermore, partial agonism can be induced and controlled by homodimers. Such homodimers can possibly bind to two distinct binding sites, orthosteric and allosteric, or to an orthosteric and a metastable binding site, located in the extracellular vestibule, in the same receptor. Homodimers could also target two orthosteric sites in a dimeric receptor.[3] The quaternary and tertiary homodimers were either built out of two iperoxo-moieties or out of two acetylcholine-moieties connected through alkyl chains of different length (Figure 1). The quaternary homodimers were investigated in binding studies on CHO-hM_2 cells for their G_i- as well as G_s signaling performed in the institute of pharmacology in Bonn. The results indicated that the G_i- as well as the G_s pathway activation depends on the linker length. In general, the shorter the linker the weaker the effect. Furthermore, the acetylcholine-related

homodimers could not reach the high maximum effect in comparison to the iperoxo-related homodimers. Furthermore, dimerization of the agonists resulted in a loss of potency compared to iperoxo or acetylcholine alone, therefore resulting in partial agonism. The closure of the so-called tyrosine lid within the receptor, formed by cation-π-interactions between three tyrosine amino acids encloses iperoxo completely in the orthosteric binding pocket as evidenced in docking studies.[4] This aromatic lid closure seems to be essential for full receptor activation. The second moiety of the homodimers, located in the gorge of the receptor hinders the closure of the tyrosine lid resulting in less receptor activation and therefore partial agonism. All in all, partial agonism can be controlled and fine-tuned by the choice of the agonist as well as by the linker length and is therefore in accordance with the concepts described for dynamic ligand binding.

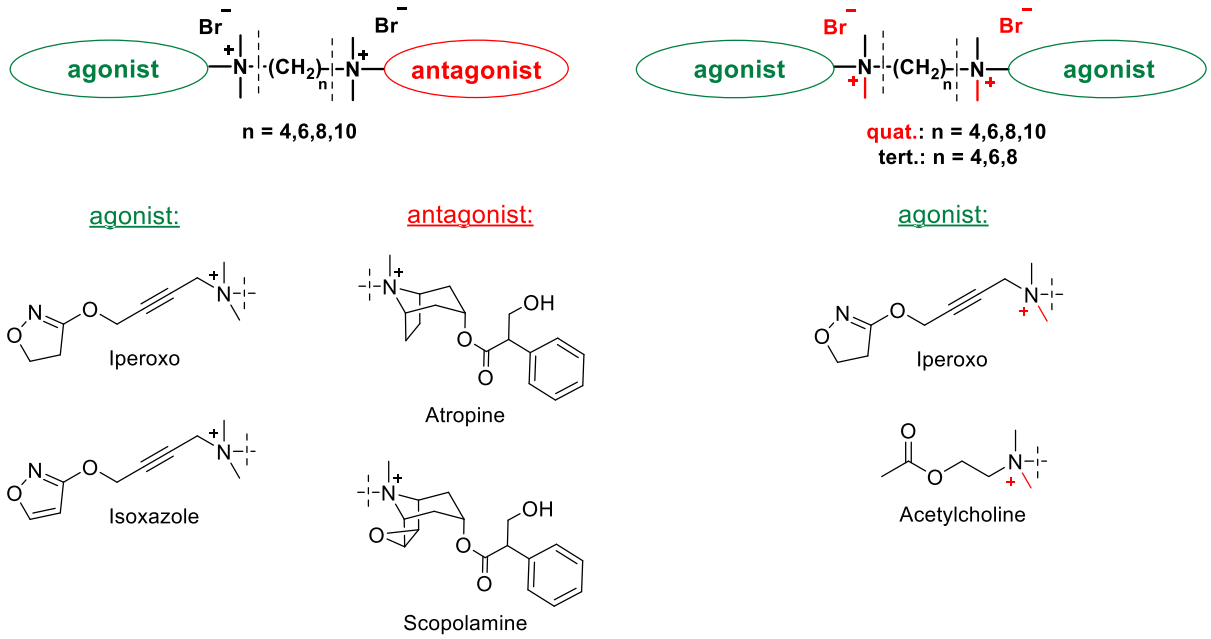

Figure 1: Overview of the designed partial agonists.

Furthermore, bipharmacophoric ligands consisting of iperoxo and a fluoro-BQCA-derived moiety linked via a hexamethylene chain were also found to act as partial hM_1 receptor agonists.[5] The benzyl quinolone carboxylic acid (BQCA) is known as M_1-selective positive allosteric modulator (PAM) with respect to orthosteric agonist binding.[6-9] On this basis, appropriate hybrid molecules with elongated alkyl chain lengths as well as fluoro-BQCA-derived hybrids connected to acetylcholine were synthesized in order to generate M_1-subtype selective partial agonists (Figure 2). FRET experiments were performed in the institute of pharmacology in Würzburg in order to get information about receptor conformational changes induced by ligand binding to the receptor. The studies confirmed a linker length dependent FRET signal. The highest positive FRET signal was observed with quinolone-C_6-

iperoxo resulting from a positive cooperativity between the two separated moieties, alloster and orthoster. Interestingly, hybrids consisting of longer linker chains showed an inverse FRET signal indicating a different binding pose to the receptor in comparison to shorter linked hybrids. Further FRET measurements using derivatives of the hybrid, namely fluoro-BQCA-derived allosteric moieties linked to alkyl chains of different length which bind to the allosteric site of the receptor, were investigated. Here, the long chain linked derivatives also resulted in inverse FRET signals, indicating that the hybrids connected to a C10 alkyl chain possibly have a purely allosteric binding mode.

Besides BQCA-derived hybrids connected through flexible alkyl chains, a BQCA-derived hybrid linked to a rigidified spacer was designed and synthesized (Figure 2). Such rigidified hybrids seem to have interesting pharmacological properties as shown for the hybrid naph-rigid-iper. Due to the missing flexibility of the rigidified linker, naph-rigid-iper is forced to bind in a purely dualsteric binding mode as confirmed in binding studies, resulting in full receptor activation and full agonism.[10] Interestingly, FRET studies of the corresponding quinolone-rigid-iper indicated a delayed kinetic. This time-delayed FRET signal is probably caused by interactions between the rigidified linker and the already mentioned aromatic lid.

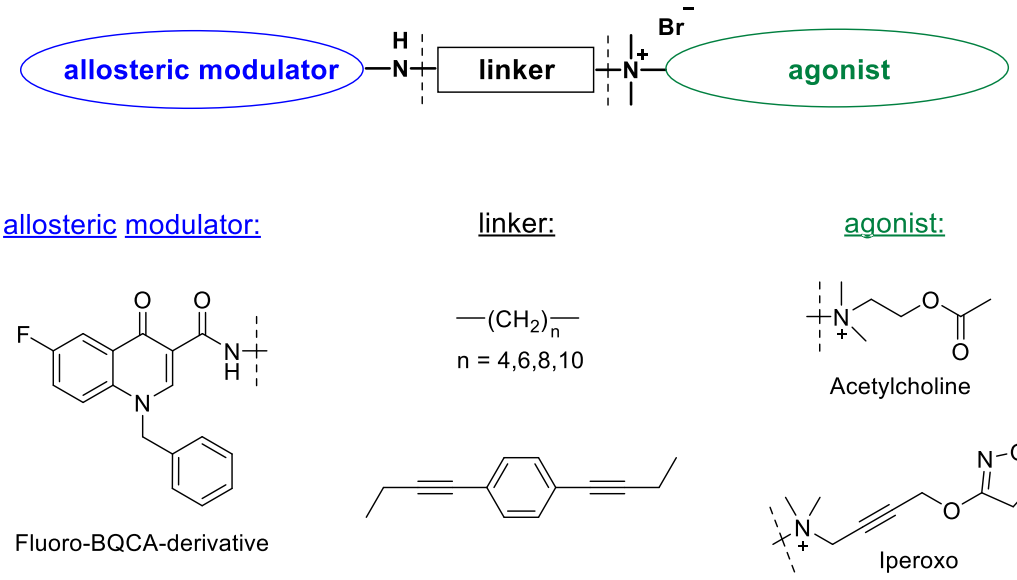

Figure 2: Overview of the M_1-subtype-selective hybrids.

Furthermore, bipharmacophoric hybrid compounds acting simultaneously as agonists at the M_1 receptor and as inhibitors against AChE and BChE, enzymes which are responsible for the rapid hydrolysis in the synaptic cleft, are promising candidates for the treatment of M. Alzheimer. Compounds such as phth-C_n-isox (Figure 3) showed good anticholinesterase activity for AChE and BChE.[11] On that basis, further newly designed hybrid sets were developed by using different pharmacophoric units with varying alkyl chain length. Thus, the

isoxazole moiety in phth-C_n-isox was exchanged by iperoxo resulting in phth-C_n-iper, replacement of the phthalyl moiety by a naphthyl moiety and tacrine, respectively, led to the hybrid compounds naph-C_n-iper and tac-C_n-iper, respectively (Figure 3). The compounds phth-C_n-iper and naph-C_n-iper were synthesized in analogy to previously reported procedures.[11] The different hybrid sets were evaluated towards BChE from equine serum as well as AChE from electric eel, and towards human ChEs. Compounds containing a naphthyl moiety have higher anticholinesterase activity than the hybrids related to phthalyl moieties. Tac-C_n-iper showed excellent inhibitory activity for both AChE (pIC_{50} = 9.81) and BChE (pIC_{50} = 8.75). According to the structure-activity relationship, the hybrids phth-C_{10}-iper, naph-C_{10}-iper, and tac-C_{10}-iper resulted in the most active compounds out of the three different hybrid sets and were investigated in computational studies performed in the institute of pharmacy and food chemistry in Würzburg. Results indicated that the second positive ammonium group available in phth-C_{10}-iper and naph-C_{10}-iper leads to unfavorable higher desolvation penalty in comparison to the uncharged alkylene chain in tac-C_{10}-iper which might explain its high anticholinesterase activity. In addition to ChE inhibitors, M receptor agonists, especially of the M_1 subtype, have gained great interest in the field of anti-Alzheimer agents. Therefore, the most active compounds tac-C_7-iper and tac-C_{10}-iper were investigated in radioligand binding studies and showed affinity to the muscarinic M_1 and M_2 receptor. These hybrids possibly have a dual mechanism of action due to their ability of inhibiting the cholinesterases combined with agonistic activity at the M_1 and M_2 receptor. Thus, the newly designed hybrids are interesting tools in the context of M. Alzheimer.[12]

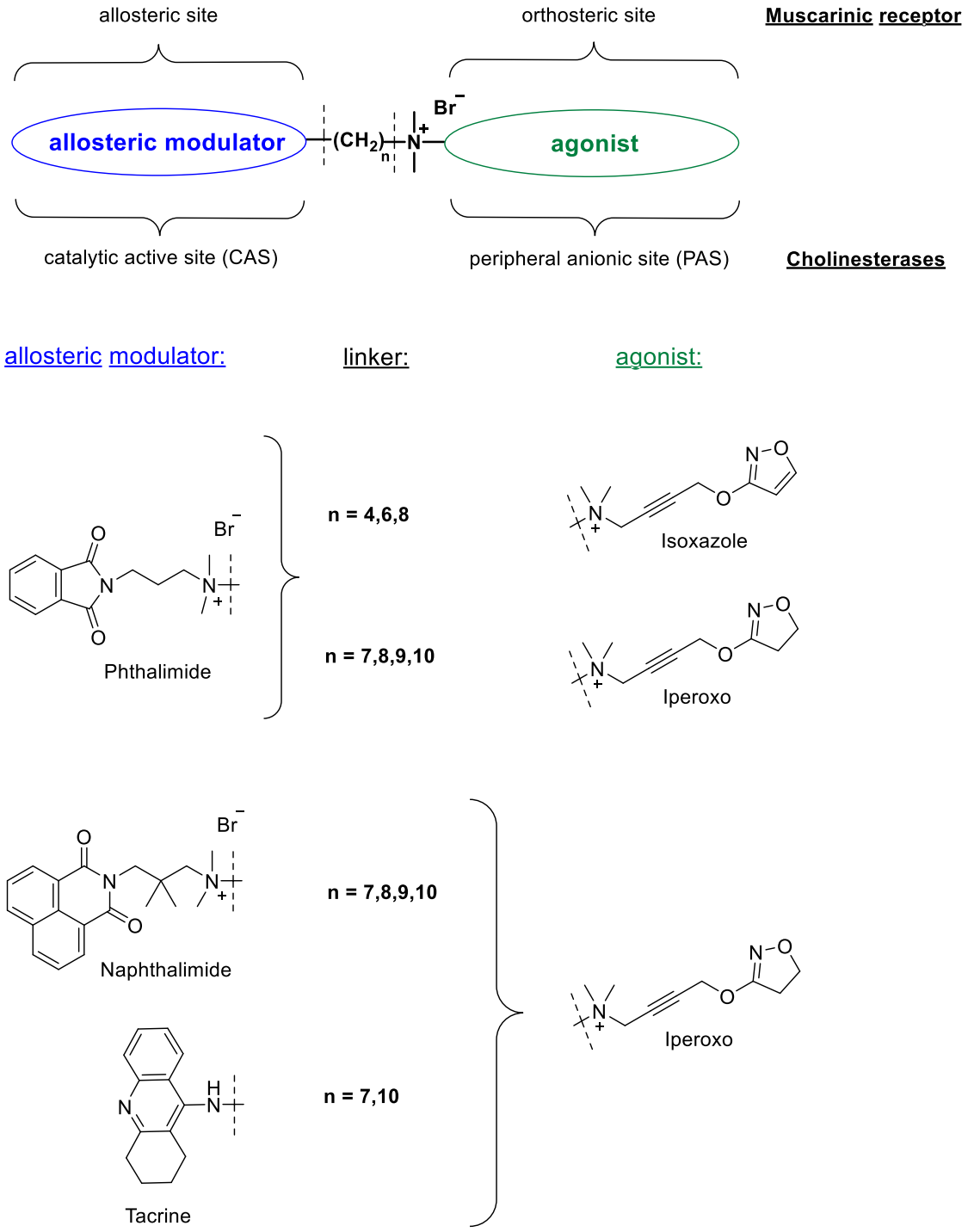

Figure 3: Overview of the newly designed hybrid inhibitors of cholinesterases.

References

[1] Bock, A., Chirinda, B., Krebs, F., Messerer, R., Batz, J., Muth, M., Dallanoce, C., Klingenthal, D., Tränkle, C., Hoffmann, C., De Amici, M., Holzgrabe, U., Kostenis, E., and Mohr, K. (2014) Dynamic ligand binding dictates partial agonism at a G protein-coupled receptor, *Nat. Chem. Biol. 10*, 18-20.

[2] Bock, A., Kostenis, E., Tränkle, C., Lohse, M. J., and Mohr, K. (2014) Pilot the pulse: controlling the multiplicity of receptor dynamics, *Trends Pharmacol. Sci. 35*, 630-638.

[3] Fronik, P., Gaiser, B. I., and Sejer Pedersen, D. (2017) Bitopic Ligands and Metastable Binding Sites: Opportunities for G Protein-Coupled Receptor (GPCR) Medicinal Chemistry, *J. Med. Chem.*

[4] Kruse, A. C., Ring, A. M., Manglik, A., Hu, J. X., Hu, K., Eitel, K., Hübner, H., Pardon, E., Valant, C., Sexton, P. M., Christopoulos, A., Felder, C. C., Gmeiner, P., Steyaert, J., Weis, W. I., Garcia, K. C., Wess, J., and Kobilka, B. K. (2013) Activation and allosteric modulation of a muscarinic acetylcholine receptor, *Nature 504*, 101-106.

[5] Chen, X., Kloeckner, J., Holze, J., Zimmermann, C., Seemann, W. K., Schrage, R., Bock, A., Mohr, K., Tränkle, C., Holzgrabe, U., and Decker, M. (2015) Rational design of partial agonists for the muscarinic m1 acetylcholine receptor, *J. Med. Chem. 58*, 560-576.

[6] Mistry, S. N., Valant, C., Sexton, P. M., Capuano, B., Christopoulos, A., and Scammells, P. J. (2013) Synthesis and pharmacological profiling of analogues of benzyl quinolone carboxylic acid (BQCA) as allosteric modulators of the M1 muscarinic receptor, *J. Med. Chem. 56*, 5151-5172.

[7] Kuduk, S. D., Chang, R. K., Di Marco, C. N., Ray, W. J., Ma, L., Wittmann, M., Seager, M. A., Koeplinger, K. A., Thompson, C. D., Hartman, G. D., and Bilodeau, M. T. (2010) Quinolizidinone carboxylic acids as CNS penetrant, selective m1 allosteric muscarinic receptor modulators, *ACS Med. Chem. Lett. 1*, 263-267.

[8] Davie, B. J., Valant, C., White, J. M., Sexton, P. M., Capuano, B., Christopoulos, A., and Scammells, P. J. (2014) Synthesis and pharmacological evaluation of analogues of benzyl quinolone carboxylic acid (BQCA) designed to bind irreversibly to an allosteric site of the M (1) muscarinic acetylcholine receptor, *J. Med. Chem. 57*, 5405-5418.

[9] Ma, L., Seager, M. A., Wittmann, M., Jacobson, M., Bickel, D., Burno, M., Jones, K., Graufelds, V. K., Xu, G., Pearson, M., McCampbell, A., Gaspar, R., Shughrue, P., Danziger, A., Regan, C., Flick, R., Pascarella, D., Garson, S., Doran, S., Kreatsoulas, C., Veng, L., Lindsley, C. W., Shipe, W., Kuduk, S., Sur, C., Kinney, G., Seabrook, G. R., and Ray, W. J. (2009) Selective activation of the M1 muscarinic acetylcholine receptor achieved by allosteric potentiation, *Proc. Natl. Acad. Sci. U. S. A. 106*, 15950-15955.

[10] Bock, A., Bermudez, M., Krebs, F., Matera, C., Chirinda, B., Sydow, D., Dallanoce, C., Holzgrabe, U., De Amici, M., Lohse, M. J., Wolber, G., and Mohr, K. (2016) Ligand Binding Ensembles Determine Graded Agonist Efficacies at a G Protein-coupled Receptor, *J. Biol. Chem. 291*, 16375-16389.

[11] Matera, C., Flammini, L., Quadri, M., Vivo, V., Ballabeni, V., Holzgrabe, U., Mohr, K., De Amici, M., Barocelli, E., Bertoni, S., and Dallanoce, C. (2014) Bis(ammonio)alkane-type agonists of muscarinic acetylcholine receptors: synthesis, in vitro functional characterization, and in vivo evaluation of their analgesic activity, *Eur. J. Med. Chem. 75*, 222-232.

[12] Messerer, R., Dallanoce, C., Matera, C., Wehle, S., Flammini, L., Chirinda, B., Bock, A., Irmen, M., Tränkle, C., Barocelli, E., Decker, M., Sotriffer, C. A., De Amici, M., and Holzgrabe, U. (2017) Novel bipharmacophoric inhibitors of the cholinesterases with affinity to the muscarinic receptors M_1 and M_2, *in preparation.*

E. Summary

The study is dealing with the synthesis and pharmacological investigation of newly designed dualsteric ligands of muscarinic acetylcholine receptors belonging to the superfamily of G protein-coupled receptors. Such bipharmacophoric ligands combine the advantages of the orthosteric binding site (high-affinity) and of the topographically distinct allosteric binding site (subtype-selectivity) resulting in compounds with reduced side effects. This opens the way to a new therapeutic approach in the treatment of e.g. chronic pain, drug withdrawal, Parkinson`s and Alzheimer`s disease. Furthermore, the newly synthesized dualsteric compounds were pharmacologically investigated in order to get a better understanding of the activation and signaling processes in muscarinic acetylcholine receptors, especially with regard to partial agonism.

The development of the “dynamic ligand binding” concept offers new perspectives for ligand binding and signaling at G protein-coupled receptors. GPCRs are no longer considered as simple on/off switches. Dualsteric ligands can bind in a dualsteric pose, reflecting an active receptor state as well as in a purely allosteric binding pose, characterized by an inactive receptor state resulting in partial agonism. The degree of partial agonism depends on the ratio of active versus inactive receptor populations. On this basis, orthosteric/orthosteric hybrid ligands consisting of the antagonist atropine and scopolamine, respectively, as well as of the agonist iperoxo and isoxazole, respectively, linked via different alkyl chain length were synthesized in order to investigate partial agonism (Figure 1).

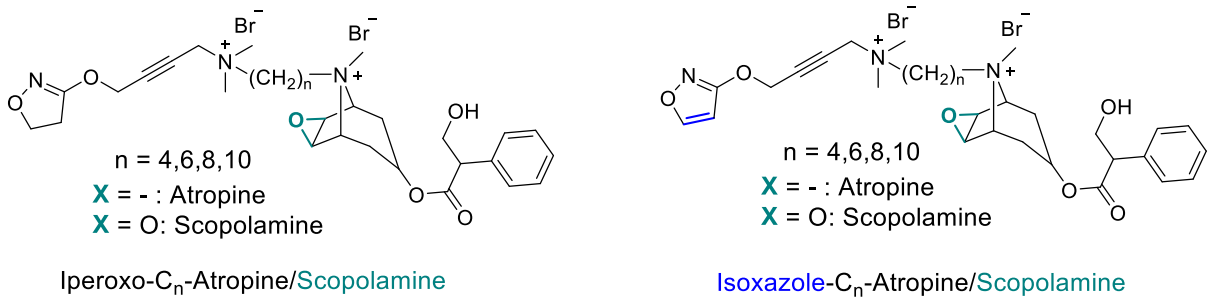

Figure 1: Structures of the synthesized iperoxo/isoxazole-atropine/scopolamine-hybrids.

Furthermore, different sets of quaternary and tertiary homodimers consisting either of two iperoxo or two acetylcholine units were synthesized in order to study their extent on partial agonism (Figure 2). The two agonists were connected by varying alkyl chain length. Binding studies on CHO-hM_2 cells of the quaternary compounds revealed that dimerization of the agonist results in a loss of potency. The iperoxo-dimers reached higher maximum effects on the G_i- as well as on the G_s pathway in comparison to the acetylcholine-dimers. Besides the choice of the orthosteric building block (potency of the agonist), the alkyl chain length is also crucial for the degree of partial agonism.

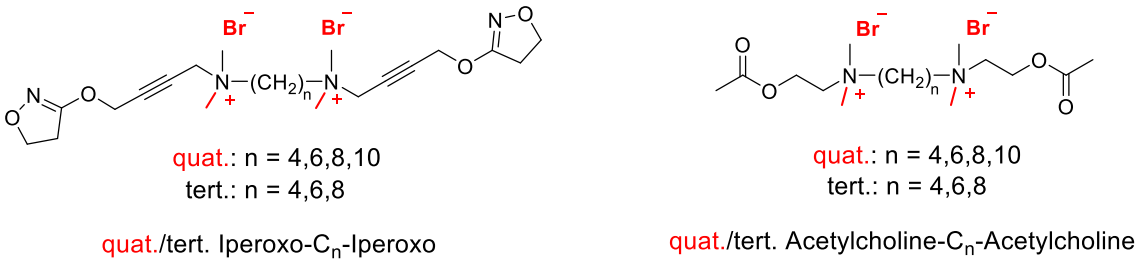

Figure 2: Structures of the synthesized quat./tert. iperoxo/acetylcholine-homodimers.

Quinolone-based hybrids connected to the superagonist iperoxo and to the endogenous ligand acetylcholine, respectively, linked through an alkyl chain of different length were synthesized in order to develop further partial agonists (Figure 3). FRET studies confirmed M_1 subtype-selectivity as well as linker dependent receptor response. The greatest positive FRET signal was observed with quinolone-C_6-iper resulting from a positive cooperativity between the two separated moieties, alloster and orthoster. However, the corresponding hybrids with a longer linker led to an inverse FRET signal indicating a different binding mode, e.g. purely allosteric, in contrast to the shorter linked hybrids. Furthermore, the flexible alkyl spacer was replaced by a rigidified linker resulting in the hybrid quinolone-rigid-iperoxo (Figure 3). FRET studies on the M_1 receptor showed reduced FRET kinetics, resulting from interactions between the bulky linker and the aromatic lid, located between the orthosteric and allosteric binding site. A bitopic binding mode of the rigidified hybrid is presumed. For further clarity, mutational studies are necessary.

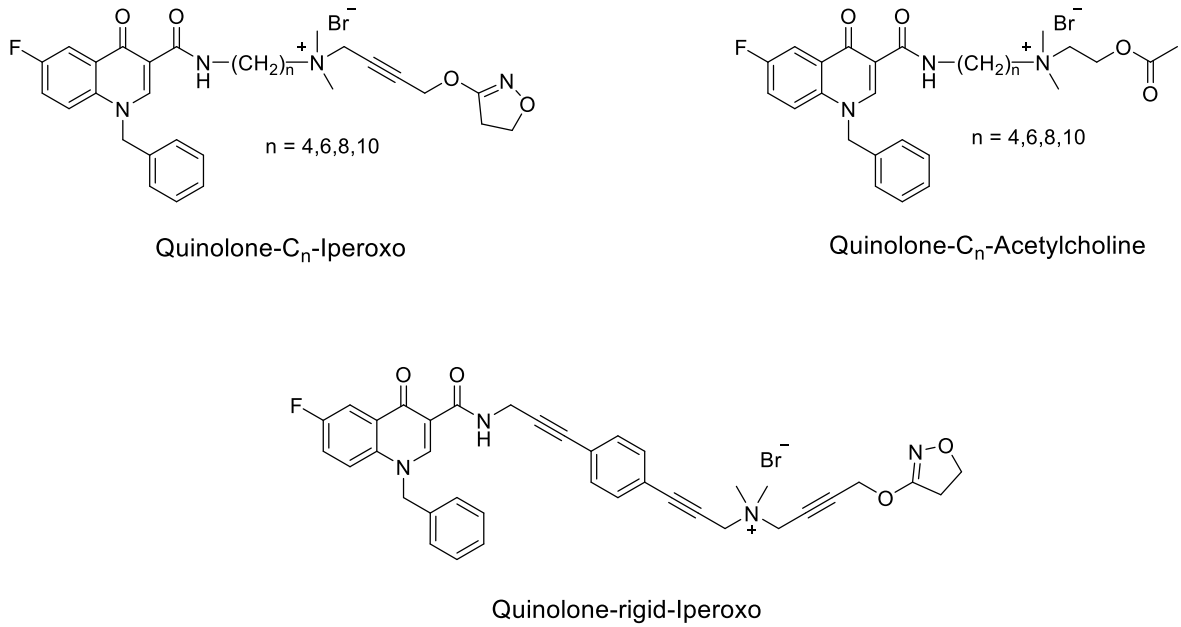

Figure 3: M_1-selective hybrid compounds.

Another aim of this work was the design and synthesis of new hybrid compounds, acting as agonists at the M_1 and M_2 receptor and as inhibitors for AChE and BChE in the context of M. Alzheimer. Several sets of hybrid compounds consisting of different pharmacophoric units (catalytic active site: phthalimide, naphthalimide, tacrine; peripheric anionic site: iperoxo, isoxazole) linked through a polymethylene chain of varying length were synthesized. Tac-C_{10}-iper (Figure 4), consisting of tacrine and the superagonist iperoxo linked by a C10 polymethylene spacer, was found to have excellent anticholinesterase activity for both AChE (pIC_{50} = 9.81) and BChE (pIC_{50} = 8.75). Docking experiments provided a structural model to rationalize the inhibitory power towards AChE. Additionally, the tacrine related hybrids showed affinity to the M_1 and M_2 receptor. Such compounds, addressing more than one molecular target are favorable for multifactorial diseases such as Alzheimer.

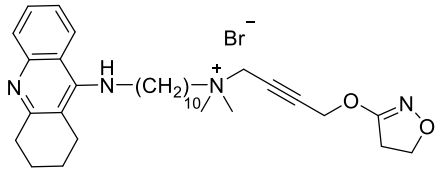

Tacrine-C_{10}-Iperoxo

Figure 4: Structure of the most active compound regarding anticholinesterase activity.

In summary, the choice of the pharmacophoric units, their connecting point as well as the nature, length, and flexibility of the linker play an important role for the activity of designed bivalent ligands. A shorter linker length cannot bridge both binding sites simultaneously in contrast to longer linker chains. On the other hand, too long linker chains can result in unwanted steric interactions. Further investigations with respect to structural variations of hybrid compounds, with or without quaternary ammonium groups, are necessary in the light of drug development.

F. Zusammenfassung

Die vorliegende Studie beschäftigt sich mit der Synthese und der pharmakologischen Untersuchung von neu entwickelten dualsteren Liganden des muskarinischen Acetylcholinrezeptors, welcher zur Superfamilie der G-Proteine gehört. In derartigen bipharmakophoren Liganden sind die Vorteile des orthosteren Bindemodus und des räumlich davon getrennten allosteren Bindemodus vereint. Der orthostere Bindemodus bewirkt eine hohe Affinität zum Rezeptor, während der allostere Bindemodus Subtypselektivität vermittelt. Dadurch weisen diese Verbindungen weniger Nebenwirkungen auf. Dies eröffnet einen neuen Therapieansatz in der medikamentösen Behandlung von z.B. chronischen Schmerzen, Drogenentzug, Morbus Parkinson und Morbus Alzheimer. Die neu synthetisierten, dualsteren Verbindungen wurden pharmakologisch untersucht, um ein besseres Verständnis über das Bindungsverhalten und die Signalweiterleitung an muskarinischen Acetylcholinrezeptoren zu erhalten, besonders in Hinblick auf Partialagonismus.

Die Entwicklung des Konzeptes der „dynamischen Ligandenbindung“ bietet neue Perspektiven in Hinblick auf das Bindungsverhalten und die Signalweiterleitung an G-Protein gekoppelten Rezeptoren. Somit werden GPCRs nicht mehr nur in ihrem aktiven oder inaktiven Zustand betrachtet. Vielmehr können dualstere Liganden sowohl einen dualsteren Bindemodus, welcher den aktiven Rezeptorzustand widerspiegelt, als auch einen rein allosteren Bindemodus, welcher durch einen inaktiven Rezeptorzustand charakterisiert ist, einnehmen, was schließlich zu Partialagonismus führt. Die Stärke des resultierenden Partialagonismus hängt vom Verhältnis zwischen aktiver und inaktiver Rezeptorbesetzung ab. Auf Basis dessen wurden orthostere/orthostere Hybridverbindungen, bestehend aus einem Antagonisten, Atropin oder Scopolamin, und einem Agonisten, Iperoxo oder Isoxazol, die über eine Alkylkette unterschiedlicher Länge miteinander verknüpft sind, synthetisiert, um mit deren Hilfe den Partialagonismus zu steuern (Abbildung 1).

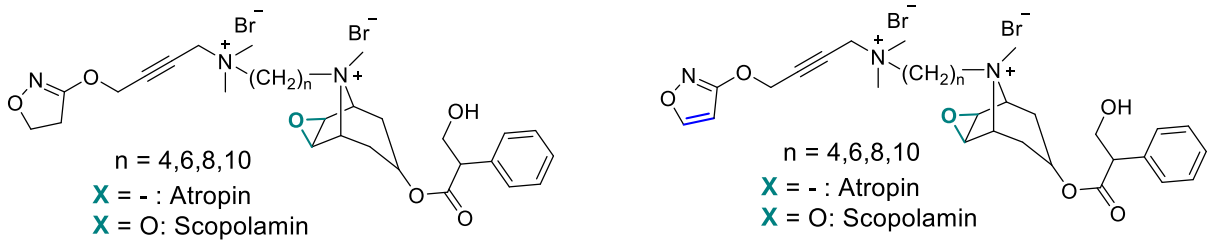

Iperoxo-C_n-Atropin/Scopolamin Isoxazol-C_n-Atropin/Scopolamin

Abbildung 1: Strukturen der synthetisierten Iperoxo/Isoxazol-Atropin/Scopolamin-Hybride.

Es wurden verschiedene quartäre sowie tertiäre Homodimere, welche entweder aus zwei Iperoxo-Einheiten oder aus zwei Acetylcholin-Einheiten bestehen, synthetisiert, um deren

Ausmaß in Bezug auf Partialagonismus untersuchen zu können (Abbildung 2). Die beiden Agonisten wurden über unterschiedlich lange Alkylketten miteinander verknüpft. Bindungsstudien an CHO-hM_2 Zellen der quartären Verbindungen zeigten, dass die Dimerisierung eines Agonisten zu einer verringerten Wirkstärke führt. Die Dimere von Iperoxo erreichten sowohl auf dem G_i- als auch auf dem G_s-Signalweg höhere Maximaleffekte als die Dimere von Acetylcholin. Neben der Wahl des orthosteren Bausteins (Wirkstärke des Agonisten) spielt auch die Länge der Alkylkette eine entscheidende Rolle für die Stärke des Partialagonismus.

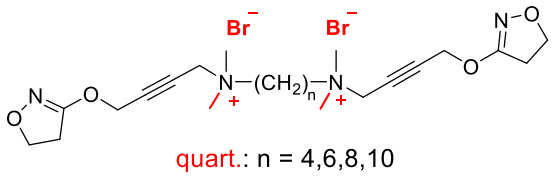

quart.: n = 4,6,8,10
tert.: n = 4,6,8

quart./tert. Iperoxo-C_n-Iperoxo

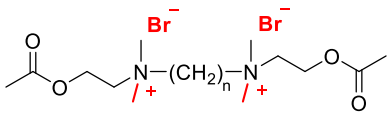

quart.: n = 4,6,8,10
tert.: n = 4,6,8

quart./tert. Acetylcholin-C_n-Acetylcholin

Abbildung 2: Strukturen der synthetisierten quart./tert. Iperoxo/Acetylcholin-Homodimere.

Um weitere Partialagonisten zu entwickeln, wurden Chinolon-basierte Verbindungen, die mit dem Superagonisten Iperoxo oder mit dem endogenen Liganden Acetylcholin über eine Alkylkette mit unterschiedlicher Länge verknüpft sind, synthetisiert (Abbildung 3). FRET-Messungen bestätigen, dass es sich bei den Hybriden um M_1-subtypselektive Substanzen handelt und das FRET-Signal von der Länge der Zwischenkette abhängig ist. Das stärkste positive FRET-Signal wurde mit der Verbindung Chinolon-C_6-Iper erzielt, welches durch positive Kooperativität zwischen den beiden Liganden, Alloster und Orthoster, zustande kommt. Im Gegensatz zu den kurzkettigen Hybriden beobachtete man bei den langkettigen Hybriden ein inverses FRET-Signal, welches auf einen anderen Bindemodus zum Rezeptor hindeutet, z.B. könnte es sich um eine rein allostere Bindung handeln. Außerdem wurde die flexible Alkylkette durch einen starren Linker ersetzt, welches im Hybrid Chinolon-rigide-Iperoxo verwirklicht ist (Abbildung 3). FRET-Messungen dieser starren Hybridverbindung am M_1-Rezeptor zeigten eine verzögerte FRET-Kinetik, welche vermutlich auf Wechselwirkungen zwischen dem starren Linker und dem aromatischen Deckel, der sich zwischen der orthosteren und der allosteren Bindestelle befindet, zurückzuführen ist. Es wird vermutet, dass das starre Hybrid bitopisch in den Rezeptor bindet. Um diese Annahme bestätigen zu können, müssten Mutationsstudien durchgeführt werden.

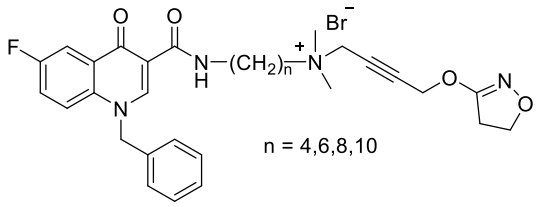

Chinolon-C_n-Iperoxo

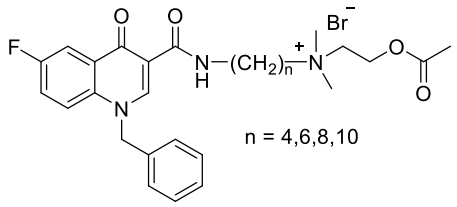

Chinolon-C_n-Acetylcholin

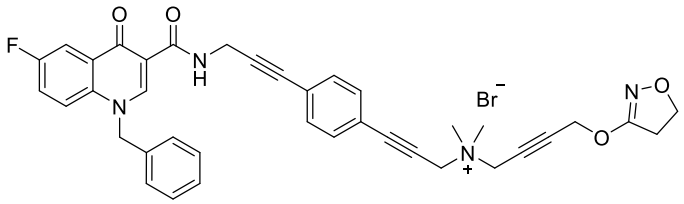

Chinolon-rigide-Iperoxo

Abbildung 3: M_1-selektive Hybridverbindungen.

Ein weiteres Ziel dieser Arbeit war das Wirkstoffdesign und die Synthese von neuen Hybridverbindungen, die als Agonisten am M_1- und am M_2-Rezeptor sowie als Inhibitoren der AChE als auch der BChE im Hinblick auf die Alzheimer`sche Krankheit wirken sollen. Verschiedenartige Hybridverbindungen, bestehend aus unterschiedlichen pharmakophoren Gruppen (katalytische, aktive Seite: Phthalimid, Naphthalimid, Tacrin; periphere, anionische Seite: Iperoxo, Isoxazol), die über eine Polymethylenkette unterschiedlicher Länge miteinander verknüpft sind, wurden synthetisiert. Tac-C_{10}-Iper (Abbildung 4), bestehend aus Tacrin und dem Superagonisten Iperoxo, welche über eine C10 Polymethylenkette miteinander verknüpft sind, zeigte exzellente Anticholinesterase-Aktivitäten sowohl für die AChE (pIC_{50} = 9.81) als auch für die BChE (pIC_{50} = 8.75). Docking-Experimente lieferten ein Strukturmodell, welches die inhibitorische Aktivität in Bezug auf die AChE begründet. Zusätzlich zeigten die aus Tacrin bestehenden Hybride Affinität zum M_1- als auch zum M_2-Rezeptor. Solche Verbindungen, die mehr als ein Zielmolekül adressieren, sind für multifaktorielle Krankheiten, wie z.B. die Alzheimer`sche Krankheit, von Vorteil.

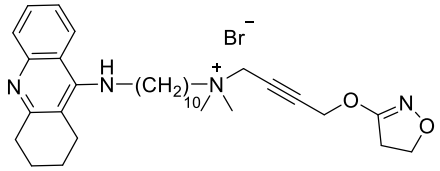

Tacrin-C_{10}-Iperoxo

Abbildung 4: Struktur der aktivsten Substanz in Bezug auf die Anticholinesterase-Aktivität.

Zusammenfassend kann festgestellt werden, dass sowohl die Wahl des Pharmakophors, deren Verbindungsstelle als auch die Zusammensetzung, Länge und Flexibilität des Linkers eine große Rolle für die Aktivität der entwickelten bivalenten Verbindungen spielen. Kurzkettige Linker können im Gegensatz zu längeren Zwischenketten nicht beide Bindestellen gleichzeitig überbrücken. Andererseits können zu lange Zwischenketten unerwünschte sterische Wechselwirkungen hervorrufen. Weitere Untersuchungen in Bezug auf strukturelle Veränderungen der Hybridverbindungen, mit oder ohne quartäre Ammoniumgruppen, sind in Bezug auf die Arzneimittelentwicklung notwendig.

G. Appendix

1. Supporting information for chapter 5

The herein described pharmacological experiments and data were gratefully investigated in the working group of PD Dr. Tränkle and Prof. Dr. Mohr by Anna Krüger (Pharmacology and Toxicology, Institute of Pharmacy, University of Bonn, Germany).

Data analysis using the operational model of agonism

The operational model of agonism correlates and quantifies the different extents of activation caused by the two signaling pathways G_i and G_s. The EC_{50}-value is affected by the binding constant (K_A) as well as by the efficacy (τ). Global fitting of the functional data (Figure 2, Figure 3, Chapter 5) with the operational model of agonism[1] provides both the binding constant (K_A) and the efficacy (τ) of the respective agonists. Furthermore, the transduction coefficient τ/K_A was calculated (τ/K_A-ratios normalized on iperoxo for the iperoxo derivatives and on acetylcholine for the acetylcholine derivatives) in order to eliminate system bias and focus on ligand bias.[2,3] However, the calculated results are influenced by the fact, that the M_2 receptor preferentially activates the G_i pathway. Therefore, the transduction coefficient of the reference substance was subtracted by the transduction coefficient of the test substance resulting in the equation $\Delta\log(\tau/K_A)$. $\Delta\Delta\log(\tau/K_A)$-values[4] eliminate system bias and indicate true test compound bias relative to the reference substance iperoxo and acetylcholine, respectively.

Data analysis of the iperoxo derivatives

Regarding the G_i signaling pathway, iperoxo displayed a significant larger efficacy τ than the corresponding derivatives (Figure S1A). Both iperoxo derivatives iper-6-iper **3-C6** and iper-6-phth resulted in similar behavior with respect to their binding constant- and efficacy values. Regarding the G_s signaling pathway, we could find a larger efficacy value for iper-6-iper **3-C6** ($\log\tau = 0.43$) than for iper-6-phth ($\log\tau = -0.88$), resulting in partial agonism for iper-6-iper **3-C6** and weak partial agonism for iper-6-phth (Figure S1A). However, iper-6-phth ($\log K_A = -6.46$) showed a higher binding constant value K_A than iper-6-iper **3-C6** ($\log K_A = -5.46$) (Figure S1A). All in all, the iperoxo derivatives displayed different behavior concerning the way of activation: iper-6-iper **3-C6** results in a higher efficacy τ, whereas iper-6-phth has the larger binding constant K_A.

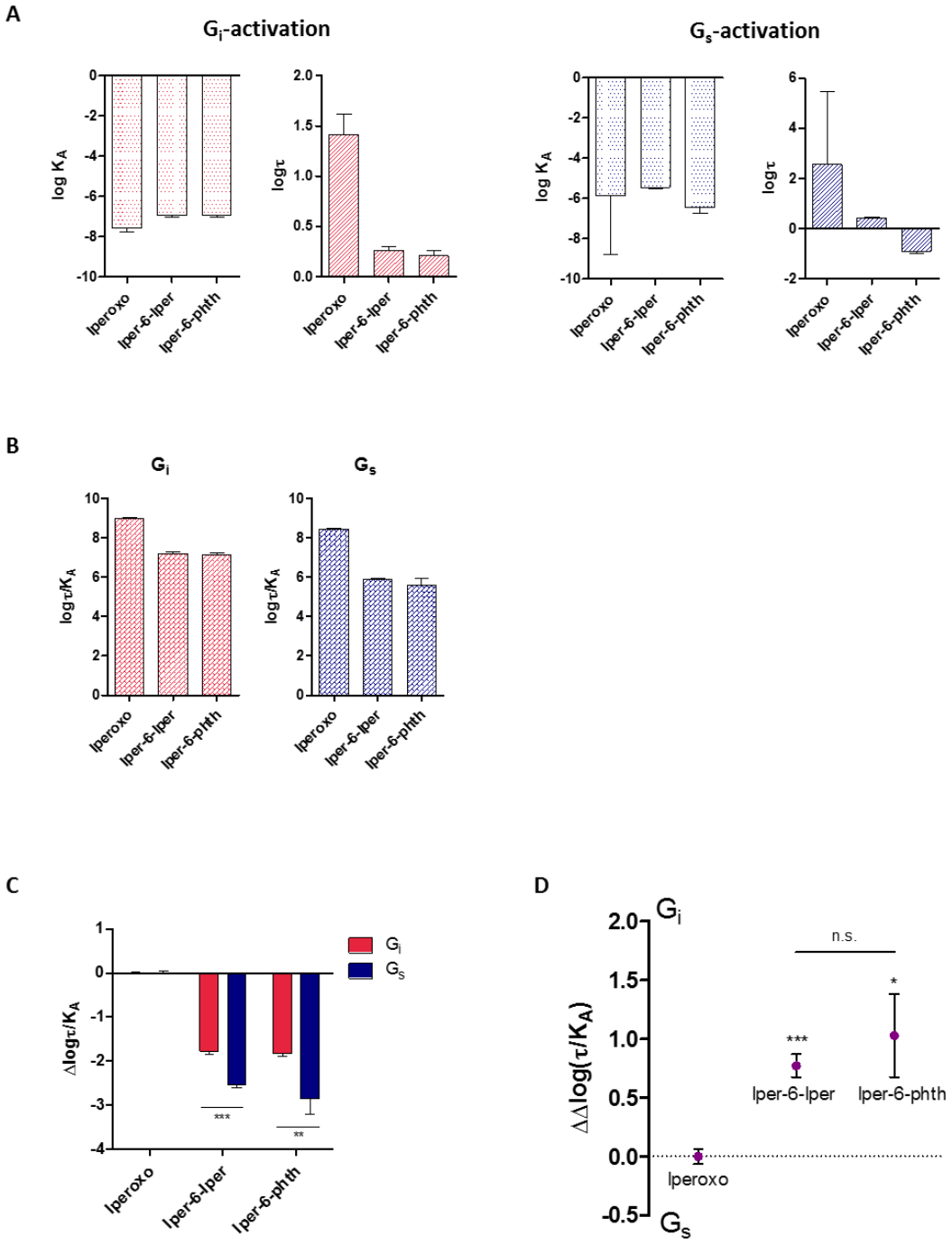

Figure S1: (**A**) Binding constant (K_A) and efficacy (τ) of iperoxo derivatives on the G_i pathway (red) and G_s pathway (blue). Determination of logK_A and logτ out of concentration effect curves by means of the operational model using iperoxo as reference agonist. (**B**) Transduction coefficients of iperoxo derivatives on the G_i pathway (red) and G_s pathway (blue). Determination of log(τ/K_A) by modified operational model.[5] (**C**) Normalized transduction coefficients of iperoxo derivatives. ** or ***: significantly different from the value obtained out of the G_i activation (t-test, P<0.01 or P<0.001). (**D**) ΔΔlog(τ/K_A) values of iperoxo derivatives. ** or ***: significantly different from the value obtained out of ΔΔlog(τ/K_A) in comparison to the reference agonist iperoxo (t-test, P<0.01 of P<0.001). n.s.: no significant difference between iper-6-Iper and iper-6-phth (P>0.05). Data are means ±s.e.m.

For the determination of ligand bias, the transduction coefficient $\log(\tau/K_A)$ was calculated. Iperoxo preferentially activates the G_i pathway at the M_2 receptor which was described earlier in literature as system bias[2,6]. The iperoxo derivatives also prefer the G_i signaling pathway confirmed through the higher transduction coefficients found (Figure S1B).

For the elimination of system bias, the equation $\Delta\log(\tau/K_A)$ was used which makes a comparison between the two signaling pathways for iper-6-iper **3-C6** and iper-6-phth possible. Both iperoxo derivatives display a significant higher activation on the G_i pathway than on the G_s (Figure S1C).

Ligand bias is expressed by the equation $\Delta\Delta\log(\tau/K_A)$, which makes a direct comparison between the two iperoxo derivatives possible. Here, both iperoxo derivatives show a significant preference for the G_i signaling pathway. Iper-6-iper **3-C6** ($\Delta\Delta\log(\tau/K_A)$ = 0.77 ± 0.09) activates the G_i pathway 6 times and iper-6-phth ($\Delta\Delta\log(\tau/K_A)$ = 1.03 ± 0.35)[6] even 11 times stronger than the G_s pathway (Figure S1D).

Data analysis of the acetylcholine derivatives

The acetylcholine derivatives were investigated with respect to their efficacy τ as well as their binding constant K_A, too. Regarding the G_i pathway, the middle chain-elongated derivatives ACh-4-ACh **5-C4** and ACh-6-ACh **5-C6** displayed low and almost similar efficacy values as well as binding constants (Figure S2A). The extension of the alkyl chain length to C_8 and C_{10} atoms resulted in much higher K_A- and efficacy-values with ACh-10-ACh **5-C10** having the highest efficacy τ ($\log\tau$ = 0.25), acting therefore as strong partial agonist similar to iper-6-iper **3-C6** ($\log\tau$ = 0.25) and iper-6-phth ($\log\tau$ = 0.21). According to (Figure 3B, Chapter 5), no G_s activation could be found for the compounds ACh-4-ACh **5-C4** and ACh-6-ACh **5-C6**. The two long chain-elongated derivatives showed no difference according to their binding constants. The low efficacy values indicate weak partial agonism (Figure S2A).

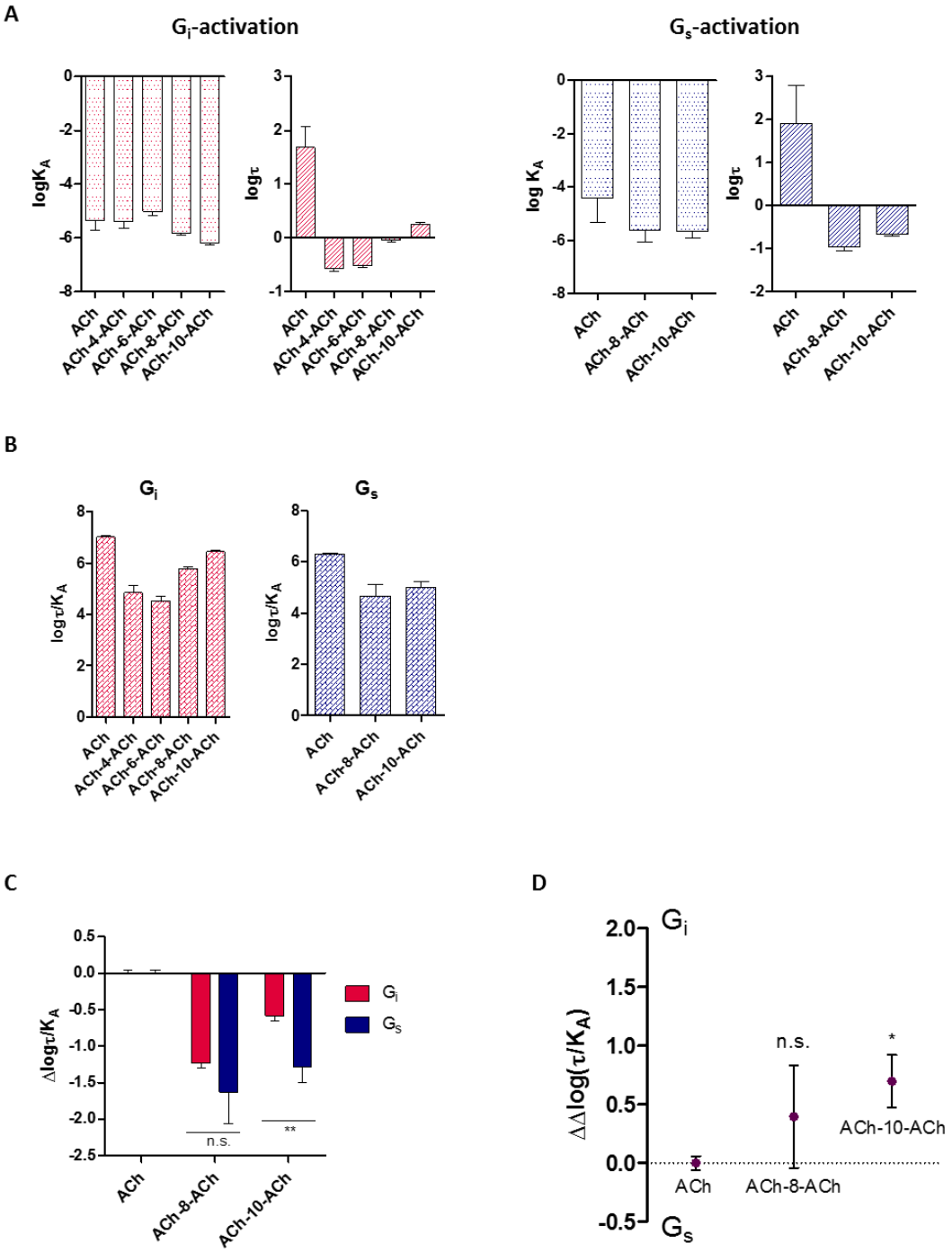

Figure S2: (**A**) Binding constant (K_A) and efficacy (τ) of acetylcholine derivatives on the G_i pathway (red) and G_s pathway (blue). Determination of $\log K_A$ and $\log\tau$ out of concentration effect curves by means of the operational model using acetylcholine as reference agonist. (**B**) Transduction coefficients of acetylcholine derivatives on G_i pathway (red) and G_s pathway (blue). Determination of $\log(\tau/K_A)$ by modified operational model.[5] (**C**) Normalized transduction coefficients of acetylcholine derivatives. **: significantly different from the value obtained out of the G_i activation (t-test, $P<0.01$). n.s.: not significantly different from the value obtained out of the G_i activation (t-test, $P>0.05$). (**D**) $\Delta\Delta\log(\tau/K_A)$ values of acetylcholine derivatives. *: significantly different from the $\Delta\Delta\log(\tau/K_A)$-value in contrast to the reference agonist acetylcholine (t-test, $P<0.05$). n.s.: not significantly different from the $\Delta\Delta\log(\tau/K_A)$-value in contrast to the reference agonist acetylcholine (t-test, $P<0.05$). Data are means ±s.e.m.

Regarding the G_i pathway, the longer the middle chain, the greater the calculated $\log(\tau/K_A)$-values. The values on the G_s pathway are distinct lower (Figure S2B).

In order to eliminate the preferred G_i signaling pathway for the M_2 receptor (system bias), the transduction coefficient was normalized. The two long chain elongated acetylcholine dimers displayed weaker activation than acetylcholine alone concerning both pathways, whereas the G_i activation was greater than the G_s activation (Figure S2C).

The calculated $\Delta\Delta\log(\tau/K_A)$-values showed a preferred tendency of G_i signaling pathway activation for ACh-8-ACh **5-C8** (statistically not significant) and ACh-10-ACh **5-C10** displayed a 5 times stronger G_i activation than G_s activation (statistically significant) (Figure S2D).

Methods

Pharmacology

Cell culture

Flp-In-Chinese hamster ovary cells (Flp-In-CHO) stably expressing the hM_2 receptor (CHO-hM_2 cells) were cultured in Ham`s nutrient mixture F-12 supplemented with 10% (v/v) fetal calf serum (FCS), 100 U/mL penicillin, 100 µg/mL streptomycin and 2 mM *L*-glutamine. All cell lines were kept at 37 °C in a humidified 5% CO_2 atmosphere.

[^{35}S]GTPγS-binding assay

[^{35}S]GTPγS-binding experiments were conducted as described earlier in the literature.[7] In brief, homogenates of membranes of CHO-hM_2 cells (40 µg/mL) were incubated with 0.07 nM [^{35}S]GTPγS and maximum agonist-induced [^{35}S]GTPγS incorporation was measured after 1 h. Experiments were measured in triplicates.

cAMP accumulation assay

Agonist-induced rise of intracellular cAMP was captured in CHO-hM_2 cells pretreated with 100 ng/mL PTX for 16-20 h as described previously[8] using the HTRF-cAMP dynamic 2 kit (Cisbio, Codolet, France) following the described procedure. Fluorescence was quantified on a Mithras LB 960 reader (Berthold Technologies, Bad Wildbad, Germany).

Calculations and data analysis

All data were analyzed using GraphPad Prism 5.03 (San Diego, CA) or Microsoft Excel 2007 (Redmont, Washington). Data obtained from [^{35}S]GTPγS-binding and cAMP accumulation assays were analyzed in two steps. First, data were fitted by a four-parameter logistic function resulting in parameter values for ligand potency (pEC_{50}) and maximum effect (E_{max}). Second, data points were analyzed by the following equation due to the operational model of agonism:[1]

$$E = \frac{E_{max} \cdot \tau \cdot [A]}{\tau \cdot [A] + ([A] + K_A)} \quad (1)$$

E_{max} is defined as the maximal response of the system induced by the maximal effect of a full agonist; τ is the coupling efficiency, indicating how efficient agonist binding is transduced into a signaling response and therefore reflects agonist efficacy; K_A is the equilibrium dissociation constant of the agonist-receptor complex and displays affinity. For the calculation of ligand bias, we used the term $\log(\tau/K_A)$, which combines information about both affinity and efficacy of the respective agonist for activating a signaling pathway.[4] The so obtained transduction coefficients were then expressed relative to the corresponding reference substance (iperoxo for the iperoxo derivatives; acetylcholine for the acetylcholine derivatives) for each pathway according to

$$\Delta log(\tau/K_A)_{agonist,pathway} = log(\tau/K_A)_{agonist,pathway} - log(\tau/K_A)_{ref.,pathway} \quad (2)$$

$\Delta\log(\tau/K_A)$-values eliminate system bias and indicate true test compound bias relative to the reference substance iperoxo and acetylcholine, respectively. The log bias scale is given by

$$\Delta\Delta log(\tau/K_A)_{agonist} = \Delta log(\tau/K_A)_{agonist,pathway1} - \Delta log(\tau/K_A)_{agonist,pathway2} \quad (3)$$

References

[1] Black, J. W., and Leff, P. (1983) Operational Models of Pharmacological Agonism, *Proc. R. Soc. Lond. B 220*, 141-162.

[2] Kenakin, T., and Christopoulos, A. (2013) Signalling bias in new drug discovery: detection, quantification and therapeutic impact, *Nat. Rev. Drug. Discov. 12*, 205-216.

[3] Kenakin, T. (2012) The potential for selective pharmacological therapies through biased receptor signaling, *BMC Pharmacol. Toxicol. 13*, 3.

[4] Kenakin, T., Watson, C., Muniz-Medina, V., Christopoulos, A., and Novick, S. (2012) A simple method for quantifying functional selectivity and agonist bias, *ACS Chem. Neurosci. 3*, 193-203.

[5] Shonberg, J., Lopez, L., Scammells, P. J., Christopoulos, A., Capuano, B., and Lane, J. R. (2014) Biased agonism at G protein-coupled receptors: the promise and the challenges--a medicinal chemistry perspective, *Med. Res. Rev. 34*, 1286-1330.

[6] Bock, A., Merten, N., Schrage, R., Dallanoce, C., Batz, J., Kloeckner, J., Schmitz, J., Matera, C., Simon, K., Kebig, A., Peters, L., Müller, A., Schrobang-Ley, J., Tränkle, C., Hoffmann, C., De Amici, M., Holzgrabe, U., Kostenis, E., and Mohr, K. (2012) The allosteric vestibule of a seven transmembrane helical receptor controls G-protein coupling, *Nat. Commun. 3*, 1044.

[7] Jäger, D., Schmalenbach, C., Prilla, S., Schrobang, J., Kebig, A., Sennwitz, M., Heller, E., Tränkle, C., Holzgrabe, U., Holtje, H. D., and Mohr, K. (2007) Allosteric small molecules unveil a role of an extracellular E2/transmembrane helix 7 junction for G protein-coupled receptor activation, *J. Biol. Chem. 282*, 34968-34976.

[8] Schröder, R., Merten, N., Mathiesen, J. M., Martini, L., Kruljac-Letunic, A., Krop, F., Blaukat, A., Fang, Y., Tran, E., Ulven, T., Drewke, C., Whistler, J., Pardo, L., Gomeza, J., and Kostenis, E. (2009) The C-terminal tail of CRTH2 is a key molecular determinant that constrains Galphai and downstream signaling cascade activation, *J. Biol. Chem. 284*, 1324-1336.

2. List of publications/manuscript and documentation of authorship

FRET studies of quinolone-based bitopic ligands and their structural analogues at the muscarinic M_1 receptor

Messerer, R., Kauk, M., Volpato, D., Alonso Canizal, M.C., Klöckner, J., Zabel, U., Nuber, S., Hoffmann, C., Holzgrabe, U.

ACS Chem. Biol., 2017, 12 (3), 833-843

doi:10.1021/acschembio.6b00828

Dynamic ligand binding dictates partial agonism at a G protein-coupled receptor

Bock, A., Chirinda, B., Krebs, F., Messerer, R., Bätz, J., Muth, M., Dallanoce, C., Klingenthal, D., Tränkle, C., Hoffmann, C., De Amici, M., Holzgrabe, U., Kostenis, E., Mohr, K.

Nat. Chem. Biol., 2014, 10, 18-20

doi:10.1038/nchembio.1384

Novel bipharmacophoric inhibitors of the cholinesterases with affinity to the muscarinic receptors M_1 and M_2

Messerer, R., Dallanoce, C., Matera, C., Wehle, S., Flammini, L., Chirinda, B., Bock, A., Irmen, M., Tränkle, C., Barocelli, E., Decker, M., Sotriffer, C., De Amici, M., Holzgrabe, U.

in preparation (unpublished)

This section contains a list of individual contribution for each author to the publications reprinted in this thesis. Unpublished manuscripts are handled, accordingly.

Messerer R, Kauk M, Volpato D, Alonso Canizal M, Klöckner J, Zabel U, Nuber S, Hoffmann C, Holzgrabe U, FRET studies of quinolone-based bitopic ligands and their structural analogues at the muscarinic M_1 receptor. ACS *Chem. Biol.* **2017**, *12* (3), 833-843.

Author	1	2	3	4	5	6	7	8	9
Compound synthesis and characterization	x		x		x				
FRET studies		x		x					
FRET-sensor characterization						x	x		
Study design/concept development	x	x						x	x
Data analysis and interpretation	x	x						x	x
Manuscript planning	x	x						x	x
Manuscript writing	x	x							
Correction of manuscript	x	x						x	x
Supervision of Regina Messerer									x

Bock A, Chirinda B, Krebs F, Messerer R, Bätz J, Muth M, Dallanoce C, Klingenthal D, Tränkle C, Hoffmann C, De Amici M, Holzgrabe U, Kostenis E, Mohr K, Dynamic ligand binding dictates partial agonism at a G protein-coupled receptor. *Nat. Chem. Biol.* **2014**, *10*, 18-20.

Author	1	2	3	4	5	6	7	8	9	10	11	12	13	14
Development of mathematical framework	x													
Binding experiments	x	x	x					x						
Compound synthesis and characterization				x		x	x							
FRET experiments					x									
Data analysis and interpretation	x								x	x	x	x		x
Manuscript planning	x									x		x	x	x
Manuscript writing	x													x
Correction of manuscript	x													x
Supervision of Regina Messerer												x		

Messerer R, Dallanoce C, Matera C, Wehle S, Flammini L, Chirinda B, Bock A, Irmen M, Tränkle C, Barocelli E, Decker M, Sotriffer C, De Amici M, Holzgrabe U, Novel bipharmacophoric inhibitors of the cholinesterases with affinity to the muscarinic receptors M_1 and M_2. **2017**, in preparation (unpublished).

Author	1	2	3	4	5	6	7	8	9	10	11	12	13	14
Compound synthesis and characterization	x	x	x											
In vitro anticholinesterase assay	x													
Rat brain anticholinesterase assay					x									
Binding experiments						x	x	x						
Measurement of logP values	x													
Calculation of LE- and LLE values	x													
Docking studies				x										
Data analysis and interpretation	x			x			x		x			x	x	x
Manuscript planning	x													
Manuscript writing	x	x		x			x		x	x				
Correction of manuscript	x	x		x						x	x	x	x	x
Supervision of Regina Messerer														x

Erklärung zu den Eigenanteilen des Doktoranden an Publikationen und Zweitpublikationsrechten bei einer kumulativen Dissertation.

Für alle in dieser kumulativen Dissertation verwendeten Manuskripte liegen die notwendigen Genehmigungen der Verlage („reprint permissions“) für die Zweitpublikation vor, außer das betreffende Kapitel ist nicht publiziert. Dieser Umstand wird einerseits durch die genaue Angabe der Literaturstelle der Erstpublikation auf der ersten Seite des betreffenden Kapitels deutlich gemacht oder die bisherige Nichtveröffentlichung durch den Vermerk „unpublished“ oder „nicht veröffentlicht“ gekennzeichnet.

Die Mitautorin der in dieser kumulativen Dissertation verwendeten Manuskripte ist sowohl über die Nutzung als auch über die oben angegebenen Eigenanteile informiert.

Die Beiträge der Mitautorin an den Publikationen sind in den vorausgehenden Tabellen aufgeführt.

Prof. Dr. Ulrike Holzgrabe	_____	_____
	Ort, Datum	Unterschrift
Regina Messerer	_____	_____
	Ort, Datum	Unterschrift

3. Conference contribution

Messerer, R., Dallanoce, C., Matera, C., Wehle, S., Flammini, L., Barocelli, E., Decker, M., Sotriffer, C., De Amici, M., Holzgrabe, U.

Novel hybrid inhibitors of cholinesterases as potential anti-Alzheimer agents.

DPhG Jahrestagung 2016, München.

4. Abbreviations

AC	adenylate cyclase
ACh	acetylcholine
AChE	acetylcholinesterase
AD	Alzheimer disease
ATC	acetylthiocholine
ATR	attenuated total reflection
BChE	butyrylcholinesterase
BOC	*tert*-butyloxycarbonyl
BQCA	benzyl quinolone carboxylic acid
BTC	butyrylthiocholine
cAMP	cyclic adenosine monophosphate
CAS	catalytic active site
CFP	cyan fluorescent protein
DAG	diacylglycerol
DMR	dynamic mass redistribution
DTNB	dithionitrobenzoic acid
ELSD	evaporative light scattering detector
ESI	electrospray ionization
FlAsH	fluoresceine arsenical hairpin binder
FRET	fluorescence resonance energy transfer
FT-IR	fourier transform infrared spectroscopy
GDP	guanosindiphosphat
G_i	inhibitory G-protein
G_q	G-protein activating phospholipase C
G_s	stimulatory G-protein
GPCR	G protein-coupled receptor
GTP	guanosintriphosphat
HPLC	high-performance liquid chromatography
IL	intracellular loop
IP_3	ionositol-1,4,5-triphosphate
LCMS	liquid chromatography mass spectrometry
M_1-M_5	muscarininc acetylcholine subtype 1-5
mAChR	muscarinic acetylcholine receptor
NA	noradrenaline
nAChR	nicotinic acetylcholine receptor
NAL	neutral allosteric modulator
NAM	negative allosteric modulator
NMR	nuclear magnetic resonance
NOE	nuclear Overhauser effect
NOESY	nuclear Overhauser enhancement spectroscopy

PAM	positive allosteric modulator
PAS	peripheral anionic site
PLC	phospholipase C
PTX	pertussis toxin
RMSD	root mean square deviation
TCM	ternary complex model
TLC	thin layer chromatography
UV-VIS	ultraviolet-visible
YFP	yellow fluorescent protein

Corrigenda

Regina Messerer, Dissertation, Synthesis of Dualsteric Ligands for Muscarinic Acetylcholine Receptors and Cholinesterase Inhibitors, 2017

Figure 6a on page 43 (C. Results; 1. FRET studies of quinolone-based bitopic ligands and their structural analogues at the muscarinic M_1 receptor) is identical to **Figure 2B** on page 72 (C. Results; 2. Synthesis and FRET studies of the quinolone-rigid-iper hybrid). In both figures the same compound was measured, but differently numbered (5-C6 in Figure 6a on page 43 and 3 in Figure 2B on page 72).

The first sentence on page 214 reads correctly:

“Die vorliegende Studie beschäftigt sich mit der Synthese und der pharmakologischen Untersuchung von neu entwickelten dualsteren Liganden des muskarinischen Acetylcholinrezeptors, welcher zur Superfamilie der G-Protein gekoppelten Rezeptoren gehört.“